Electronic Thesis and Dissertation Repository

2-13-2017 12:00 AM

Quantitative Proteomic Characterization of CX-4945, a Clinical Stage Inhibitor of Protein Kinase CK2

Adam J. Rabalski, *The University of Western Ontario*

Supervisor: Dr. David Litchfield, *The University of Western Ontario*
A thesis submitted in partial fulfillment of the requirements for the Doctor of Philosophy degree in Biochemistry
© Adam J. Rabalski 2017

Follow this and additional works at: https://ir.lib.uwo.ca/etd

Part of the Biochemistry Commons

Abstract

Protein phosphorylation is controlled by protein kinases, and represents a critical signaling mechanism involved in the regulation of fundamental biological processes. Furthermore, the aberrant regulation of kinase activity is implicated in diseases such as cancer and has resulted in efforts to target kinases therapeutically. Protein kinase CK2, although frequently considered constitutively active, has emerged as a clinical target on the basis of its altered expression in different types of human cancers and its regulatory participation in multiple biological processes. In fact, CX-4945, a small molecule ATP-competitive inhibitor of CK2 has advanced to clinical trial and has been widely used to interrogate CK2-dependent signaling events in cells. Despite its widespread applications, an understanding of the mechanism of action of CX-4945 on cells remains limited.

In this thesis, comparison of proteomic sample preparation strategies led to the development of a phosphoproteomic workflow that enabled the enrichment of phosphopeptides conforming to the CK2 consensus sequence. Using the optimized workflow, phosphoproteomic profiling was conducted in HeLa cells treated with CX-4945. Several phosphorylation sites conforming to the recognition motif for CK2 phosphorylation displayed significantly decreased phosphorylation in response to CX-4945. Kinase substrate enrichment analysis also revealed a broad impact of CX-4945 on several kinases other than CK2. Profiling of the kinome utilizing multiplexed inhibitor beads also revealed changes in the activity of other kinases including activation of the ERK MAPK pathway and inhibition of the PI3K/Akt/mTOR pathway. Studies with Inhibitor VIII, an unrelated CK2 inhibitor, also resulted in activation of the ERK MAPK pathway suggesting that CK2 has a role in regulating this pathway. By comparison, the PI3K/Akt/mTOR pathway was not affected by

Inhibitor VIII indicating that the effects of CX-4945 on that pathway are independent of CK2.

Overall, this investigation provides valuable insight into the regulation of the phosphoproteome and the kinome in response to CX-4945 in HeLa cells. Dynamic markers of CK2 activity in cells were identified and putative CK2-independent effects of CX-4945 were revealed. Collectively, these studies illustrate the utility of global proteomic approaches to elucidate the cellular effects of clinical-stage kinase inhibitors.

Keywords: CK2, proteomic, phosphorylation, CX-4945, kinase inhibitors, mass spectrometry

Co-Authorship Statement

All chapters in this thesis were written by Adam Rabalski and edited by David Litchfield. Excerpts in chapter 1 have been previously published in: Rabalski, A. J., Gyenis, L., and Litchfield, D. W. (2016) Molecular Pathways: Emergence of Protein Kinase CK2 (CSNK2) as a Potential Target to Inhibit Survival and DNA Damage Response and Repair Pathways in Cancer Cells. *Clin. Cancer Res.* **22**, 2840–2847. Laszlo Gyenis conceptualized figures reproduced from this publication, with input from David Litchfield and Adam Rabalski.

Adam Rabalski performed all experiments and data analysis presented in this thesis. In chapter 4, Stephen Sherman and Miljan Kuljanin assisted in the acquisition and analysis of flow cytometry data.

Table of Contents

List of Figures

List of Supplemental Figures

List of Appendices

The following tables are provided in an accompanying file.

List of Abbreviations Used

°C   degrees centigrade

4E-BP1   eukaryotic translation initiation factor 4E-binding protein 1

7-AAD   7-amino-actinomycin D

Å   angstrom

ABC   ammonium bicarbonate

ACN   acetonitrile

AGC   automatic gain control

Akt1   protein kinase B alpha

ATP   adenosine triphosphate

BEH   ethylene-bridged hybrid

BET   Bromodomain and extra-terminal protein

BRAF   B-Raf proto-oncogene serine/threonine protein kinase

BRD4   Bromodomain containing protein 4

BSA   bovine serum albumin

c-Raf   Raf-1 proto-oncogene serine/threonine kinase

C18   octadecyl carbon chain

CDK   cyclin dependent kinase

CID   collision induced dissociation

CK2   protein kinase CK2

CK2α   catalytic isoform of CK2 alpha, CSNK2A1

CK2α'   catalytic isoform of CK2 alpha prime, CSNK2A2

CK2β   catalytic isoform of CK2 beta, CSNK2B

CLL   chronic lymphocytic leukemia

CML   chronic myelogenous leukemia

CX-4945   5-((3-chlorophenyl)amino)benzo[c][2,6]naphthyridine-8-carboxylic acid

Da   Dalton

DDR   DNA Damage Response

DMEM   Dulbecco's modified Eagle medium

DMSO   dimethyl sulfoxide

DSB   DNA doubled-strand break

DTT   DL-Dithiothreitol

EDTA   ethylenediaminetetraacetic acid

EGF   epidermal growth factor

EGFR   epidermal growth factor receptor

EGTA   ethylene glycol-bis(β-aminoethyl ether)-N,N,N',N'-tetraacetic acid)

EIF2S1   eukaryotic translation initiation factor 2 subunit 1

EIF2S2   eukaryotic translation initiation factor 2 subunit 2

ER   endoplasmic reticulum

ERK   extracellular signal-regulated kinase

FA   formic acid

FACS   fluorescence activated cell sorting

FASP   Filter aided sample preparation

FBS   fetal bovine serum

FDR   false discovery rate

FHA   forkhead associated domain

g	relative centrifugal force
GAM	goat-anti-mouse
GAPDH	glyceraldehyde 3-phosphate dehydrogenase
GAR	goat-anti-rabbit
HCD	higher energy collisional dissociation
HeLa	human cervical cancer cell line
HEPES	4-(2-hydroxyethyl)-1-piperazineethanesulfonic acid
HPLC	high performance liquid chromatography
IAA	iodoacetamide
Inhibitor VIII	4-(2-(4-methoxybenzamido)thiazol-5-yl)benzoic acid
IRAK1	interleukin-1 receptor-associated kinase 1
KCl	potassium chloride
kDa	kiloDalton
L	liter
LC	liquid chromatography
LC3	microtubule-associated proteins 1A/1B light chain 3
Lys-C	endoproteinase Lys-C
m/*z*	mass-to-charge ratio
MAPK	mitogen activated protein kinase
MDC1	mediator of DNA damage checkpoint protein 1
MED1	mediator of RNA polymerase II transcription subunit 1
MEK	MAPK/ERK kinase
mg	milligram

MIB	multiplexed inhibitor bead
mL	millilitre
mM	millimolar
MRN	MRE11A-RAD50-NBN complex
MS	mass spectrometer
MS1	survey scan of mass spectrometer cycle
MS2	dependent scan of mass spectrometer cycle
mTOR	mechanistic target of rapamycin
NBN	Nijmegen breakage syndrome protein 1
NCE	normalized collision energy
NCS	neocarzinostatin
nm	nanometre
NP-40	Nonidet P-40
OTUB1	ubiquitin thioesterase OTUB1
p38MAPK	mitogen activated protein kinase p38
p70S6K	ribosomal protein S6 kinase beta-1, RPS6KB1
p90RSK	ribosomal protein S6 kinase alpha-1, RPS6KA1
PARP	poly (ADP-ribose) polymerase
PBS	phosphate buffered saline
PBST	phosphate buffered saline + 0.1% Tween-20
PGC	porous graphitic carbon
pH3Ser10	phospho-Histone 3 serine 10
PI3K	phosphatidylinositol 3-kinase

PMSF	phenylmethylsulfonylfluoride
PP	protein precipitation on-pellet digestion
PP2A	protein phosphatase 2
ppm	parts per million
PRM	parallel reaction monitoring
PVDF	polyvindylidine fluoride
RAD51	DNA repair protein RAD51 homolog1
SCX	strong cation exchange chromatography
SDS	sodium dodecyl sulfate
SDS-PAGE	sodium dodecyl sulfate – polyacrylamide gel electrophoresis
Sgk1	serum/glucocorticoid-regulated kinase 1
SILAC	Stable Isotope Labeling of Amino Acids in Cell Culture
SPE	solid phase extraction
STS	staurosporine
TBST	Tris buffered saline + 0.05% Tween-20
TCA	trichloroacetic acid
TCOF1	Treacle protein
TOP2A	topoisomerase 2 alpha
Torin1	1-[4-[4-(1-Oxopropyl)-1-piperazinyl]-3-(trifluoromethyl)phenyl]-9-(3quinolinyl)-benzo[*h*]-1,6-naphthyridin-2(1*H*)-one
TP53BP1	tumor suppressor p53-binding protein 1
TRAIL	Tumor necrosis factor-related apoptosis-inducing ligand

Tris	tris(hydroxymethyl)aminomethane
UPLC	ultra performance liquid chromatography
Ulk1	Unc-51 like kinase 1
UTA6	human osteosarcoma cell line
VIN1	vinculin
XRCC1	x-ray repair cross-complementing protein 1
XRCC4	x-ray repair cross-complementing protein 4
γH2AX	phospho-histone H2A Ser139
μg	microgram
μL	microlitre
μm	micrometre
μM	micromolar

Ala	A	alanine
Arg	R	arginine
Asn	N	asparagine
Asp	D	aspartic acid
Cys	C	cysteine
Gln	Q	glutamine
Glu	E	glutamic acid
Gly	G	glycine
His	H	histidine
Ile	I	isoleucine
Leu	L	leucine
Lys	K	lysine
Met	M	methionine
Phe	F	phenylalanine
Pro	P	proline
Ser	S	serine
Thr	T	threonine
Trp	W	tryptophan
Tyr	Y	tyrosine
Val	V	valine

1 Chapter 1 – Introduction

1.1 General Introduction[1]

The reversible phosphorylation of cellular proteins that is catalyzed by protein kinases represents a central mechanism for the transmission of intracellular signals (1). In eukaryotes, protein kinases catalyze the transfer of phosphate from ATP to the hydroxyl group located on side chains of amino acids serine, threonine and tyrosine. The phosphate group can be removed by a specific phosphatase when no longer required (2). Phosphorylation plays a pivotal regulatory role in a broad array of cellular responses including activation of transcription factors (3), conformational change in protein structure (4), and the mediation of protein-protein interactions which comprise signal transduction pathways (5). Approximately 700,000 potential phosphorylation sites could exist in the human proteome (6), with nearly three quarters of proteins that are detectable by mass spectrometry being phosphorylated, demonstrating the widespread impact of phosphorylation in maintaining cellular processes (7). Not surprisingly, because of the critical role in regulatory signaling pathways, the deregulation of kinases can lead to pathophysiological processes such as cancer (8) and has prompted interest in kinases as drug targets for cancer therapeutics (9).

1.2 Protein Kinase CK2

Protein kinase CK2 represents one small protein kinase family that has recently emerged as a potential therapeutic target based on alterations in its expression or activity in a number of cancers (10). CK2 is composed of two closely related catalytic isoforms CK2α

---

[1] Excerpts of this chapter are reproduced with permission from:
Rabalski, A. J., Gyenis, L., and Litchfield, D. W. (2016) Molecular Pathways: Emergence of Protein Kinase CK2 (CSNK2) as a Potential Target to Inhibit Survival and DNA Damage Response and Repair Pathways in Cancer Cells. *Clin. Cancer Res.* **22**, 2840–2847

and CK2α' (encoded by CSNK2A1 and CSNK2A2 genes respectively) that both display catalytic activity in the presence or absence of its regulatory CK2β (CSNK2B) subunit. The regulatory CK2β subunit is not essential for activity, but can impact the ability of the catalytic subunits to phosphorylate certain substrates (11). CK2 has also been shown to be essential for viability, as deletion of CK2α or CK2β leads to embryonic lethality in mice (12, 13). A recent analysis of transcript expression profiles for CSNK2A1, CSNK2A2 and CSNK2B in neoplastic tissues versus normal tissues deposited in the Oncomine database revealed varying degrees of altered expression of individual CK2 subunits suggesting that deregulation of CK2 subunit expression profiles promotes cancer (14). To this point, the CK2-dependent phosphoproteome has not yet been fully elucidated and the impact of alterations in CK2 on the phosphoproteome has not yet been systematically investigated. Nevertheless, it is evident both from an extensive literature and computational predictions of its substrates based on its consensus recognition motif (S/T-X-X-D/E/pS/pY) that CK2 could be implicated in a vast landscape of biological processes (Figure 1.1) with >2000 putative phosphorylation sites in the human proteome (15). While more comprehensive discussions of CK2 can be found elsewhere (16, 17), we will highlight the involvement of CK2 in specific cellular processes, including its convergence with caspase pathways and its roles in DNA response and repair pathways, which have inspired ongoing efforts to exploit CK2 as a therapeutic target.
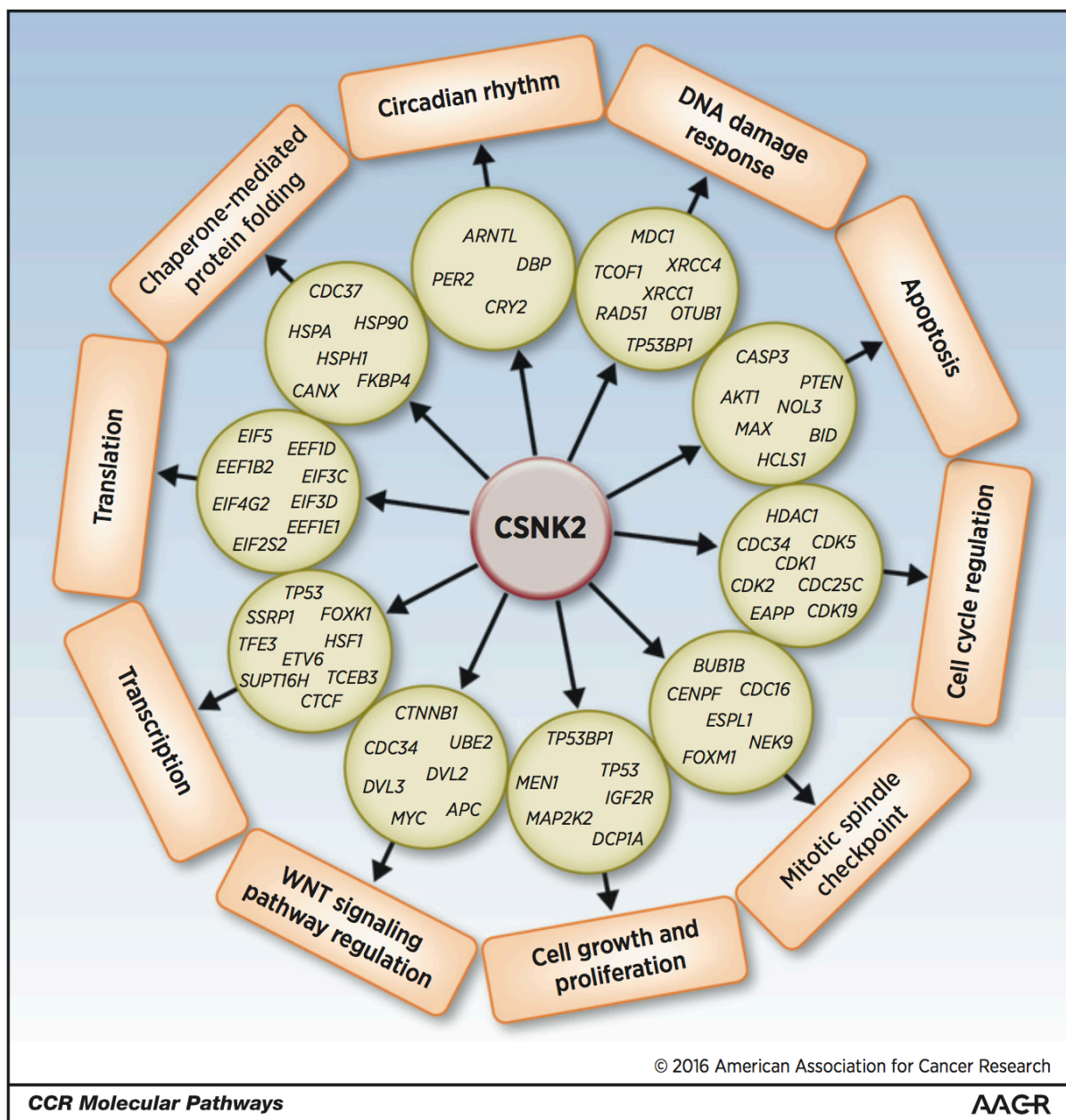
Figure 1.1 Protein Kinase CK2 is Implicated in Different Biological Processes
CK2 (referred to as CSNK2 in the figure) is presented with examples of putative substrates or interacting proteins involved in each biological process listed. These proteins were identified using gene ontology biological processes according to the following databases: UniProt, Reactome, PHOSIDA and PubMed. This figure is reproduced with permission from AACR.

1.3 Convergence of CK2 with Caspase Pathways

CK2 is generally considered to be a constitutively active enzyme (ie. its catalytic subunits do not require activating phosphorylation, association with its regulatory subunit or the presence of second messengers to be catalytically active), which is expressed at higher levels in many forms of human cancer (14, 18-20). These observations are particularly intriguing when considering the remarkable resemblance of the consensus recognition motif of CK2 with that of caspases (Figure 1.2 A) which cleave substrates at aspartic acid residues during the progression of apoptosis. In fact, several published examples (Figure 1.2 A) demonstrate that caspase substrates, including Bid which promotes apoptotic progression when it is cleaved, can be phosphorylated by CK2 at sites adjacent to caspase cleavage sites. Since phosphorylation adjacent to caspase cleavage sites blocks cleavage, these observations suggest that increased phosphorylation by CK2 could promote cell survival by inhibiting caspase action (21-26).

Building on these observations, a combined computational and biochemical approach revealed an extensive repertoire of proteins with overlapping CK2 and caspase recognition motifs suggesting that CK2 could have widespread impact on caspase action (27). In addition to the identification of many proteins known to be caspase substrates, these studies also demonstrated that CK2 could phosphorylate caspase-3 to prevent its cleavage by upstream caspases activated by intrinsic and extrinsic apoptotic stimuli (Figure 1.2 A). Collectively, these findings demonstrate that CK2 has the potential to inhibit caspase action at both the level of caspase activation and cleavage of downstream substrates. Furthermore, these findings raise the prospect that the higher (ie. pathological) levels of CK2 that are observed in cancer cells could result in the pathological rewiring of caspase pathways to

promote cell survival. Interestingly, further characterization of the relationship between CK2 and caspases revealed intriguing isoform specificity. In this respect, caspase-3 appears to be preferentially phosphorylated by CK2α' rather than CK2α despite the fact that these two isoforms of CK2 have very similar enzymatic characteristics (33). Furthermore, CK2β attenuated phosphorylation suggesting that misregulation of CK2 subunits in cells could be an additional mechanism to affect the regulation of apoptosis (24). The capacity of CK2 to promote cancer cell survival *in vitro* was also revealed in a recent large scale screen utilizing RNAi knockdown and cDNA overexpression of kinases in DLD-1 colorectal adenocarconima cells where overexpression of CK2α promoted resistance to TRAIL as determined by flow-cytometry utilizing antibodies against cleaved PARP and cleaved caspase-3 (34). Overall, while CK2 is only one of many constituents that intersect caspase pathways, its ability to modulate caspase action through phosphorylation of caspase substrates (potentially including caspases themselves) represents one potential mechanism by which CK2 might be exploited to neutralize cancer cell survival.
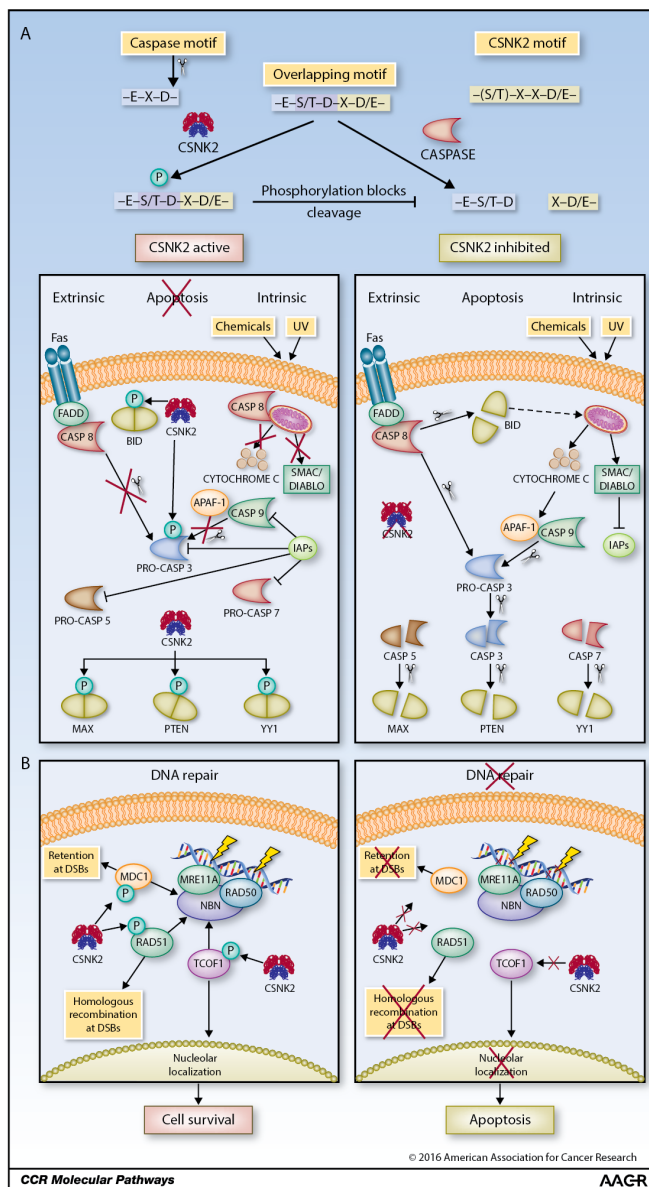
Figure 1.2 CK2 in the Control of Cell Survival and Response to DNA Damage
A) On the basis of the remarkable similarity of the consensus recognition motifs for phosphorylation by CK2 (S/T-D-X-X-D/E) and cleavage by caspases (E-X-D), it is evident that there are many cellular proteins where CSNK2 phosphorylation could occur adjacent to caspase cleavage sites to block their cleavage by caspases (27). B) Proteins shown here are involved in DNA damage repair, which requires phosphorylation by CK2 to execute respective DNA repair processes. A recurring theme with the illustrated proteins (i.e., MDC1, RAD51, and TCOF1) is the ability of CK2 to promote phosphorylation-dependent interactions with the FHA domain of the NBN component of the MRN complex (28-32). Reproduced with permission from AACR.

1.4   CK2 and DNA Damage Response & Repair Pathways

Another manner in which CK2 may contribute to the regulation of cancer cell survival that might be exploited for intervention is through its involvement in DNA damage response (DDR) and DNA repair pathways (Figure 1.2 B). In this respect, recent large-scale phosphoproteomic analyses of G361 melanoma cells and GM00130 B lymphocyte cells treated with the radiomimetric drug neocarzinostatin or with ionizing radiation to induce DNA double-stranded breaks (DSBs) respectively, demonstrated a dynamic response in motifs preferential for CK2 phosphorylation in many proteins. These results reveal a previously under-appreciated role for CK2 as an important mediator in the cellular response to DSBs (35, 36). Other indications that CK2 is involved in DDR and DNA repair pathways include the demonstration that CK2α localizes to perinuclear structures whereas CK2α' becomes nuclear in response to DSBs caused by ionizing radiation (37). Some of the putative CK2 substrates that are involved in DDR are scaffold proteins such as mediator of DNA damage checkpoint 1 (MDC1), where phosphorylation of serine-aspartate-threonine repeats regulates retention of the MRE11A-RAD50-NBN (MRN) complex at DSBs through interactions with Forkhead-associated (FHA) domains in the NBN (Nijmegen breakage syndrome protein 1) component of the MRN complex (28, 29). Another critical interaction for NBN is co-localization to the nucleolus which is dependent on the phosphorylation of TCOF1 by CK2 at threonine 210, independent of MRE11A (30, 31). In terms of regulating processes tasked with repairing damaged DNA, the phosphorylation of XRCC1 by CK2 is required for single-strand break repair (38) and phosphorylation of XRCC4 is necessary for non-homologous end joining repair (39). In homologous recombination, phosphorylation of RAD51 by PLK1 at serine 14 primes the phosphorylation of threonine 13 by CK2, regulating

binding to the NBN component of the MRN complex and facilitating recruitment of RAD51 to damaged DNA (32). In another recent study, it was determined that the phosphorylation of a deubiquitylase OTUB1 by CK2 is necessary for its nuclear accumulation in order to promote the formation of TP53BP1 repair foci at DSBs (40). While there are undoubtedly many details regarding its roles in DDR and DNA repair pathways that remain to be elucidated, these examples demonstrate that CK2 may have an important role in several discrete aspects of these processes. A recurring theme that is highlighted by these examples is that phosphorylation by CK2 promotes phosphorylation-dependent interactions such as those involving the FHA domain of the NBN component of the MRN complex. Overall, the widespread involvement in these processes could be relevant to the development of strategies that neutralize the advantages or exploit the unique vulnerabilities of cancer cells.

1.5   Protein Kinase CK2 Inhibitors

As CK2 is implicated in a number of fundamental biological processes, and found at varying levels of deregulation in human cancers, there has been widespread interest in targeting this kinase therapeutically (10, 14). While there are many inhibitors described in the literature (41, 42), the following sections focus on the use of CX-4945.

1.5.1   CX-4945: an ATP-competitive CK2 Inhibitor in Clinical Trial

CX-4945 was developed by Cylene Pharmaceuticals Inc. and is a potent and selective ATP-competitive inhibitor (K_i = 0.38 nM for CK2α and CK2α' with an IC$_{50}$ of 1 nM) with no extensive inhibitory activity detected against a panel of 238 kinases (43, 44). Characterization of its *in vitro* effects revealed varying degrees of activation of caspase 3 and caspase 7 in cancer cells with no detectable change of caspase 3/7 activity in normal cells (44). Interestingly, CX-4945 elicited differential effects on the cell cycle with BT-474 breast

cancer cells arresting in G2/M transition and BxPC-3 prostate cancer cells arresting in G1 (44). *In vitro* studies employing CX-4945 in combination with gemcitabine or cisplatin revealed enhanced anti-proliferative effects in A2780 and SKOV-3 ovarian cancer cells. Anti-proliferative activity was 23-38% higher based on a Bliss Independence model when CX-4945 was added to cells after treatment with gemcitabine or cisplatin. These treatments were also accompanied by decreased phosphorylation of the CK2 substrates XRCC1 and MDC1 and accumulation of single-stranded and double-stranded DNA breaks (45). These data are in agreement with the observations of CK2 localizing to the nucleus in response to double-stranded breaks and for the role of CK2 in the DDR and DNA repair mechanisms (37, 38, 46, 47). Currently CX-4945 is in Phase I/II clinical trial in the U.S., South Korea and Taiwan for the treatment of cholangiocarcinoma (bile duct cancer) in combination with gemcitabine and cisplatin (ClinicalTrials.gov Identifier NCT02128282). The aim of this trial is to determine its maximum tolerable dose in patients followed by a randomized Phase II assessment using CX-4945 in combination with gemcitabine and cisplatin versus the standard of care.

1.5.2   Emerging Prospects for Combinatorial Treatments Involving CK2 Inhibition

CX-4945 has been used in combination with other agents and has shown promise for targeting a number of malignancies. For example, CX-4945 has been studied *in vitro* in combination with DNA-damaging agents such as in acute myeloid leukemia cell lines and patient-derived leukemia cells (48). In another study of hematological malignancies, CX-4945 demonstrated a significant decrease in cell viability of patient-derived chronic lymphocytic leukemia (CLL) cell lines *in vitro* (49). When CX-4945 was combined with GS-1101 (PI3KD inhibitor), ibrutinib (BTK inhibitor), or fludarabine, synergistic responses were

observed in CLL cell lines that were not observed in the unpaired treatments with combination indices (using the Chou-Talalay method) of 0.46, 0.56 and 0.30 for CX-4945 and GS-1101, ibrutinib and fludarabine, respectively. Combinations of CX-4945 and bortezomib using patient-derived cells from multiple myeloma and mantle cell lymphoma also demonstrated enhanced mitochondria dependent apoptosis associated with suppression of NFKB1 and STAT3 target genes leading to 50% reduction of *NOS2* and *BCL2* gene expression (50). In other *in vitro* cell models of cancer such as A431 epidermal carcinoma cells and H2170 lung cancer cells, combining erlotinib and CX-4945 resulted in suppression of Akt1 phosphorylation in addition to down-regulation of phosphorylation sites on Akt1 and mTOR substrates (51). Combined treatment resulted in 3-fold increases in apoptosis as determined by caspase-3 and caspase-7 activity assays in comparison to treatment by CX-4945 or erlotinib alone. This enhanced anti-proliferative effect was also demonstrated in mouse xenograft models with the greatest reduction in tumor volume resulting from combined treatment in both A431 and H2170 xenograft mice (51).

Since resistance is commonly observed with both chemotherapy and targeted therapy involving kinase inhibitors, inhibition of CK2 has also been explored as a strategy for overcoming both *de novo* resistance and acquired resistance. Analysis of several multidrug-resistant cell lines revealed that CX-4945 sensitized cells to vinblastine and doxorubicin, resulting in reduction of cell viability by 50% when treating with vinblastine and a two-fold increase in doxorubicin accumulation in resistant cells (52). These results indicate that CK2 inhibition may have utility for over-coming *de novo* resistance.

There is also mounting evidence to suggest that CK2 inhibition may be effective to combat adaptive resistance. Investigation of imatinib-resistant chronic myeloid leukemia cell

lines revealed two-fold higher protein and activity levels of CK2, along with increased localization of CK2α and CK2β to the cytoplasm of imatinib-resistance cells in comparison to imatinib-sensitive cells (53). Interestingly, treatment with CX-4945 abrogated CK2α and Bcr-Abl interaction as determined by co-immunoprecipitation and glycerol gradient sedimentation leading to the induction of apoptosis in resistant cell lines at concentrations that failed to promote PARP cleavage in imatinib-sensitive CML. Furthermore, treatment of imatinib-resistant CML cells with CX-4945 or siRNA targeting CK2α promoted higher sensitivity to lower concentrations of imatinib, suggesting that the kinome had adapted in response to Bcr-Abl inhibition by imatinib leading to increased dependence on CK2 activity (53). In an *in vitro* cell model of T-cell acute lymphoblastic leukemia, CX-4945 downregulated the unfolded protein response as determined by HSPA5 expression and caused increased ERN1, phosphorylated EIF2S1, and DDIT3 indicating ER stress. When paired with thapsigargin or temsirolimus the synergistic cytotoxicity was further potentiated in these cell based assays (54). More recently, analysis of acquired resistance in triple negative breast cancer using SUM149 and SUM159 cell lines revealed that resistance to the BET bromodomain inhibitor JQ1 was associated with increased binding of BRD4 to MED1 in a bromodomain-independent manner, and dependent on BRD4 phosphorylation by CK2α, which keeps transcriptional regulation of genes promoting cellular proliferation active (55). Utilization of CK2 inhibitor or protein phosphatase PP2A activators such as perphenazine decreased phosphorylation of BRD4, suggesting a rationale combination for tackling BET bromodomain inhibitor resistance in triple negative breast cancer. Collectively, these observations raise the prospect that CK2 inhibitors could be utilized to enhance the effectiveness of other interventions.

1.6   Mass Spectrometry-Based Proteomics

The study of the protein-encoded complement of the genome on a global scale is referred to as proteomics. This analysis also includes the corresponding factors that can regulate protein function, such as posttranslational modifications and abundance. Mass spectrometry-based proteomics takes advantage of the ability to acquire high quality spectra of analyte derived from protein sources in complex samples such as human cells or tissue (56). This analysis can be accomplished rapidly with current mass spectrometry instrumentation enabling the identification of thousands of proteins in a limited amount of time (57). The most common form of mass spectrometry-based proteomics is the "bottom up" approach, where proteins are digested by proteases resulting in short peptides that are then analyzed (Figure 1.3). Peptides are delivered to the mass spectrometer using micro or nano-scale high-performance liquid chromatography columns. Peptides injected onto the column are eluted using an increasing gradient of organic solvent which separates the peptides on the basis of hydrophobicity when using stationary matrices such as reversed-phase C18 material. The eluted peptides are then ionized at the point of entry to the mass spectrometer by the application of electric potential across an emitter needle, using a process called electrospray ionization (58). The ionized peptides are measured on the basis of their mass-to-charge (m/z) ratio. In data-dependent analysis, peptide ions are detected and analyzed typically in two stages. In the first stage (MS1), the mass analyzer performs a survey scan selecting specific precursor ions, usually on the basis of abundance. These selected precursor ions are then fragmented in a collision cell and detected in a second mass analyzer (MS2). A commonly used fragmentation mode, collision-induced dissociation (CID), creates ion fragments through collisions with inert gas molecules, generating ions that originate from the amino terminus (b ions) and carboxy

terminus (y ions). The basis of peptide sequence identification results from the calculation of the differences in mass observed between fragment ions, which can represent an amino acid (59). The assigned precursor and fragment masses can then be searched against a database to identify the sequence and can be statistically validated using decoy search strategies to estimate the rate of false positive identification (reviewed in (60, 61)). A complete review of the mass spectrometry instrumentation and technology used to generate data presented in this thesis is beyond the scope of this thesis and can be found in (62-64).

1.7   Quantitative Proteomics

Quantitative proteomic strategies can be employed to better understand the context of the biological system being analyzed. This approach moves away from simply identifying a protein of interest using mass spectrometry towards an approach that enables characterization of dynamic features of the protein or system of interest. Quantitative strategies can be applied at the protein or peptide level. Labeling techniques such as isobaric tags for relative and absolute quantitation (iTRAQ) (65), tandem mass tags (TMTs) (66), or dimethyl labeling (67) are performed at the peptide level. This results in peptides that can be distinguished in a mass spectrometer between different conditions or treatments. A commonly used approach involves labeling at the protein level *in vivo* in the system of interest. Stable isotopic labeling of amino acids in cell culture (SILAC) involves the metabolic labeling of amino acids containing ^{13}C or ^{15}N into the proteome of a cell (68, 69). By using arginine and lysine amino acids that are labeled with "heavy" ^{13}C or ^{15}N isotopes and a protease such as trypsin that cleaves after the c-terminus of arginine and lysine residues, one can obtain a sample where theoretically all peptides are labeled (Figure 1.4). SILAC-labeled samples are mixed at a 1:1 ratio at the protein level prior to sample digestion and handling. This ensures that samples

that were differentially treated within the biological context of interest undergo the same handling steps and minimizes the likelihood of sample loss in one label versus the other. Peptides from SILAC samples elute at the same time during chromatographic analysis, and are distinguishable due to the difference in mass introduced by the presence of "heavy" amino acid. The abundance of a peptide can then be determined by relative quantitation. MaxQuant, a freely available mass spectra data analysis software can detect the three-dimensional characteristics of a SILAC pair in MS1 using m/z, signal intensity and elution time, enabling the accurate identification and quantitation of thousands of peptides detected in an LC-MS/MS acquisition (70, 71).
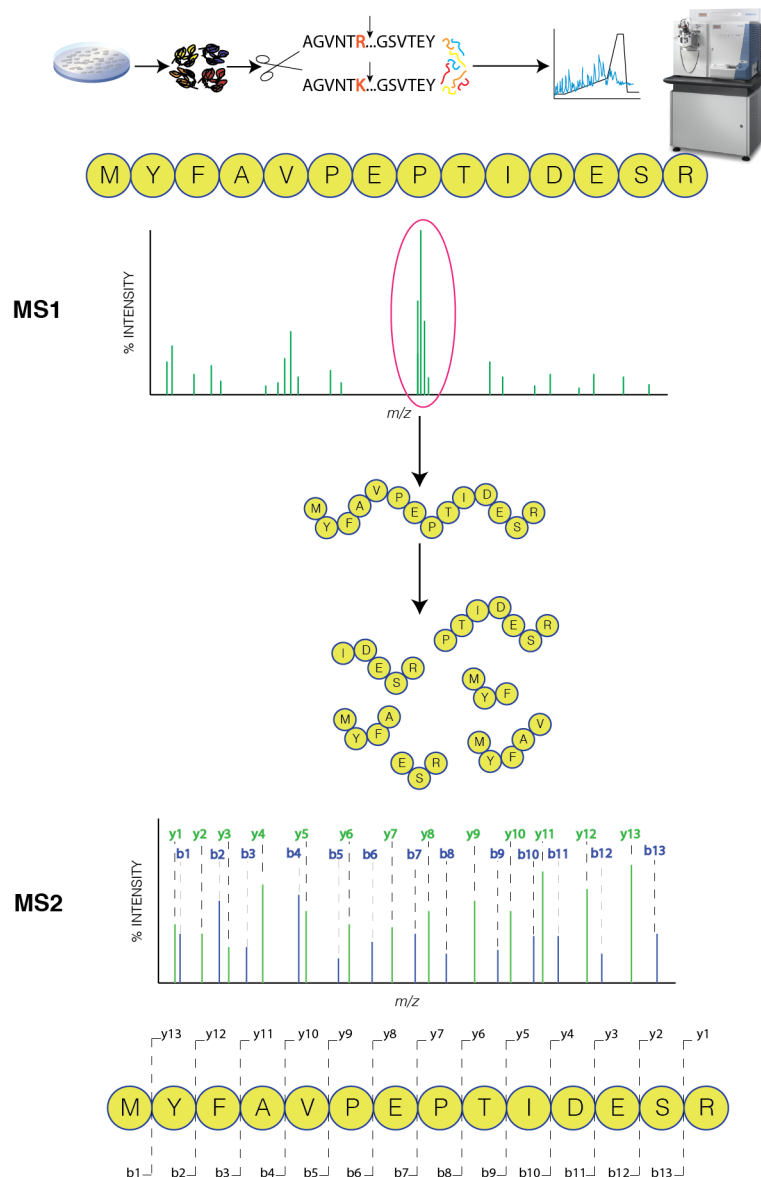
Figure 1.3 Identification of Peptides Using Mass Spectrometry

Peptides generated from protein samples using proteases such as trypsin can be ionized using electrospray ionization and delivered into the mass spectrometer by liquid chromatography. Ions are selected on the basis of abundance in MS1 during data-dependent analysis, and fragmented for detection in MS2. CID fragmentation results in b and y ions. The difference in mass from the resulting fragments can be used to identify the amino acid sequence of the peptide.
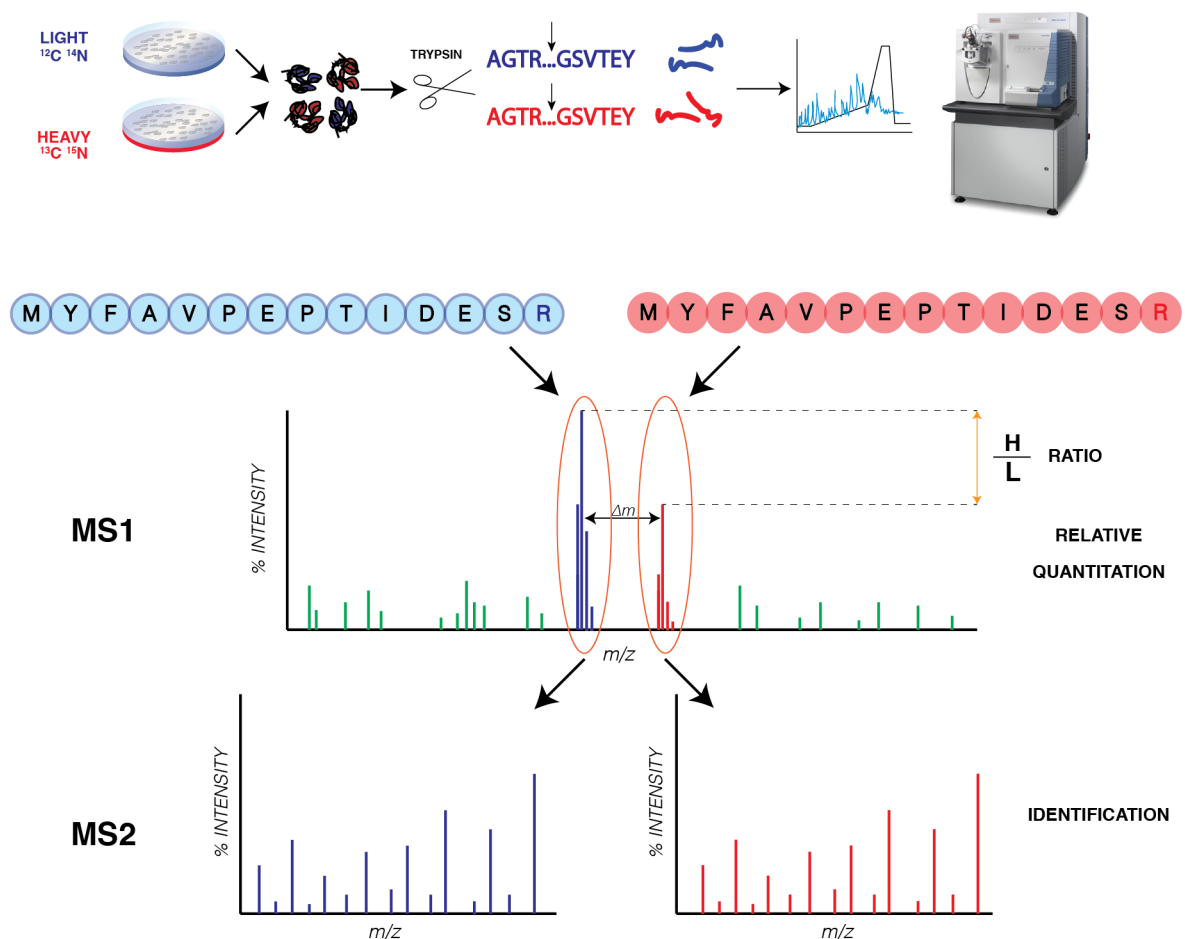
Figure 1.4 Quantitative Proteomics Using SILAC
SILAC enables the labeling of proteins in cellular systems using amino acids containing [13]C
and ^{15}N isotopes. When arginine and lysine amino acids are used as the source of metabolic
labeling, proteolytic cleavage using trypsin will result in a sample of peptides that are labeled
with a "heavy" amino acid at the carboxy-terminus. SILAC labeled peptide pairs will elute at
the same time during liquid chromatography separation, and will be distinguishable in the
mass spectrometer due to the labeled amino acid-specific mass shift. Relative quantitation is
achieved during MS1 where a ratio can be calculated based on the intensity of each peptide
ion peak. Detection of peptide ion fragments in MS2 ensures appropriate sequence
identification.

1.8   Phosphoproteomics

Phosphorylation is a posttranslational modification which can be dynamically regulated through kinases and phosphatases. Quantitative phosphoproteomic strategies have been successfully employed to study signaling networks involved in cell cycle regulation (72) and the response to kinase inhibitors (73). Due to the nature of data-dependent acquisition where peptide ions are selected based on abundance, unphosphorylated peptides typically predominate the peptides selected for fragmentation and MS2 detection, therefore limiting the analysis of phosphopeptides (74). Consequently, phosphopeptide enrichment strategies are typically required to overcome this obstacle and enable detection of phosphopeptides. One commonly used enrichment strategy is metal oxide affinity chromatography using TiO_2, which captures phosphopeptides through the interaction of the phosphate anion in a "bridging-bidentate" mode with TiO_2 (75). The selectivity of enrichment is further enhanced by using acid modifiers such as lactic acid (76), during washes and incubation steps which prevent the binding of non-phosphorylated peptides through carboxylic groups. When coupled with a quantitative label such SILAC, the relative comparison of the abundance of a phosphopeptide can enable the quantitation of phosphorylated residues (referred to as phosphorylation sites) localized to that peptide. Bioinformatics approaches can then be employed to assign kinase-substrate relationships using linear motifs (77). A recent comprehensive review of phosphoproteomic strategies and workflows is described in (78).

1.9   Chemical Proteomic Approaches to Study the Kinome

In addition to the development of phosphoproteomic profiling to monitor the phosphorylation status of protein kinase substrates, complementary strategies have emerged to directly

monitor the kinome. The capture of kinases using chemical biology approaches was first demonstrated using adenosine-5'-(γ-4-aminophenyl)triphosphate-sepharose affinity chromatography to isolate MEK from rabbit skeletal muscle (79). This approach was further advanced using ATP-competitive inhibitors to identify targets of cyclin dependent kinase and glycogen synthase kinase-3, demonstrating the utility of this methodology to profile off-target effects of kinase inhibitors (80, 81). Studies expanding on the types of inhibitor resins available for chromatography have devised combinations of inhibitors that achieve broad capture and selective capture of kinases. These latter developments have enabled the identification of the broad impact of kinase inhibitors on the kinome and revealed target profiles of clinical stage inhibitors (82). Quantitative applications using SILAC labeling have also been used to monitor the changes in the phosphorylation status of the kinome during the cell cycle, identifying regulated phosphorylation sites on kinases that were previously uncharacterized in the regulation of the cell cycle (83). Building on this approach, optimization of the kinase inhibitor mix utilized by Daub *et al*. (83) led to the development of the Multiplexed Inhibitor Bead (MIB) protocol by Duncan *et al*. (84). MIBs have been used as a means to capture and infer the activity of hundreds of active kinases (ie. the active kinome) from cell extracts. With triple-negative breast cancer cells and mouse models, this approach revealed activation of receptor tyrosine kinases such as PDGFRβ and DDR1 in response to the MEK inhibitors selumetinib or trametinib, which in turn activated downstream kinases capable of activating the MAPK pathway through an alternative route to circumvent inhibition (84).

1.10 Rationale for Study

With recent advances in mass spectrometry-based proteomics and the increased sophistication of computational approaches, it is now possible to explore cellular responses to kinase inhibition on a proteome-wide scale. In addition to identification of direct targets of individual kinases within cells, phosphoproteomic studies are also revealing new relationships between different kinases or kinases-mediated pathways within the complex and intricate regulatory networks that orchestrate cellular processes. For example, in a thyroid cancer cell line harboring the BRAF V600E mutation, phosphoproteomic analysis following short-term treatment (15 or 30 minutes) with vemurafenib (PLX4032) or MEK inhibitor selumetinib (AZD6244) revealed increased phosphorylation of numerous sites. Interestingly approximately 50% of the up-regulated sites conformed to the CK2 consensus motif suggesting that CK2 activity is impacted by inhibition of MAPK signaling (85). Building on that observation, combination of CX-4945 with vemurafenib demonstrated a synergistic effect in reducing cell viability by 60% in V600E mutant thyroid cancer cells and in mutant melanoma cell lines. In another global phosphoproteomic study, CK2 phosphorylation sites had increased phosphorylation site stoichiometry in gefitinib-resistant PC9 lung cancer cells in comparison to gefitinib-sensitive cells, in addition to having higher phosphorylation stoichiometry than MAPK or EGFR regulated phosphorylation sites (86). Collectively, these large-scale phosphoproteomics studies imply that CK2 may have an important role in drug resistance mechanisms and offers new insights regarding pathways that may be regulated or influenced by CK2.

In this respect, applications of proteomic and phosphoproteomic strategies for profiling CK2 inhibitors would undoubtedly be invaluable in assessing the prospect of

resistance to CK2 inhibition and revealing the relationships of CK2 with other constituents of the regulatory kinase networks. Given the emergence of CX-4945 as a clinical-stage inhibitor, it has become widely used in the CK2 field to study cellular processes that CK2 is implicated in regulating. Therefore, an investigation into effect of CX-4945 on a global scale is warranted, and characterization of the effects of CX-4945 in an unbiased manner will highlight the CK2-dependent and independent effects in cells.

1.11 Thesis Objective

In chapter 2, development and optimization of a phosphoproteomics workflow was performed. We identified that the use of specific types of sorbents for sample preparation can impact the ability to enrich for phosphopeptides that match the CK2 consensus. We also compared workflows to evaluate the utility of using chromatographic separation to fractionate phosphopeptide mixtures prior to LC-MS/MS analysis and demonstrated that fractionation did not dramatically improve the detection of phosphopeptides and that omission of the chromatographic fractionation has the advantage of reduced sample handling and instrument time. The sample preparation protocol was further refined by comparing two different methods for proteolytic digestion of protein samples, with one method outperforming the other in the number of phosphorylation sites identified.

In chapter 3, we performed unbiased phosphoproteomic profiling of the effect of CX-4945 on HeLa cells using a quantitative SILAC strategy. This resulted in the identification of several dynamic markers of CK2 activity that displayed larger magnitudes of de-phosphorylation in comparison to a *bona fide* substrate, EIF2S2 Ser2 that has been previously utilized as a biomarker for CK2 activity. CK2 phosphorylation sites were located on several proteins involved in DNA repair and translation, highlighting the importance of

CK2 in regulating these processes. Overall, interrogation of the phosphoproteome revealed a broad impact on several kinases when kinase-substrate enrichment analysis was performed, suggestive of both CK2-dependent and CK2-independent effects of CX-4945 in cells.

In chapter 4, we performed MIB profiling of the kinome in HeLa cells to corroborate the phosphoproteomic data. This resulted in the identification of kinases downstream of PI3K/Akt/mTOR pathway that are down regulated by CX-4945 treatment, and the demonstration that the ERK MAPK pathway is activated following CX-4945 treatment. Further studies were performed with an unrelated inhibitor of CK2, "Inhibitor VIII," (Figure 1.5). These studies revealed that CX-4945 and Inhibitor VIII have some overlapping effects but also putative divergent functions. In this respect, treatment with either CK2 inhibitor resulted in activation of ERK whereas inhibition of the mTOR pathway was exclusively observed with CX-4945. Additional characterization using flow cytometry and western blotting revealed differential effects of these two inhibitors in cells, raising speculation about the mechanism of action in cells.

Taken together, the proteomic characterization of cells treated with CX-4945 has identified dynamic markers of CK2 activity and also revealed the broad impact of CX-4945 on the phosphoproteome which suggests that CK2 is intricately involved in regulatory kinase networks and that CX-4945 may also elicit CK2-independent effects in cells.
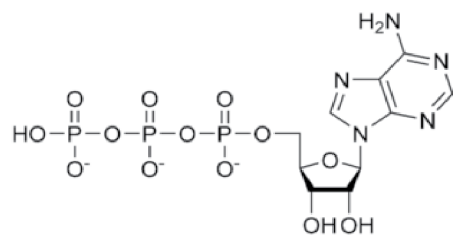
ATP
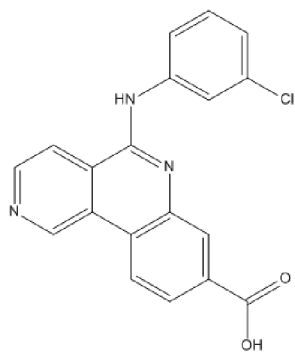
CX-4945
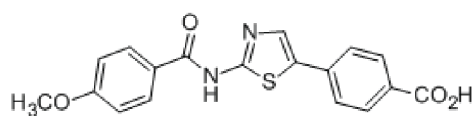
Inhibitor VIII

Figure 1.5 Structures of ATP-competitive CK2 Inhibitors CX-4945 and Inhibitor VIII
CX-4945 (5-((3-chlorophenyl)amino)benzo[c][2,6]naphthyridine-8-carboxylic acid) is described in (43, 44). Inhibitor VIII (4-(2-(4-methoxybenzamido)thiazol-5-yl)benzoic acid) is described in (87).

2   Chapter 2 – Development of a Mass Spectrometry – Based Phosphoproteomics Workflow

2.1   Introduction

The phosphorylation of proteins by protein kinases is a critical post-translational modification required in the regulation of cellular homeostasis (88). Advances in mass spectrometry have enabled not only the identification of phosphorylation sites but the quantitative dynamics of this modification on a large scale (89). However, enrichment strategies are still required in order to detect phosphorylated peptides and different options exist such as immobilized metal ion affinity chromatography using iron (Fe^{3+}) (90) or metal oxide affinity chromatography using TiO_2 (91).

Protein kinase CK2 is involved in a multitude of cellular processes by virtue of the number of proteins that it can phosphorylate and is necessary for cell survival and proliferation (16). The specificity determinants of protein kinase CK2 dictate the phosphorylation of target protein substrates, with acidic residues such aspartic acid or glutamic acid in the n + 3 position (relative to the phospho-acceptor residue) serving as critical elements (92-95). Bioinformatic analyses have demonstrated that in addition to the n +3 position, CK2 substrates generally display large stretches of acidic residues rendering sequences hydrophilic in nature (15). Contemporary sample preparation methods in phosphoproteomic workflows require steps for desalting of peptides prior to phosphopeptide enrichment (96, 97). The use of reverse-phased columns for desalting can affect the recovery of hydrophilic peptides (98, 99). This poses a challenge for the detection of phosphorylated peptides that are putative substrates of CK2. Therefore, the investigation of different solid phase extraction (SPE) columns for peptide desalting was undertaken to determine if phosphorylated

hydrophilic peptides containing a CK2 consensus sequence could be retained and later detected by LC-MS/MS. A comparison of porous graphitic carbon (PGC) and octadecyl carbon chain (C18) SPE columns was undertaken in combination with a strong cation exchange chromatography (SCX) fractionation workflow (Figure 2.1). This resulted in the generation of four datasets: phosphopeptides from samples fractionated using SCX and without fractionation, respectively desalted by PGC and C18 SPE columns. Integrating a combined PGC and C18 SPE desalting step, the phosphoproteomic workflow was further developed by comparing the preparation of protein lysates using Filter Aided Sample Preparation (FASP) or protein precipitation (PP) prior to phosphopeptide enrichment. This enabled the evaluation of the respective protein preparation methods and their respective effect in identifying phosphorylation sites and protein groups reproducibly.
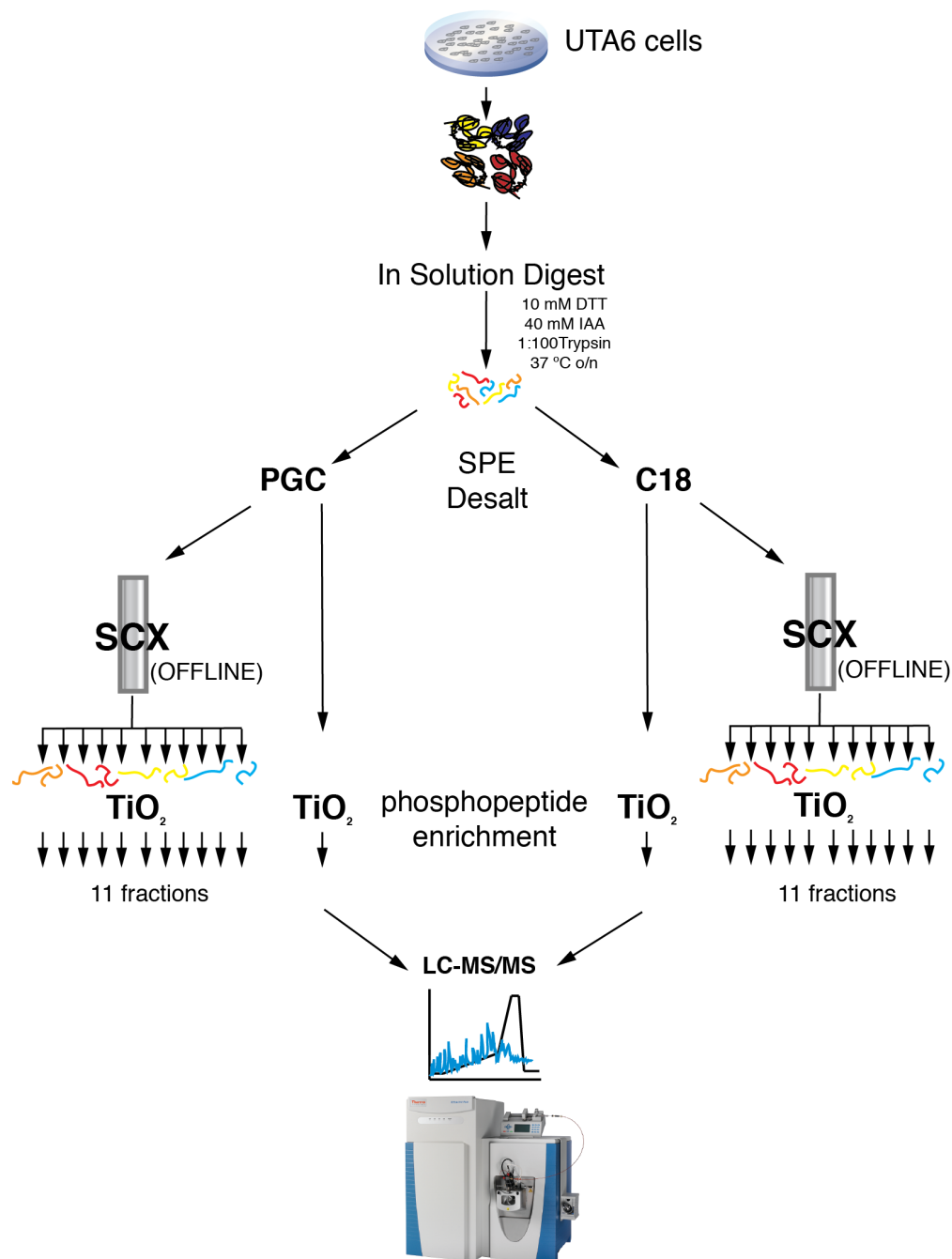
Figure 2.1 Schematic for Comparison of Phosphopeptide Enrichment Workflows.
Lysate from UTA6 cells was digested in-solution with trypsin and desalted with PGC or C18
SPE columns. 75% of peptides were fractionated by SCX chromatography prior to
phosphopeptide enrichment with TiO_2 and 25% were directly enriched for phosphopeptides
using TiO_2. All samples were analyzed by LC-MS/MS using a QExactive mass spectrometer
operated in data-dependent acquisition mode and resulting raw spectra were analyzed in
PEAKS 7.0.

2.2   Results

2.2.1   Evaluation of PGC and C18 SPE for Phosphopeptide Identification

A comparative analysis of phosphopeptides derived from peptide mixtures that were desalted by PGC or C18 SPE columns was performed to investigate the utility of fractionation for a phosphoproteomics workflow. Analysis of unique variants of phosphopeptides in PEAKS software (non-unique amino acid sequences, but unique patterns of variable modifications) that were detected by LC-MS/MS revealed distinct but overlapping sets of phosphopeptide identification between PGC and C18 SPE desalted samples (Figure 2.2). PGC SCX-TiO_2 yielded more phosphopeptides than C18 SCX-TiO_2, identifying a total of 3118 phosphopeptides of which 338 were shared by the C18 SCX-TiO_2 method that in total only yielded 678 phosphopeptides. When comparing the respective SPE sorbents with or without SCX fractionation, both the PGC and C18 methods without fractionation outperformed the SCX-fractionation method in terms of phosphopeptide yield. C18 TiO_2 yielded 4,402 phosphopeptides identified, exceeding that of PGC TiO_2 that identified 3,842 phosphopeptides, with 1,560 phosphopeptides shared between the two methods. Considering the increased yield of phosphopeptides from workflows without SCX fractionation and the increased complexity of the SCX-fractionation workflows that require multiple desalting steps in contrast to the single step desalt with the unfractionated samples, we focused the comparison of phosphopeptides from unfractionated samples desalted with PGC and C18.

2.2.2   Comparison of Phosphorylation Motifs Obtained from PGC and C18 SPE

To compare the utility of PGC and C18 SPE columns for desalting tryptic digests prior to phosphopeptide enrichment for the identification of hydrophilic phosphopeptides that could be putative phosphorylation sites by CK2, we analyzed the phosphopeptides obtained from the phosphoproteomic workflows using a bioinformatics tool, *motif-x* (100, 101). Statistically significant over-represented motifs from modified serine residues were identified in each of the samples (Figure 2.3). Both SPE columns retained phosphopeptides that were enriched for phosphorylation motifs containing proline in the n +1 with comparable performance based on the fold increase. However, the PGC SPE column exhibited the best performance in the identification of acidic motifs reminiscent of the specificity determinants of CK2 with two motifs matching the CK2 consensus sequence being enriched 61.87-fold and 49.47-fold over the background frequency of serine residues in the human proteome. This result demonstrates the utility of a different sorbent to achieve desalting prior to phosphopeptide enrichment as opposed to a silica-based C18 reverse-phase material for the purposes of identifying phosphopeptides that display the specificity determinants for phosphorylation by CK2.
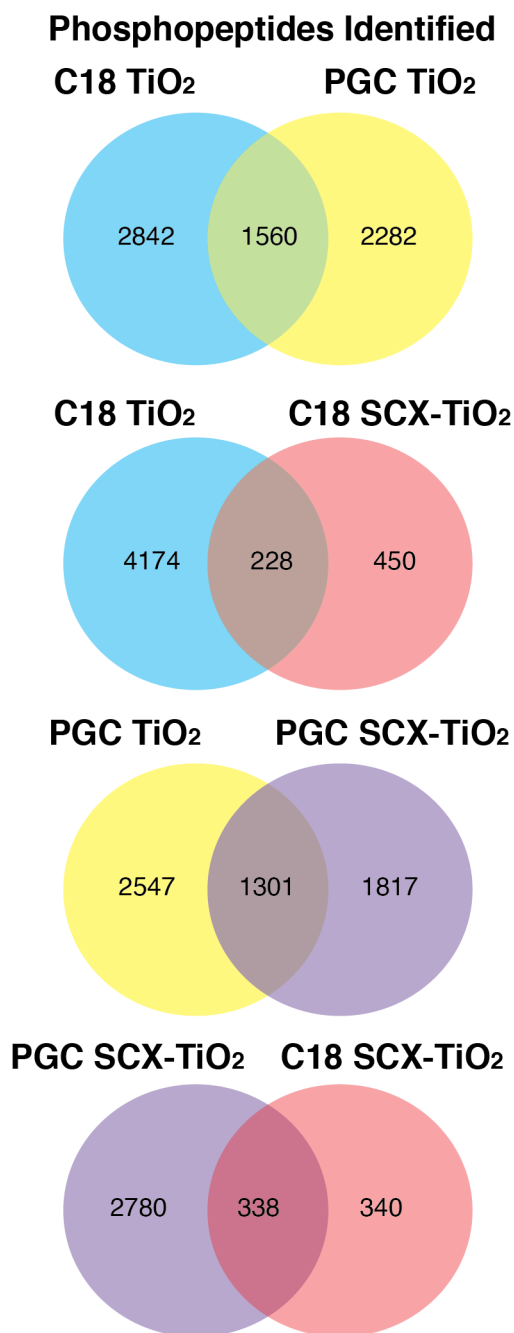
Figure 2.2 Comparative Analysis of Phosphopeptides Identified Using Different Sample Preparation Workflows

Phosphopeptides enriched from SCX-fractionated and unfractionated samples using TiO_2 were analyzed by LC-MS/MS and searched in PEAKS 7.0. Phosphopeptide variants (unique modification pattern) were considered for comparison between SCX-fractionated and unfractionated samples that were desalted with PGC or C18 SPE columns.
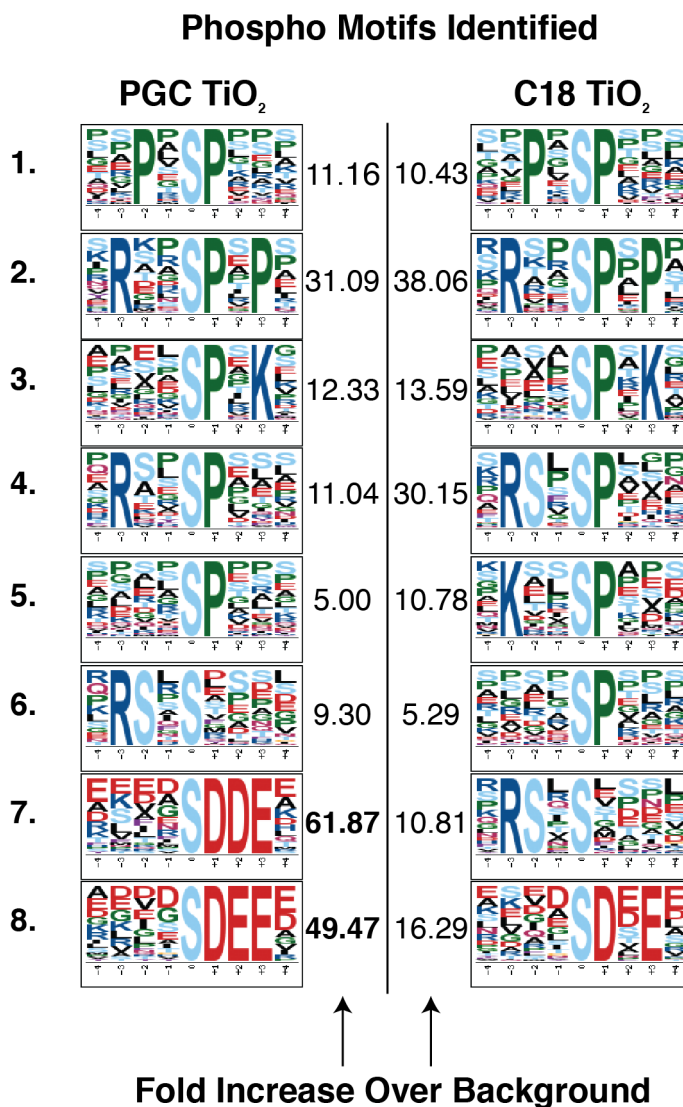
Figure 2.3 Analysis of Phosphoserine-containing Phosphopeptides with *motif-x*
Phosphorylated peptides from unfractionated samples desalted with PGC and C18 SPE columns were analyzed using *motif-x*. Linear motifs were searched with a minimum number of 20 occurrences and a 9 residue window (plus/minus 4 residues from the modified serine) with a default value of significance threshold set to 0.000001 searching against the International Protein Index human sequence database. The top 8 most abundant motifs are listed in descending order based on foreground size (number of phosphopeptides matching the motif) with respective fold increase values over the background frequency of serine residues.

2.2.3   Evaluation of FASP and PP Methods to Prepare Samples for Phosphopeptide Enrichment

Building on the result that PGC exhibited increased performance in the identification of hydrophilic phosphopeptides that conformed to the consensus sequence of CK2, the investigation of the utility of two sample preparation methods that are widely used in the proteomics field for the preparation of proteomic samples was undertaken (Figure 2.4). This comparison was performed in order to determine if proteome sample preparation would affect phosphoproteome yield. Filter Aided Sample Preparation (FASP) uses a filtration concentrator (in this case with a molecular weight limit of 10,000 Da) to exchange buffers during the process of reduction, alkylation and proteolytic digestion. Digested peptides are then collected by spinning the concentrator in a centrifuge, resulting in removal of any undigested peptides or proteins that are retained by the membrane (102-104). Protein precipitation (PP) has been previously used in proteomics to remove non-compatible buffer components or detergents from protein extracts prior to proteolytic digestion (105). This strategy has also been adapted with the demonstration of the utility of on-pellet digestion using a protease rather than re-suspension in a denaturing solution (106). Our phosphopeptide enrichment protocol was also modified to include double incubations with TiO_2 based on literature reports of increased identification of phosphorylation sites using this strategy (107). Furthermore, we followed the protocol from Kettenbach et al. (108), for enrichment from unfractionated samples that employed the use of bulk TiO_2 beads as a substitute for the enrichment step in a spin-tip format.
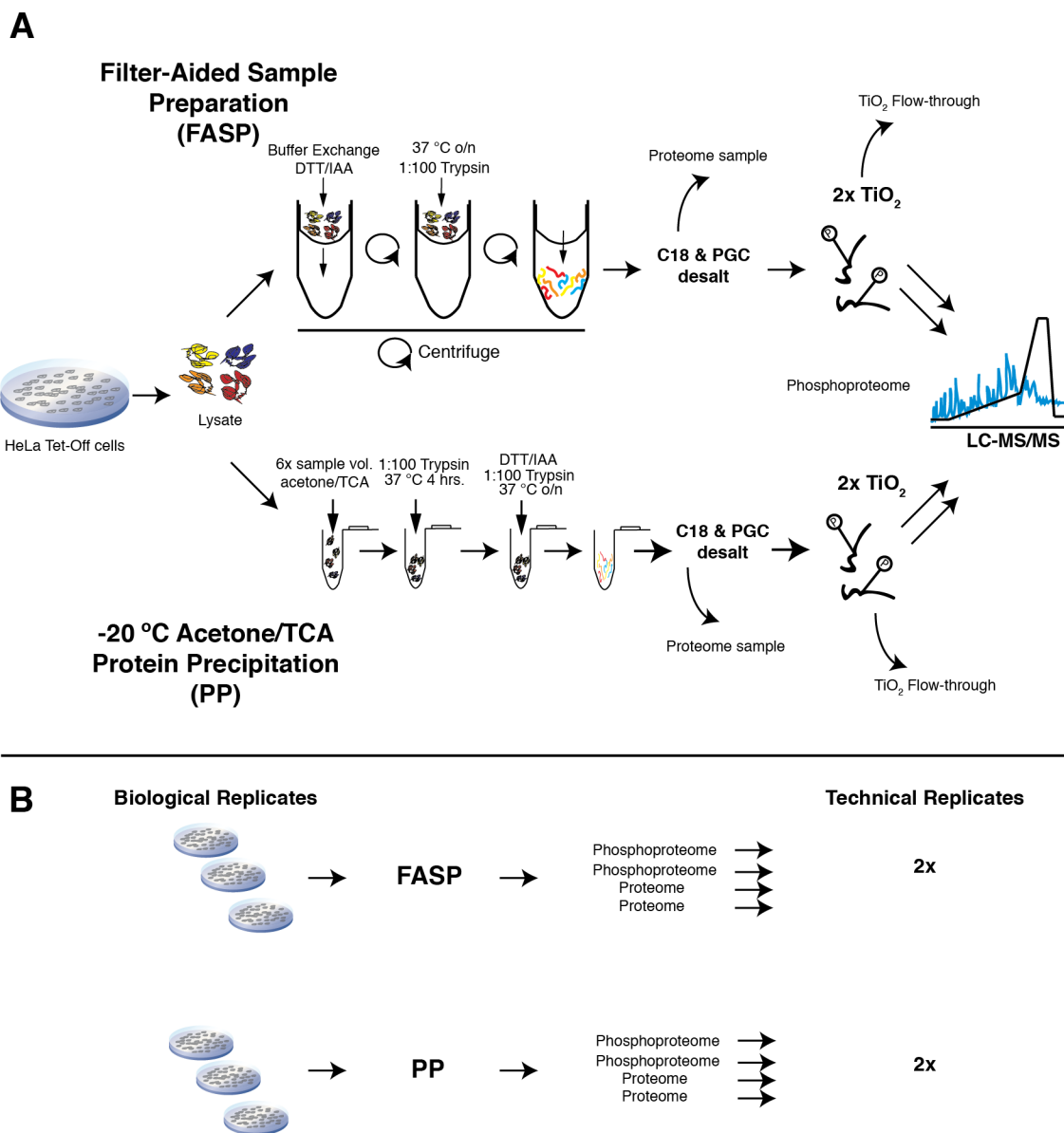
Figure 2.4 Schematic for Comparative Analysis of FASP and PP Workflows
(A) Protein lysate from HeLa Tet-Off cells was divided equally into two fractions and processed using FASP or PP protocols. Proteome (2) and phosphoproteome (2) samples were collected using both workflows and analyzed by LC-MS/MS using a Orbitrap Elite mass spectrometer. (B) Overview of samples analysis. Each workflow was performed with samples from 3 biological replicates that were each processed and analyzed in technical duplicate. All acquired spectra were analyzed in MaxQuant v1.5.3.8.

Taken together, the two methods identified a total of 6,153 phosphorylation sites with a localization score greater than 0.75 (a maximum score is 1.00), with 63% overlap in terms of the sites identified in at least one biological replicate from each of the workflows (Figure 2.5 A). A phosphorylation site is defined as an identified amino acid residue that is occupied by a phosphate and can be identified from multiple phosphopeptides. Notably, twice as many phosphorylation sites were exclusively identified using PP. The number of phosphorylation sites identified in all three biological replicates using FASP and PP were 2,511 and 3,111 respectively (Figure 2.5 B). The percentage of biological replicates where the same site was identified in independent LC-MS/MS acquisitions ranged from 41.4 – 48.9% for both methods. (Figure 2.5 C). Slightly more than 50% of the identified phosphorylation sites were present in all three biological replicates when using each method (Figure 2.5 D). In terms of the identification of protein groups using FASP and PP, both methods achieved similar yields in terms of the total number of protein groups identified in at least one biological replicate (Figure 2.5 A). A protein group is defined as a collection of proteins that cannot be individually distinguished based on the identified peptides, such as in the case of protein isoforms. Both methods identified slightly over 5,000 protein groups in all three biological replicates (Figure 2.5 B). The replicable identification of protein groups was much higher in contrast to phosphorylation site identification, with approximately 90% of protein groups being identified in both technical LC-MS/MS analyses (Figure 2.5 C), and approximately 92% of protein groups identified in all three biological replicates (Figure 2.5 D). In summary, the use of protein precipitation in preparing samples for proteomic analysis is advantageous given the increased number of phosphorylation sites yielded and the reduction in the number of sample handling steps.

Phosphorylation Sites | Protein Groups

A

Phosphorylation Sites: FASP 737, overlap 3881, PP 1535

Protein Groups: FASP 232, overlap 5262, PP 225

B

# SITES (P loc. > 0.75)		
(# with > 1/3) BIOLOGICAL REPLICATES	FASP	4618
	PP	5416
(# with 3/3) BIOLOGICAL REPLICATES	FASP	2511
	PP	3111

# PROTEIN GROUPS		
(# with > 1/3) BIOLOGICAL REPLICATES	FASP	5494
	PP	5487
(# with 3/3) BIOLOGICAL REPLICATES	FASP	5093
	PP	5079

C

REPLICABILITY		1	2	3
(% with 2/2) TECH. REPLICATES	FASP	41.4	48.9	42.8
	PP	47.4	45.7	48.8

REPLICABILITY		1	2	3
(% with 2/2) TECH. REPLICATES	FASP	90.7	91.8	86.9
	PP	88.3	87.5	89.3

D

(% with 3/3) BIOLOGICAL REPLICATES	FASP	54.3
	PP	57.4

(% with 3/3) BIOLOGICAL REPLICATES	FASP	92.7
	PP	92.5

Figure 2.5 Comparison of FASP and PP Workflows for Phosphoproteomics
FASP and PP workflows were compared on the basis of identification of phosphorylation sites and protein groups. Phosphorylation sites were considered when P localization > 0.75. (A) Comparison of sites and protein groups identified in at least one biological replicate. (B) Number of sites and protein groups identified in at least one biological replicate and number of sites and protein groups identified in all biological replicates. (C) Technical replicability of identified sites and protein groups in the same biological replicate. (D) Percentage of phosphorylation sites and protein groups that were identified in all three biological replicates.

2.3   Discussion

The specificity determinants of CK2 substrates can render stretches of amino acid sequences on a protein hydrophilic (15). In order to implement a phosphoproteomics workflow capable of identifying phosphopeptides derived from CK2 substrates, we compared solid phase extraction adsorbents for sample preparation and desalting in combination with testing SCX-fractionation prior to phosphopeptide enrichment.

The use of SCX-fractionation appeared to be of limited utility considering the lower yield of phosphopeptides identified when either C18 or PGC SPE columns were used for desalting steps in comparison to samples that were not fractionated. Furthermore, considering the amount of LC-MS/MS time required to analyze 11 SCX fractions (1100 minutes) in comparison to 300 minutes for an unfractionated sample, the return on phosphopeptide identification with limited sample handling and reduction of desalting steps renders the unfractionated "shotgun" approach considerably more advantageous. The requirement for desalting after SCX-fractionation may contribute to the lower yield of phosphopeptides. To some degree, our results contrast a previous study. In this respect, the utility of SCX-fractionation has been investigated previously in the application of phosphoproteomics (108) where it was demonstrated that fractionation into 24 samples in comparison to an unfractionated sample yielded a comparable number of unique phosphorylation sites. In an SCX gradient, peptides with lower net charge elute earlier, with multiply-charged species eluting later. Multiply-phosphorylated peptides will have a net charge less than zero and will elute in the earliest fractions collected. Peptides generated with trypsin will have a net charge of +2 at pH 2.7 (in the case of no missed cleavages) when accounting for the N-terminus and C terminal arginine or lysine sidechain group, so a singly phosphorylated peptide will have a

net charge of +1 (109). SCX fractionation may enable the separation of phosphopeptides from non-phosphopeptides but this approach does not drastically outperform the unfractionated approach in terms of phosphopeptides identified.

The utility of PGC SPE columns in desalting digested peptides was demonstrated in the analysis of phosphorylation motifs identified using *motif-x* from unfractionated samples. Although more phosphopeptides were identified using the C18 SPE columns, the identification of phosphorylation motifs reminiscent of the specificity determinants of protein kinase CK2 from porous graphitic carbon SPE columns was more prevalent when analyzing the enrichment of phosphorylation motifs against a background of the human proteome. The ability to enrich phosphopeptides matching the specificity determinants of protein kinase CK2 using PGC is advantageous. Previous reports using graphite and porous graphitic carbon as desalting adsorbents prior to LC-MS/MS analysis have also highlighted the utility of this sorbent in phosphoproteomics (98, 99, 110).

The comparison of FASP and PP as methods to prepare proteomic and phosphoproteomic samples for LC-MS/MS analysis highlighted similar yields in protein group identification across all biological replicates that were processed. Furthermore, there was similar technical replicability in terms of protein group identification from LC-MS/MS run to run. Given that several unique peptides can identify a protein, the identification of protein groups using a data-dependent acquisition method does not suffer the same constraints that phosphorylation site identification does. Few phosphopeptides can contribute to the identification of a phosphorylation site. This is reflective of the stochastic nature of data-dependent acquisition and the identification of a labile post-translational modification within the constraint of a minimum localization score of 0.75. This issue in data-dependent

phosphoproteomics has been identified previously and one alternative to improve future analyses within the context of this project would be targeted acquisition of precursor ion although this precedes the discovery proteomics stage. Applications of targeted phosphoproteomics have increased the identification of phosphosites in technical replicates up to 88% (111). Compared to FASP, the protein precipitation (PP) approach yielded approximately 24% more phosphosite identifications with the same amount of input material, suggesting a better recovery of phosphorylated proteins when precipitating in comparison to retention using centrifuge spin concentrators. FASP has been investigated by other groups in addition to the development of newer protocols with adjustments made to the types of buffers and detergents used for sample processing (112, 113) to increase sample recovery. In addition to protocol evolution, the integration of multiple enzyme digestion to generate a different pool of peptides has been incorporated (114) and warrants future investigation to identify optimal combinations of proteases which would serve in the identification of putative CK2 motifs on phosphopeptides.

The comparative analysis of sample preparation approaches prior to phosphopeptide enrichment revealed the advantage of using unfractionated protein samples in addition to the use of different adsorbent materials for peptide desalting. Considering the amount of instrument time that is logged using a fractionated strategy, the unfractionated approach is advantageous in the delivery of LC-MS/MS results in a timely manner. An unfractionated approach for phosphoproteome enrichment within this time constraint also enables the analysis of more time-points or cellular contexts. Future phosphoproteomic investigations will incorporate C18 and porous graphitic carbon in combination with protein precipitation in order to identify phosphopeptides conforming to the CK2 consensus sequence by LC-

MS/MS. In summary, these analyses establish a foundation upon which the development of a phosphoproteomic-workflow evolved in order to address the identification of putative CK2 substrates in future experiments.

2.4 Experimental Methods

2.4.1 Cell Culture

UTA6 cell line – U2-OS-derived UTA6 cells (a gift from Dr. Christoph Englert, Forschungszentrum Karlsruhe, Germany, as previously described in (115)) were cultured in Dulbecco's modified Eagle's medium (DMEM) containing 10% fetal bovine serum (FBS), penicillin (100 U/mL) and streptomycin (100 µg/mL) on 15 cm dishes. Cells were lifted off the dish with PBS-EDTA (), centrifuged at 200 x g, rinsed with phosphate-buffered saline (PBS), transferred to 1.5 ml micro-centrifuge tubes and snap frozen in liquid nitrogen before storage at -80 °C until further use.

HeLa Tet-Off cell line – HeLa Tet-Off cells (Clontech) were cultured in Dulbecco's modified Eagle's medium (DMEM) containing 10 % FBS, penicillin (100 U/mL) and streptomycin (100 µg/mL) on 15 cm dishes.

2.4.2 Cell Lysis

UTA6 cell line – Cell pellets were lysed on ice for 30 minutes with denaturing lysis buffer [1% octyl-β-D-glucopyranoside (Sigma-Aldrich), 100 mM ammonium bicarbonate (Fluka) pH 8.5, 6 M urea (Sigma-Aldrich), 10% acetonitrile (ACN) (Fisher Scientific), 1 mM β-glycerophosphate (Sigma-Aldrich), 1 µM okadaic acid (Bioshop), 25 mM sodium fluoride (Sigma-Alrich), 1 µM microcystin-LR (Cayman Chemical), pepstatin (10 µg/mL) (Sigma-Aldrich)]. Lysates were spun for 10 minutes at 16,000 x g at 4 °C, upon which the

supernatant was retained and protein concentration was determined using a Bradford assay (Bio-Rad).

HeLa Tet-Off cell line – Media was aspirated from culture dishes and cells were rinsed with ice cold PBS. Cells were lysed on ice in [1% octyl-β-D-glucopyranoside (Sigma-Aldrich), 50 mM Tris (tris(hydroxymethyl)aminomethane) (Bioshop) pH 8.5, 6 M urea (Sigma-Aldrich), 25 mM β-glycerophosphate (check), 1 µM okadaic acid (Bioshop), 50 mM sodium fluoride (Sigma-Aldrich), 1 µM microcystin-LR (Cayman Chemical), 10 mM sodium orthovanadate (Aldrich), 5 mM sodium pyrophosphate (Sigma-Aldrich), pepstatin (10 µg/mL) (Sigma-Aldrich)]. Samples were sonicated 2 x 15 seconds on ice then spun for 10 minutes at 16,000 x g at 4 °C, upon which the supernatant was retained and protein concentration was determined using a Bradford assay (Bio-Rad).

2.4.3 Sample Preparation for Comparison of Unfractionated vs. Strong Cation Exchange-Fractionated Phosphoproteome of UTA6 Cells

Protein lysate from UTA6 cells (a total of 20 mg) was divided into microfuge tubes in 2.5 mg aliquots and processed for in-solution digestion. Samples were reduced with 10 mM DTT (Sigma Aldrich) for 45 minutes at room temperature and then alkylated with 40 mM iodoacetamide (IAA) (Sigma Aldrich) in the dark for 45 minutes at room temperature, followed by quenching the reaction with the addition of 10 mM DTT for 45 minutes at room temperature. Samples were then diluted 1:4 using 50 mM ammonium bicarbonate pH 8.5 (ABC) and digested overnight for 18 hours at 37 °C with trypsin (Pierce) at a ratio of 1:100 (w/w). The next morning the reaction was stopped by the addition of 10% formic acid (FA). Peptides were desalted by solid phase extraction (SPE) using porous graphitic carbon (PGC) (HyperSep Hypercarb, Thermo Scientific) and C18 (Strata, Phenomenex) columns. PGC

columns were activated with 3 x 1 mL of 70% (v/v) ACN, 0.1% (v/v) FA, followed by 3 x 1

mL with 0.1% (v/v) FA. 10 mg of digested peptides were loaded on each column followed by

washing with 3 x 1 mL of 0.1% (v/v) FA and eluted using 1 mL 70% (v/v) ACN, 0.1% (v/v)

FA. C18 columns were activated with 3 x 1 mL of 0.1% FA (v/v) in ACN, followed by 3 x 1

mL of 0.1% (v/v) FA. 10 mg of digested peptides were loaded on columns followed by 3 x 1

mL of 0.1% (v/v) FA and eluted using 1 mL 50% (v/v) ACN, 0.1% (v/v) FA. Samples were

then concentrated in a vacuum centrifuge until near-dryness and reconstituted in 0.1% (v/v)

FA. 75% of the sample was designated for fractionation by strong cation exchange (SCX)

chromatography with 25% of the sample designated for immediate phosphopeptide

enrichment.

2.4.4   Offline Fractionation of Digested UTA6 Peptides Using Strong Cation Exchange Chromatography

Peptides desalted by C18 and PGC SPE columns were reconstituted in 100 μL of 0.1

FA and fractionated offline in SCX mode using a poly(2-sulfoethyl aspartamide) column

(100 x 4.6 mm, 5 μm, 200 Å) (PolySULFOETHYL A, PolyLC Inc.) connected to an Agilent

1100 HPLC with quaternary pump at a flowrate of 1.5 mL/min, monitoring absorbance at

220 nm. Mobile phase A consisted of 10 mM KH_2PO_4 pH 2.7, 20% ACN (v/v) and mobile

phase B consisted of 10 mM KH_2PO_4 pH 2.7, 500 mM KCl, 20% ACN (v/v). Fractionation

was performed using an 85 minute method consisting of a linear gradient as follows: 0% B

from 0 to 13 minutes, 25% B from 14 to 43 minutes, 100% B from 44 to 53 minutes, 100% B

from 53 to 60 minutes, with fractions collected every minute. Samples that were initially

desalted by PGC and C18 prior to SCX fractionation were again desalted by the respective

SPE column after pooling both sets of respective samples into 11 fractions based on absorbance at wavelength 220 nm.

2.4.5 Phosphopeptide Enrichment of UTA6 SCX-Fractionated and Unfractionated Peptides

SCX-fractionated and unfractionated peptides prepared from UTA6 cell lysate were enriched for phosphopeptides using a TiO_2 phosphopeptide enrichment kit (Cat #88301, Pierce) following the manufacturer's instructions.

2.4.6 Filter Aided Sample Preparation (FASP) of HeLa Tet-Off lysates

Protein lysate (2 mg) from each biological replicate was reduced with 5 mM DTT for 30 minutes at room temperature. Centrifugal filter units with 10 kDa – cutoff membranes (Amicon Ultra 15 mL, Millipore) were conditioned with 50 mM Tris pH 8.5, 8 M urea as per the manufacturer's instructions. Samples were then added to centrifugal filter units and mixed with 4 mL of 50 mM Tris pH 8.5, 8 M urea and spun at 4, 925 x g for 15 minutes at room temperature, repeating the addition of 4 mL 50 mM Tris pH 8.5, 8 M urea and centrifugation. Samples were then alkylated with 10 mM IAA for 20 minutes in the dark, followed by the addition of 4 mL 50 mM Tris pH 8.5, 8 M and centrifugation which was repeated twice. The concentration of urea was then diluted by the addition of 4 mL 100 mM Tris pH 8.5 and centrifugation, which was repeated twice. After the final dilution step trypsin (Pierce) was added at a ratio of 1:100 (w/w) and samples were digested overnight for 18 hours at 37 °C. Samples were then added to new centrifugal filter units with 10 kDa – cutoff (Amicon Ultra 0.5 mL, Millipore) which had been previously conditioned with 100 mM Tris, pH 8.5 as per the manufacturer's instructions. Samples were then spun at 14,000 x g until all of the filtrate was collected, and acidified with 10% FA. An aliquot was desalted by C18

StageTips (116), with the remainder of the digested peptides were desalted using C18 SPE columns, from which the flow-through and wash fractions were retained and desalted on PGC SPE columns. Samples were then concentrated in a vacuum centrifuge until near-dryness and reconstituted in 0.1% (v/v) FA.

2.4.7 Protein Precipitation and On-Pellet Digestion (PP) of HeLa Tet-Off Lysates

Protein lysate (2 mg) from each biological replicate was precipitated by the addition of 6 sample volumes of 10% trichloroacetic acid (TCA) (v/v) (BDH Chemicals) in acetone (EMD Millipore) at − 20 °C overnight. Samples were spun at 16,000 x g for 10 min at 4 °C to pellet precipitated protein, followed by removal of supernatant using vacuum aspiration, and ice-cold acetone was added to wash the pellet, followed by centrifugation and a subsequent wash step. Protein pellets were reconstituted in twice the original lysate sample volume in 50 mM Tris-HCl pH 8.5, 0.02% ProteaseMAX (Promega) with 1:100 trypsin (w/w) and digested for 4 hours at 37 °C with agitation in a shaking incubator. Samples were then reduced with 5 mM DTT for 30 minutes, followed by alkylation with IAA for 20 minutes in the dark. Alkylation was quenched with 5 mM DTT for 30 minutes, and an additional aliquot of 1:100 trypsin was added to samples before samples were incubated overnight for 18 hours at 37 °C with agitation. The next day samples were acidified with 10% FA, spun at 3,000 x g to remove insoluble debris, after which a small aliquot was desalted by C18 StageTips (116), while the remainder of the digested peptides were desalted using C18 SPE columns, from which the flow-through and wash fractions were retained and desalted on PGC SPE columns. Samples were then concentrated in a vacuum centrifuge until near-dryness and reconstituted in 0.1% (v/v) FA.

2.4.8 Phosphopeptide Enrichment of FASP and PP Digested Peptides

Reconstituted peptides desalted by C18 and PGC columns were measured using A_{280} absorbance on a Nanodrop (Thermo Scientific) to estimate peptide yield and combined. Samples were adjusted to 2 M lactic acid (Sigma-Aldrich), 50% ACN (v/v) and mixed. Bulk 10 μM titanium dioxide (TiO_2) beads (5020-75010, GL Sciences) previously washed and incubated in 2 M lactic acid, 50% ACN (v/v) (binding buffer) were added to peptides at a ratio of 4:1 (w/w) (400 μg of TiO_2 beads per 100 μg of peptides) in micro-centrifuge tubes and incubated for 30 minutes at room temperature with end-over-end rotation. Samples were then spun at 8,000 x g for 1 minute, after which the supernatant was removed and transferred to a new tube for a second incubation with TiO_2 beads. After a second incubation with TiO_2 beads for 30 minutes, the supernatant was retained, vacuum centrifuged, and desalted using C18 micro-columns (C18 StageTips) (116). TiO_2 beads were then washed twice by adding 500 μL of binding buffer and mixing vigorously using a vortex genie, followed by centrifugation at 8,000 x g for 1 minute. TiO_2 beads were then reconstituted in 500 μL of 50% ACN (v/v) and transferred to new micro-centrifuge tubes, followed by centrifugation at 8,000 x g for 1 minute, vacuum aspiration of supernatant and washed with 500 μL of 50% ACN (v/v). This wash process was repeated for a total of three times. Phosphopeptides bound to the TiO_2 beads were eluted with two volumes of 300 μL of 5% NH_4OH (v/v) (Fluka), 50% ACN (v/v) (elution buffer) using centrifugation to pellet the beads in order to remove the eluate. The eluate was passed through a StageTip containing one layer of C18 material by centrifugation at 3000 x g for 2 minutes to retain any TiO_2 beads, followed by the addition of 100 μL of 80% ACN (v/v). Filtered eluate was concentrated using vacuum centrifugation until near dryness and reconstituted in 1% FA.

2.4.9 LC-MS/MS Data Acquisition of UTA6 SCX-Fractionated and Unfractionated Phosphopeptides

Samples were injected using a NanoAcquity UPLC (Waters) onto a Symmetry C18 trapping column (20 mm x 180 μm i.d., 5 μm, 100 Å) at a flow rate of 10 μL/min in 99% mobile phase A (0.1% FA (v/v), 1% mobile phase B (0.1% FA (v/v) in ACN) for 4 minutes. Samples were then separated on a NanoAcquity Peptide BEH C18 analytical column (250 mm x 75 μm i.d., 1.7 μm, 130 Å) at a flow rate of 300 nL/min by a linear gradient of increasing mobile phase B. Fractionated samples were separated using a gradient from 7.5% to 37.5% mobile phase B over 60 minutes (total run time 100 minutes per sample) and unfractionated samples were separated using a gradient from 5% to 37.5% mobile phase B over 240 minutes (total run time 300 minutes per sample). Separated peptides were ionized using a nano-Electro Spray Ionization source connected to the analytical column by a fused-silica capillary emitter (New Objective). Ionized peptides were analyzed using a QExactive Hybrid Quadrupole-Orbitrap mass spectrometer (Thermo Scientific) operated by Thermo XCalibur (software version 2.2.1.1646) in data-dependent mode. Full MS1 scans were performed at 70,000 resolution, scanning from $400 - 1800$ m/z with AGC set to 1×10^{6} ions and an isolation window of 4.0 m/z. The top 12 most abundant ions were selected for MS2 for SCX-fractionated samples and the top 24 most abundant ions were selected for MS2 for unfractionated samples. A lock mass ion was enabled for 445.120025 m/z (117). Maximal injections times for MS1 acquisition was 120 ms and 30 ms for SCX-fractionated and unfractionated samples, respectively. Peptide ions were fragmented using HCD with NCE set to 23% and data-dependent MS2 scans were performed at 17,000 resolution with a dynamic

exclusion window of 60 seconds. Maximal injection times for MS2 acquisition was 120 ms and 100 ms for SCX-fractionated and unfractionated samples, respectively.

2.4.10 LC-MS/MS Data Acquisition of HeLa Tet-Off FASP and PP Phosphopeptides

Samples were injected using a NanoAcquity UPLC (Waters) onto a Symmetry C18 trapping column (20 mm x 180 μm i.d., 5 μm, 100 Å) at a flow rate of 10 μL/min in 99% mobile phase A (0.1% FA (v/v), 1% mobile phase B (0.1% FA (v/v) in ACN) for 4 minutes. Samples were then separated on a NanoAcquity Peptide BEH C18 analytical column (250 mm x 75 μm i.d., 1.7 μm, 130 Å) at a flow rate of 300 nL/min by a linear gradient of increasing mobile phase B from starting condition 7.5% to 25% for 180 minutes, followed by 25% to 32.5% for 40 minutes, and culminating at 60% at 240 minutes. Separated peptides were ionized using a nano-Electro Spray Ionization source connected to the analytical column by a fused-silica capillary emitter (New Objective). Ionized peptides were analyzed using a Orbitrap Elite Hybrid Ion Trap-Orbitrap mass spectrometer (Thermo Scientific) operated by Thermo XCalibur (software version 2.7.0.1094) in data-dependent mode. Full MS1 scans were performed at 120,000 resolution, scanning from 400 – 1450 *m/z* with AGC set to 5 x 10^2 ions and an isolation window of 1.0 *m/z*. The top 20 most abundant ions were selected for MS2. A lock mass ion was enabled for 445.120025 *m/z* (117). Maximal injection time for MS1 acquisition was 200 ms and 50 ms for MS2. Peptide ions were fragmented using CID with NCE set to 35% with activation time set to 10 ms and a Q value of 0.25. Data-dependent MS2 scans were acquired in the linear ion trap using rapid scan selection, with a dynamic exclusion window of 60 seconds.

2.4.11 Data Analysis of UTA6 SCX-Fractionated and Unfractionated Phosphopeptides

Raw mass spectra were analyzed in PEAKS version 7.0 (Bioinformatics Solutions Inc.) (118, 119). Once loaded in PEAKS, mass spectra were refined and analyzed by *de novo* sequencing with the following parameters; parent mass error tolerance 20.0 ppm, fragment mass error tolerance 0.02 Da, enzyme specificity trypsin, fixed modification cysteine carbamidomethylation (+ 57.0215), variable modifications methionine oxidation (+15.9949), asparagine and glutamine deamidation (+0.9840 Da), serine and threonine phosphorylation (+79.9663). The maximum number of variable modifications was set to 4. Following *de novo* sequencing, data were searched against the UniProt sequence database (*homo sapiens* taxon, accessed on March 11, 2014) using the same parameter constraints as *de novo* sequencing in addition to 3 maximum missed cleavages for sequence matching. Peptide spectrum matches were restricted to a 1% false discovery rate (FDR) threshold against a target-based decoy database. Identified phosphopeptides were compared amongst the four datasets (SCX-fractionated and unfractionated samples desalted by PGC or C18) for shared or complementary sets of phosphopeptides. Using *motif-x* (100, 101), identified peptide sequences from PGC and C18 unfractionated samples that were exported from PEAKS were searched for statistically over-represented linear motifs centered on phosphorylated serine residues against the human proteome fasta sequence database of the International Protein Index built into motif-x. Linear motifs were considered with a minimum number of 20 occurrences and a 9 residue window (plus/minus 4 residues from the modified serine) with a default value of significance threshold set to 0.000001.

2.4.12 Data Analysis of HeLa Tet-Off FASP and PP Phosphopeptides

Raw mass spectra files were analyzed in MaxQuant version 1.5.3.8 (70, 71, 120) and searched against the Uniprot sequence database (*homo sapiens* taxon, accessed on June 10, 2015). Mass tolerances were set to 4.5 ppm for the parent ion mass (MS) and 0.5 Da for the fragment ion mass (MS/MS). The minimum number of amino acids in a peptide was set to 7, with a peptide spectrum match (PSM) and protein match set to 1% FDR and protease selectivity for trypsin/P. A maximum number of 3 missed cleavages was selected. The option for second peptide search was selected, as was the use of "Match Between Runs" for respective pairs of samples between biological replicates, using the default matching parameters. A maximum number of variable modifications per peptide was 5, with methionine oxidation (+15.9949), asparagine and glutamine deamidation (+0.9840 Da), and serine and threonine phosphorylation (+79.9663) selected. Cysteine carbamidomethylation (+ 57.0215) was set as a fixed modification. Raw mass spectra files were defined as separate groups using the experimental setup option. The minimum score for modified peptides was set to 40, and the decoy-database setting was "Revert." Output data from MaxQuant was then loaded into Perseus version 1.5.2.6 (121). For the comparison of proteome data between FASP and PP, the "proteinGroups.txt" file was first removed of entries marked as reverse decoy database hits, contaminants, and protein identifications that were only matched to modified peptides. Proteins were considered identified in each biological replicate if identified in at least one of two technical replicates. For the comparison of the phosphoproteome data between FASP and PP, the "Phospho (ST)Sites.txt" file was removed of entries marked as reverse decoy database hits and filtered to only contain phosphorylation

sites with localization probability greater than 0.75. Phosphosites were considered identified

in each biological replicate if identified in at least one of two technical replicates.

2.5   Supplemental
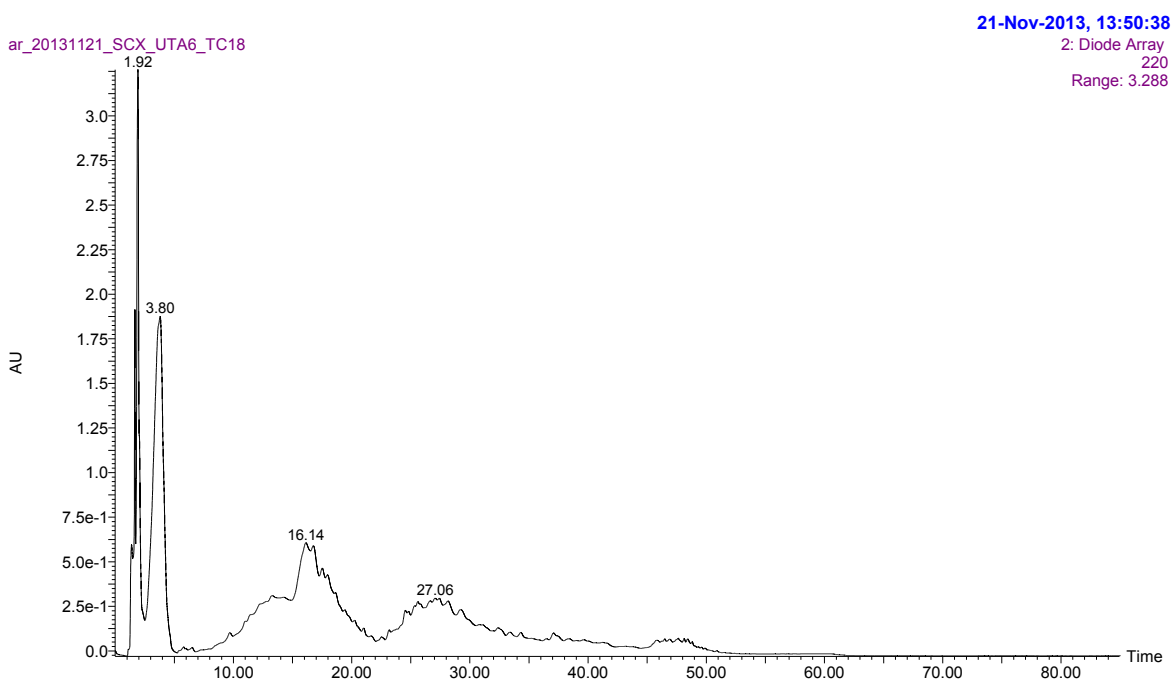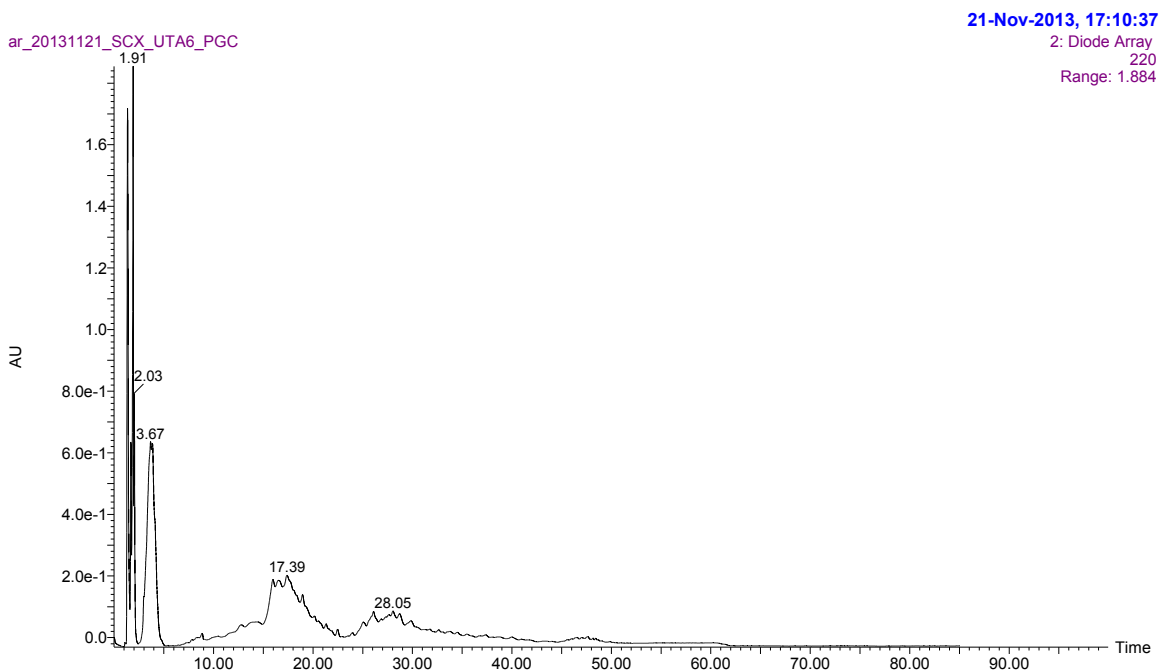
Supplemental Figure 2.1 Companion to Figure 2.2
Chromatograms for SCX separation of peptides desalted using PGC (top) and C18 (bottom.)
Peptides were separated at a flow-rate of 1.5 mL/min, monitoring absorbance at 220 nm.

3   Chapter 3 – Investigation of the Phosphoproteome in Response to CX-4945 Treatment

3.1   Introduction

It is estimated that potentially 700,000 phosphorylation sites may exist in the human proteome (6). Furthermore, current "deep" proteomic profiling methods can identify up to 50,000 phosphorylation sites in human cells, representing three quarters of the proteins that are detectable by mass spectrometry (7). The regulation of phosphorylation is a central component in maintaining cellular homeostasis and is regulated by protein kinases which catalyze the transfer of phosphate from ATP to serine, threonine or tyrosine residues (122). Not surprisingly, these enzymes have quickly emerged as potential therapeutic targets of interest for the treatment of a number of human diseases (9). Protein kinase CK2 has attracted interest as a potential therapeutic target since it has been identified as a kinase that is expressed at high levels in different types of human cancers (16). A recent report has also noted that de-regulation of expression exists at the transcript level for the catalytic and regulatory subunits of CK2 (14). The first orally-bioavailable inhibitor of CK2, CX-4945 (44), recently entered clinical trial for the treatment of cholangiocarcinoma in combination with gemcitabine and cisplatin, and is touted as a highly selective and specific inhibitor of CK2 (123). CX-4945 has been used extensively in the literature in different models of multiple myeloma, lymphoma, and leukemia (50, 53, 54, 124, 125), and these studies have implicated CK2 activity in the regulation of different pathways. Characterization of the impact of CX-4945 on a cellular phosphoproteome would enable a better understanding of the processes and pathways that that enable cell death via CK2 inhibition. Additionally, it would allow for an unbiased assessment of the potential for the regulation of other kinases

considering this inhibitor is ATP-competitive. To date, proteomics strategies have not been applied for characterizing the phosphoproteome of cells treated with CX-4945, and the most recent studies with an inhibitor of CK2, quinalizarin, have not capitalized on translational capacity due to its limited clinical utility (126, 127).

In this chapter the phosphoproteomics workflow that was optimized previously in Chapter 2 is used to perform unbiased quantitative phosphoproteomic profiling of HeLa cells treated with CX-4945 within a window of 240 minutes. SILAC (Stable Isotopic Labeling of Amino Acids in Cell Culture) was utilized in order to perform relative quantification of the phosphoproteome and proteome. To identify phosphorylated substrates that could serve as dynamic markers of CK2 activity, a bioinformatics approach was undertaken and a kinase-substrate prediction tool, KinomeXplorer (77) was utilized. In order to gauge the impact of CX-4945 treatment on the phosphoproteome and to identify kinases-substrate relationships that were perturbed in response to CX-4945 treatment, the PHOXTRACK tool (128) was also employed. A global assessment of the biological processes and pathways with phosphorylation sites perturbed by CX-4945 was performed using gene enrichment analysis with g:Profiler (129). Collectively, these analyses reveal a broad impact of CX-4945 on several different processes and distinct areas of regulation.

3.2   Results

3.2.1   Evaluation of CK2 Inhibition Using a Bona-Fide Substrate EIF2S2

A previous study by Geiger *et al.* identified that amongst 11 commonly used cell line models there is ubiquitous expression of proteomes (130). Taking into consideration the availability of existing cell line models in our laboratory and the use of a commercially available HeLa proteome standard for LC-MS/MS analysis, we performed experiments in the

HeLa cell line. Prior to embarking on a quantitative phosphoproteomic analysis of CX-4945 in HeLa cells, we adapted the cell line in SILAC medium for a period of 7 days and 3 sub-passages to ensure that proteins were isotopically-labeled to greater than 95% as is routinely performed (69). We used medium containing proline to prevent arginine-to-proline conversion (131). Heavy labeled samples were digested and raw spectra acquired by LC-MS/MS, followed by analysis in MaxQuant to assess the extent of isotopic labeling of proteins (70, 71, 120). The median incorporation efficiency was over 96% (Supplemental Figure 3.13.1) and the distribution of incorporation amongst all peptides detected and quantified was skewed towards 100% incorporation. Following confirmation of successful incorporation of isotopically-labelled amino acids, a time-course experiment was performed using CX-4945 at 20 μM up to 24 hours of treatment in HeLa cells to identify a window of time in which inhibition of CK2 would precede secondary signaling events such as DNA damage or apoptosis, given that CK2 has previously been demonstrated to regulate the phosphorylation of constituents of the DNA damage and repair pathways (29, 37, 132, 133) and implicated in the regulation of apoptotic pathways (27, 34). Confirmation of CK2 inhibition was based upon the phosphorylation status of a well-characterized bona fide substrate, EIF2S2 (11, 134), for which a phospho-specific antibody was raised in our laboratory. Western blotting with antibodies directed against phospho-EIF2S2 Ser2, PARP, and γH2AX Ser139 identified a period of time up to 4 hours in which the lysates derived from CX-4945 treated samples were comparable to an untreated sample in terms of appearance of cleaved PARP and γH2AX Ser139 (Supplemental Figure 3.23.2), suggesting that within this window of time the inhibition of CK2 preceded the activation of other

signaling pathways which could interfere with the interpretation of events succeeding CK2 inhibition.

3.2.2 Unbiased Phosphoproteomic Evaluation of HeLa Cells Treated with CX-4945

Following confirmation of CK2 inhibition using anti-phospho-EIF2S Ser2 antibody to probe unlabeled lysates derived from HeLa cells treated with CX-4945, SILAC labeled HeLa cells were treated with 20 μM CX-4945 or with DMSO for periods of 60, 135, 180 and 240 minutes. These samples were separated by SDS-PAGE, transferred to membrane and probed using antibodies against phospho-EIF2S2 Ser2, PARP, phospho-ATM Ser1981, and γH2AX Ser139 (Supplemental Figure 3.33.3-3.5). Western blotting confirmed that over the time-course of 240 minutes, the inhibition of CK2 using CX-4945 was apparent with the decrease in phospho-EIF2S2 Ser2 signal. During the period in which CX-4945 treatment occurred, CK2 inhibition was not secondary to events such as the activation of apoptosis or the activation of DNA-damage. These processes would be apparent with the cleavage of PARP or increase of γH2AX Ser139 respectively. By comparison, lysates derived from cells treated with a promiscuous kinase inhibitor such as staurosporine or a chemical which induces DNA damage such as neocarzinostatin, displayed activation of apoptosis and evidence of DNA damage. Next, equal amounts of light and heavy lysates were combined and digested with trypsin and Lys-C proteases, followed by desalting and phosphopeptide enrichment. Proteome samples were retained as well. By combining samples prior to processing and enrichment, bias in phosphopeptide abundance between a treated and a control sample was eliminated. Quantitative analysis by mass spectrometry enables the MS1 peptide features to be utilized to measure the difference in abundance between SILAC pairs of peptides, and the MS2 spectrum confirms peptide sequence identity and phosphorylation site localization

(Figure 3.1). In total, 48 fractions derived from four time-point datasets of three biological replicates were analyzed by LC-MS/MS in technical duplicate (Figure 3.2 A). This resulted in the identification and quantification of 3,003 phosphorylation sites and 2,805 protein groups in three out of three biological replicates across all time-points that were profiled (Figure 3.2 B, C, D). Phosphorylation sites were categorized on the magnitude of change and whether the change was statistically significant based on a one-sample Student's t test with Benjamini Hochberg FDR of 0.05 for multiple hypothesis correction (Figure 3.2 C and Supplemental Figure 3.63.6-3.9). Of these, sites which are predicted to be phosphorylated by CK2 as identified using KinomeXplorer (77) constitute a small number of the sites that decrease greater than log2 -1 (a two-fold change). To note, the magnitude of change in phosphorylation of TOP2A at Ser1377, a well-characterized CK2 substrate (135), is substantially greater when compared to EIF2S2 Ser2 at 60 minutes of CX-4945 treatment and over the period of inhibitor treatment up to 240 minutes (Figure 3.3). Other phosphorylation sites from bona fide CK2 substrates within this period of treatment do not show as dynamic de-phosphorylation. This suggests preferential activity of phosphatases directed towards sites of phosphorylation by CK2. The broader impact on the phosphoproteome can be visualized using volcano plots (Figure 3.4-3.7), where it is evident based on the distribution of phosphorylation sites that increase and decrease upon treatment that CX-4945 elicits a dynamic phosphoproteome.

3.2.3   Dynamic Phosphorylation is Independent of Protein Abundance

In parallel with phosphopeptide analysis to investigate the phosphoproteome of HeLa cells perturbed with CX-4945, proteomic samples were analyzed by LC-MS/MS as well to quantify the proteome. When surveying the distribution of quantified proteins in each particular time-point, the distribution of quantified protein group ratios falls within log2 -/+ 0.5, suggesting that the proteome in general does not change in cells that are treated with CX-4945 up to a period of 240 minutes (Supplemental Figure 3.10-3.13). Additionally, those phosphorylation sites that were categorized as statistically significant were plotted against the corresponding protein ratio (Figure 3.8-11) for each individual time-point dataset to confirm that the change in the phosphoproteome is independent of protein abundance. Phosphorylation sites identified as CK2 substrates showed dramatic decrease in phosphorylation upon CX-4945 treatment and this was not due changes in protein abundance.
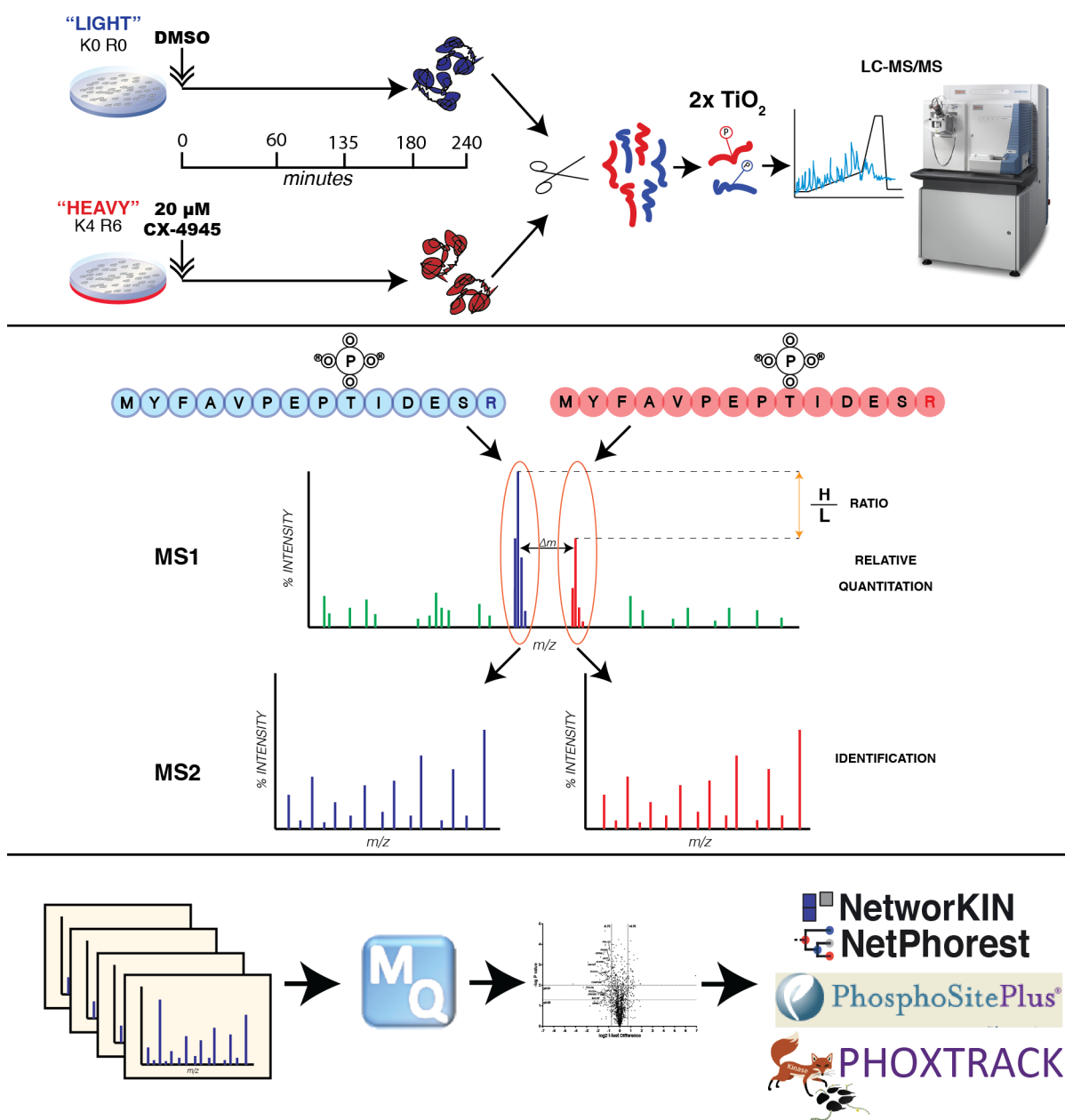
Figure 3.1 Phosphoproteomics Workflow to Investigate CX-4945 in HeLa Cells.
HeLa cells were adapted in SILAC media and treated with CX-4945 for a period up to 240 minutes. Lysates were mixed 1:1 and digested with trypsin and Lys-C, followed by phosphopeptide enrichment and analysis by LC-MS/MS. Relative quantitation was performed on raw mass spectra using MaxQuant and identified and quantified sites were analyzed using bioinformatics tools to investigate kinase-substrate relationships.

A

Biological Replicates

Technical Replicates

DMSO
"LIGHT"
K0 R0

20 µM CX-4945
"HEAVY"
K4 R6

Phosphoproteome →
→ Phosphoproteome →
Proteome →
Proteome →

2x

0   60   135   180   240
minutes
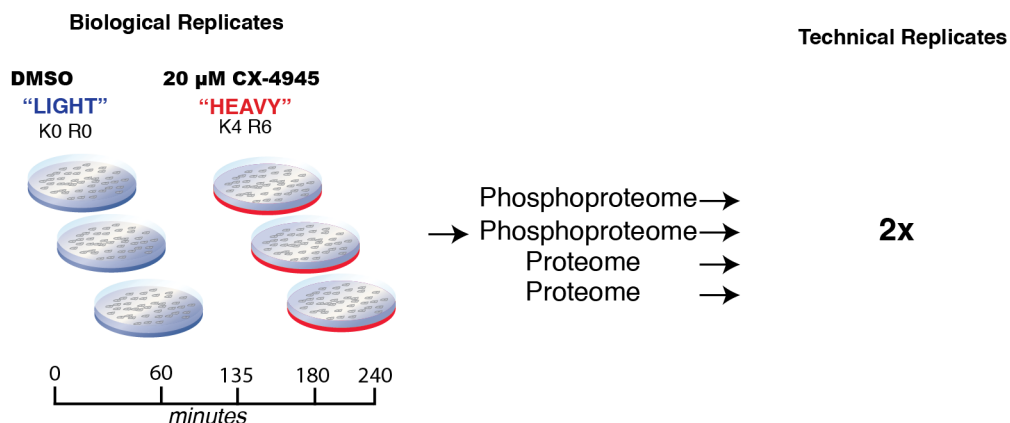
B

MS¹ SPECTRA
1,060,922

MS² SPECTRA
8,296,813

C

	# Phosphorylation Sites (P loc. > 0.75) (3/3 Biological Replicates)		# UP >1	# DOWN <-1	# DOWN CK2
3003 in all replicates and timepoints	**60 min**	**4277**	53 (1.2%)	246 (5.8%)	17
	135 min	**4762**	95 (1.9%)	354 (7.4%)	36
	180 min	**5273**	307 (5.8%)	420 (7.9%)	49
	240 min	**4455**	147 (3.3%)	356 (8.0%)	35

D

	# Proteins (3/3 Biological Replicates)	
2805 in all replicates and timepoints	**60 min**	**3096**
	135 min	**3212**
	180 min	**3260**
	240 min	**3149**

Figure 3.2 Experimental Layout and Data Summary
(A) Processing of treated and control samples for LC-MS/MS analysis resulted in four fractions per biological replicate which were analyzed in technical duplicate. (B) Summary of total number of spectra acquired. (C) Number of phosphorylation sites identified and quantified in 3/3 biological replicates and number that changed in response to CX-4945 that met significance criteria. (D) Number of protein groups identified in 3/3 biological replicates.
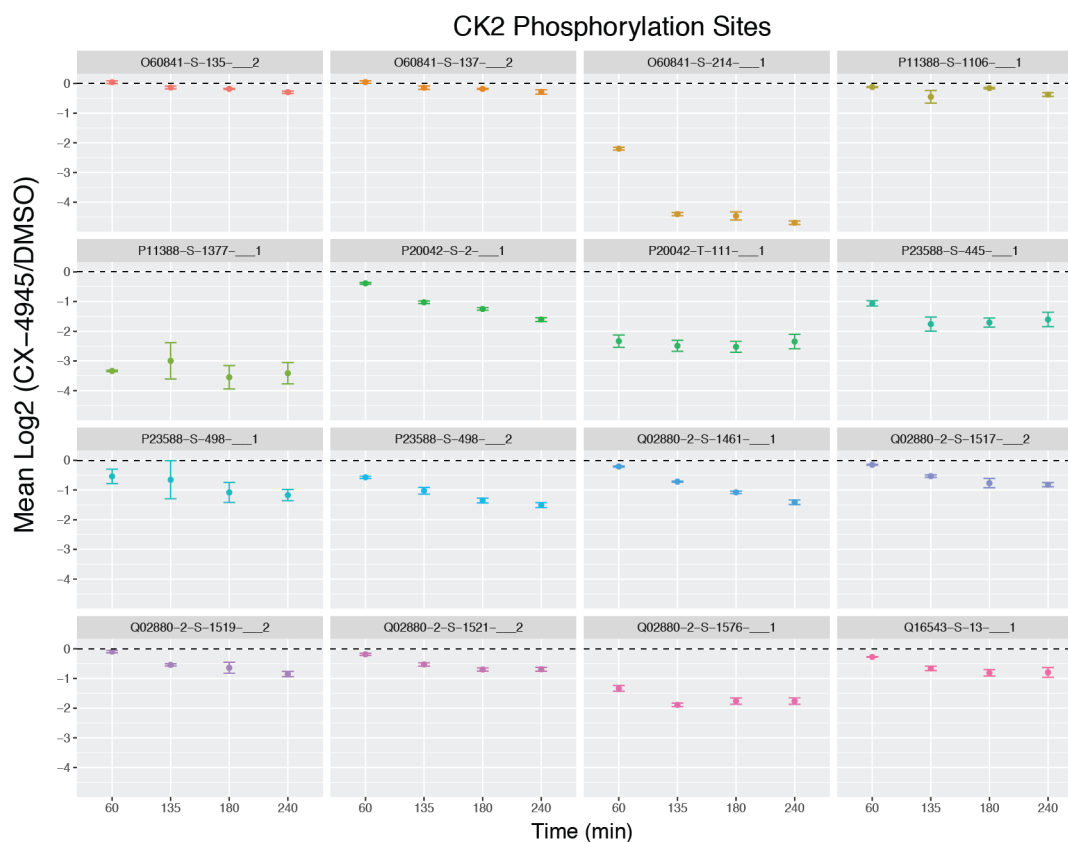
Figure 3.3 Phosphorylation Dynamics of Identified CK2 Sites Using KinomeXplorer.
Subset of phosphorylation sites identified as CK2 substrates that were quantified in all biological replicates and time-points. In each panel header a concatenated identifier consisting of the protein Uniprot accession code, amino acid residue, sequence position of the phosphorylation site and multiplicity is shown. Error bars denote standard deviation of all three biological replicates quantified.
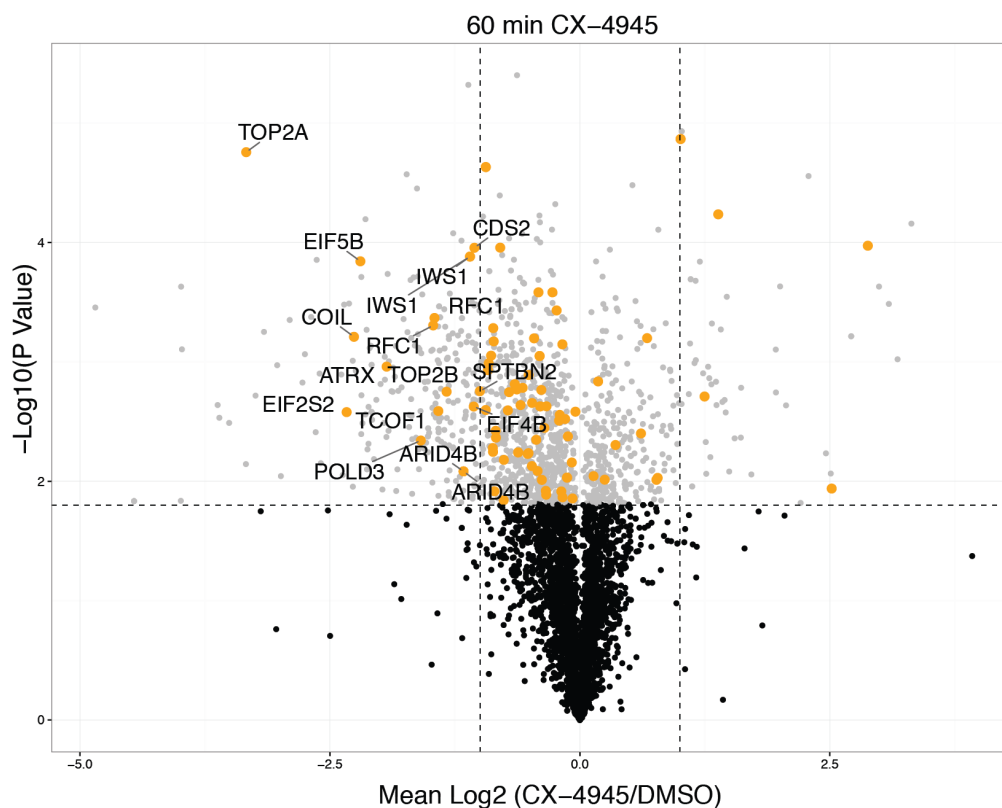
Figure 3.4 Volcano Plot of Quantified Phosphorylation Sites from HeLa Cells Treated with 20 µM CX-4945 for 60 Minutes.
Quantified phosphorylation sites were tested for significance using a one-sample Student's t-test with FDR correction (<0.05). Points in grey exceed statistical significance cut-off. CK2 phosphorylation sites identified by KinomeXplorer are highlighted in orange. Labeled sites exceed log2 -1 and are significant. Vertical dashed lines denote -1 and +1 Log2 cutoffs; horizontal line denotes FDR threshold of $P < 0.05$.
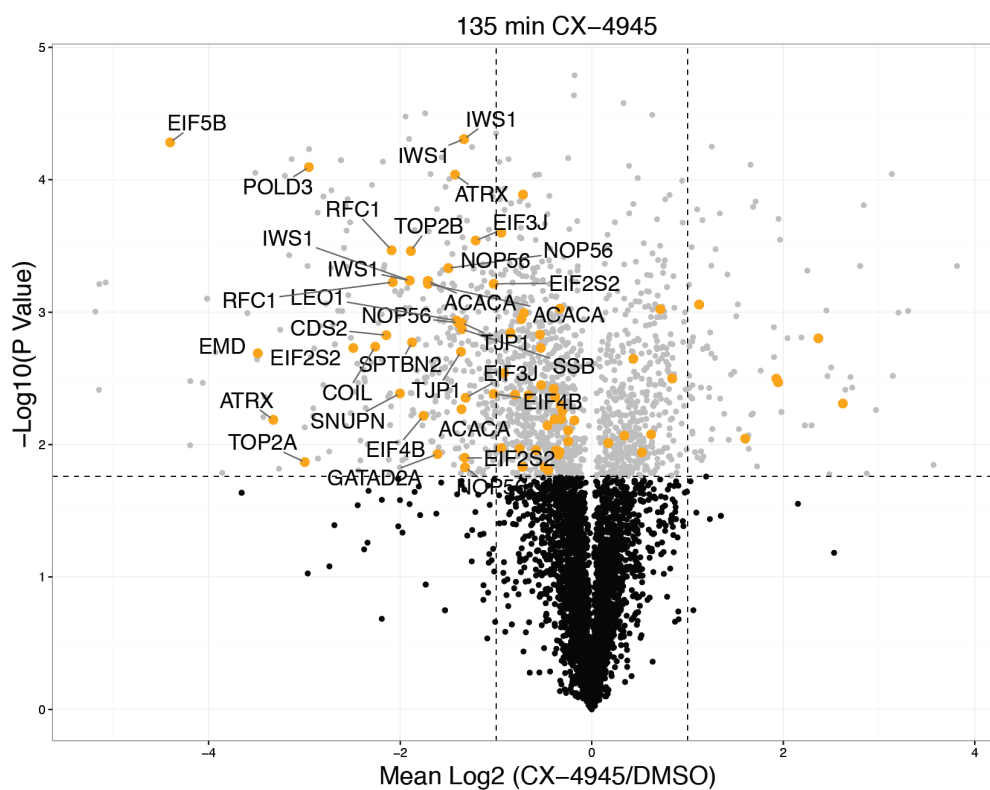
Figure 3.5 Volcano Plot of Quantified Phosphorylation Sites from HeLa Cells Treated with 20 μM CX-4945 for 135 Minutes.
Quantified phosphorylation sites were tested for significance using a one-sample Student's t-test with FDR correction (< 0.05). Points in grey exceed statistical significant cut-off. CK2 phosphorylation sites identified by KinomeXplorer are highlighted in orange. Labeled sites exceed log2 -1 and are significant. Vertical dashed lines denote -1 and +1 Log2 cutoffs; horizontal line denotes FDR threshold of P < 0.05.
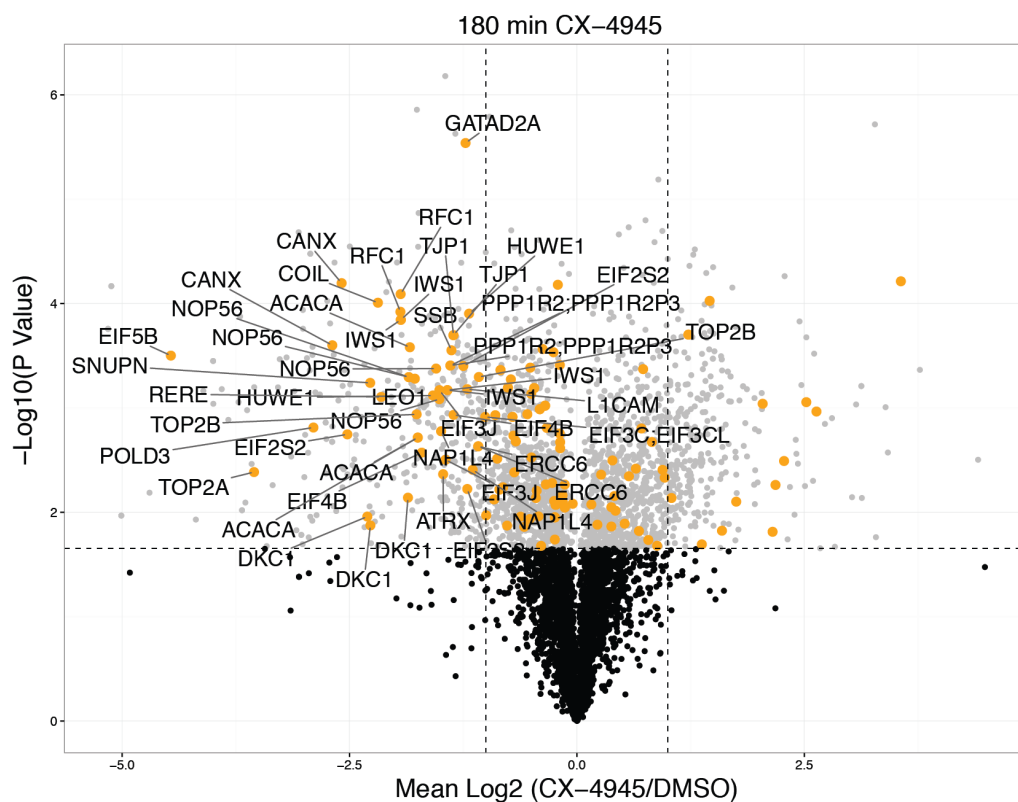
Figure 3.6 Volcano Plot of Quantified Phosphorylation Sites from HeLa Cells Treated with 20 μM CX-4945 for 180 Minutes.
Quantified phosphorylation sites were tested for significance using a one-sample Student's t-test with FDR correction (< 0.05). Points in grey exceed statistical significance cut-off. CK2 phosphorylation sites identified by KinomeXplorer are highlighted in orange. Labeled sites exceed log2 -1 and are significant. Vertical dashed lines denote -1 and +1 Log2 cutoffs; horizontal line denotes FDR threshold of P < 0.05.
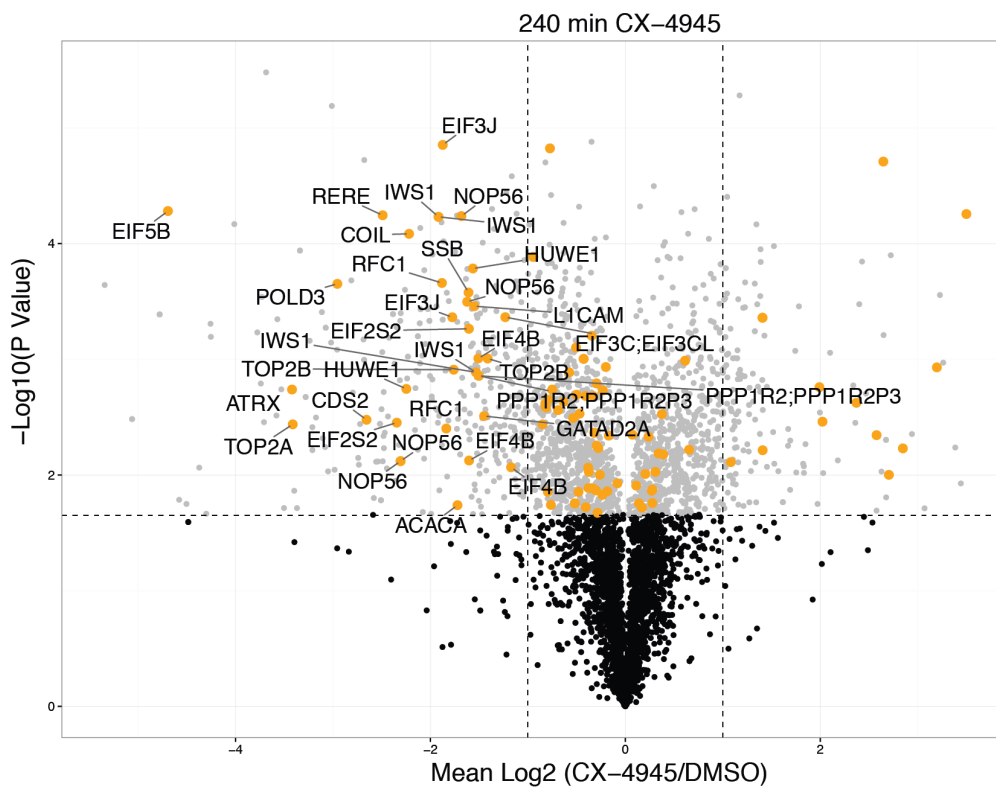
Figure 3.7 Volcano Plot of Quantified Phosphorylation Sites from HeLa Cells Treated with 20 μM CX-4945 for 240 Minutes.
Quantified phosphorylation sites were tested for significance using a one-sample Student's t-test with FDR correction (< 0.05). Points in grey exceed statistical significance cut-off. CK2 phosphorylation sites identified by KinomeXplorer are highlighted in orange. Labeled sites exceed log2 -1 and are significant. Vertical dashed lines denote -1 and +1 Log2 cutoffs; horizontal line denotes FDR threshold of $P < 0.05$.
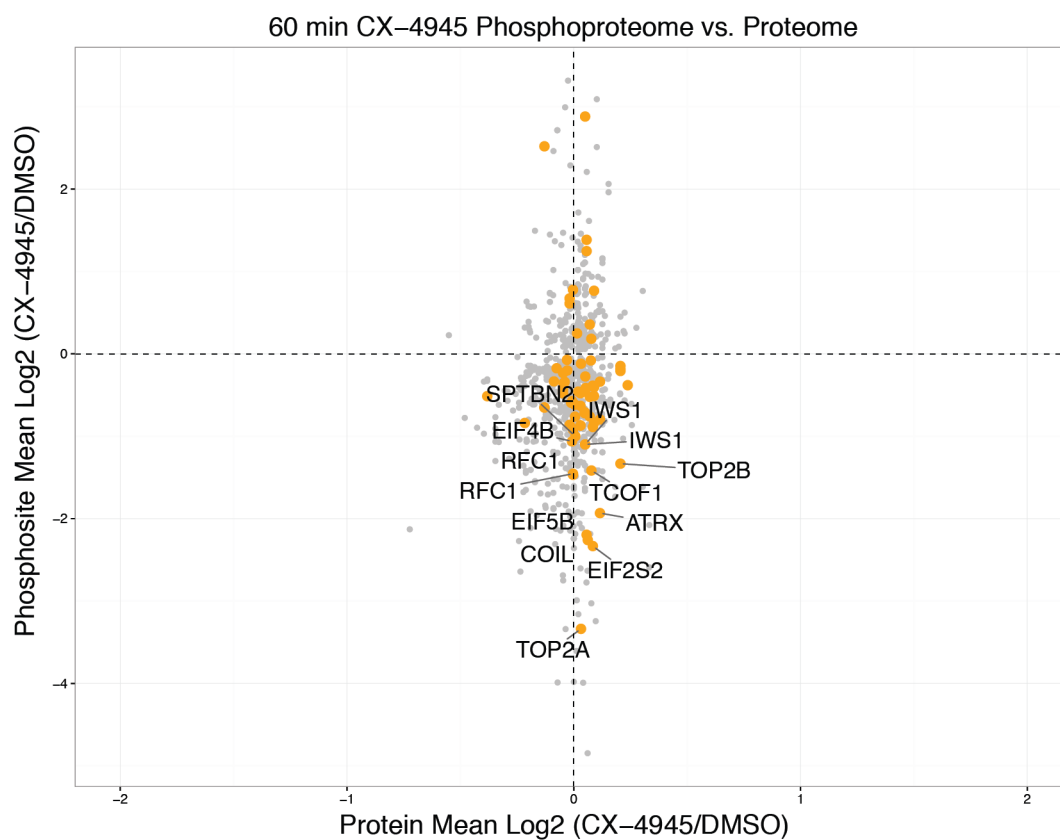
Figure 3.8 Comparison of Phosphorylation Site vs. Protein Abundance in HeLa Cells Treated with 20 μM CX-4945 for 60 Minutes.
Phosphorylation sites that were statistically significant were plotted against the respective protein ratio. Displayed are the mean Log2 ratios for a phosphorylation site and the mean Log2 ratio for the respective protein abundance, all derived from three biological replicates. CK2 phosphorylation sites are highlighted in orange. Labeled sites exceed Log2 -1.
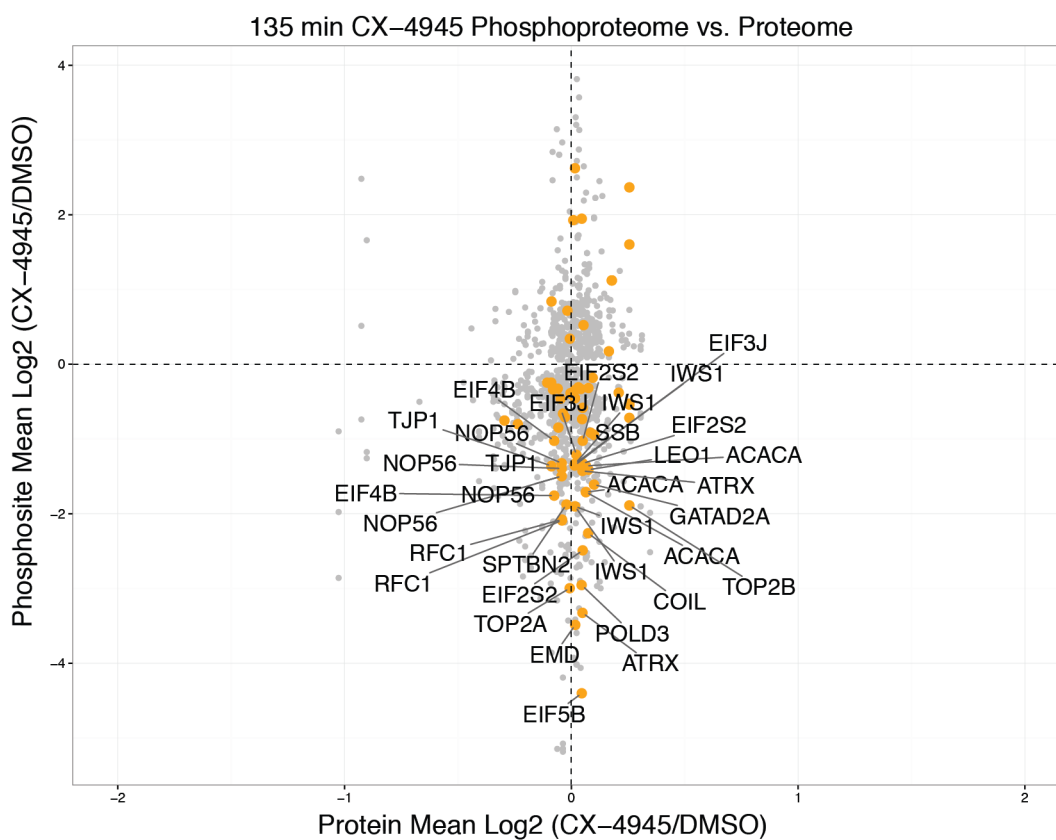
Figure 3.9 Comparison of Phosphorylation Site vs. Protein Abundance in HeLa Cells Treated with 20 μM CX-4945 for 135 Minutes.
Phosphorylation sites that were statistically significant were plotted against the respecrive protein ratio. Displayed are the mean Log2 ratios for a phosphorylation site and the mean Log2 ratio for the respective protein abundance, all derived from three biological replicates. CK2 phosphorylation sites are highlighted in orange. Labeled sites exceed Log2 -1.
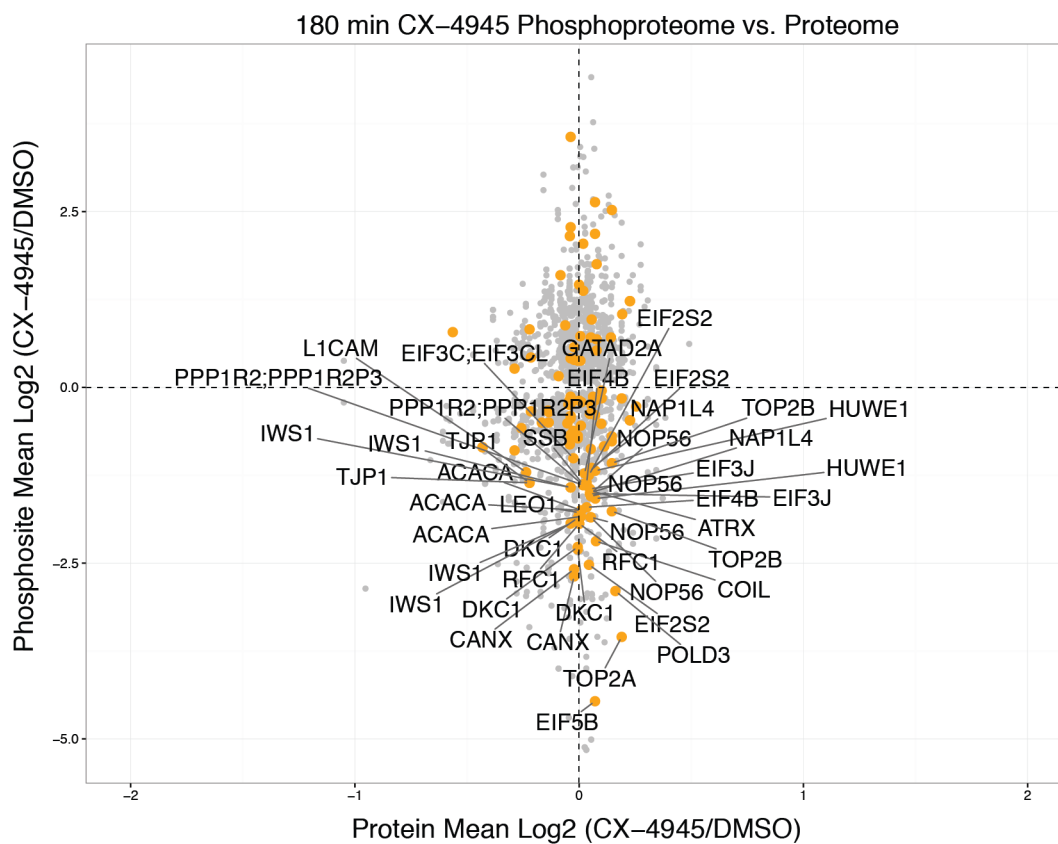
Figure 3.10 Comparison of Phosphorylation Site vs. Protein Abundance in HeLa Cells Treated with 20 μM CX-4945 for 180 Minutes.
Phosphorylation sites that were statistically significant were plotted against the respective protein ratio. Displayed are the mean Log2 ratios for a phosphorylation site and the mean Log2 ratio for the respective protein abundance, all derived from three biological replicates. CK2 phosphorylation sites are highlighted in orange. Labeled sites exceed Log2 -1.
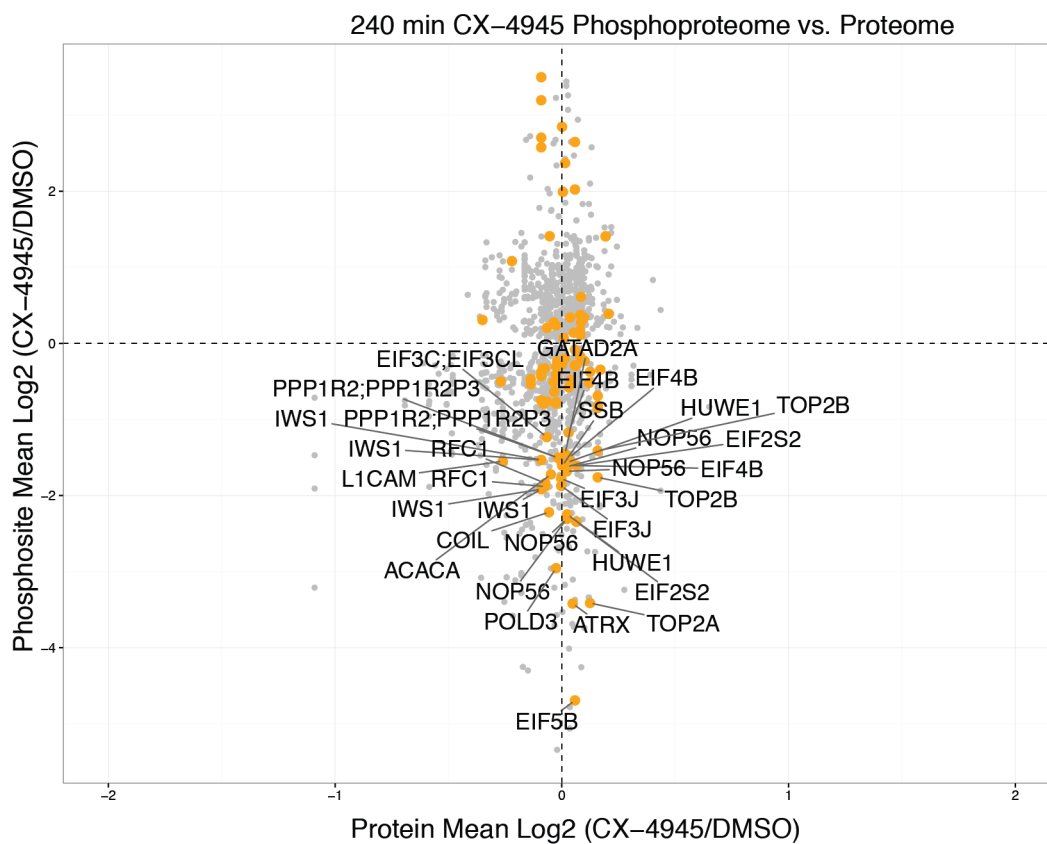
Figure 3.11 Comparison of Phosphorylation Site vs. Protein Abundance in HeLa Cells Treated with 20 μM CX-4945 for 240 Minutes.
Phosphorylation sites that were statistically significant were plotted against the respective protein ratio. Displayed are the mean Log2 ratios for a phosphorylation site and the mean Log2 ratio for the respective protein abundance, all derived from three biological replicates. CK2 phosphorylation sites are highlighted in orange. Labeled sites exceed Log2 -1.

3.2.4 CX-4945 Treatment Affects Phosphorylation Mediated by Kinases Other Than CK2

CK2 can regulate the activity of other kinases by phosphorylation of cdc37 Ser13 (136), which is a kinase-chaperone that can regulate client kinases concurrently with Hsp90 (137). CX-4945 itself is a small molecule ATP-competitive inhibitor, and could target other kinases other than CK2 in the cell. Considering these points, kinase-substrate enrichment analysis was performed using PHOXTRACK (128) to investigate the impact of CX-4945 treatment. This analysis was performed using information found in PhosphoSitePlus and the kinase-substrate relationships that are listed (138). Phosphorylation sites quantified in each time-point dataset were analyzed separately and Kolmogorov-Smirnov unweighted running sum statistics were calculated. PHOXTRACK scores for a particular kinase reflect the enrichment value as computed by running sum statistics for the set of phosphorylation sites that are attributed to a particular kinases and are adjusted using the false-discovery rate (FDR). Activation or inhibition of a particular kinase can be inferred by the trend of attributed phosphorylation sites; whether these sites are trending as increased in phosphorylation or decreased in phosphorylation. Analysis using PHOXTRACK revealed kinases (FDR < 0.25) that were inhibited or activated as inferred by the quantification of attributed phosphorylation sites in PhosphoSitePlus for the four time-point datasets (Figure 3.12). Interestingly, at 60 minutes of CX-4945 treatment, mTOR and Akt are down-regulated with CDK1, CDK2 and LATS1 being up-regulated. The phosphorylation of several CK2 substrates suggests that there is inhibition of CK2 although the bioinformatics analysis derived from information attributed in PhosphoSitePlus does not meet the FDR cut-off of 0.25. Notably, in agreement with previous analysis using KinomeXplorer, there are
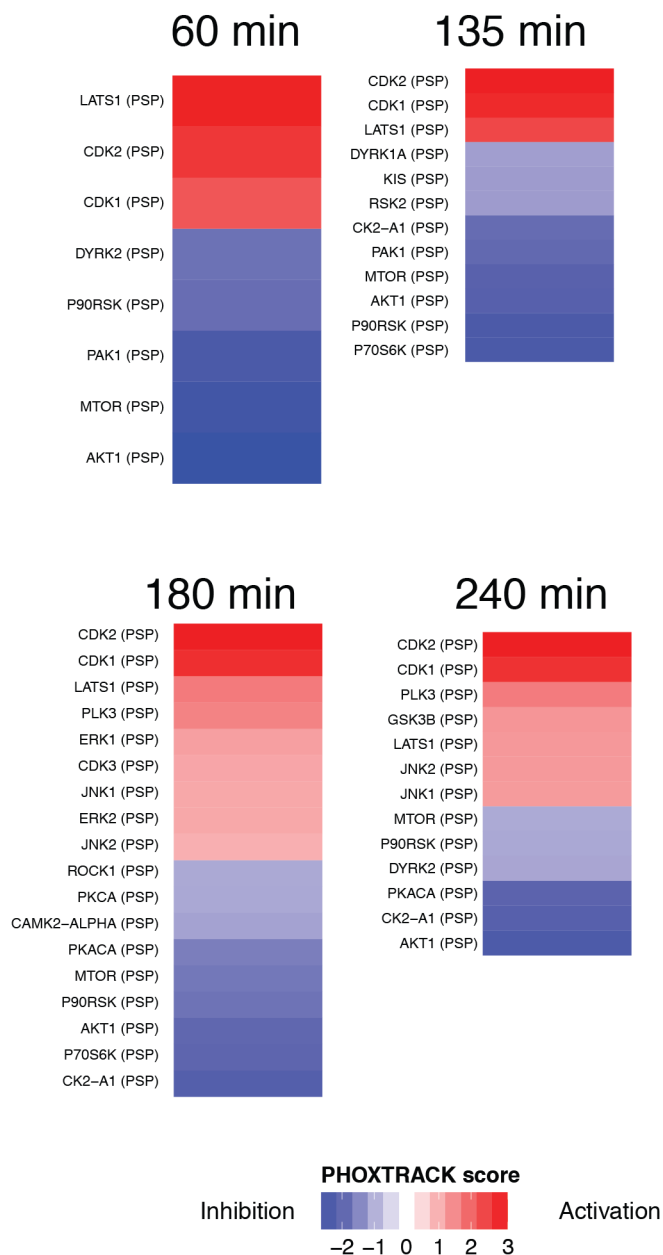
Figure 3.12 PHOXTRACK Analysis of Phosphorylation Sites Quantified at Each Time-Point.
Phosphorylation sites were analyzed using PHOXTRACK which uses Kolmogorov-Smirnov unweighted running sum statistics to calculate activation or inhibition of a kinase based on the assigned substrates in PhosphoSitePlus database . Shown are heat maps with kinases that exceeded a FDR threshold of < 0.25 in each time-point.
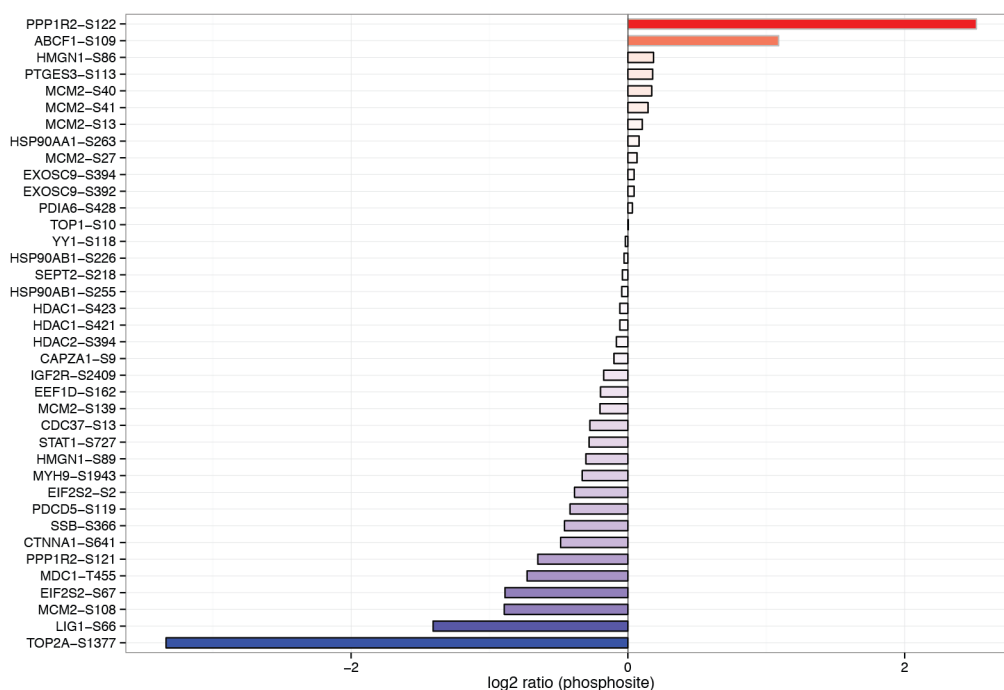
Figure 3.13 Quantified CK2 Phosphorylation Sites in PhosphoSitePlus from HeLa Cells Treated with 20 μM CX-4945.
Phosphorylation sites listed as CK2 substrates in PhosphoSitePlus database are presented. The mean log2 ratio from three biological replicates is used to calculate the change represented by each bar for a given phosphorylation site.
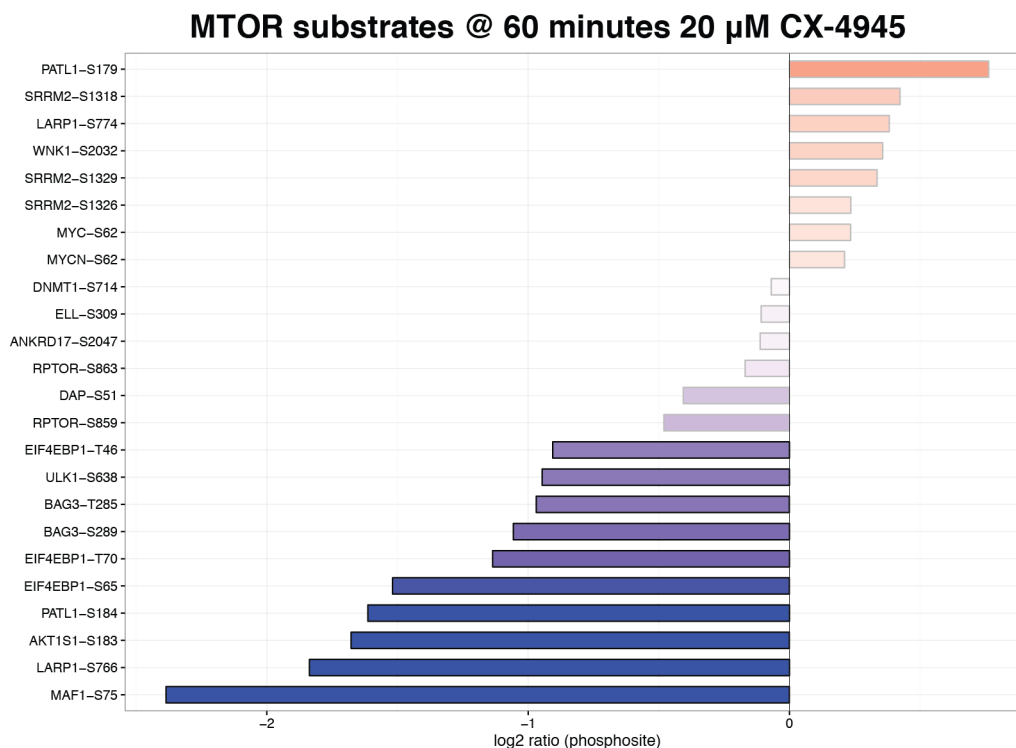
Figure 3.14 Quantified mTOR Phosphorylation Sites In PhosphoSitePlus from HeLa Cells Treated with 20 μM CX-4945.
Phosphorylation sites listed as mTOR substrates in PhosphoSitePlus database are presented. The mean log2 ratio from three biological replicates is used to calculate the change represented by each bar for a given phosphorylation site.
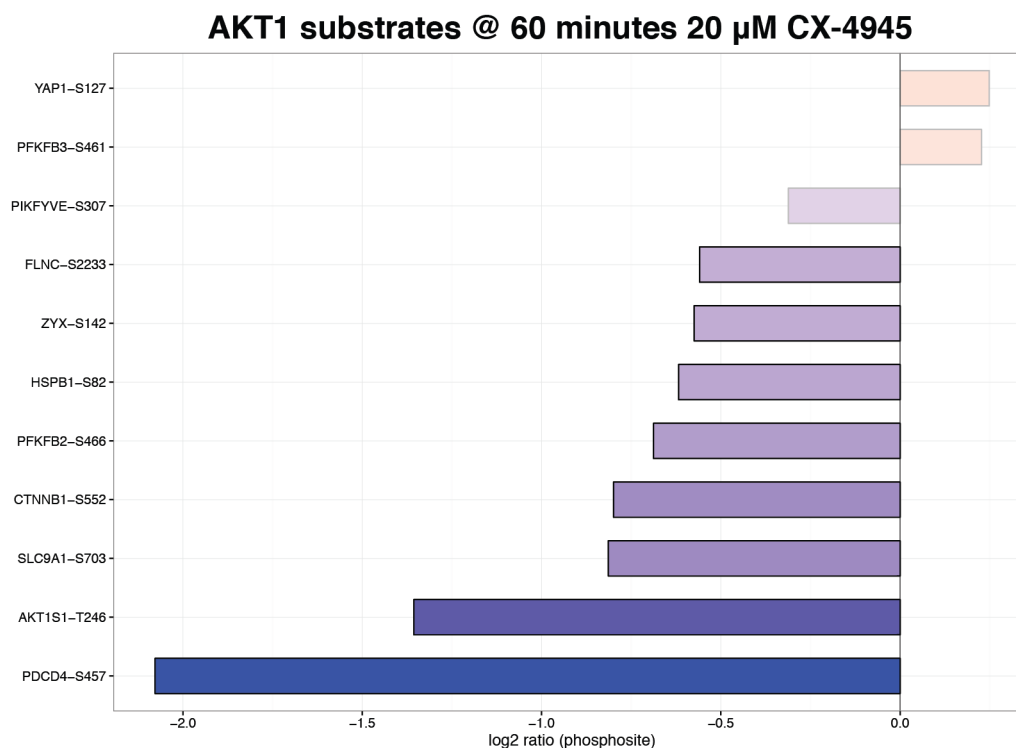
Figure 3.15 Quantified Akt Phosphorylation Sites in PhosphoSitePlus from HeLa Cells Treated with 20 μM CX-4945.
Phosphorylation sites listed as CK2 substrates in PhosphoSitePlus database are presented. The mean log2 ratio from three biological replicates is used to calculate the change represented by each bar for a given phosphorylation site.

substrates of CK2 that decrease in response to CX-4945 (Figure 3.13). Substrates of the mTOR and Akt kinases also decreased in phosphorylation (Figure 3.14-3.15) including EIF4EBP1 Thr46/Ser65/Thr70 and AKT1S1 Thr246, suggesting that CX-4945 down-regulates the mTOR/Akt pathways, although at this point it is unclear whether this is the result of a CK2-dependent or independent inhibition.

3.2.5 CX-4945 Impacts Distinct Biological Processes and Pathways in HeLa Cells

To investigate the biological processes and pathways that could be affected by CX-4945 treatment, gene enrichment analysis was performed using g:Profiler (129) and gene ontology (GO) terms for biological processes (139), KEGG pathways (140), and Reactome pathways (141) were queried. Statistically significant phosphorylation sites across the four time-point datasets were pooled into three groups: those with quantified ratios less than log2 -1 (i.e. a reduction in phosphorylation by more than 50%), greater than log2 +1 (increase in phosphorylation by two-fold) and those sites that were identified as CK2 substrates which decreased greater than log2 -1. Enriched terms were visualized using Cytoscape and the EnrichmentMap plugin (Figure 3.16-3.17 – and Supplemental Figure 3.14-3.15)(142). Processes that were identified from phosphorylation sites that decreased in response to CX-4945 treatment are involved in mTOR signaling, ribosome biogenesis, RNA splicing, cytoskeletal organization, chromosome condensation and nuclear envelope assembly (Figure 3.16 A). Processes that were identified from CK2 substrates were involved in DNA repair and translation (Figure 3.16 B). Processes that were identified from phosphorylation sites that increased in response to CX-4945 are involved in nuclear transport, RNA splicing, negative cell cycle regulation,
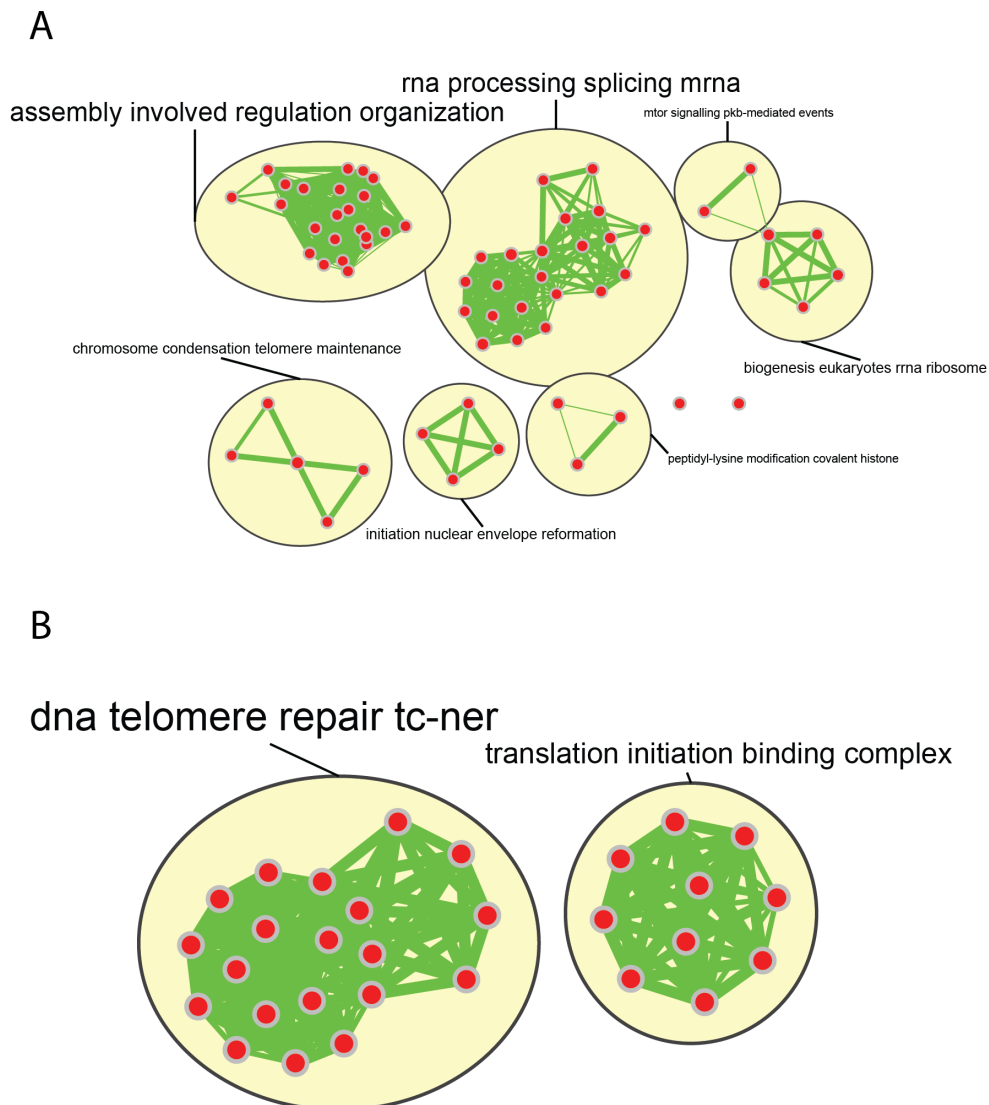
Figure 3.16 EnrichmentMap Network of Biological Processes Enriched from Decreasing Quantified Phosphorylation Sites Using g:Profiler.
Phosphorylation sites that decreased across all time-points greater than log2 -1 were used for gene enrichment using g:Profiler. Networks were constructed in Cytoscape with a similarity score cut-off of 0.5 and a FDR q value of 0.005. Nodes represent GO pathways, processes and functions and are connected by edges where edge thickness corresponds to the number of genes shared between two different nodes. Labels and font size correspond with overrepresented terms. (A) Phosphorylation sites that decreased in response to CX-4945. (B) Phosphorylation sites identified as CK2 using KinomeXplorer.
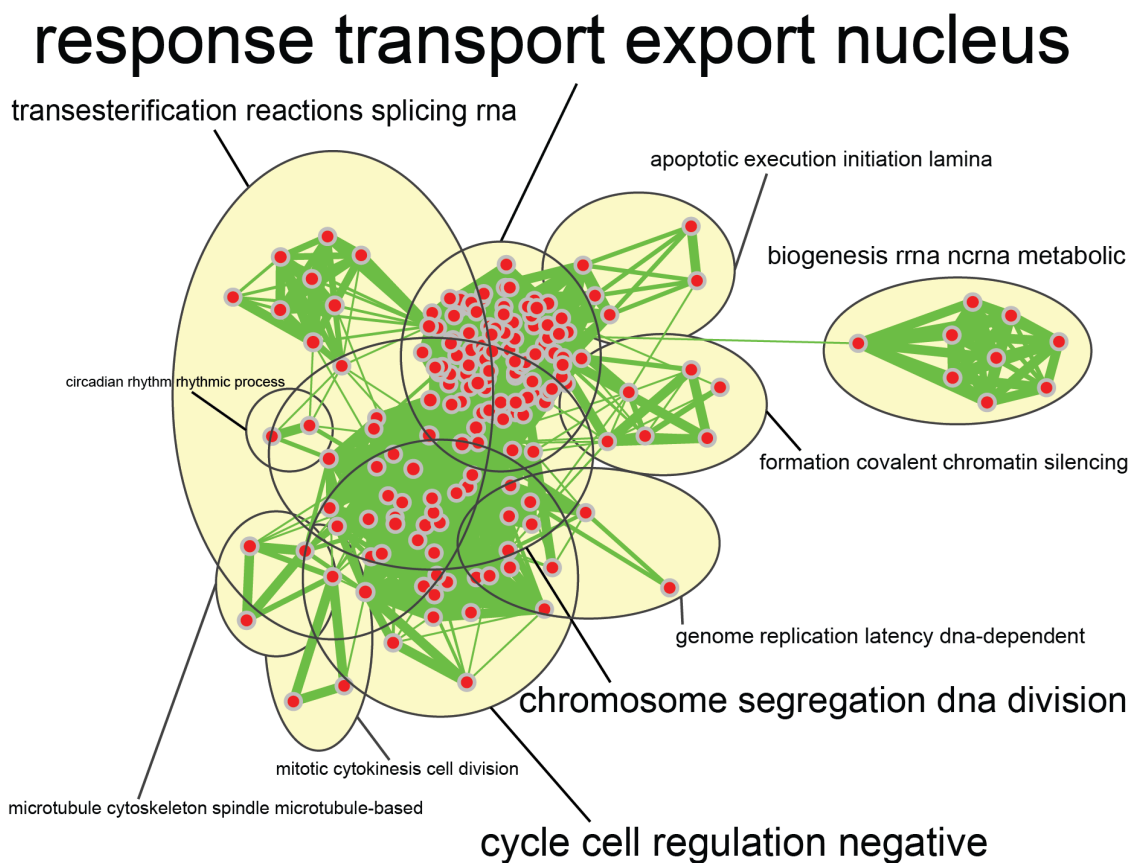
Figure 3.17 EnrichmentMap Network of Biological Processes Enriched from Increasing Quantified Phosphorylation Sites Using g:Profiler.
Phosphorylation sites that increased across all time-points greater than log2 +1 were used for gene enrichment using g:Profiler. Networks were constructed in Cytoscape with a similarity score cut-off of 0.5 and a FDR q value of 0.005. Labels and font size correspond with overrepresented terms.

74

apoptotic execution and microtubule regulation (Figure 3.17). The topology of the biological

processes and pathways that are affected by CX-4945 suggests a broad network that could be

regulated by CK2, however complementary sets within phosphorylation sites that decrease

and those that are CK2 substrates suggests divergent function of CX-4945 with respect to

CK2-dependent processes.

3.3   Discussion

Protein kinase CK2 expression is de-regulated in different types of human cancers, as

evidenced by a recent study of mRNA expression data in the Oncomine database (14). CK2

is implicated in the regulation of different cellular pathways by virtue of the identification of

protein substrates bearing the specificity determinants for phosphorylation (15). Given the

signaling network that CK2 is involved in, it has emerged as a therapeutic target. CX-4945 is

the first clinical-stage, orally-bioavailable small molecule ATP-competitive inhibitor of CK2

(44). Therefore, we sought to use phosphoproteomics to profile CX-4945 treatment in HeLa

cells to identify dynamic markers of CK2 activity and to monitor the effect of CK2 inhibition

on signaling pathways, in addition to profiling potentially divergent (CK2 independent)

functions of CX-4945 in cells.

Initial profiling of CX-4945 in HeLa cells revealed a window of time of up to 240

minutes where signaling events associated with apoptosis or DNA damage were not

activated, suggesting CX-4945 dependent effects would be the primary stimulus for signaling

events occurring. Utilizing a phospho-specific antibody for the bona fide CK2 substrate

EIF2S2, confirmation of CK2 inhibition suggested that CX-4945 treatment antagonized CK2

activity in HeLa cells. Subsequent analysis of quantified phosphorylation sites that changed

in response to CX-4945 in HeLa revealed several sites that displayed dynamic levels of

reduced phosphorylation to a greater extent than that of EIF2S2 Ser2. Among theses sites that change dramatically, a well-characterized substrate of CK2 such as TOP2A Ser1377 (135), decreased approximately 8 times more than DMSO vehicle treatment, suggesting that inhibition of CK2 was achieved. Utilizing KinomeXplorer and Phoxtrack, three phosphorylation sites matching the specificity determinants of CK2 were quantified from EIF2S2: Ser2, Ser67 and Thr111. Both Ser2 and Ser67 are annotated in the PhosphoSitePlus database as substrates of CK2 and both have been previously validated in experimental studies (134, 143). By comparison, although detected in previous studies, Thr111 as a substrate of CK2 has remained unexplored. Thr111 shows the largest change in response to CX-4945, and the rate of de-phosphorylation over the 240 minute treatment differs between Ser2 and Thr111 (Ser67 was not quantified in all time-points), suggesting differential activity towards these phosphorylation sites by protein phosphatases, given that CK2 has constitutive activity in cells (16). Ser2 and Ser67 have been identified as substrates of protein phosphatase-1 (144) while the phosphatase activity towards Thr111 remains to be determined. Ser2 has been characterized as a CK2β-dependent phosphorylation site and cannot be phosphorylated by the free catalytic subunit CK2α (11), which raises interesting questions regarding the de-phosphorylation of sites that are dependent on holo-enzyme activity versus catalytic subunits when cells are treated with an inhibitor of CK2. It should be noted that a few CK2 phosphorylation sites appear to increase in response to CX-4945 treatment. This may be the result of a loss of phosphorylation on a multiply-phosphorylated peptide which increases the stoichiometry of a corresponding doubly or singly phosphorylated peptide at a different phospho-acceptor residue on the peptide. This trend has been previously identified with a different inhibitor of CK2, quinalizarin (127). Another

possibility might be the proximity of other phospho-acceptor residues serving as specificity determinants for hierarchical phosphorylation by CK2 (145), that when de-phosphorylated result in an apparent increase in phosphopeptide containing the CK2 phosphorylation site. More importantly, the phosphorylation sites that demonstrate the largest change in de-phosphorylation not only serve as useful indicators of activity in cells but also provide further insight into the critical pathways that CK2 can regulate as these sites would be indicative of rapid turnover in regards to phosphatase activity. Previous investigations into large-scale phosphorylation stoichiometry in cells identified sites matching CK2 motifs possessing the highest phosphorylation stoichiometry in comparison to other kinases identified (146). The ability to quantify the proteome in parallel enabled the confident analysis of phosphorylation sites displaying dynamic regulation as it was determined that protein abundance during the length of CX-4945 treatment did not differ.

Treatment with CX-4945 results in a dynamic phosphoproteome, creating changes in phosphorylation sites that can be attributed to kinases other than CK2. Interestingly, CK2 can regulate the activity of other kinases through phosphorylation of cdc37 Ser13, which in conjuction with Hsp90 can stabilize client kinases (136). Quantification of cdc37 Ser13 phosphorylation did not change dramatically in response to CX-4945 treatment at 60 minutes, suggesting that the dynamic regulation of phosphorylation sites attributed to other kinases is not necessarily through a CK2-dependent inhibition mechanism via the phosphorylation status of cdc37 Ser13. Analysis of the phosphoproteome using PHOXTRACK revealed that the activity of kinases such as mTOR and Akt are down-regulated upon treatment with CX-4945. CK2 is known to phosphorylate Ser129 on Akt and this phosphorylation has been reported to contribute to Akt activity (147) which may provide

an explanation for the decreased phosphorylation of Akt substrates following CX-4945 treatment. Previous reports utilizing CX-4945 demonstrated down-regulation of mTOR substrates in different cancer lines after a period of 240 minutes (44, 51), and are in agreement with the phosphoproteomic data presented here. Long term treatment of CX-4945 can result in autophagy, as documented by Kim et al (148). Through phosphorylation of ULK1 Ser638, mTOR can repress autophagy activation (149), and given that ULK1 Ser638 decreased in phosphorylation after 60 minutes of CX-4945 treatment, the possibility for a CK2-independent activation of autophagy exists with CX-4945 treatment. Another interesting phosphorylation site that may be attributable to mTOR activity is EIF5B Ser214, which showed drastic de-phosphorylation in response to CX-4945 but displays specificity determinants for CK2. A recent study investigating the phosphoproteome in cells treated with rapamycin for 2 hours found decreased phosphorylation of EIF5B Ser214, suggesting this site is a target of mTOR (150). This information raises speculation about the promiscuity of CX-4945 in cultured human cells, although IC_{50} values for kinases in the PI3K/Akt pathway and mTOR that were assayed *in vitro* were more than 500 times higher than for CK2 (44).

Phosphorylation sites that showed an increase in response to CX-4945 treatment were attributed to CDK1 and CDK2 kinases. These results are interesting considering that CK2 is known to phosphorylate Cyclin H in the Cyclin-dependent kinase (CDK) Activating Complex (CAK) to regulate the activity of this complex (151), which is required for cell cycle progression through phosphorylation of CDK1 and CDK2 at Thr160/161 (reviewed in (152)). Inhibition of CK2 would suggest a decrease in CAK activity and therefore a decrease in CDK1 and CDK2 activity. One plausible consideration is the activity of phosphatase cdc25C, which can remove inhibitory phosphorylation at Thr14 and Tyr15 (reviewed in

(153)). Phosphorylation of cdc25C by CK2 at Thr236 results in delayed cytoplasmic-to-nuclear transfer of cdc25C, and inhibition of CK2 *in vivo* results in enhanced nuclear localization (154), consistent with the suggestion that treatment with CX-4945 inhibits CK2 phosphorylation of cdc25C, enabling increased activity towards the removal of inhibitor phosphorylation on CDK1 and CDK2. More recent experiments investigating cdc25C expression levels determined that long-term treatment with CK2 inhibitors actually decreases the levels of cdc25C and CDK1 (155). Given the short period of time in which HeLa cells are treated with CX-4945 in this phosphoproteomic investigation, and the utilization of an asynchronous population, subtle differences in cell cycle regulation may be more apparent in comparison to cells that have been treated for extended periods of time with inhibitor.

A topological analysis of biological processes and pathways affected by CX-4945 performed using gene enrichment analysis revealed widespread impact on the phosphoproteome. The enrichment of terms from biological processes derived from phosphorylation sites which increased were nuclear transport, RNA splicing, negative cell cycle regulation, apoptotic execution and microtubule regulation. Not surprisingly, CK2 is known to oppose apoptosis, given that it can translocate to the nucleus following DNA damage (37) and overexpression of CK2α can promote resistance to TRAIL-induced apoptosis (34, 156, 157). The large number of phosphorylation sites that increase on proteins enriched in these pathways can be interpreted as an extensive cellular response to CX-4945, attributable to the inhibition of not only CK2 but through the up-regulation and de-regulation of kinases in response to CX-4945.

Phosphorylation sites that decreased were located on proteins involved in mRNA splicing, mTOR signaling, cytoskeletal organization, chromosome maintenance and nuclear

envelope formation. It is interesting to note that a recent report demonstrated that CX-4945 regulated mRNA splicing independent of CK2 inhibition and that this could be attributed to the inhibition of Clk (Cdc2-like-kinase) kinases (158), although CK2 is known to phosphorylate and regulate the activity of RNA splicing activator RNPS1 (159) and has a large number of *in vitro* proteins that are involved in splicing (160). The enrichment of processes specific to proteins identified as CK2 substrates that decreased in response to CX-4945 was divergent from the group of phosphorylation sites that decreased overall, with enrichment in DNA repair and translation processes. CK2 constitutively phosphorylates several proteins involved in DNA repair, such as XRCC1 (161), XRCC4 (39), and MDC1 (29), which generates binding sites for FHA (Fork-head associated) domains to recruit other factors to sites of DNA repair. These data collectively suggest that inhibition of CK2 with CX-4945 in HeLa cells primarily results in drastic de-phopshorylation of proteins involved in DNA repair and translation, with secondary effects that are putatively CK2-independent with respect to processes involved with mRNA splicing and mTOR signaling for that matter.

The investigation of CX-4945 using phosphoproteomics in HeLa cells has revealed a substantial impact of this CK2 inhibitor in the regulation of phosphorylation of protein involved in broad range of biological processes. Utilizing bioinformatics tools, the identification of dynamic markers of CK2 activity was achieved; noting that many of these phosphorylation sites exhibited de-phosphorylation of a greater magnitude than previously standardized substrates. A number of interesting responses in the phosphoproteome were elicited, with many of these changes in phosphorylation sites attributed to other kinases, suggesting a divergence of specificity for CX-4945 in HeLa cells. Taken together these

findings demonstrate the utility of phosphoproteomics to characterize the effects of a small-molecule ATP-competitive inhibitor.

3.4 Experimental Methods

3.4.1 Cell Culture, Lysis & Western Blotting for Preliminary 24 Hour CX-4945 Treatment

HeLa Tet-Off cells (Clontech) were cultured in Dulbecco's modified Eagle's medium (DMEM) (Corning) containing 10 % FBS, penicillin (100 U/mL) and streptomycin (100 µg/mL) on 10 cm dishes. Cells were treated with 20 µM CX-4945 (MedKoo Biosciences) from at various intervals from 1 to 24 hours. Media was vacuum-aspirated and cells were washed with ice cold PBS, followed by lysis on ice [1% octyl-β-D-glucopyranoside (Sigma-Aldrich), 50 mM Tris (tris(hydroxymethyl)aminomethane) (Bioshop) pH 8.5, 6 M urea (Sigma-Aldrich), 25 mM β-glycerophosphate (Bioshop), 1 µM okadaic acid (Bioshop), 50 mM sodium fluoride (Sigma-Aldrich), 1 µM microcystin-LR (Cayman Chemical), 10 mM sodium orthovanadate (Sigma-Aldrich), 5 mM sodium pyrophosphate (Sigma-Aldrich), pepstatin (10 µg/mL) (Sigma-Aldrich)]. Samples were sonicated 2 x 15 seconds on ice then spun for 10 minutes at 16,000 x g at 4 °C. The supernatant was retained and protein concentration was determined using a Bradford assay (Bio-Rad). An equal amount of each sample (20 µg) was loaded per lane and separated by SDS-PAGE. Proteins were transferred to PVDF membrane (Millipore) using a wet-transfer apparatus (Bio-Rad) at 400 mA for 60 minutes at 4 °C followed by incubation in blocking buffer (LI-COR Biosciences) for 60 minutes. Primary antibodies were incubated overnight at 4 °C in 3% BSA-TBST or 3% BSA-PBST. Antibodies against PARP (9542, Cell Signaling Technologies), γH2AX S139 (ab26350, Abcam), GAPDH (MAB374, Millipore) and pEIF2S2 S2 (YenZym Laboratories,

raised against ac-pS-GDEMIFDPTMSKC-amide) were used. Secondary antibodies used were GAR-800 (926-32211), GAM-800 (926-32210), and GAM-680 (926-32220) (LI-COR Biosciences) in 3% BSA-TBST or 3% BSA-PBST, with incubation for 45 minutes. Following 3 x 5 minute washes with TBST or PBST, membranes were scanned using an Odyssey scanner (LI-COR Biosciences) at 700 nm and 800 nm wavelengths. Raw data scans were loaded into ImageStudioLite v5.2.5 (LI-COR Biosciences) and exported as .TIFF image files.

3.4.2   SILAC Medium Formulation

SILAC-dropout DMEM (Life Technologies) lacking L-arginine, L-lysine and L-glutamine was supplemented with isotope-encoded L-arginine ($^{13}C_6$) and L-lysine (4,4,5,5-D4) (Cambridge Isotope Laboratories Inc.) at respective concentrations of 86.2 mg/L (0.398 mM) and 61.16 mg/L (0.274 mM) to create a "heavy" medium. "Light" medium was created using the SILAC-dropout DMEM by supplementing with equivalent molar amounts of unlabeled L-arginine (83.9 mg/L) and L-lysine (60.04 mg/L). All media used for SILAC studies were supplemented with 10% 10 kDa-dialyzed FBS (Corning), penicillin (100 U/mL), streptomycin (100 mg/mL), L-glutamine (2 mM) (Life Technologies), and L-proline (400 mg/L) (Cambridge Isotope Laboratories Inc.) in order to prevent arginine to proline conversion (131, 162). Media was filter-sterilized prior to use for cell culture.

3.4.3   SILAC Incorporation of HeLa Tet-Off Cells

HeLa Tet-Off cells were adapted over a period of 7 days with 3 sub-passages after being switched to SILAC medium. An aliquot of protein lysate from heavy labeled cells was precipitated using 6 sample volumes of 10% TCA in acetone (v/v) and digested on-pellet (refer to Chapter 2.4.7 for digestion procedure). Trypsin-Lys-C (Promega) at 200:1 (w/w)

was used for the first 4 hour digestion step and Trypsin at 100:1 (Pierce) was used for the overnight incubation step. Digested peptides were desalted using a C18 StageTip (Empore) (163). LC-MS/MS parameters for data acquisition followed those presented in Chapter 2.4.10, with data acquisition performed on an Orbitrap Elite mass spectrometer. Raw spectra were analyzed using MaxQuant v1.5.3.8 (70, 71, 164) and searched against the Swissprot-Uniprot sequence database (*homo sapiens* taxon, accessed on December 26, 2015). Samples were searched using a Multiplicity set to 2, with "heavy" labels selected as Arg6 and Lys4. Mass tolerances were set to 4.5 ppm for the parent ion mass (MS) and 0.5 Da for the fragment ion mass (MS/MS). The minimum number of amino acids in a peptide was set to 7, with a peptide spectrum match (PSM) and protein match set to 1% FDR and protease selectivity for trypsin/P. A maximum number of 3 missed cleavages was selected. The number of variable modifications per peptide was 5, with methionine oxidation (+15.9949), protein N-terminus acetylation (+42.0105), asparagine and glutamine deamidation (+0.9840 Da) selected. Cysteine carbamidomethylation (+ 57.0215) was set as a fixed modification. Re-Quantify option was turned on. The minimum score for modified peptides was set to 40, and the decoy-database setting was "Revert." Output data from MaxQuant was then loaded into Perseus version 1.5.2.6 (121). The "evidence.txt" file was used to extract information about peptides that were quantified in MS1 and identified in MS2, from which reverse hits and contaminants were removed. The heavy and light intensity values from MS1 quantitation were used to calculate H/L ratios. Two formulae were applied to calculate the incorporation for each peptide: H/L ratios larger than 1 were calculated with (100 − (1/ratio)*100), and ratios less than 1 were calculated with (ratio * 100). The median of all incorporation values

for each individual SILAC pair was calculated and represents the incorporation efficiency for the labeled amino acids.

3.4.4 CX-4945 Treatment and Lysis of SILAC HeLa Tet-Off Cells

HeLa Tet-Off cells were cultured in heavy or light-labeled SILAC medium. Cells were maintained in 15 cm cell culture plates until reaching approximately 80% confluence. Heavy labeled cells were treated with 20 μM CX-4945 (MedKoo Biosciences) for 60, 135, 180 and 240 minutes, with light labeled cells treated with DMSO vehicle. Three 15 cm plates (representing three independent biological replicates) were harvested for each labeled population for each time-point. Following treatment, media was vacuum-aspirated and cells were washed with ice cold PBS, followed by lysis on ice in 750 μL of lysis buffer [1% octyl-β-D-glucopyranoside (Sigma-Aldrich), 50 mM Tris (tris(hydroxymethyl)aminomethane) (Bioshop) pH 8.5, 6 M urea (Sigma-Aldrich), 25 mM β-glycerophosphate (Bioshop), 1 μM okadaic acid (Bioshop), 50 mM sodium fluoride (Sigma-Aldrich), 1 μM microcystin-LR (Cayman Chemical), 10 mM sodium orthovanadate (Aldrich), 5 mM sodium pyrophosphate (Sigma-Aldrich), pepstatin (10 μg/mL) (Sigma-Aldrich)]. Samples were sonicated for 2 x 15 seconds on ice then spun for 10 minutes at 16,000 x g at 4 °C. The supernatant was retained and protein concentration was determined using a Bradford assay (Bio-Rad). Samples were frozen at – 80 °C until processing.

3.4.5 Western Blotting of CX-4945 Treated Samples for Phosphoproteomics

An equal amount of each sample (20 μg) was loaded per lane and separated by SDS-PAGE. Proteins were transferred to PVDF membrane (Millipore) using a wet-transfer apparatus (Bio-Rad) at 400 mA for 60 minutes at 4 °C followed by block in blocking buffer (LI-COR Biosciences) for 60 minutes. Primary antibodies were incubated overnight 4 °C in 3% BSA-

TBST or 3% BSA-PBST. Antibodies against PARP (9542, Cell Signaling Technologies), γH2AX S139 (ab26350, Abcam), GAPDH (MAB374, Millipore), pATM S1981 (ab81292, Abcam), hVIN1 (V9131, Sigma) and pEIF2S2 S2 (YenZym Laboratories, raised against ac-pS-GDEMIFDPTMSKC-amide) were used. Secondary antibodies used were GAR-800 (926-32211), GAM-800 (926-32210), and GAM-680 (926-32220) (LI-COR Biosciences) in 3% BSA-TBST or 3% BSA-PBST, with incubation for 45 minutes. Data was acquired as previously outlined in Chapter 3.4.1. Lysates derived from unlabeled HeLa Tet-Off cells treated with staurosporine (2 μM) (LC Laboratories), 20 ng/mL neocarzinostatin (Sigma), or DMSO (Fisher) for 3 hours were used as controls.

3.4.6 Sample Digestion and Phosphopeptide Enrichment

Prior to sample processing, 2 mg of protein lysate derived from light labeled cells (DMSO treated) and 2 mg of protein lysate derived from heavy labeled cells (CX-4945 treated) from each respective biological replicate was mixed, resulting in 12 samples. Samples were then processed using protein precipitation, and digested following the methods outlined in Chapter 2.4.7 with some alterations. Trypsin-Lys-C (Promega) at 200:1 (w/w) was used for the first 4 hour digestion step and Trypsin at 100:1 (Pierce) was used for the overnight incubation step. Phosphopeptides were enriched following the methods outlined in Chapter 2.4.8.

3.4.7 LC-MS/MS Data Acquisition

Samples were analyzed using an Orbitrap Elite Hybrid Ion Trap-Orbitrap mass spectrometer using the acquisition parameters and settings previously described in Chapter 2.4.10. Three biological replicates per time-point were analyzed in technical duplicate, generating a total of 96 raw mass spectra files. Raw mass spectra files were analyzed in MaxQuant version 1.5.3.8

(70, 71, 164) and searched against the Swissprot-Uniprot sequence database (*homo sapiens* taxon, accessed on December 26, 2015). Samples were searched using a Multiplicity set to 2, with "heavy" labels selected as Arg6 and Lys4. Mass tolerances were set to 4.5 ppm for the parent ion mass (MS) and 0.5 Da for the fragment ion mass (MS/MS). The minimum number of amino acids in a peptide was set to 7, with a peptide spectrum match (PSM) and protein match set to 1% FDR and protease selectivity for trypsin/P. A maximum number of 3 missed cleavages was selected. The option for second peptide search was selected, as was the use of "Match Between Runs" for respective pairs of samples between biological replicates, using the default matching parameters. Raw mass spectra files were defined as separate groups using the experimental setup option. Cysteine carbamidomethylation (+ 57.0215 Da) was set as a fixed modification. For phosphopeptide samples, the number of variable modifications per peptide was 6, with methionine oxidation (+15.9949 Da), protein N-terminus acetylation (+42.0105 Da), asparagine and glutamine deamidation (+0.9840 Da) and serine, threonine, and tyrosine phosphorylation (+79.9663) selected. For proteome samples the maximum number of variable modifications was set to 5, and phosphorylation as a variable modification was excluded from these samples. The minimum score for modified peptides was set to 40, and the decoy-database setting was "Revert." For quantification of protein groups, unmodified peptides and those with carbamidomethylation, methionine oxidation, protein N-terminus acetylation or asparagine and glutamine deamidation were included. Peptides for which the corresponding heavy or light modified peptide were not quantified were excluded from the protein groups quantitation. Output data from MaxQuant was then loaded into Perseus version 1.5.2.6 (121). For the analysis of proteome data, the "proteinGroups.txt" file was first processed to remove entries marked as reverse decoy

database hits, contaminants, and protein identifications that were only matched to modified peptides. MaxQuant-generated normalized ratios were utilized, and the log base 2 of the normalized ratios was calculated for each protein. Proteins were considered identified in each biological replicate if identified in at least one of two technical replicates. For the analysis of the phosphoproteome data, the "Phospho (STY)Sites.txt" file was first processed to remove entries marked as reverse decoy database hit and contaminants, and filtered to only contain phosphorylation sites with localization probability greater than 0.75. Phosphorylation sites were expanded in Perseus to obtain information from instances of quantified sites being derived from singly, doubly and triply-phosphorylated peptides. Rows where no quantification was present were removed, and phosphorylation sites were considered quantified in each biological replicate if they were identified in at least one of two technical replicates.

3.4.8   Data Analysis

A one-sample Student's t-test with multiple hypothesis correction using Benjamini Hochberg FDR = 0.05 was used to identify statistically significant phosphorylation sites that responded to CX-4945 treatment for each respective time-point dataset. A list of all phosphosites identified with putative upstream kinases was generated using KinomeXplorer (77) following criteria outlined in Schoof *et al.* (165) for kinase prediction and filtering, excluding prediction scores for a phosphorylation site that was less than 1 and predicting only one kinase per site. Phosphoproteomic and proteomic data were visualized using the ggplot2 package within the R framework (v3.2.3). PHOXTRACK (128) was used to identify kinase-substrate relationships that are indicative of up or down-regulation of kinases. The PhosphositePlus database (138, 166) was queried with uploaded mean log2 ratios of

phosphorylation sites from each time-point dataset. An unweighted Kolmogorov-Smirnov running sum statistic was calculated for the query list of phosphorylated sites with the number of permutations set to 10,000 and the minimum number of phosphosites per kinase set to 3 with, retaining kinase hits which were < 0.25 FDR and the respective information of the phosphorylation mark with the upstream kinase. To perform gene enrichment analysis, statistically significant phosphorylation sites across all time-points were grouped together into three groups: sites which increased greater than log2 ratio 1, sites which decreased greater than log2 ratio -1, and sites that decreased greater than log2 -1 and were identified as CK2 phosphorylation sites. Gene identifiers from these phosphorylation sites were queried with g:Profiler (129), using the following parameters: the minimum and maximum size of functional category was 5 and 500 respectively, no electronically inferred GO annotations, only significant hits displayed, hierarchical filtering enabled, minimum size of gene list and functional category overlap was 2, significance threshold was set to Benjamini Hochberg and GO biological process, KEGG pathways and Reactome pathways were queried. The output was saved in generic enrichment map format and loaded into Cytoscape v3.3.0 (167). Enriched biological processes and pathways were visualized using the EnrichmentMap v2.1.0 plugin (142), building the network with minimum similarity score of 0.5 and maximum q-value (FDR adjusted P value) of 0.005 The AutoAnnotate v1.1.0 plugin (168) was used to generate word-clouds depicting over-represented terms in the biological processes and pathways that were clustered together in order to summarize terms for each cluster.

3.5 Supplemental Figures

HeLa-Tet Off SILAC Amino Acid Incorporation

Median Incorporation = 96.47 %
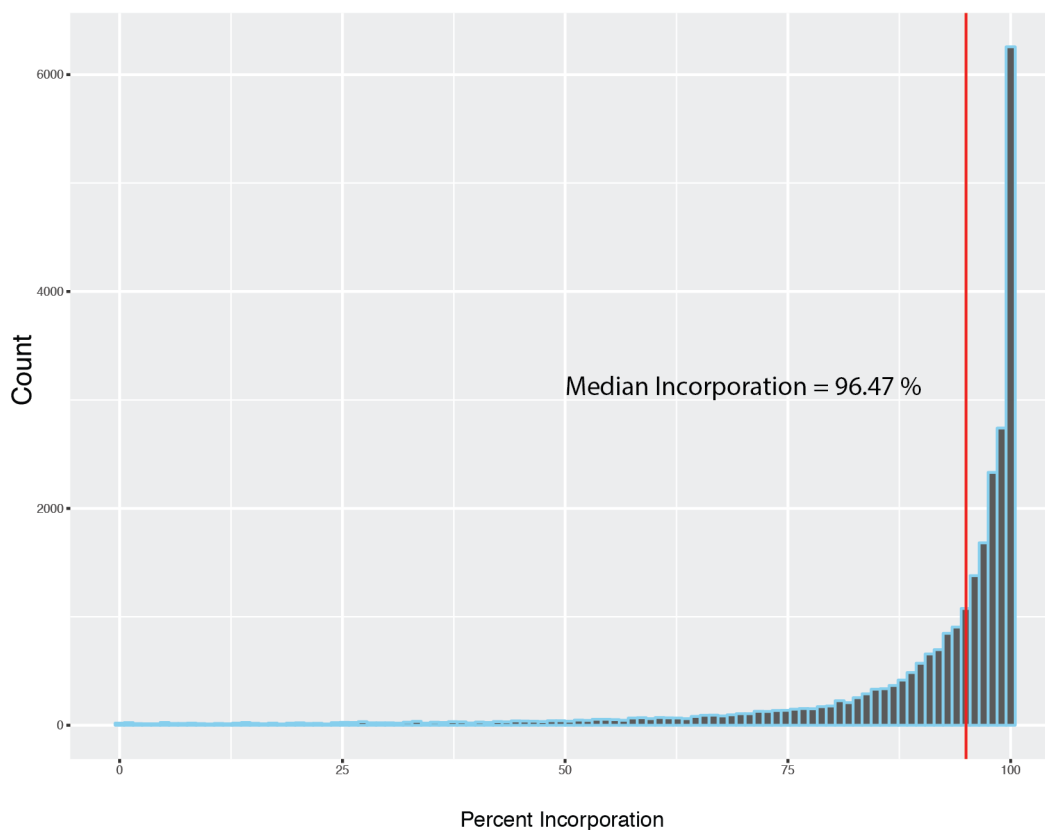
Supplemental Figure 3.1 Frequency Distribution of SILAC Arginine and Lysine Incorporated Peptides.
HeLa cells were adapted in SILAC medium over 7 days with 3 sub-passages. An aliquot of heavy labeled cells was processed as described in 3.4.3. Distribution is representative of all arginine and lysine peptides that were quantified. Red vertical line indicates 95% incorporation. Median incorporation was calculated as 96.47 %.
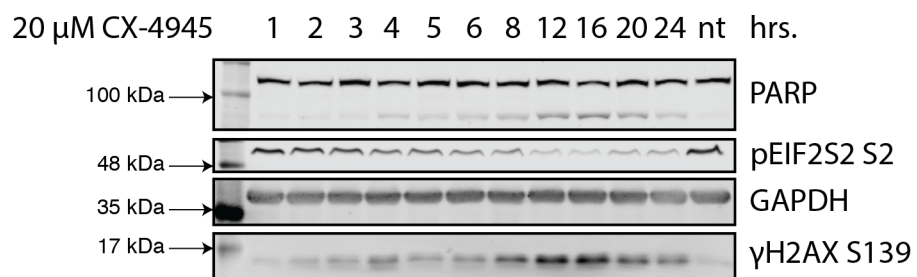
Supplemental Figure 3.2 Preliminary Time-Course Treatment of HeLa Cells with 20 µM CX-4945.
HeLa cells were treated for intervals up to 24 hours with CX-4945 followed by lysis. Lysates were separated by SDS-PAGE, transferred and western blotted using antibodies against PARP, GAPDH, γH2AX and phospho-EIF2S2. Refer to 3.4.1 for methods.

t (min)	60		135		180		240		180		
20 ng/mL NCS	-	-	-	-	-	-	-	-	-	-	+
2 µM STS	-	-	-	-	-	-	-	-	-	+	-
20 µM CX-4945	-	+	-	+	-	+	-	+	-	-	-

pATM S1981
245 kDa

135 kDa — VIN1

100 kDa — PARP

48 kDa — pEIF2S2 S2

35 kDa — GAPDH

17 kDa
γH2AX S139
11 kDa

Biological Replicate 1
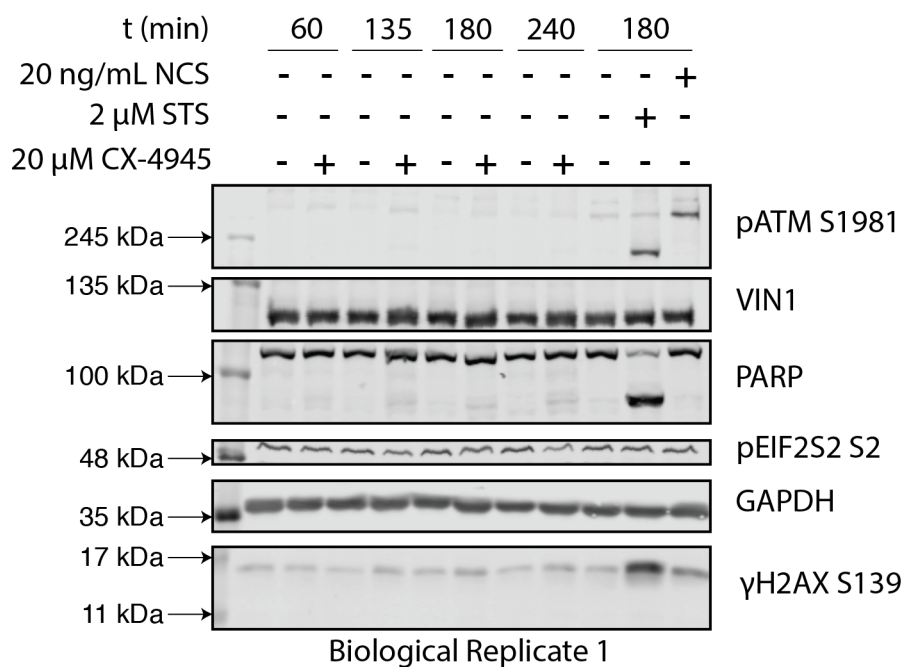
Supplemental Figure 3.3 Biological Replicate 1 of SILAC Labeled Cells Treated with CX-4945 and Analyzed by LC-MS/MS.
Heavy labeled HeLa cells were treated with 20 µM CX-4945 and light labeled cells were treated with DMSO for indicated times. HeLa cells treated with staurosporine (STS) or neocarzinostatin (NCS) served as positive controls. Refer to 3.4.5 for methods.
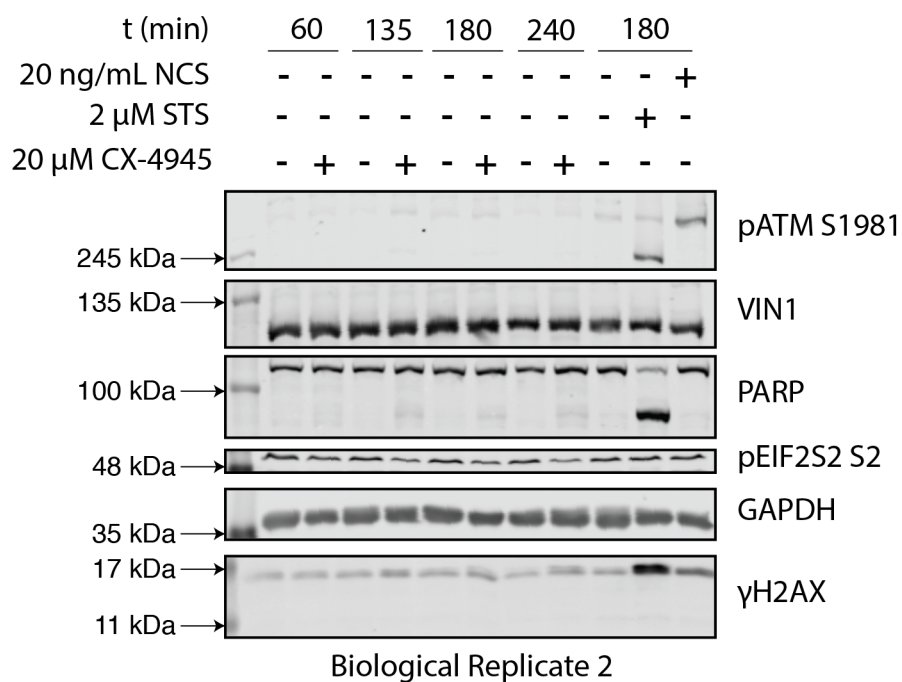
Supplemental Figure 3.4 Biological Replicate 2 of SILAC Labeled Cells Treated with CX-4945 and Analyzed by LC-MS/MS.
Heavy labeled HeLa cells were treated with 20 μM CX-4945 and light labeled cells were treated with DMSO for indicated times. HeLa cells treated with staurosporine (STS) or neocarzinostatin (NCS) served as positive controls. Refer to 3.4.5 for methods.

t (min)	60		135		180		240		180		
20 ng/mL NCS	-	-	-	-	-	-	-	-	-	-	+
2 µM STS	-	-	-	-	-	-	-	-	-	+	-
20 µM CX-4945	-	+	-	+	-	+	-	+	-	-	-
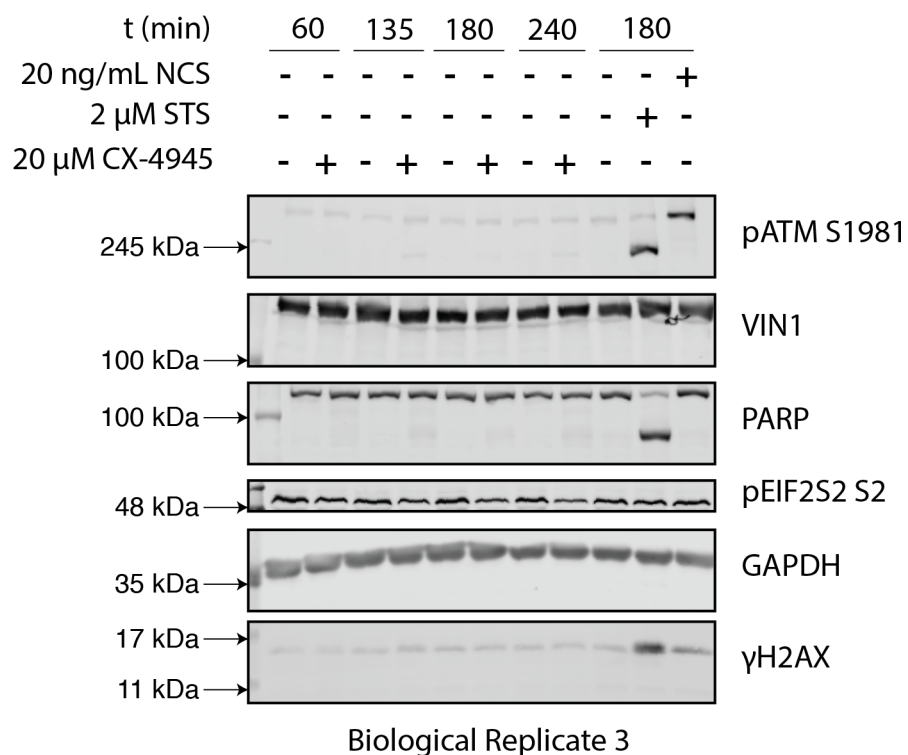
Supplemental Figure 3.5 Biological Replicate 3 of SILAC Labeled Cells Treated with CX-4945 and Analyzed by LC-MS/MS.
Heavy labeled HeLa cells were treated with 20 µM CX-4945 and light labeled cells were treated with DMSO for indicated times. HeLa cells treated with staurosporine (STS) or neocarzinostatin (NCS) served as positive controls. Refer to 3.4.5 for methods.
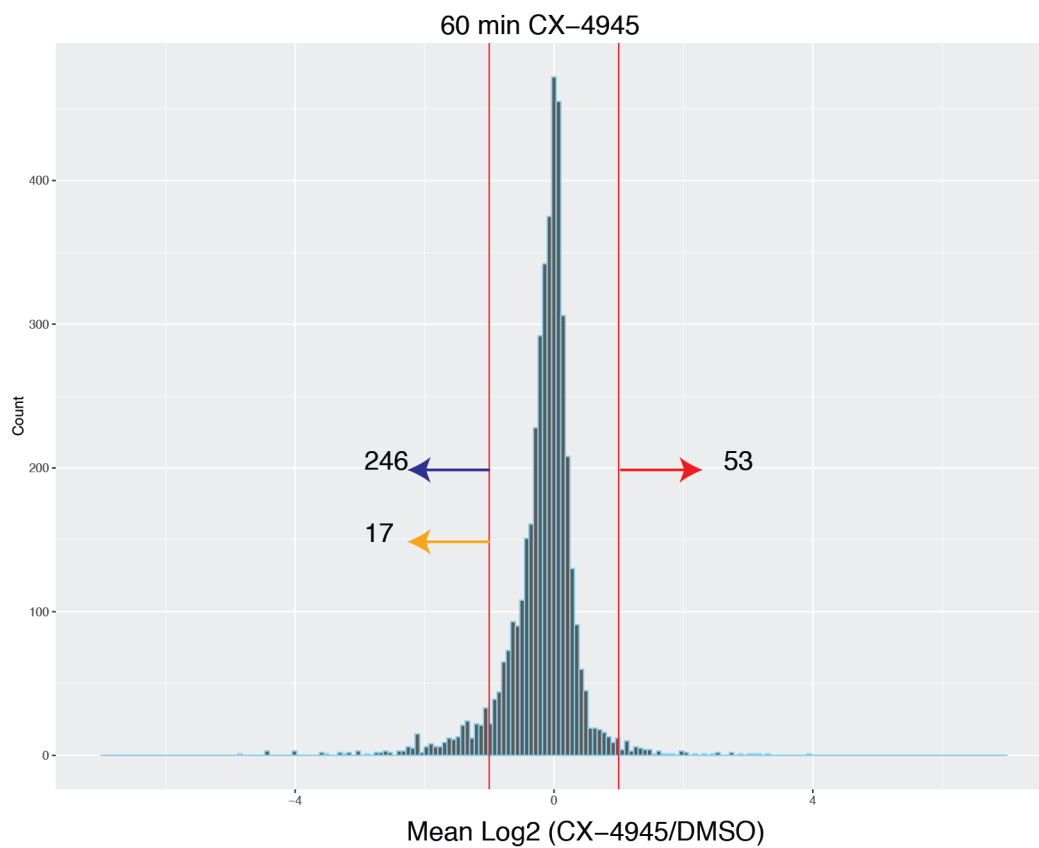
Supplemental Figure 3.6 Frequency Distribution of Phosphorylation Site Mean Log2 Ratio In HeLa Cells Treated with CX-4945 for 60 Minutes.
The mean log2 ratio of three biological replicates for each site identified and quantified is represented in this frequency distribution of all quantified sites from HeLa cells treated with 20 μM CX-4945 for 60 minutes. Numbers correspond to sites down or up-regulated in Figure 3.2 C. Coloured arrows correspond to increasing, decreasing or decreasing CK2 sites.
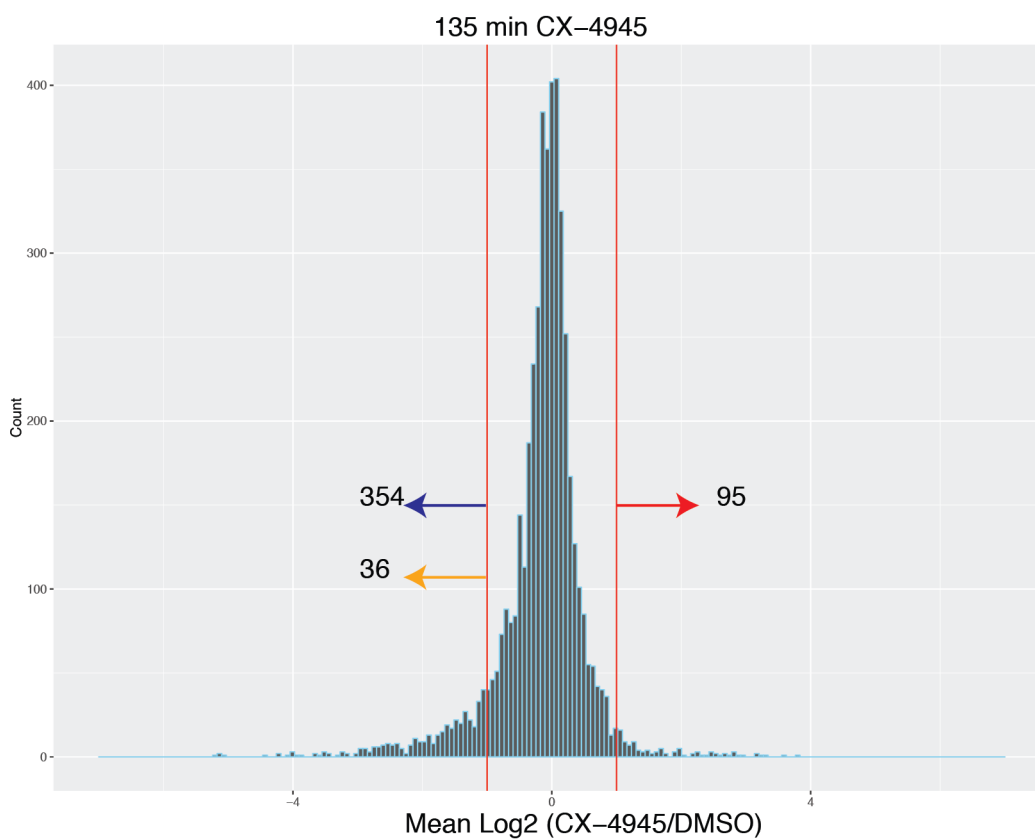
135 min CX−4945

Supplemental Figure 3.7 Frequency Distributino of Phosphorylation Site Mean Log2 Ratio In HeLa Cells Treated with CX-4945 for 135 Minutes.
The mean log2 ratio of three biological replicates for each site identified and quantified is represented in this frequency distribution of all quantified sites from HeLa cells treated with 20 μM CX-4945 for 135 minutes. Numbers correspond to sites down or up-regulated in Figure 3.2 C. Coloured arrows correspond to increasing, decreasing or decreasing CK2 sites.
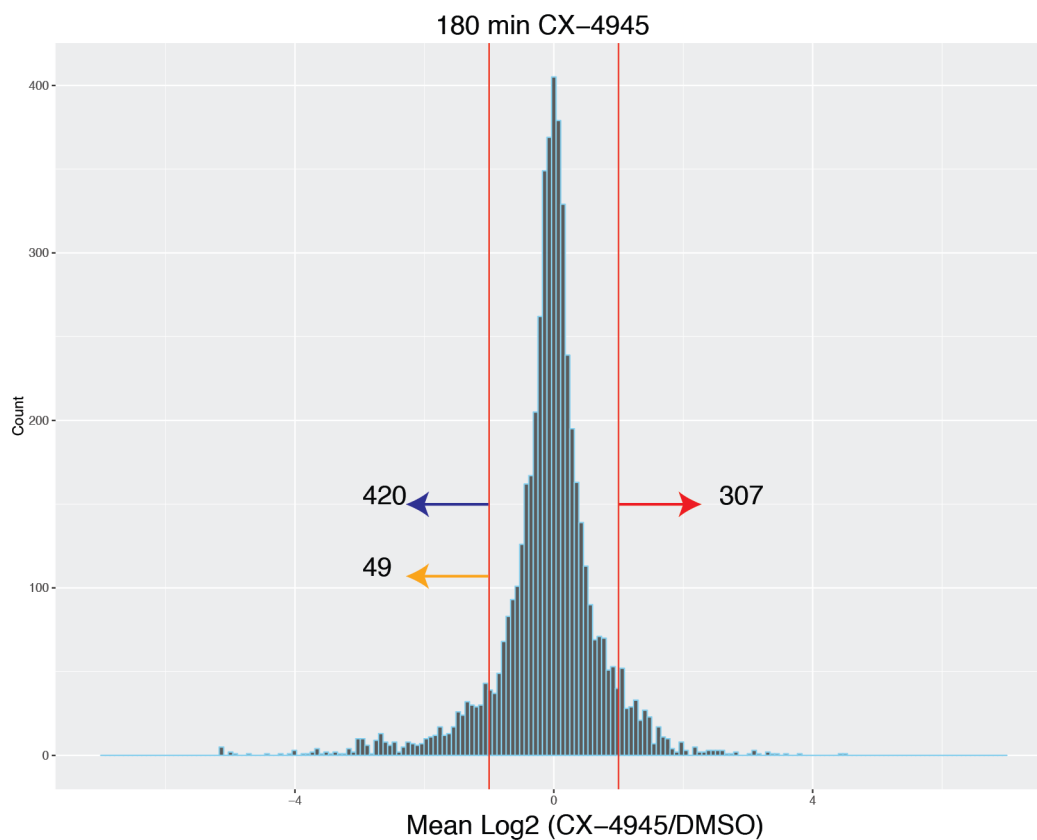
Supplemental Figure 3.8 Frequency Distribution of Phosphorylation Site Mean Log2 Ratio In HeLa Cells Treated with CX-4945 for 180 Minutes.
The mean log2 ratio of three biological replicates for each site identified and quantified is represented in this frequency distribution of all quantified sites from HeLa cells treated with 20 μM CX-4945 for 180 minutes. Numbers correspond to sites down or up-regulated in Figure 3.2 C. Coloured arrows correspond to increasing, decreasing or decreasing CK2 sites.
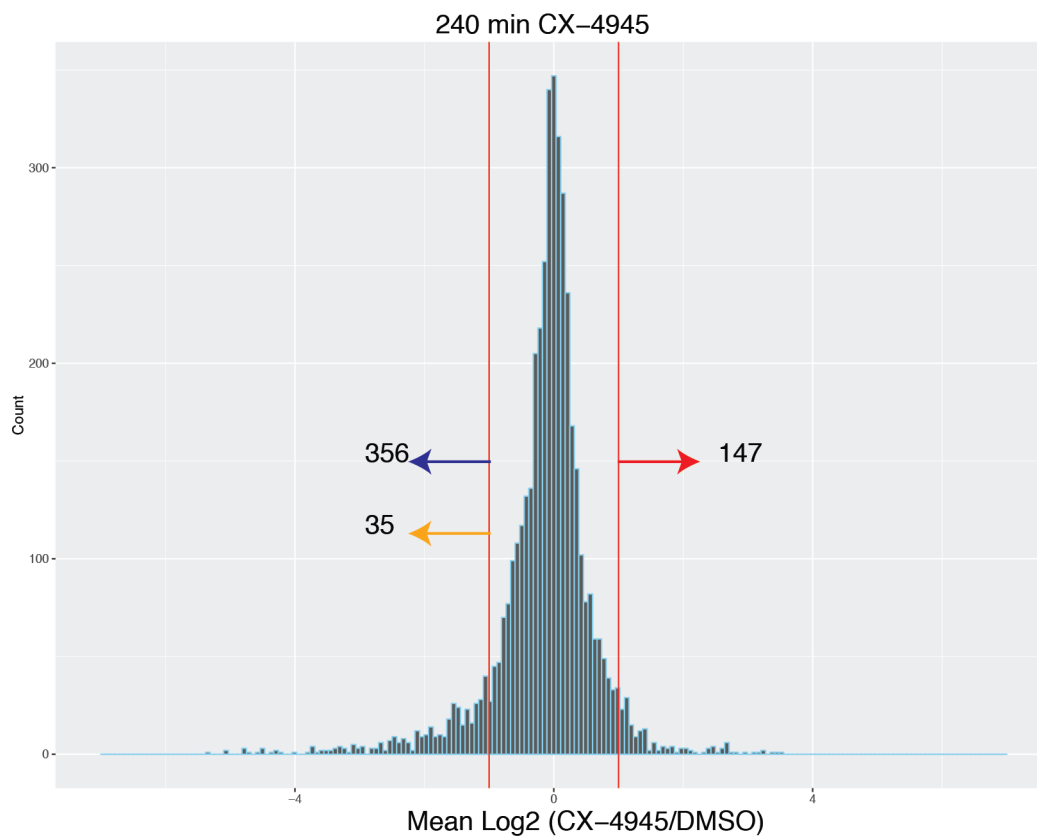
Supplemental Figure 3.9 Frequency Distribution of Phosphorylation Site Mean Log2 Ratio in HeLa Cells Treated with CX-4945 for 240 Minutes.
The mean log2 ratio of three biological replicates for each site identified and quantified is represented in this frequency distribution of all quantified sites from HeLa cells treated with 20 μM CX-4945 for 240 minutes. Numbers correspond to sites down or up-regulated in Figure 3.2 C. Coloured arrows correspond to increasing, decreasing or decreasing CK2 sites.
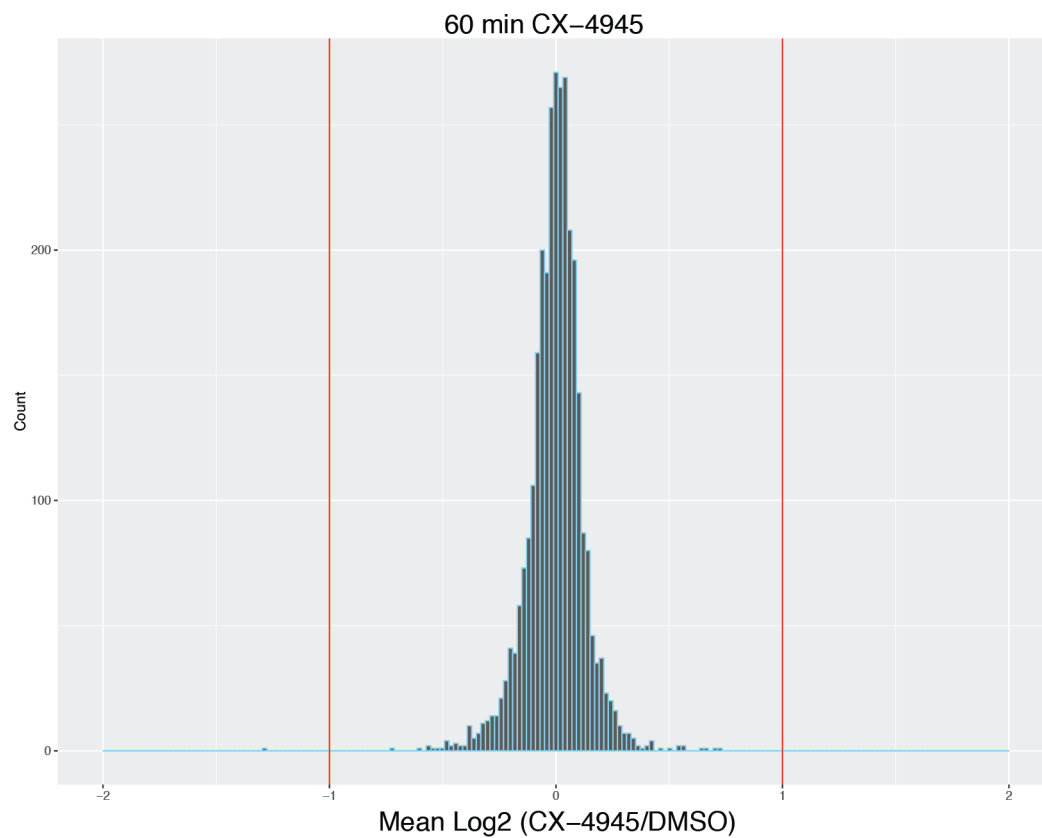
Supplemental Figure 3.10 Frequency Distribution of Protein Mean Log2 Ratio in HeLa Cells Treated with CX-4945 for 60 Minutes.
The mean log2 ratio of three biological replicates for each protein identified and quantified is represented in this frequency distribution of all quantified proteins from HeLa cells treated with 20 μM CX-4945 for 60 minutes.
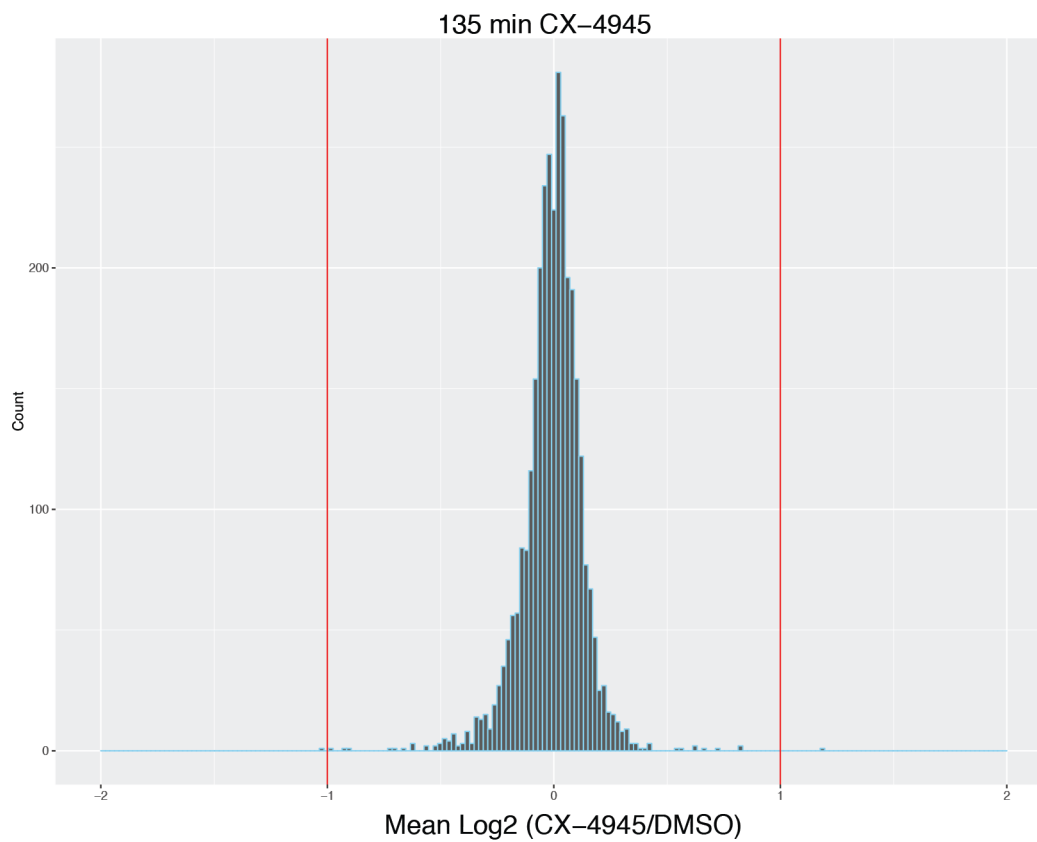
135 min CX−4945

Supplemental Figure 3.11 Frequency Distribution of Protein Mean Log2 Ratio in HeLa Cells Treated with CX-4945 for 135 Minutes.
The mean log2 ratio of three biological replicates for each protein identified and quantified is represented in this frequency distribution of all quantified proteins from HeLa cells treated with 20 μM CX-4945 for 135 minutes.
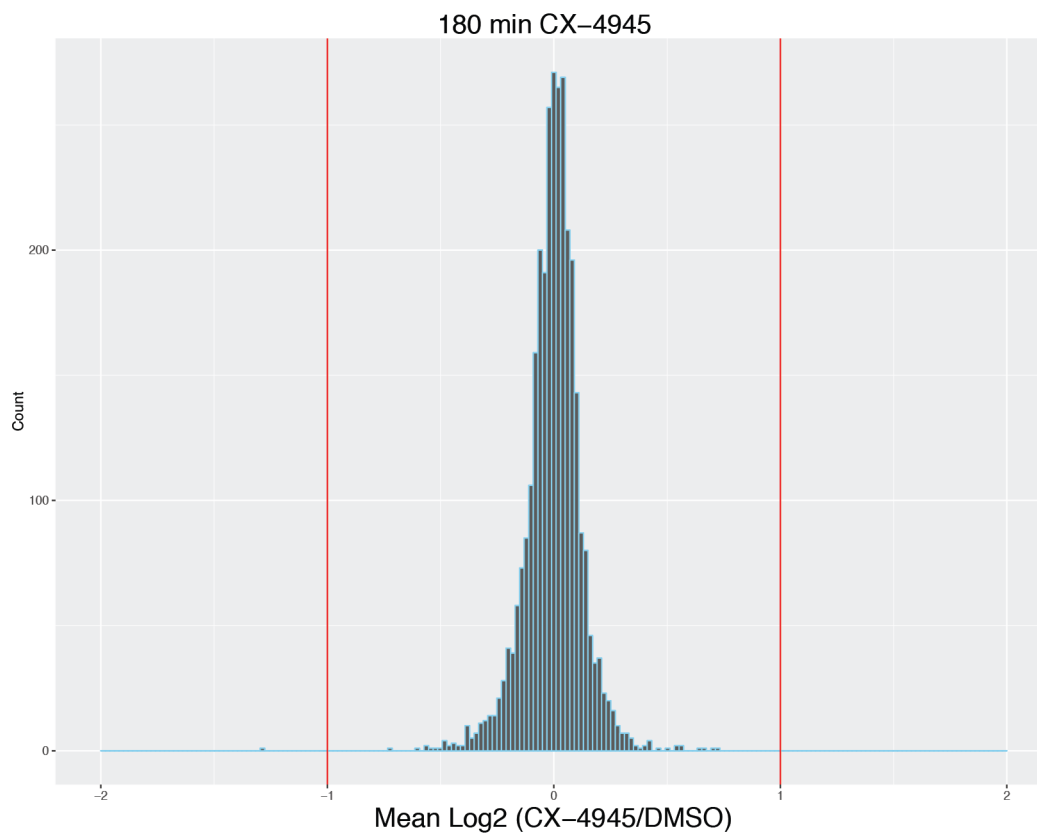
Supplemental Figure 3.12 Frequency Distribution of Protein Mean Log2 Ratio in HeLa Cells Treated with CX-4945 for 180 Minutes.
The mean log2 ratio of three biological replicates for each protein identified and quantified is represented in this frequency distribution of all quantified proteins from HeLa cells treated with 20 μM CX-4945 for 180 minutes.
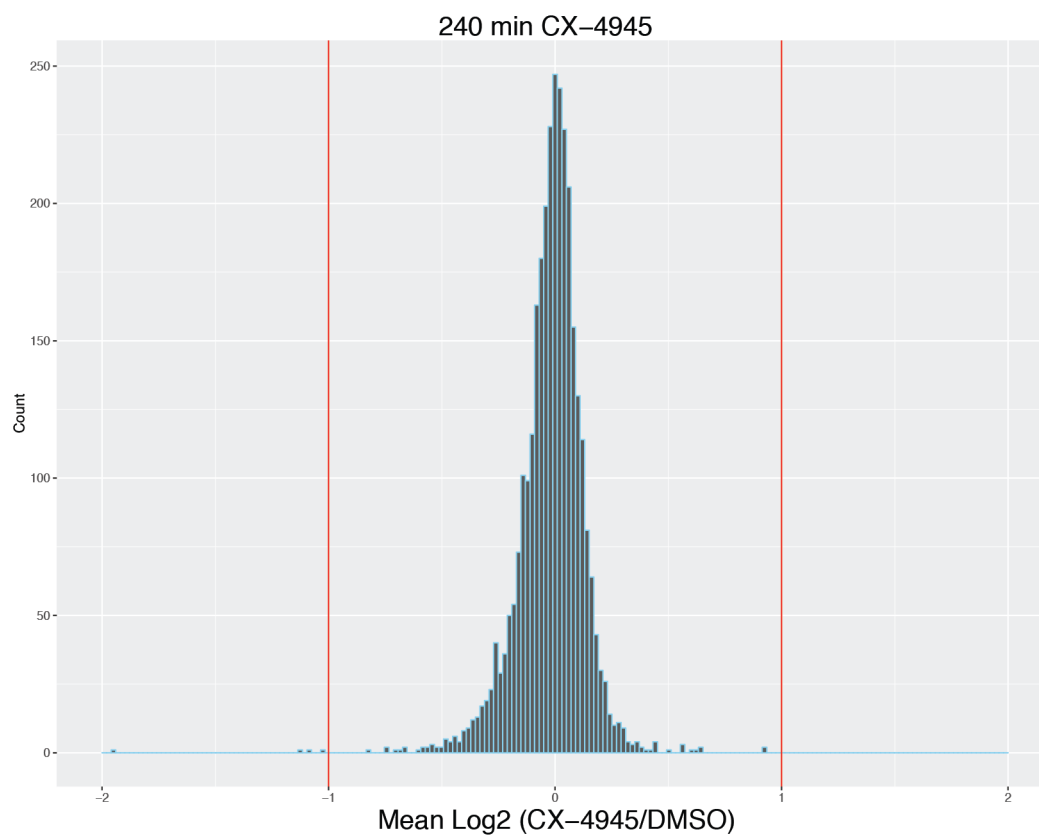
Supplemental Figure 3.13 Frequency Distribution of Protein Mean Log2 Ratio in HeLa Cells Treated with CX-4945 for 240 Minutes.
The mean log2 ratio of three biological replicates for each protein identified and quantified is represented in this frequency distribution of all quantified proteins from HeLa cells treated with 20 µM CX-4945 for 240 minutes.

Supplemental Figure 3.14 Companion Figure for Figure 3.16
Biological process terms are shown for each node in the network.

Supplemental Figure 3.15 Companion Figure for Figure 3.17
Biological process terms are shown for each node in the network.

4   **Chapter 4 – Functional Characterization of the Kinome in Response to CX-4945 Treatment**

4.1   Introduction

Protein kinases play a critical role in the regulation of cellular processes through the phosphorylation of proteins. Historically, strategies have focused on the modulation of individual phosphorylation sites by individual kinases in distinct cellular contexts. The emergence of high-throughput phosphoproteomic analyses using mass spectrometry has enabled the quantitative profiling of the phosphorylation status of thousands of modified sites in the proteome, and can deliver insights into signaling mechanisms at play in the regulation of a protein's function at a network level (56). In such approaches the regulation of kinases has been studied through the interpretation of the modulation of phosphorylation sites in distinct cellular contexts or using kinase inhibitors (72, 73). Furthermore, recent developments in chemical proteomics and mass spectrometry have enabled the enrichment for kinases to enable profiling of kinase expression and activity at the level of the kinome. One of the strategies for kinome profiling exploits multiplexed inhibitor beads (MIBs) (82, 83). Multiplexed inhibitor beads consist of sepharose beads conjugated with ATP-competitive inhibitors that have a broad range of specificity, which enables the capture of a large number of protein kinases. When coupled with LC-MS/MS, MIBs enable the quantitative profiling of kinase activity within a cellular context. MIBs can also be applied to evaluate kinome responses in cells treated with kinase inhibitors and for the systematic profiling of kinase inhibitor specificity (169).

In an effort to relate responses to CX-4945 that were identified using phosphoproteomics in the previous chapter, MIB profiling was undertaken to study the effect of CX-4945 at the

kinome level. Two complementary sample preparation approaches were utilized in order to profile the kinome of HeLa cells that were treated with CX-4945 for 240 minutes. Utilizing MIBs enables the quantitative comparison of the amount of kinase bound to the inhibitor resin, enabling identification of kinases that are up-regulated or down-regulated in response to inhibitor treatment. Given the enrichment of kinases in comparison to the general proteome, MIB profiling also enables the identification of phosphorylated kinases, lending more insight into kinase activity, particularly for the many kinases that are regulated by phosphorylation (170). Our studies have also incorporated utilization of another CK2 inhibitor "Inhibitor VIII," which was designed using virtual screening and structure-based-guided methods (87). Inhibitor VIII was exploited for discrimination between CK2-dependent or CK2-independent effects of CX-4945 within the CX-4945 dependent phosphoproteome that was characterized in Chapter 3.

4.2   Results

4.2.1   Multiplexed Inhibitor Bead Profiling Reveals Kinome Perturbation in Response to CX-4945

In an effort to complement previous phosphoproteomic analysis of CX-4945 in HeLa cells, multiplexed inhibitor bead (MIB) profiling was performed utilizing two different inhibitor-based MIB resins that have been previously described (171, 172). This workflow consisted of treating SILAC labeled HeLa cells for 240 minutes with either CX-4945 or DMSO. Three biological replicates consisting of heavy-labeled cells (CX-4945 treated) and light-labeled cells (DMSO treated) were profiled using the six-inhibitor mix and the four-inhibitor mix, resulting in two datasets. A separate experiment consisting of one biological replicate with heavy-labeled cells (DMSO treated) and light-labeled cells (CX-4945 treated) was profiled

using the four-inhibitor mix (Figure 4.1). MIB profiling enables the capture of active kinases to the inhibitor resin, allowing quantitative comparison by LC-MS/MS of labeled peptides derived from the captured kinases within a given biological context (84). Utilizing these two different inhibitor resins, profiling of SILAC labeled HeLa cells revealed regulation of kinase activity in response to CX-4945 treatment, quantifying between 148-217 kinases in separate analyses (Figure 4.2) in addition to 30-77 phosphorylation sites that were identified on kinases. The identification of several kinases related to the PI3K/Akt/mTOR pathways that decreased in activity in response to CX-4945 supported the data previously presented in chapter 3 which quantified a decrease in phosphorylation on substrates of these kinases (Figure 4.3, Figure 4.5, Figure 4.7). Kinases such as AKT1 (Akt1), SGK1 (Sgk1), and RPS6KB1 (p70S6K) decreased approximately 25% (log2 value of -0.4) in response to CX-4945, suggesting that inhibition of mTOR occurred with CX-4945 treatment (173-175). Pyruvate kinase (PKM), which regulates glycolysis and can be controlled by mTOR activity (176), decreased approximately 3x (log2 value of -1.5). Interestingly, the decrease in CK2 activity (CSNK2A1) was approximately 25%, suggesting that MIB profiling was able to detect inhibition of CK2 in cells treated with CX-4945. Quantification of CK2 activity was only detected in samples processed using the six-inhibitor mix. Samples profiled using the four-inhibitor mix revealed other targets that could be regulated by mTOR, with a decrease in Akt2 activity of approximately 30%, and an increase in Ulk1 activity of approximately 100% (Figure 4.7). The change in activity of kinases regulated by mTOR further supports the notion that CX-4945 treatment results in down-regulation of mTOR.

The capture of kinases using MIBs enabled the identification and quantification of phosphorylation sites located on kinases that was not previously documented using the

phosphoproteomics workflow presented in chapter 3, owing largely in part to constraints in detecting lower-abundance proteins in data-dependent acquisition of a complex lysate mixture (170). Treatment with CX-4945 resulted in the increase of phosphorylation on several kinases that are a part of the mitogen activated protein kinase (MAPK) pathway (Figure 4.4). Thr185/Tyr187 of MAPK1 (ERK2) and Thr202/Tyr204 of MAPK3 (ERK1) increased in phosphorylation more than 2x, with a downstream target of ERK, RPS6KA1 Ser380 increasing almost 4x in phosphorylation, suggesting activation of the MAPK pathway after treatment with CX-4945. The increase in MAPK1 phosphorylation sites was documented using the four-inhibitor MIB beads as well (Figure 4.6). In addition to the quantification of phosphorylation sites on kinases from MAPK pathway, the quantitation at the protein level for interleukin-1 receptor-associated kinase (IRAK1) demonstrated a large increase that was detected using both MIB mixes (Figure 4.3, Figure 4.5). The activity of IRAK1 has been demonstrated to be required for the phosphorylation of ERK1/2 in the context of interleukin-mediated signaling (177). Lysates used for proteomic profiling were analyzed using western blotting, probing against different constituents of the MAPK pathway using phospho-specific antibodies (Figure 4.9). These results corroborate the quantification of the phosphorylation sites from kinases captured by the MIBs.
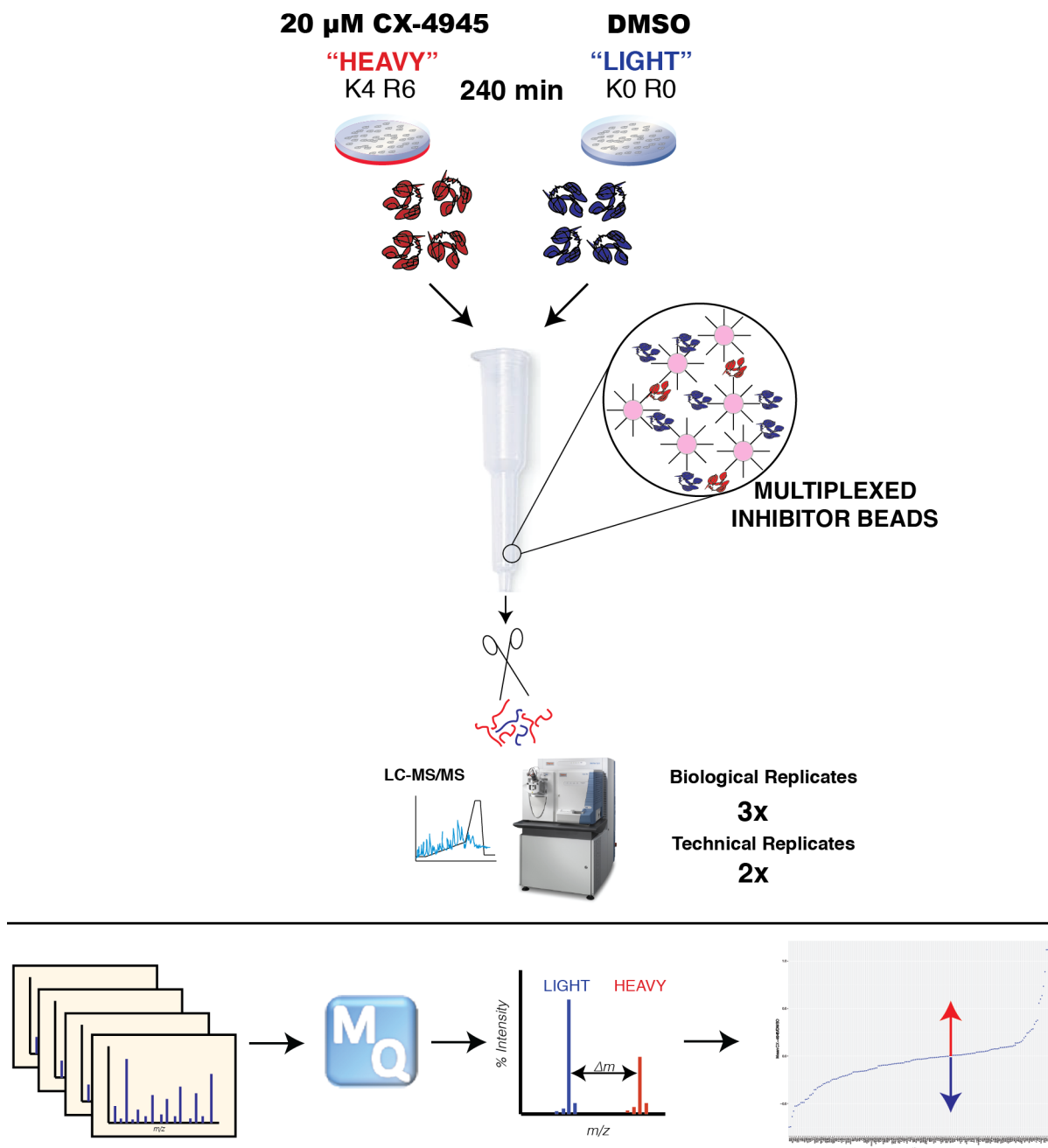
Figure 4.1 Workflow Overview for Multiplexed Inhibitor Bead Profiling
SILAC-adapted HeLa cells were treated with CX-4945 or DMSO for 240 minutes followed by lysis. Samples were combined 1:1 based on protein amount and processed using MIBs that contained either a 6-Inhibitor or 4-Inhibitor mix. Peptides derived from captured kinases were acquired by LC-MS/MS and raw mass spectra were quantified using MaxQuant v1.5.3.8.

MIB mix	Kinases	Phosphosites	n
6-mix	217	77	2/3
4-mix	148	30	2/3
4-mix (swap)	183	49	1

Figure 4.2 Summary of Kinases Identified and Quantified by MIB Profiling
Quantitative information from samples processed using the 6-Inhibitor mix was filtered on the basis of identification and quantification in two out of three biological replicates. For samples processed using the 4-Inhibitor mix, two out of three biological replicates were considered separately from the sample in which the light label was treated with CX-4945 and the heavy label was treated with DMSO. Phosphorylation sites were considered only if localization exceeded a probability of 0.75.
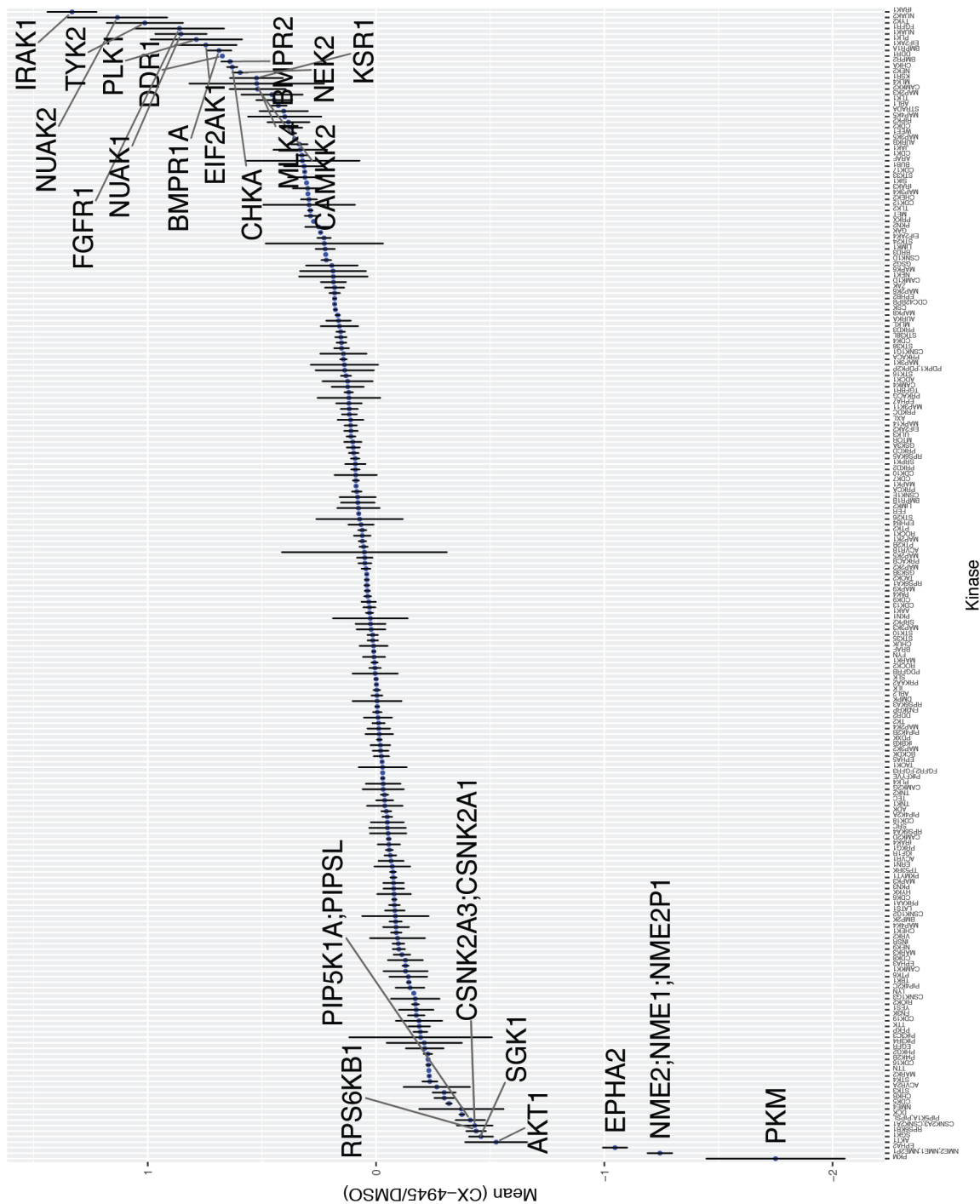
Figure 4.3 Quantification of Kinases Using 6-Inhibitor MIBs
The mean log2 (CX-4945/DMSO) ratio is presented from 2 out of 3 biological replicates. Bars denote standard variation where quantitative information was obtained from 3 biological replicates. Labeled kinases increased > log2 + 0.5 or decreased > log2 - 0.4.
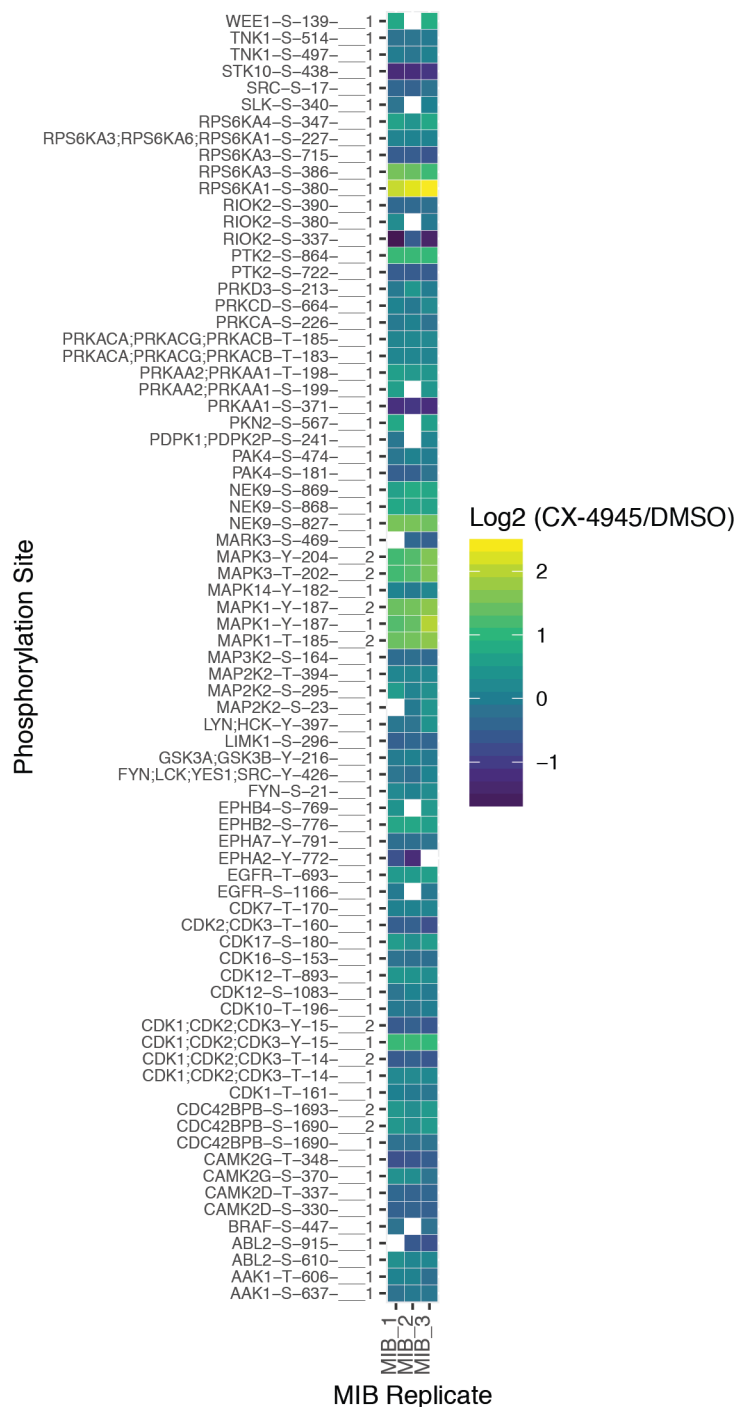
Figure 4.4 Quantification of Kinase Phosphorylation Sites Using 6-Inhibitor MIBs
Phosphorylation of Ser, Thr, and Tyr residues as a variable modification was included in the database searching in MaxQuant but excluded in the quantification of protein groups. Phosphorylation sites that exceeded localization probability of 0.75 are presented. Blank squares denote values for phosphorylation sites where quantitation was not present in a biological replicate.

111
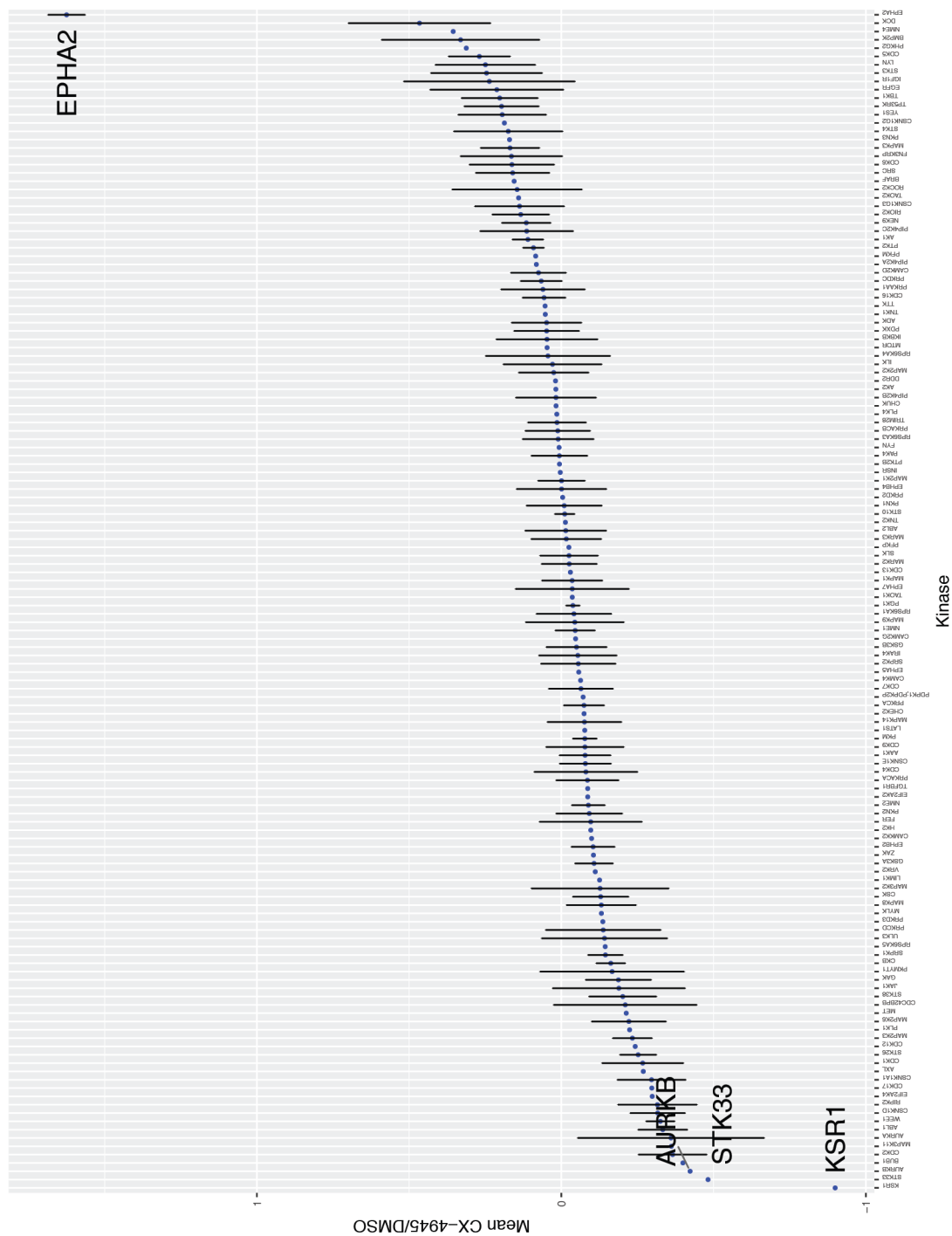
Figure 4.5 Quantification of Kinases Using 4-Inhibitor MIBs
The mean log2 (CX-4945/DMSO) ratio is presented from 2 out of 3 biological replicates. Bars denote standard variation where quantitative information was obtained from 3 biological replicates. Labeled kinases increased > log2 + 0.5 or decreased > log2 - 0.4.
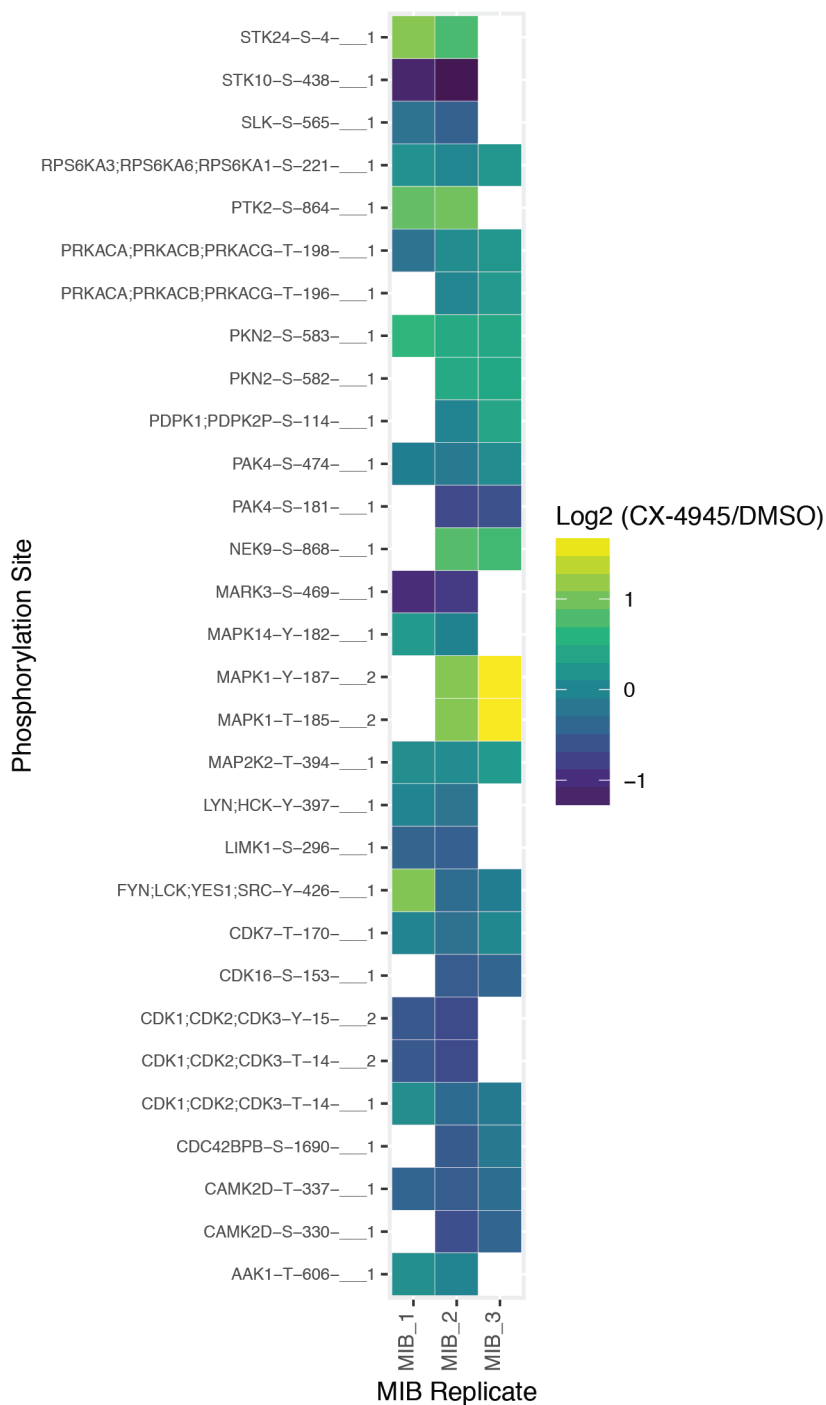
Figure 4.6 Quantification of Kinase Phosphorylation Sites Using 4-Inhibitor MIBs
Phosphorylation of Ser, Thr, and Tyr residues as a variable modification was included in the database searching in MaxQuant but excluded in the quantification of protein groups. Phosphorylation sites that exceeded localization probability of 0.75 are presented. Blank squares denote values for phosphorylation sites where quantitation was not present in a biological replicate.
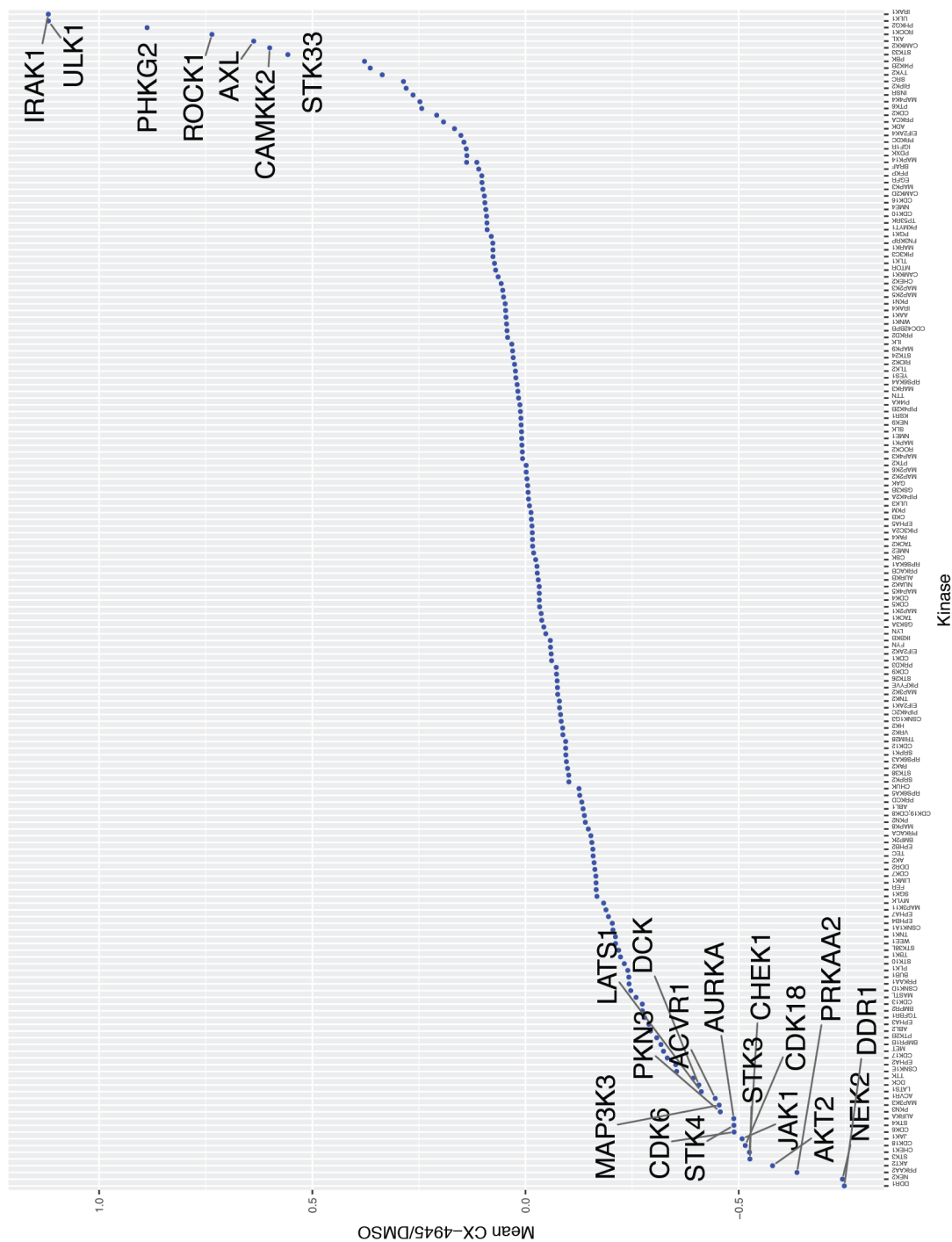
Figure 4.7 Quantification of Kinases Using 4-Inhibitor MIBs in Label Swap
The mean log2 (CX-4945/DMSO) ratio is presented from the label swap, where light HeLa cells were treated with CX-4945. Labeled kinases increased > log2 + 0.5 or decreased > log2 - 0.4.
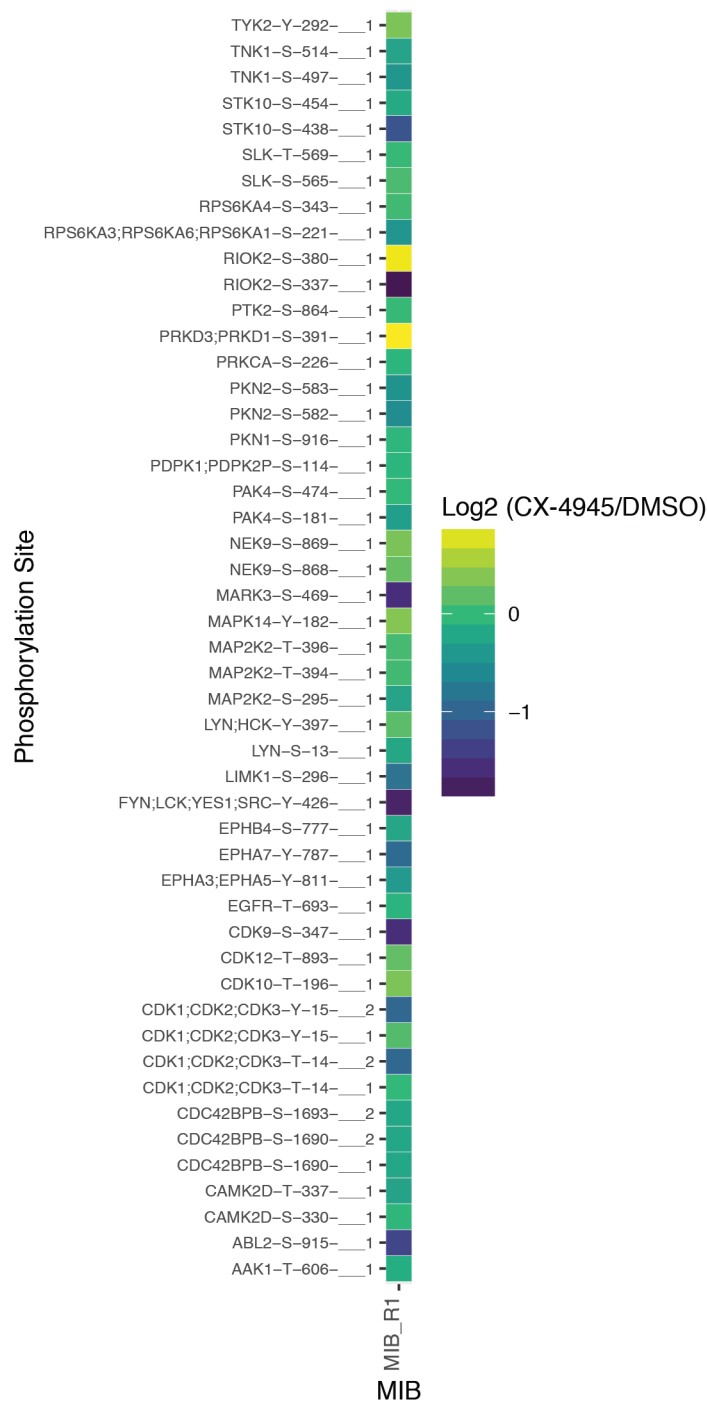
Figure 4.8 Quantification of Kinase Phosphorylation Sites Using 4-Inhibitor MIBs in Label Swap
Phosphorylation of Ser, Thr, and Tyr residues as a variable modification was included in the database searching in MaxQuant but excluded in the quantification of protein groups. Phosphorylation sites that exceeded localization probability of 0.75 are presented.

Interestingly, the increase of Tyr15 phosphorylation on CDK1 was detected in response to CX-4945 from singly phosphorylated peptides that were identified and quantified when profiling lysates using the six-inhibitor mix (Figure 4.4). The Tyr15 phosphorylation site was quantified as decreasing in phosphorylation from doubly phosphorylated peptides which also contain phosphorylation at Thr14. Due to isoform similarity between the CDK-family kinases, the phosphopeptides which have the localized phosphorylation site match multiple CDK kinases. Using the four-inhibitor mix, the quantification of Tyr15 from multiply phosphorylated peptides decreased (Figure 4.6, Figure 4.8)..The quantitation of Tyr15 from singly phosphorylated peptides was only observed in samples profiled by the four-inhibitor mix when light-labeled cells were treated with CX-4945 in a label swap experiment. In this instance only a small increase in phosphorylation was observed in comparison to quantification obtained when samples were profiled using the six-inhibitor MIBs (Figure 4.6, Figure 4.8). Given the relative quantitation between singly and doubly phosphorylated peptides containing phosphorylated Tyr15, and the increase in the singly phosphorylated form of the Tyr15 site and decrease in the doubly phosphorylated form, this suggests an overall increase at this phosphorylation site on CDK. The phosphorylation of Tyr15 is inhibitory to the activity of CDK kinase (178) and can impede the progression from G2 to M phases of the cell cycle, suggesting that CX-4945 down-regulates the CDK1 activity after 240 minutes of treatment.
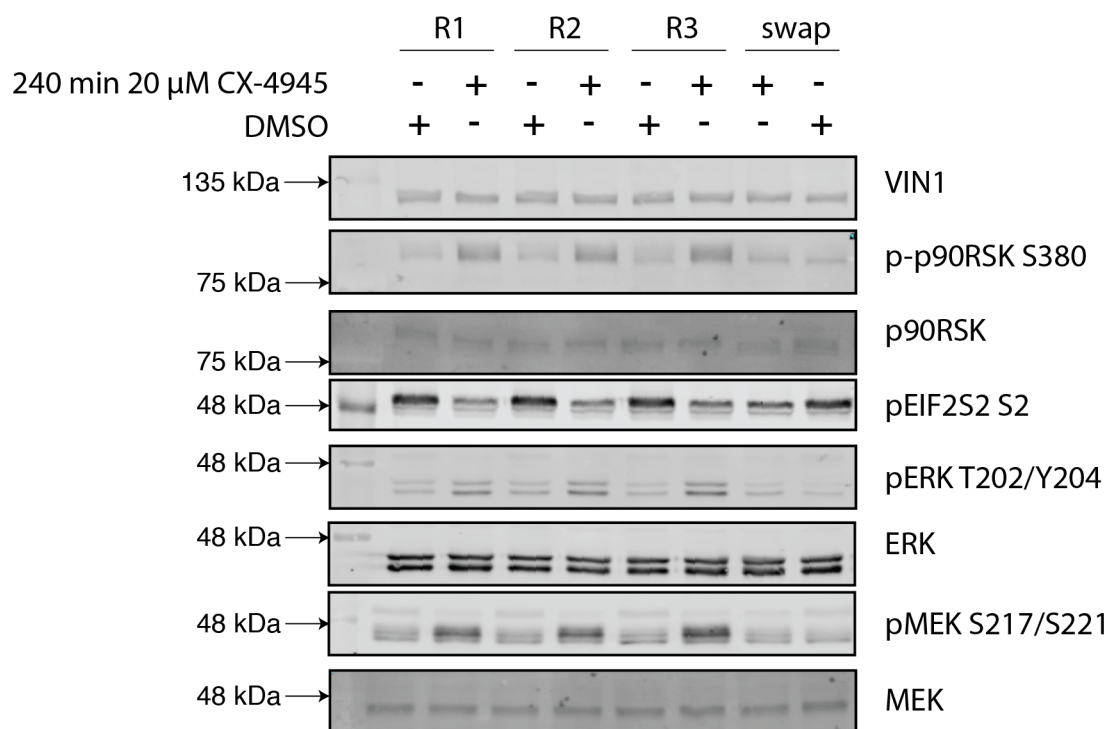
Figure 4.9 MIBs Profiling Reveals Activation of the ERK MAPK Pathway in Response to CX-4945

Western blot of samples utilized for MIB profiling. 10 μg of lysate was separated by SDS-PAGE, transferred to PVDF membrane and probed against antibodies listed to the right of each panel. R1, R2, R3 and swap denote the four biological replicates that were processed. Heavy-labeled SILAC HeLa cells from replicates R1-R3 were treated with 20 μM CX-4945 with light-labeled cells being treated with DMSO. In the label swap, treatment and control samples were switched.

4.2.2   CX-4945 and Inhibitor VIII Activate MAPK Pathway

To test whether the activation of the MAPK pathway by CX-4945 was independent of CK2 inhibition, an unrelated small molecule inhibitor of CK2, "Inhibitor VIII" (87) was utilized in subsequent assays in parallel with CX-4945 treatment. Given that SILAC media requires growth conditions using FBS that is dialyzed against a 10 kDa membrane in order to prevent small unlabeled peptides or amino acids from interfering with the adaptation of heavy labeled amino acids, and that the presence of FBS in cell culture media can induce phosphorylation of constituents of the MAPK pathway, assays were performed with or without an overnight serum starve prior to inhibitor treatment. Treatment with 20 μM CX-4945 or 15 μM Inhibitor VIII resulted in increased phosphorylation of ERK1/2, which was observed in tandem with decreased phosphorylation of EIF2S2 Ser2 (Figure 4.10). Following this observation, samples from this treatment were run against samples from HeLa cells treated with neocarzinostatin, staurosporine, MG-132 or torin to investigate whether this increase in phosphorylation was p38 MAPK-dependent, which can become activated in cellular stress contexts (179, 180) (Figure 4.11), and can be regulated by IRAK1 activity (177). Interestingly, unlike the treatment with neocarzinostatin or staurosporine, inhibition of CK2 utilizing CX-4945 or Inhibitor VIII for 240 minutes did not induce p38 MAPK phosphorylation on Thr180/Tyr182 suggesting a p38 MAPK-independent activation of ERK1/2. Phosphopeptides from p38 MAPK were detected using MIBs, although only the singly phosphorylated form with localized site Tyr182 which did not change (Figure 4.4, Figure 4.8). A differential decrease in phospho-4E-BP1 was also noted between CX-4945 and Inhibitor VIII treated cells.
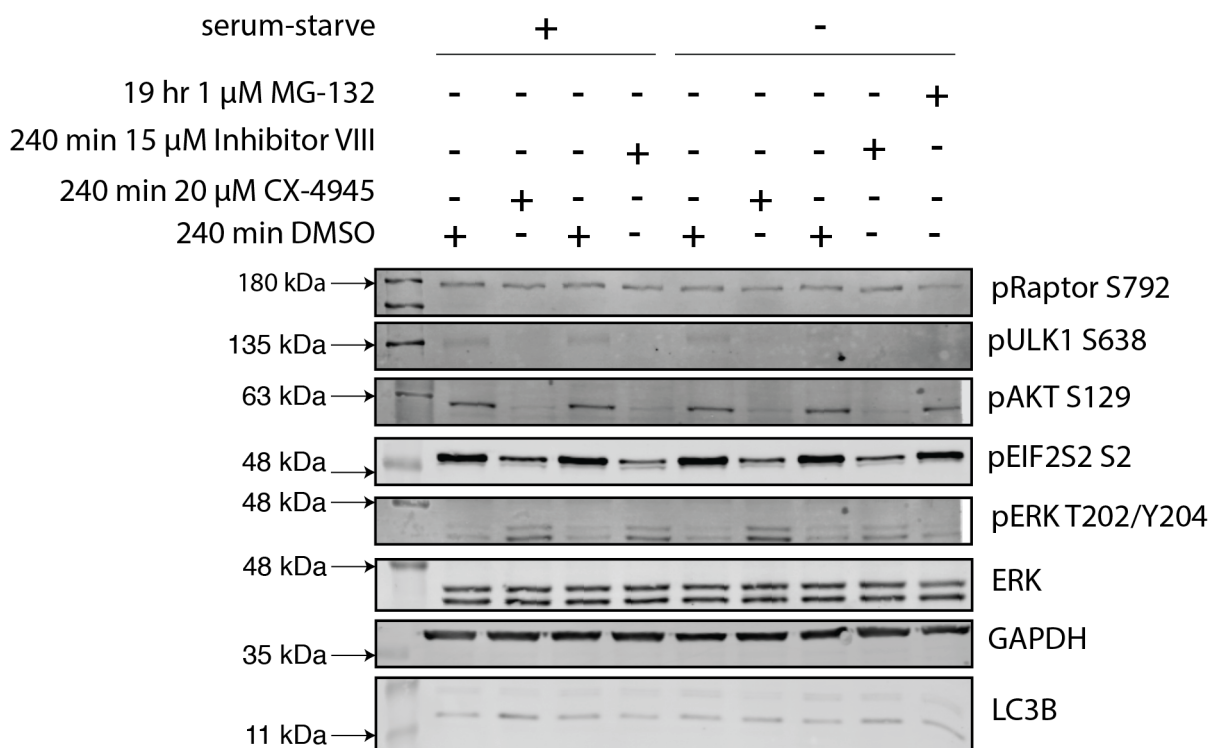
Figure 4.10 Activation of the ERK MAPK Pathway in Response to CX-4945 is Independent of Media Supplementation
Parental HeLa cells were serum starved for 18 hours prior to treatment as noted in the figure. Cells were then treated with CX-4945 or Inhibitor VIII for 240 minutes. In parallel, HeLa cells were treated with 1 μM of proteasomal inhibitor MG-132 for 19 hours. All treatments were performed by delivering drugs that were diluted in cell culture media without FBS supplementation. Samples presented in this panel were collected in MIBs lysis buffer.
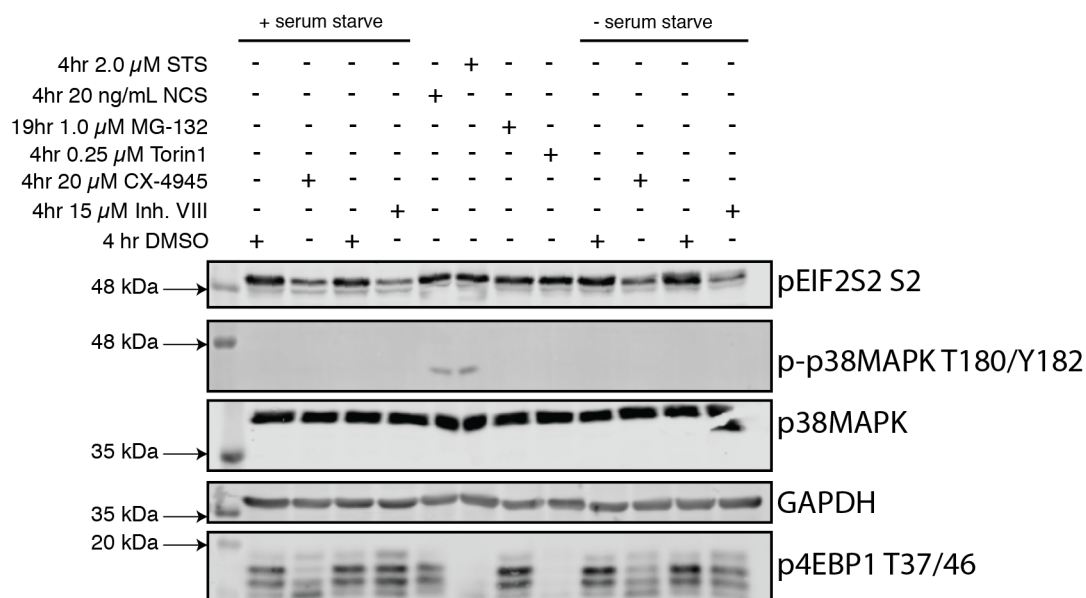
Figure 4.11 CX-4945 Activation of the ERK1/2 MAPK Pathway is Independent of p38 MAPK
Parental HeLa cells were serum starved for 18 hours prior to treatment as noted in the figure. Lysates from HeLa cells previously analyzed by western blotting in Figure 4.10 were re-analyzed by western blotting in comparison to extracts derived from HeLa cells treated with staurosporine (STS), neocarzinostatin (NCS) or Torin1 at indicated concentrations for 4 hours. All treatments were performed by delivering drugs that were diluted in cell culture media without FBS supplementation. Samples presented in this panel were collected in MIBs lysis buffer.

4.2.3 CX-4945 and Inhibitor VIII Display Differential Inhibition of Phospho-4E-BP1

Having observed a decrease in phospho-4E-BP1 (Figure 4.11) and being unable to confidently identify changes in LC3-II (a marker of autophagy induction, which can be regulated through mTOR activity towards Ulk1 (181)), HeLa cells that were previously grown in the presence of FBS were treated with for 240 minutes with CX-4945, Inhibitor VIII and torin1, followed by sample collection using a lysis buffer containing different detergents. Lysates were probed with antibodies for components of the PI3K/Akt/mTOR signaling pathways (Figure 4.12). This experiment confirmed that treating HeLa cells with CX-4945 led to a decrease of phospho-4E-BP1 signal to a different extent than that seen with Inhibitor VIII despite both inhibitors decreasing the level of phospho-EIF2S2 to a similar extent. Torin1 and staurosporine abolished the presence of LC3-I (higher migrating band) and CX-4945 decreased this to a similar extent in comparison to Inhibitor VIII and DMSO control. Despite poor resolution of the band by SDS-PAGE because of its high molecular weight, a decrease in phosphorylation of mTOR at Ser2448 is more noticeable in response to CX-4945 as compared to Inhibitor VIII treatment.

4.2.4 CX-4945 Induces Rapid Activation of MAPK Pathway and Down-regulation of PI3K/Akt/mTOR Pathways

Since previous investigation of CX-4945 treated HeLa cells covered time-points that spanned between 60 and 240 minutes, assays were performed within a window of time which preceded 60 minutes in order to explore whether CX-4945 effects would be evident. Indeed, the activation of the MAPK pathway was rapid, occurring within a span of 15 minutes as evidenced by increases in phosphorylation of ERK1/2 and MEK1/2 (Figure 4.13).

Interestingly the phosphorylation of p70S6K Thr389 was reduced quickly in comparison to

EIF2S2 Ser2 and Akt Ser129. The phosphorylation of c-Raf Ser338,
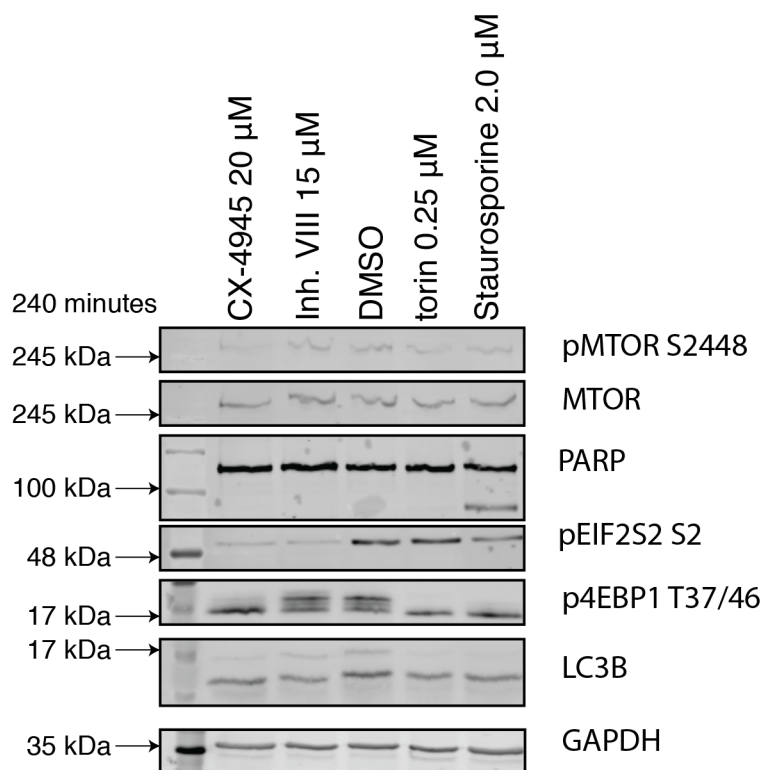
Figure 4.12 Differential Inhibition of mTOR Using CX-4945 and Inhibitor VIII
HeLa cells were grown in media supplemented with FBS, followed treated with CX-4945, Inhibitor VIII, Torin1 or staurosporine for 240 minutes at indicated concentrations. Samples collected in this panel were collected in a RIPA lysis buffer.
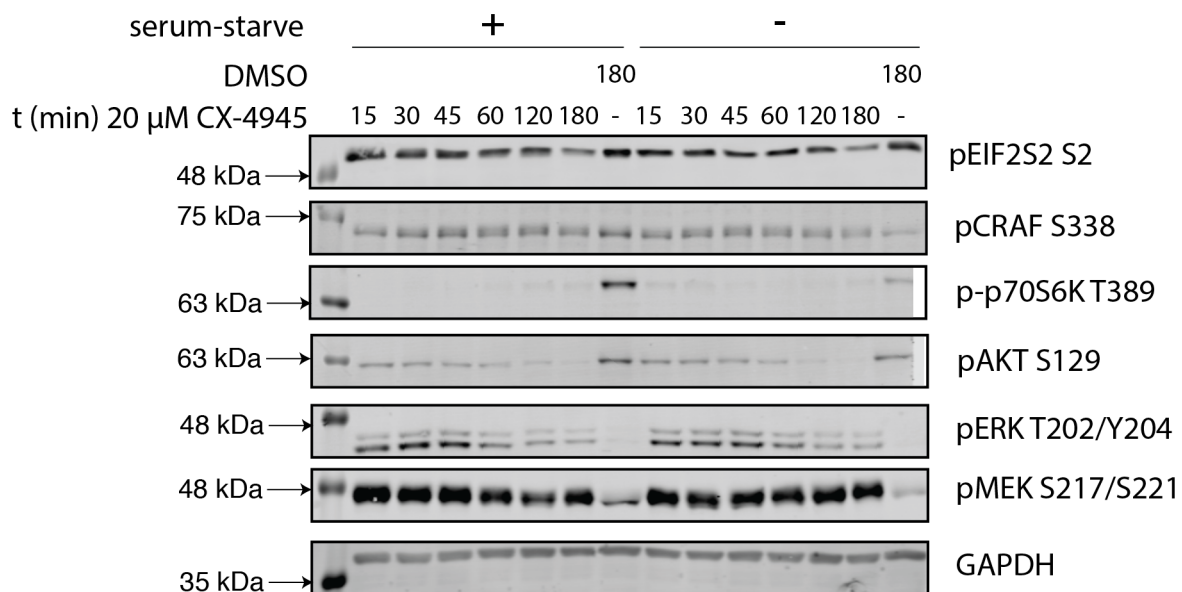
Figure 4.13 Activation of the ERK MAPK Pathway in Reponse to CX-4945 is Rapid
HeLa cells were serum starved for 18 hours prior to treatment as noted in the figure. Cells were then treated with CX-4945 for indicated time-points up to 180 minutes. All treatments were performed delivering drugs that were diluted in cell culture media without FBS supplementation. Samples collected in this panel were collected in RIPA lysis buffer.

which contributes to the activity of c-Raf (182, 183), did not change in response to CX-4945 within 180 minutes of treatment. c-Raf activity can also be regulated at Ser259 through phosphorylation by Akt, which is inhibitory as it can be sequestered by 14-3-3 proteins (184-186) and can be de-phosphorylated by protein phosphatase 2A (PP2A) (187). In a follow-up experiment, HeLa cells were serum starved overnight followed by pre-treatment with or without PP2A inhibitor okadaic acid (1 μM) for 15 minutes followed by treatment with CX-4945 to test if the phosphorylation status at c-Raf Ser259 could be contributing to MEK1/2 and ERK1/2 activity (Figure 4.14). The phosphorylation status at Ser259 of c-Raf did not change in the presence or absence of okadaic acid when cells were treated with CX-4945, suggesting that the phosphorylation status of Ser338 and Ser259 on c-Raf is not a requirement for activation of MEK1/2 and ERK1/2 in response to CX-4945. The induction of ERK1/2 phosphorylation can be achieved in a span of 10 minutes of treatment with CX-4945 or Inhibitor VIII and is nearly comparable to the induction observed using EGF within the same time (Supplemental Figure 4.14.1). Treatment with CX-4945 resulted in decreased phosphorylation of Akt Ser473 and Thr308, with pre-treatment using okadaic acid resulting in complete reduction of phosphorylation at these sites when treated with CX-4945 in comparison to cells that did not receive okadaic acid prior to CX-4945.

124

20 µM CX-4945	+	+	+	+	+	+	+	+	+	+	+	+	-	-
1 µM OKA	-	-	-	-	-	-	+	+	+	+	+	+	+	-
t (min)	0	5	10	15	30	60	0	5	10	15	30	60	75	0

63 kDa → pAKT T308

63 kDa → pAKT S473

63 kDa → pCRAF S338

63 kDa → pCRAF S259

48 kDa → pERK T202/Y204

48 kDa → tERK

48 kDa → pMEK S217/S221

48 kDa → tMEK

35 kDa → GAPDH
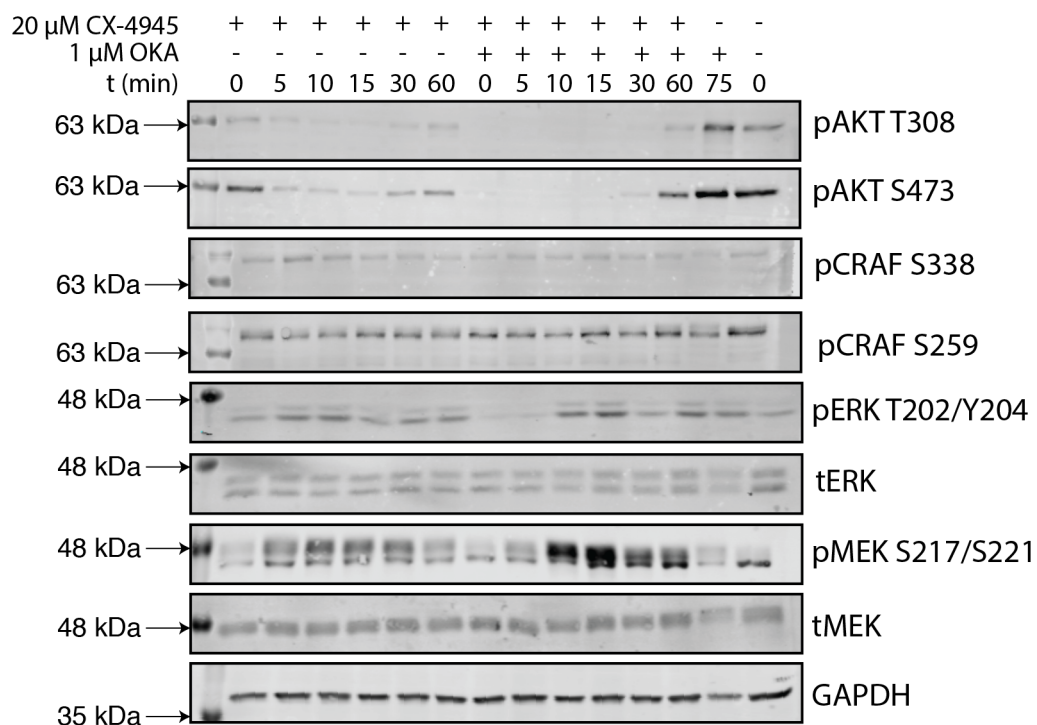
Figure 4.14 Activation of ERK MAPK is Independent of c-Raf Ser259
HeLa cells were serum starved for 18 hours prior to treatment as noted in the figure. Cells were pre-treated with or without 1 µM okadaic acid for 15 minutes prior to treatment with CX-4945 at indicated time-points. All treatments were performed delivering drugs that were diluted in cell culture media without FBS supplementation. Samples collected in this panel were collected in a RIPA lysis buffer.

4.2.5   CX-4945 and Inhibitor VIII Affect Cell Cycle Regulation

Previous phosphoproteomic analysis suggested an increase in CDK1 and CDK2 activity in response to CX-4945 treatment, while identification of phosphopeptides enriched from MIB profiling suggested an increase in Tyr15 which results in an inhibition of CDK activity. To investigate this discrepancy, HeLa cells were arrested in specific phases of the cell cycle and analyzed using western blotting with antibodies against cell cycle markers in addition to profiling using flow cytometry (Figure 4.15, Supplemental Figure 4.44.4). Treatment with 20 μM CX-4945 did not result in an evident increase in Tyr15 phosphorylation on CDK1 in comparison to DMSO after 240 minutes of treatment. Strikingly, treatment with 15 μM Inhibitor VIII resulted in increase phosphorylation of histone H3 Ser13 in comparison to either DMSO or CX-4945 within this period of time. This result is completely reversed upon longer treatment for 22 hours with either inhibitor, with complete abolishment of phospho-histone H3 Ser10 in cells treated with Inhibitor VIII. The increase in histone H3 Ser10 phosphorylation and total cyclin B1 suggests a G2/M phase arrest. Analysis using a two-colour method to analyze cell-cycle phase by flow cytometry (188) with the same clone for phospho-histone H3 Ser10 confirmed this result (Figure 4.16, Figure 4.17). Treatment of HeLa cells with CX-4945 for 4 hours results in an increase in G2 specific cells in comparison to DMSO while the mitotic population remains similar. In contrast, Inhibitor VIII causes a 4x increase in the mitotic population. In agreement with the western blot analysis, long-term treatment with CX-4945 created a G2/M specific arrest, although there is a substantial amount of cells that are apoptotic (Figure 4.17). This apoptotic population is underestimated given the reliance on gating forward scatter and side scatter profiles of singlet
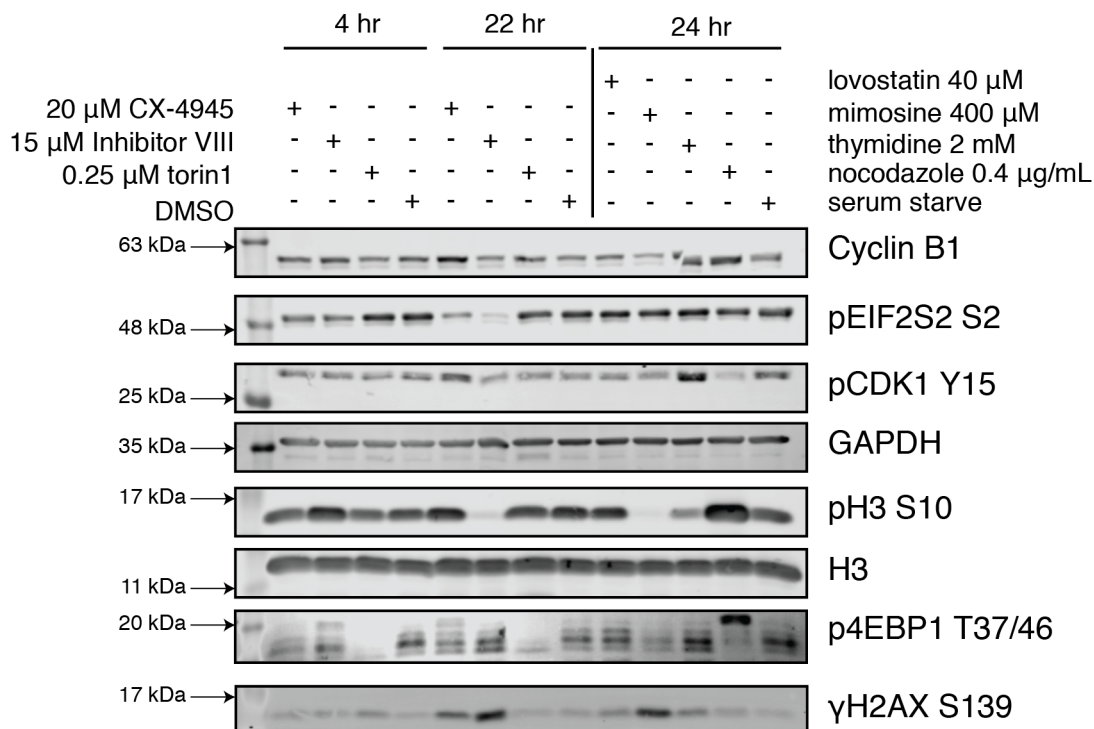
Figure 4.15 CX-4945 and Inhibitor VIII Perturb Cell Cycle Regulation
HeLa cells were grown in media supplemented with FBS, followed treated with CX-4945,
Inhibitor VIII, Torin1 or staurosporine for 240 minutes or 22 hours at indicated
concentrations. In parallel HeLa cells were treated with lovastatin, mimosine, thymidine or
nocodazole for 24 hours at indicated concentrations. All treatments were performed by
delivering drugs that were diluted in cell culture media without FBS supplementation.
Samples collected in this panel were collected in a RIPA lysis buffer.
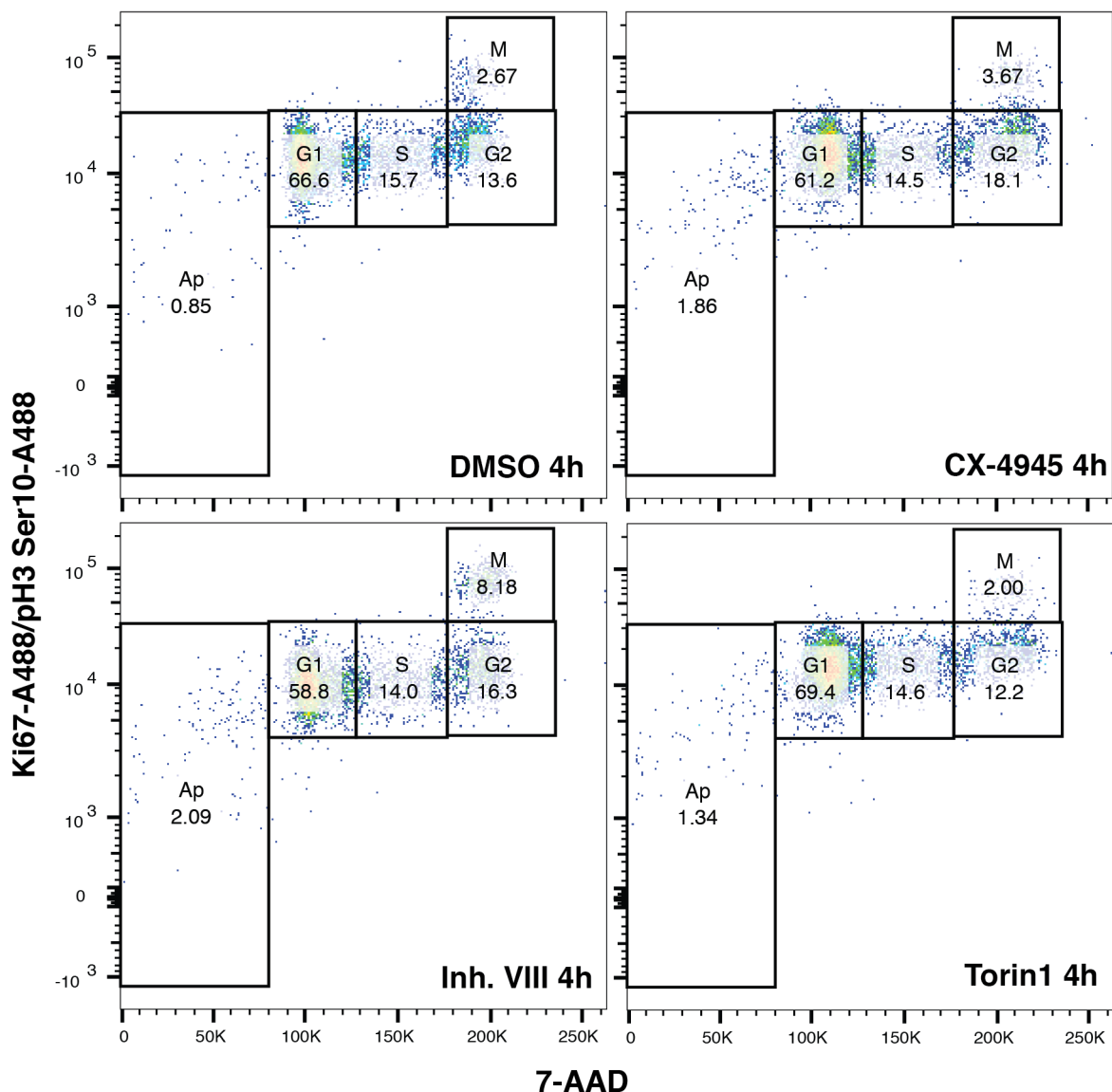
Figure 4.16 CX-4945 and Inhibitor VIII Exert Differential Effect on Histone H3 Phosphorylation
HeLa cells were grown in media supplemented with FBS, followed by treated with CX-4945, Inhibitor VIII, Torin1 or staurosporine for 240 minutes. Cells were processed for cell cycle analysis by flow cytometry, staining with 7-AAD, and antibodies against Ki-67 and phospho-histone H3 Ser10, both conjugated to AlexaFluor-488. Gating was performed on forward and side scatter profiles to isolate single cells, and samples derived from HeLa cells arrested in specific phases of the cell cycle were used to appropriately gate cell populations presented. All treatments were performed delivering drugs that were diluted in cell culture media without FBS supplementation.
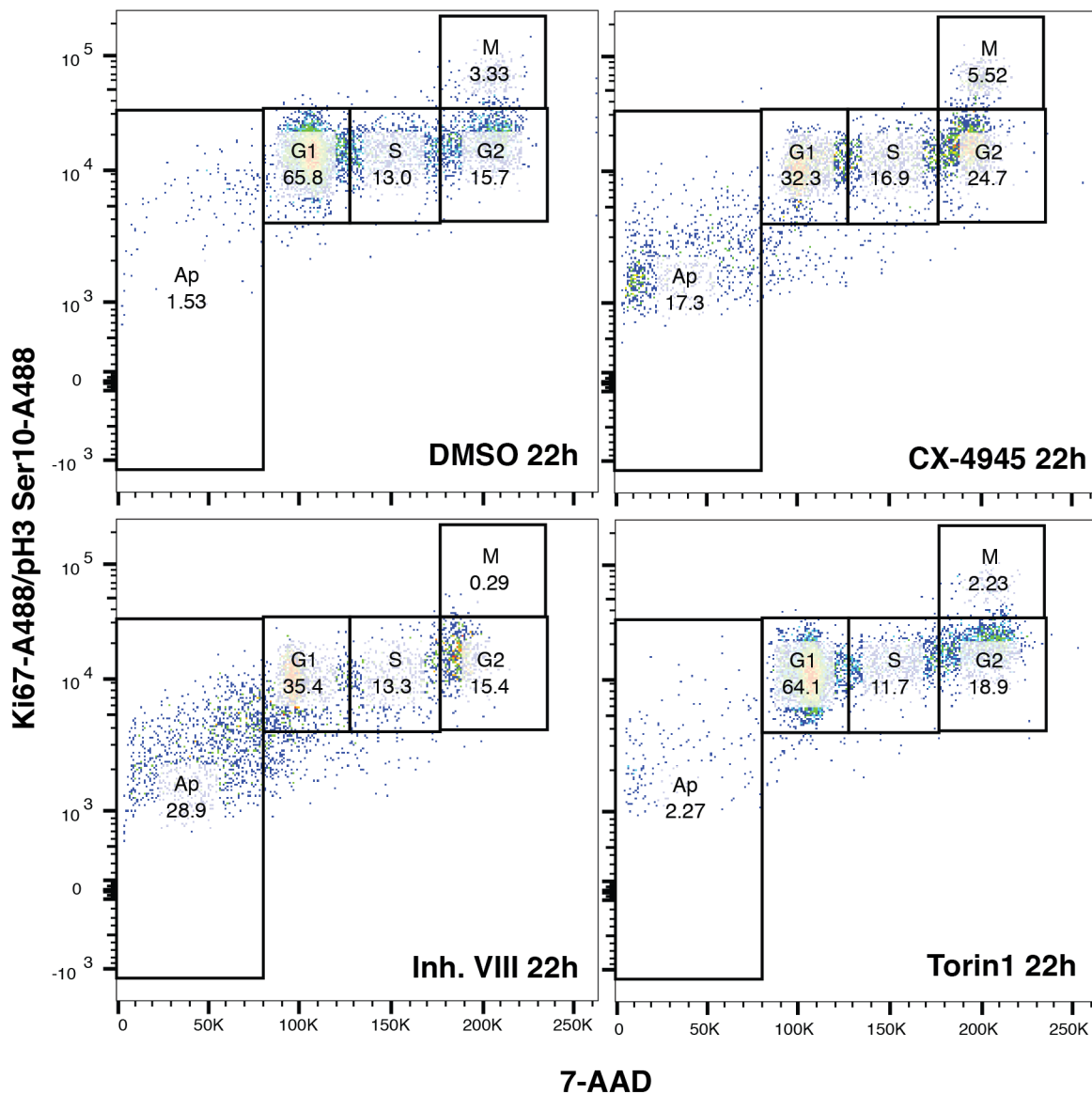
Figure 4.17 CX-4945 and Inhibitor VIII Result In Divergent Cell Cycle Arrest
HeLa cells were grown in media supplemented with FBS, followed by treated with CX-4945, Inhibitor VIII, Torin1 or staurosporine for 22 hours. Cells were processed for cell cycle analysis by flow cytometry, staining with 7-AAD, and antibodies against Ki-67 and phospho-histone H3 Ser10, both conjugated to AlexaFluor-488. Gating was performed on forward and side scatter profiles to isolate single cells, and samples derived from HeLa cells arrested in specific phases of the cell cycle were used to appropriately gate cell populations presented. All treatments were performed delivering drugs that were diluted in cell culture media without FBS supplementation.

cells within this assay which can occlude cells that have changed in shape and size as a result of undergoing apoptosis. Using a flow cytometry assay that directly measures cell viability using 7-AAD and annexin-V staining, 51% and 34% of HeLa cells treated with 20 μM CX-4945 or 15 μM Inhibitor VIII respectively remain viable (Supplemental Figure 4.24.2).

4.3   Discussion

Investigation of the phosphoproteome presented previously in this thesis revealed a dynamic regulation of phosphoproteins in response to CX-4945 treatment in HeLa cells, suggesting a dynamic change in the activity of protein kinases responsible for phosphorylation of these substrates. MIBs allow the quantitative profiling of the kinome and have been utilized to study the effects of small-molecule ATP-competitive inhibition of kinases (84). To corroborate the putative regulation of kinases, we utilized two different inhibitor combinations for MIB profiling in order to monitor the kinase activity in extracts from HeLa cells treated with CX-4945 for 240 minutes.

The identification of the down-regulation of activity for kinases in the PI3K/Akt/mTOR pathways such as Sgk1, Akt and RPS6KB1 and the up-regulation of Ulk1 activity validates the phosphoproteomic data presented earlier. The down-regulation of Sgk1, Akt and RPS6KB1 which are downstream of mTOR is in agreement with the literature which has identified CX-4945 treatment affecting Akt and mTOR activity (51, 54, 189). By comparison, the activity of mTOR as detected by MIB profiling did not appear to change using either MIB mix. One constituent that is regulated by mTOR, PKM, decreased in activity in response to CX-4945 and highlights a previously uncharacterized effect of this inhibitor with dramatic implications on metabolic regulation of glycolysis. CK2 has been implicated in regulation of metabolism, through the phosphorylation of phosphoglucose

isomerase (PGI) which is involved in glycolysis (190). A role in the regulation of the PI3K/Akt/mTOR pathways by CK2 has been previously implicated through the phosphorylation of phosphatase and tensin homolog (PTEN), which can stabilize the phosphatase preventing activity that is inhibitory towards the PI3K/Akt axis (191, 192). In a different investigation by So *et al.*, treatment of cells with CX-4945 for extended periods of time in PC9 cells induced autophagy (193). LC3 can be used as a marker for autophagy, and when conjugated to phosphatidylethanolamine (denoted as LC3-II), it can be detected as a lower migrating band using SDS-PAGE/immuno-blotting (194). In contrast to the findings by So *et al.*, experiments performed here used HeLa cells with initial western blotting failing to yield a clear difference in accumulation of LC3-II. When samples were collected using a denaturing buffer with NP-40 detergent, there was no apparent difference in LC3-II among samples treated with CX-4945, Inhibitor VIII or torin1. The presence of LC3-I (the higher migrating band) was slightly reduced with CX-4945 treatment in comparison to Inhibitor VIII and was comparable to treatment with torin1 or staurosporine. This may suggest an activation of autophagy as a result of mTOR inhibition, given that MIB profiling identified an increase in Ulk1 activity. Taking these details into perspective, it is interesting that when western blotting was performed using antibodies against phospho-4E-BP1 in lysates derived from HeLa cells that were treated with two unrelated inhibitors of CK2, a differential effect in the level of phosphorylation was noted between CX-4945 and Inhibitor VIII treatment. Both CK2 inhibitors reduced the phosphorylation level of EIF2S2, confirming inhibition of CK2 by both inhibitors and suggesting a potential divergence in the specificity between these two inhibitors when investigating the PI3K/Akt/mTOR pathway.

The intersection of the PI3K/Akt/mTOR and MAPK pathways has been previously proposed (as reviewed in (195)). Treatment with CX-4945 resulted in the activation of kinases that comprise the ERK MAPK pathway, with increased phosphorylation of ERK1/2, MEK1/2, and p90-RSK as quantified using MIB profiling. CK2-dependent inhibition is suggested as a potential mechanism given that two unrelated inhibitors of CK2 result in increased phosphorylation of ERK1/2 Thr202/Tyr204. This effect was determined to be independent of p38 MAPK activation, as treatment with either CK2 inhibitor did not result in phosphorylation of p38 MAPK. Interestingly, the activity of IRAK1 increased in response to CX-4945, and it has been documented that IRAK1 activation can lead to p38 MAPK activation dependent on Ras activation (196). The phosphorylation status of Ser259 on c-Raf did not change in this context, suggesting that the intersection of the PI3K/Akt pathway does not regulate this arm of the MAPK pathway. The activity of IRAK1 upstream of Ras suggests this pathway could still be activating c-Raf, given that other phosphorylation sites on c-Raf that modulate activity were not profiled. Previous investigation of CK2 in glioblastoma cells highlighted the activation of ERK in response to CK2 knockdown in the presence or absence of neocarzinostatin, although the presence of neocarzinostatin substantially enchanced ERK phosphorylation (197). The results presented here support the activation of the ERK MAPK pathway when cells are treated with CX-4945 or Inhibitor VIII, suggesting a CK2-dependent role in this manner. In contrast to this, more recent studies conducted in melanoma cell lines identified a CK2-dependent role for proteasomal degradation of dual specificity phosphatase-6 (DUSP6), which can reverse the activating phosphorylation on ERK mediated by MEK (198). Knock-down of CK2α resulted in increased levels of DUSP6, while high expression of CK2α maintained ERK

phosphorylation. A cell-line dependent effect may be plausible for the differences documented in terms of ERK phosphorylation, warranting further investigation. Despite apparent cell type specific contexts, these observations all suggest that CK2 can modulate the ERK MAPK pathway.

The identification of CDK phosphorylation at Tyr15 using MIB profiling suggested that in response to CX-4945 treatment HeLa cells undergo cell cycle arrest. The phosphorylation at Tyr15 is well known to inhibit the activity of CDK1 (178). In contrast, the phosphoproteomic investigation revealed that CDK1 and CDK2 substrates increased in phosphorylation in response to CX-4945 suggesting a progression in cell cycle from G2 to M phase. Western blotting and flow cytometry analysis were performed to investigate this difference. In agreement with the existing literature, CX-4945 treatment resulted in a G2/M accumulation during longer periods of treatment (44, 45). Shorter treatment of 240 minutes saw an increase in the G2 population in comparison to DMSO, suggesting cell cycle arrest occurred rapidly. These effects were not evident by western blotting at shorter time-points given that the markers used were specific for identifying the mitotic phase. Remarkably, treatment with Inhibitor VIII increased the phosphorylation of histone H3 Ser10 at 240 minutes but abolished it completely at 22 hours. One possible hypothesis is that treatment with this inhibitor drives cell cycle progression into mitosis, given that reports of histone H3 Ser10 phosphorylation as a result MAPK activation have been documented (199). The increase in mitotic phase cells was not as pronounced with CX-4945 treatment, and given the complete abolishment of histone H3 Ser10 phosphorylation at 22 hours of treatment with Inhibitor VIII, the specific reason for why histone H3 Ser10 phosphorylation occurs is difficult to reconcile without further investigation. Inhibitor VIII may exert a stimulatory

effect upon the kinase responsible for phosphorylation of histone H3 Ser10, Aurora B kinase (200, 201), or it may antagonize phosphatase activity towards this site (202, 203). This previously undocumented divergence between Inhibitor VIII and CX-4945 further calls into question the specificity of these CK2 inhibitors given differential outcomes in the phosphorylation status of proteins involved in distinct cellular processes.

Kinome profiling using MIBs enabled the characterization of kinase activity and validation of phosphoproteomic profiling of HeLa cells treated with CX-4945. A broad effect on kinase activity was documented, corroborating changes in the activity of kinases as inferred by phosphoproteomic analysis of HeLa cells treated with CX-4945 in earlier investigations in this thesis. Taken together, the analysis of the kinome and phosphoproteome identify CK2-dependent and CK2-independent effects in HeLa cells. Utilization of a different CK2 inhibitor further substantiates CK2-independent effects of CX-4945, as suggested by the incomplete overlap between the cellular effects of CX-4945 and Inhibitor VIII. These revelations call into question the utility of CX-4945 as an inhibitor of CK2 to study putative CK2-dependent processes in cells and warrant future studies to characterize putative CK2-independent effects.

4.4   Experimental Methods

4.4.1   Cell Culture and Lysis for Multiplexed Inhibitor Bead Profiling

SILAC-dropout DMEM (Life Technologies) supplemented with light and heavy isotope-encoded L-arginine and L-lysine was prepared as previously described in Chapter 3.4.2. HeLa Tet-Off cells that were previously adapted in SILAC media were grown in 15 cm dishes. Three biological replicates (consisting of three independent cell culture plates harvested on the same day) of heavy labeled cells were treated with 20 μM CX-4945

(MedKoo Biosciences) for 240 minutes with light labeled cells being treated with DMSO. In a "label-swap experiment" one biological replicate was used where the heavy labeled cells were treated with DMSO and the light labeled cells were treated with 20 μM CX-4945. Cells were rinsed with ice-cold PBS and lysed in MIB lysis buffer [0.5% Triton X-100 (Sigma), 50 mM (4-(2-hydroxyethyl)-1-piperazineethanesulfonic acid) (HEPES) pH 7.5 (Bioshop), 1 mM EDTA, 1 mM EGTA, 10 mM sodium fluoride, 1 μM microcystin-LR, 2.5 mM sodium orthovanadate, pepstatin (2.0 μg/mL), 0.2 mM phenylmethylsulfonyl fluoride (PMSF), leupeptin (20 μg/mL), aprotinin (4 μg/mL), and 1x phosphatase inhibitor cocktail 2 & 3 (Sigma P5726, P0044)]. Samples were sonicated for 3 x 10 seconds on ice then spun for 10 minutes at 16,000 x *g* at 4 °C. The supernatant was collected and clarified once more using a 0.2 μm syringe filter and protein concentration was determined by Bradford Assay (Bio Rad) before being stored at -80 °C until further processing. Aliquots of samples were diluted in sample loading buffer and 10 μg of sample was loaded per lane and separated by SDS-PAGE. Proteins were transferred to PVDF membrane (Millipore) using a wet-transfer apparatus (Bio-Rad) at 400 mA for 60 minutes at 4 °C followed by block in blocking buffer (LI-COR Biosciences) for 60 minutes. Primary antibodies were incubated overnight at 4 °C in 3% BSA-TBST or 3% BSA-PBST. Antibodies against GAPDH (MAB374, Millipore) and pEIF2S2 S2 (YenZym Laboratories, raised against ac-pS-GDEMIFDPTMSKC-amide) were used. Secondary antibodies used were GAR-800 (926-32211), GAM-800 (926-32210), and GAM-680 (926-32220) (LI-COR Biosciences) in 3% BSA-TBST or 3% BSA-PBST, with incubation for 45 minutes. Membranes were scanned using an Odyssey scanner (LI-COR Biosciences) at 700 nm and 800 nm wavelengths. Raw data scans were loaded into ImageStudioLite v5.2.5 (LI-COR Biosciences) and exported as .TIFF image files.

4.4.2 Multiplexed Inhibitor Bead Profiling Using a 6-Inhibitor Mix

MIB profiling of SILAC-labelled HeLa cells treated with CX-4945 was adapted from the protocol that was previously described by Qin et al (171). The MIB mix utilized was a generous gift from Dr. Lee M. Graves at the University of North Carolina, Chapel Hill, NC, and consisted of six kinase inhibitors each conjugated to ECH sepharose 4B: Shokat (204), PP58 (205, 206), VI16832 (83), Ctx-0294885 (207), purvalanol-B (208), and pan-Akt inhibitor UNC21474 (171). Chemical structures of these kinase inhibitors are displayed in Supplemental Figure 4.5. Equivalent amounts (2.5 mg) of heavy and light SILAC lysates were brought to 1M NaCl and equalized for volume prior to mixing. Samples were first passed over a column (Bio-Rad) containing ECH sepharose 4B, followed by passage over a column containing MIBs. MIB columns were then washed with 5 mL MIB lysis buffer containing 1M NaCl, followed by 5 mL MIB lysis buffer and 0.5 mL MIB lysis buffer containing 0.1% (w/v) SDS. Captured proteins were eluted twice with 0.5 mL [0.5% (w/v) SDS, 1% beta-mercaptoethanol, 100 mM Tris-HCl pH 6.8] by incubating at 95 °C for 15 minutes. Samples were then reduced with 5 mM DTT (Sigma) for 25 minutes at 60 °C, alkylated with 20 mM IAA (Sigma) for 30 minutes at room temperature in the dark and quenched with the addition of 10 mM DTT. Samples were then concentrated using 0.5 mL 10 kDa-cutoff spin filters (Millipore) and reduced to approximately 100 μL of volume. Samples were precipitated following chloroform (Sigma) and methanol (Fisher) extraction, using methanol, chloroform and water at a ratio of 4:1, 1:1 and 3:1 respectively to sample volume. Precipitated protein was pelleted by centrifugation at 16, 000 x *g* for 10 minutes followed by two washes with 0.5 mL of methanol. Pellets were digested using 1 μg trypsin-Lys-C (Promega) for 4 hours at 37 °C and topped up with 1 μg trypsin (Pierce) for overnight

digestion in 50 mM ammonium bicarbonate. Samples were then desalted using C18 StageTips, concentrated in a SpeedVac vacuum centrifuge and stored at -80 °C until LC-MS/MS analysis.

4.4.3 Multiplexed Inhibitor Bead Profiling Using a 4-Inhibitor Mix

MIB profiling of SILAC-labelled HeLa cells treated with CX-4945 was performed as previously described in Kurimchak *et al.* (172) and followed procedures similar to that used with the 6-Inhibitor mix. The MIB mix utilized was a generous gift from Dr. James S. Duncan at Fox Chase Cancer Center, Philadelphia, PA, and consisted of four inhibitors: PP58 (205, 206), VI16832 (83), Ctx-0294885 (207) and purvalanol-B (208). Heavy and light SILAC-labelled lysates (3-5 mg) were brought to 1M NaCl and equalized for volume prior to mixing. Samples were first passed over a column (Bio-Rad) containing beads conjugated with inhibitors PP-58, VI-16832 and purvalanol-B, followed by passage over a second column containing Ctx-0294885. MIB columns were then washed separately with 2 x 10 mL MIB lysis buffer containing 1M NaCl, followed by 10 mL MIB lysis buffer. Samples were then eluted from each column and combined prior to concentration. All subsequent steps in sample preparation followed the 6-Inhibitor mix procedure outlined in section 4.4.2.

4.4.4 LC-MS/MS Analysis of Samples Profiled by Multiplexed Inhibitor Beads

Samples were analyzed using an Orbitrap Elite Hybrid Ion Trap-Orbitrap mass spectrometer using the acquisition parameters and settings previously described in Chapter 2.4.10. Biological replicates were each analyzed in technical duplicate. Raw mass spectra files were analyzed in MaxQuant version 1.5.3.8 (70, 71, 164) and searched against the Swissprot-Uniprot sequence database (*homo sapiens* taxon, accessed on December 26, 2015). Samples were searched using a Multiplicity set to 2, with "heavy" labels selected as Arg6 and Lys4.

Mass tolerances were set to 4.5 ppm for the parent ion mass (MS) and 0.5 Da for the fragment ion mass (MS/MS). The minimum number of amino acids in a peptide was set to 7, with a peptide spectrum match (PSM) and protein match set to 1% FDR and protease selectivity for trypsin/P. A maximum number of 3 missed cleavages was selected. The option for second peptide search was selected, as was the use of "Match Between Runs" for respective pairs of samples between biological replicates, using the default matching parameters. Raw mass spectra files were defined as separate groups using the experimental setup option. Cysteine carbamidomethylation (+ 57.0215 Da) was set as a fixed modification. The number of variable modifications per peptide was 5, with methionine oxidation (+15.9949 Da), protein N-terminus acetylation (+42.0105 Da), asparagine and glutamine deamidation (+0.9840 Da) and serine, threonine, and tyrosine phosphorylation (+79.9663) selected. The minimum score for modified peptides was set to 40, and the decoy-database setting was "Revert." For quantitation of protein groups, unmodified peptides and those with carbamidomethylation, methionine oxidation, protein N-terminus acetylation or asparagine and glutamine deamidation were included. Peptides for which the corresponding heavy or light modified peptide was not quantified were excluded from the protein groups quantitation. Output data from MaxQuant was then loaded into Perseus version 1.5.2.6 (121). For the analysis of proteome data, the "proteinGroups.txt" file was first processed to remove entries marked as reverse decoy database hits, contaminants, and protein identifications that were only matched to modified peptides. MaxQuant-generated normalized ratios were utilized, and the log base 2 of the normalized ratios was calculated for each protein. Proteins were considered identified in each biological replicate if identified in at least one of two technical replicates. For the analysis of the phosphoproteome data, the "Phospho

(STY)Sites.txt" file was first processed to remove entries marked as reverse decoy database hit and contaminants, and filtered to only contain phosphorylation sites with localization probability greater than 0.75. Phosphorylation sites were expanded in Perseus to obtain information from instances of quantified sites being derived from singly, doubly and triply-phosphorylated peptides. Rows where no quantification was present were removed, and phosphorylation sites were considered quantified in each biological replicate if they were identified in at least one of two technical replicates.

4.4.5   Cell Culture and Lysis for Analysis of mTOR/Akt and MAPK Pathways

HeLa Tet-Off cells (Clontech) were cultured in Dulbecco's modified Eagle's medium (DMEM) (Corning) containing 10 % FBS, penicillin (100 U/mL) and streptomycin (100 µg/mL) on 10 cm dishes or in 6-well plates. Cells were either grown in media containing 10% FBS or were serum starved for 18 hours prior to treatment with inhibitors. Cells were treated with 20 µM CX-4945 (MedKoo Biosciences), 15 µM Inhibitor VIII (Calbiochem), 0.25 µM Torin1 (Selleckchem), 1 µM MG-132 (Sigma), 20 ng/mL neocarzinostatin (Sigma), 2 µM staurosporine (LC Laboratories) or DMSO diluted in media without FBS for indicated time-points. Cells were rinsed with PBS on ice prior to lysis. For experiments used to generate Figures 4.10-4.11, HeLa cells were lysed in MIB lysis buffer that is described in section 4.4.1. For all remaining experiments, HeLa cells were lysed in a RIPA lysis buffer [1% NP-40 Alternative (Calbiochem), 50 mM Tris pH 7.5, 150 mM sodium chloride 0.5% sodium deoxycholate (Sigma), 0.2% SDS, 1 mM EDTA, 25 mM β-glycerophosphate, 1 µM okadaic acid, 50 mM sodium fluoride, 1 µM microcystin-LR, 10 mM sodium orthovanadate, 5 mM sodium pyrophosphate, pepstatin (10 µg/mL), 1 mM phenylmethylsulfonyl fluoride (PMSF), leupeptin (100 µg/mL), and aprotinin (20 µg/mL)]. Samples were sonicated for 2 x

15 seconds on ice then spun for 10 minutes at 16,000 x *g* at 4 °C, upon which the supernatant was retained and protein concentration was determined using a BCA assay (Pierce). Samples (10 μg each) were separated by SDS-PAGE and transferred to PVDF membranes for Western blotting using procedures outlined in Chapter 4.4.1. Antibodies against phospho-p90RSK S380 (9335), p90RSK (9355), phospho-ERK1/2 T202/Y204 (9106), ERK (9102), phospho-MEK1/2 S217/221 (9154), MEK1/2 (4694), phospho-p38 MAPK T180/Y182 (9216), p38 MAPK (8690), phospho-Akt T308 (13038), phospho-Akt S473 (4060), phospho-c-Raf S338 (9427), phospho-c-Raf S259 (9421), phospho-mTOR S2448 (5536), mTOR (2983), LC3B (3868), phospho-Raptor S792 (2089), phospho-Ulk1 S638 (14205), p70S6K T389 (9234), PARP (9542), phospho-4E-BP1 T37/46 (2855) (all from Cell Signaling Technologies), hVIN1 (V9131, Sigma), γH2AX S139 (ab26350, Abcam), phospho-Akt S129 (ab133458, Abcam), GAPDH (MAB374, Millipore), and phospho-EIF2S2 S2 (YenZym Laboratories, raised against ac-pS-GDEMIFDPTMSKC-amide) were used.

4.4.6 Cell Culture and Sample Preparation for Cell Cycle Analysis using Flow Cytometry and Western Blotting

HeLa Tet-Off cells (Clontech) were cultured in Dulbecco's modified Eagle's medium (DMEM) (Corning) containing 10 % FBS, penicillin (100 U/mL) and streptomycin (100 μg/mL) on 10 cm dishes. Cells were treated with 20 μM CX-4945 (MedKoo Biosciences), 15 μM Casein Kinase II Inhibitor VIII (Calbiochem), 0.25 μM Torin1 (Selleckchem) or DMSO for 240 minutes or 22 hours. In parallel, cells were treated with 40 μM lovastatin (Sigma-Aldrich), 400 μM mimosine (Sigma-Aldrich), 2 mM thymidine (Sigma-Aldrich), nocodazole (0.4 μg/mL) (Sigma-Aldrich) or were serum-starved for 24 hours to generate arrested populations to aid in the setting of cell-cycle specific gated populations for flow cytometry

and for the comparison by Western blotting using cell-cycle markers. After treatment, media was retained and adherent cells were washed with PBS, then incubated with 0.25% trypsin, 0.02% EDTA solution at 37 °C to lift the cells. Cells were suspended in collected media, centrifuged at 100 x *g* then suspended in fresh serum-free DMEM. An aliquot was stained with 0.08% trypan blue solution (Sigma-Aldrich) and the concentration of cells was determined using a hemocytometer. Aliquots of 1 million cells were centrifuged at 100 x *g* and washed with PBS. For Western blotting, cell pellets were lysed in 300 μL lysis buffer [1% NP-40 Alternative (Calbiochem), 50 mM Tris pH 7.5, 150 mM sodium chloride 0.5% sodium deoxycholate (Sigma), 0.2% SDS, 1 mM EDTA, 25 mM β-glycerophosphate, 1 μM okadaic acid, 50 mM sodium fluoride, 1 μM microcystin-LR, 10 mM sodium orthovanadate, 5 mM sodium pyrophosphate, pepstatin (10 μg/mL), 1 mM phenylmethylsulfonyl fluoride (PMSF), leupeptin (100 μg/mL), and aprotinin (20 μg/mL)]. Samples were sonicated for 2 x 15 seconds on ice then spun for 10 minutes at 16,000 x *g* at 4 °C, upon which the supernatant was retained and protein concentration was determined using a BCA assay (Pierce). Samples (10 μg each) were separated by SDS-PAGE and transferred to PVDF membranes for Western blotting using procedures outlined in Chapter 4.4.1. Antibodies against phospho-histone H3 S10 (9542), histone H3 (9715), cyclin B1 (12231), - phospho-cdc2 Y15 (4539), phospho-4EBP1 T37/46 (2855) (all from Cell Signaling Technologies), γH2AX S139 (ab26350, Abcam), GAPDH (MAB374, Millipore), and phospho-EIF2S2 S2 (YenZym Laboratories, raised against ac-pS-GDEMIFDPTMSKC-amide) were used. For flow cytometry analysis, samples were processed as previously described in Vignon *et al*. (188) with some modifications. Cell pellets were suspended in 1 mL PBS and added drop-wise to 5 mL of ice cold 95% ethanol with agitation between drop-

wise addition then fixed overnight at − 20 °C. Samples were centrifuged at 500 x *g* for 5 minutes at room temperature, followed by aspiration of ethanol and suspended in PBS before being transferred to FACS tubes. Samples were then washed twice with 3 mL PBS, followed by two washes with 1 mL 0.25% Triton X-100, 1% FBS in PBS (PFT). Samples were stained in 200 µL of PFT for 30 minutes in the dark, after being mixed with 15 µg of 7-aminoactinomycin (7-AAD) (A1310, Thermo Scientific), 3 µL of anti-phospho-histone H3 Ser10 conjugated to AlexaFluor-488 (3465, Cell Signaling Technology), and 3 µL of anti-Ki67 conjugated to AlexaFluor-488 (11882, Cell Signaling Technology). Single stain and iso-type controls were processed in parallel. Samples were then washed twice with 1 mL PFT and once with 1mL PBS. Cells were analyzed on a Becton Dickinson FACSCanto cytometer using FACSDiva software, acquiring 10,000 cell events per sample. Data generated were analyzed using FLOWJo software v10.2 (FLOWJo, LLC, Ashland, Oregon), gating populations according to forward and side scatter profiles and setting cell-cycle specific populations according to positive control populations arrested in specific phases of the cell cycle.

4.4.7   Cell Culture and Sample Preparation for Cell Viability Analysis using Flow Cytometry

HeLa Tet-Off cells (Clontech) were cultured in Dulbecco's modified Eagle's medium (DMEM) (Corning) containing 10 % FBS, penicillin (100 U/mL) and streptomycin (100 µg/mL) on 10 cm dishes. Cells were treated with 20 µM CX-4945, 15 µM Casein Kinase II Inhibitor VIII, or DMSO for 240 minutes or 22 hours. In parallel, cells were treated with 2 µM staurosporine as a positive control for gating live and dead cell populations. After treatment, media was retained and adherent cells were washed with PBS, then incubated with

0.25% trypsin, 0.02% EDTA solution at 37 °C to lift the cells. Cells were suspended in collected media, centrifuged at 500 x g then suspended in warm 5% FBS in PBS. An aliquot was stained with 0.08% trypan blue solution (Sigma-Aldrich) and the concentration of cells was determined using a hemocytometer. 100,000 cells were aliquoted into FACS tubes, centrifuged at 100 x g and suspended in 200 μL Annexin V binding buffer (Biolegend). 4 μL of anti-annexin-V conjugated to Brilliant Violet 421 (640923, Biolegend) was added to the sample and incubated in the dark for 15 minutes. Single colour and unstained live and dead cell populations were processed as well. Samples were then diluted with 1 mL of 5% FBS in PBS and centrifuged at 500 x g. The volume was reduced to approximately 200 μL by vacuum aspiration and 4 μL of 7-AAD solution (420404, Biolegend) was added prior to analysis on a Becton Dickinson FACSCanto cytometer using FACSDiva software, acquiring 10,000 cell events per sample. Data generated were analyzed using FLOWJo software v10.2 (FLOWJo, LLC, Ashland, Oregon), gating populations according to forward and side scatter profiles and setting live and dead specific populations according to positive control populations and single colour stains.

4.5   Supplemental
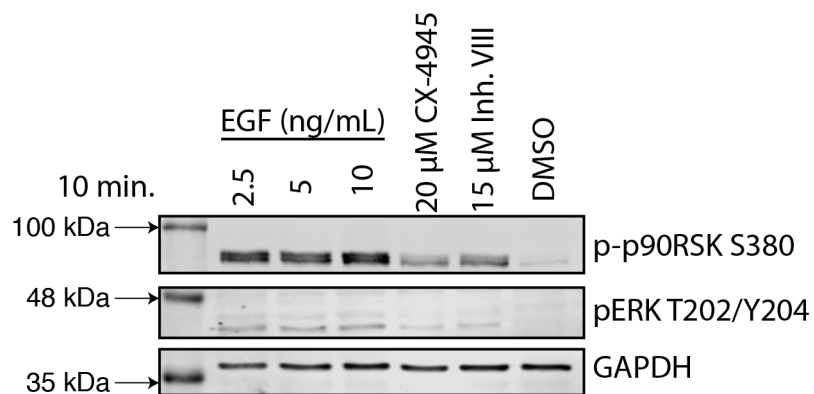
Supplemental Figure 4.1 CX-4945 and Inhibitor VIII Stimulate ERK1/2 Phosphorylation
HeLa cells were serum starved for 18 hours prior to treatment with EGF, CX-4945, Inhibitor VIII or DMSO at indicated concentrations for 10 minutes.
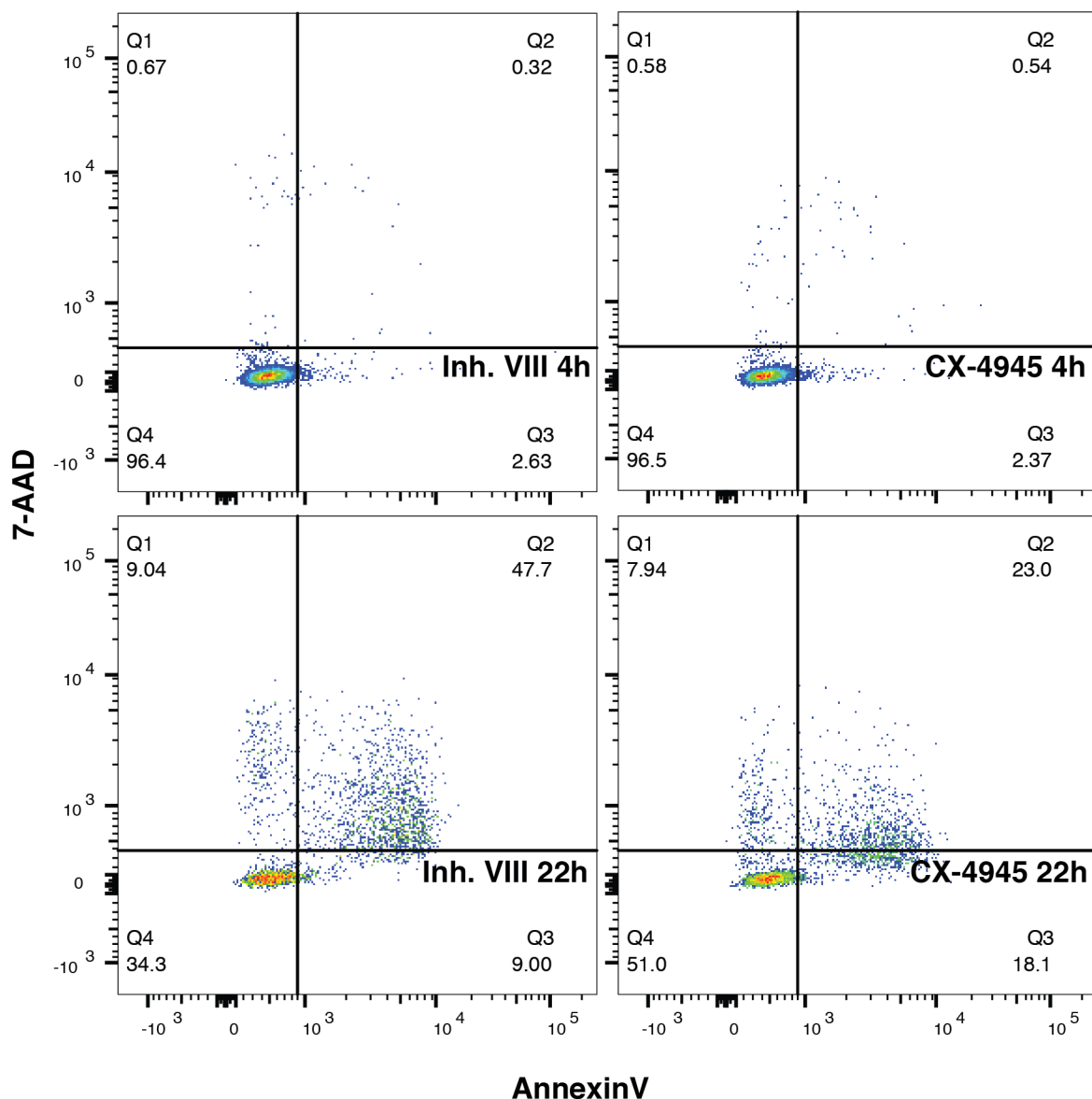
Supplemental Figure 4.2 Cell Viability of HeLa Cells Treated with CX-4945 and Inhibitor VIII
HeLa cells were grown in media supplemented with FBS, followed by treatment with CX-4945, Inhibitor VIII, Torin1 or staurosporine for 4 or 22 hours. Cells were processed for cell viability analysis by flow cytometry, staining with 7-AAD, and an antibody against annexin-V conjugated to BV-421. Non-viable cells are located in quadrant Q2.
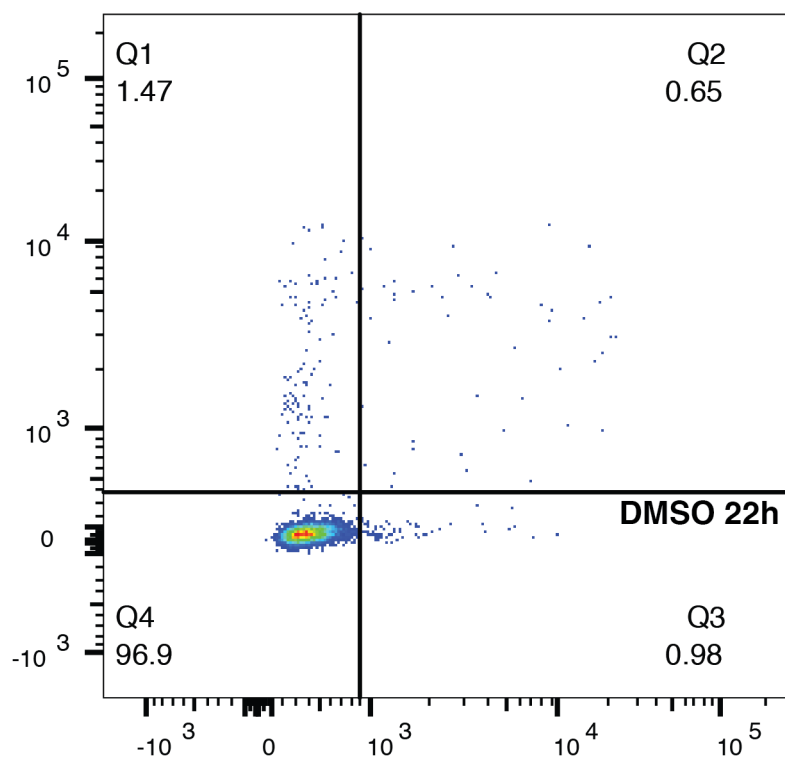
Supplemental Figure 4.3 Cell Viability of HeLa Cells Treated with DMSO
HeLa cells were grown in media supplemented with FBS, followed by treatment with DMSO for 22 hours. Cells were processed for cell viability analysis by flow cytometry, staining with 7-AAD, and an antibody against annexin-V conjugated to BV-421.
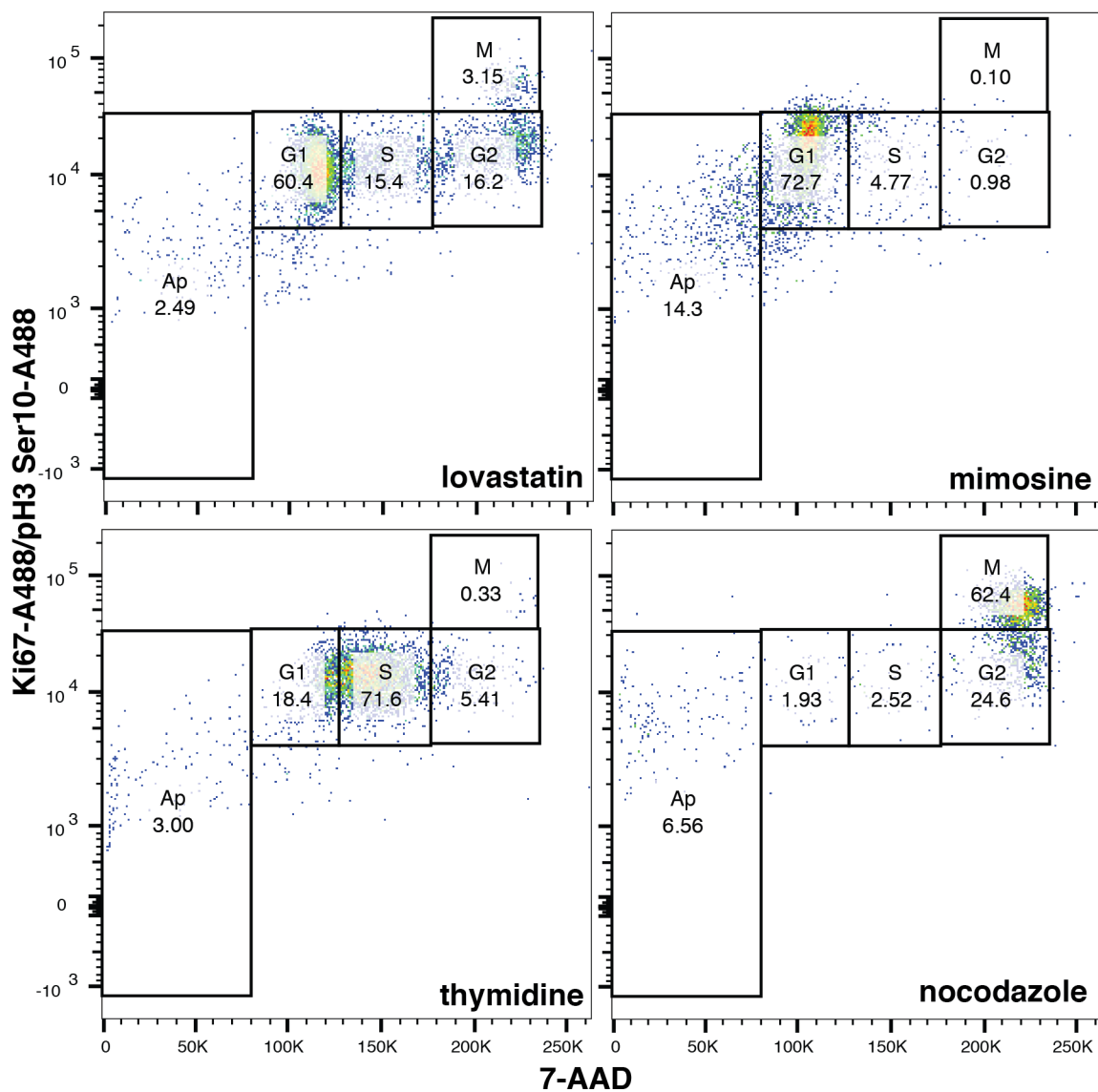
Supplemental Figure 4.4 HeLa Cells Arrested in Specific Phases of Cell Cycle
HeLa cells were treated with lovastatin, mimosine, thymidine or nocodazole for 24 hours.
Cells were processed for cell cycle analysis by flow cytometry, staining with 7-AAD, and
antibodies against Ki-67 and phospho-histone H3 Ser10, both conjugated to AlexaFluor-488.
Gating was performed on forward and side scatter profiles to isolate single cells.
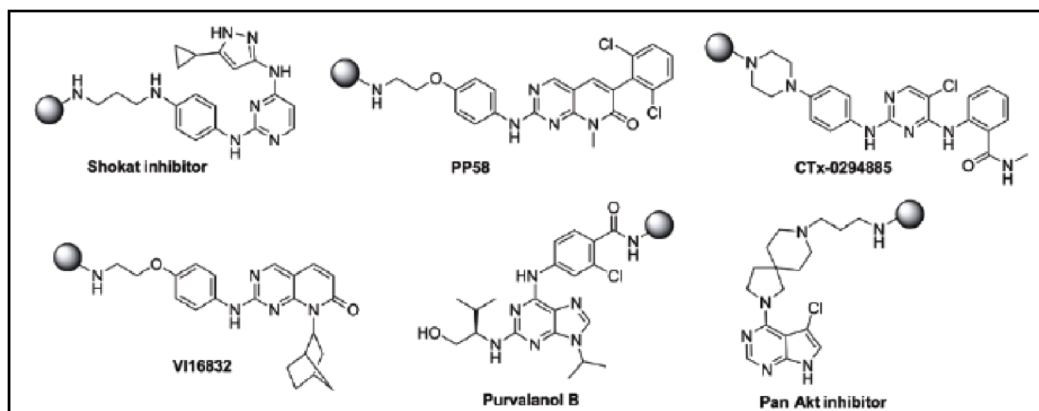
Inhibitor	Specificity
Shokat	broad
PP58	broad
CTx-0294885	broad
VI16832	broad
Purvalanol B	CDK family
Pan Akt (UNC21474)	Akt family

Supplemental Figure 4.5 Chemical Structures of Multiplexed Inhibitor Beads

5   Chapter 5 – Discussion

5.1   Introduction

The phosphorylation of proteins at serine, threonine and tyrosine residues is a critical post-translational modification involved in the transmission of regulatory signals that control cellular homeostasis. The addition of phosphate to these phospho-acceptor amino acid residues is mediated by protein kinases in eukaryotes. Expectedly, deregulation of kinase activity can contribute to aberrant signaling processes implicating kinases in the progression of diseases such as cancer (8). The work presented in this thesis has been focused on protein kinase CK2, a small family of enzymes that has been traditionally classified as serine/threonine specific but also demonstrated to be capable of phosphorylating tyrosine residues (209). Considering the number of proteins that are phosphorylated by CK2 implicating it in the regulation of several pathways (15), and its deregulated expression in several different types of human cancer (14), CK2 has emerged as a therapeutic target. In fact, an orally bioavailable small molecule ATP-competitive inhibitor of CK2, CX-4945, has recently progressed into clinical trial (44). Given the emergence of CK2 as a therapeutic target, the goal of this thesis was to utilize a mass-spectrometry based proteomics approach to perform unbiased profiling of CX-4945. This approach enabled the identification of dynamic markers of CK2 inhibition and CK2-dependent processes in cells treated with CX-4945, as well as revealing potential CK2-independent effects of CX-4945.

5.2   Summary of Research Contributions

5.2.1   Development of a Phosphoproteomic Workflow

Prior to directly undertaking a phosphoproteomics approach to characterize the effects of CX-4945 in HeLa cells, a comparative investigation of sample preparation methods

was performed in order to determine an optimized phosphoproteomics workflow. Conventional phopshoproteomic strategies typically take advantage of large-scale fractionation methods such as strong-cation exchange chromatography to increase the enrichment of lower abundance phosphopeptides (96). With recent advances in mass spectrometry, strategies for phosphopeptide enrichment that do not require fractionation have also been developed and have been documented to perform comparably to fractionation approaches such as strong cation exchange chromatography (108). In chapter 2, comparison of strategies for phosphopeptide enrichment performed both with and without fractionation by strong cation exchange demonstrated that the two approaches were comparable in phosphopeptide identification. By comparing different sorbents for sample desalting, I observed that using porous graphitic carbon for sample desalting resulted in an enrichment of phosphopeptides that contained a CK2 consensus motif. Considering that the amino acid specificity determinants for CK2 can render a peptide sequence hydrophilic in nature (92-95), matching a sorbent such as porous graphitic carbon which is selective for polar compounds enables better identification of CK2 phosphopeptides than using a reverse-phase C18 sorbent. Another recent development in a phosphopeptide enrichment protocol termed "EasyPhos" utilizes a digestion buffer compatible with phosphopeptide enrichment thereby omitting desalting prior to enrichment, and takes advantage of mixed-mode styrene-divinyl-benzene reverse phase sulfonate sorbent (SDB-RPS) for desalting prior to LC-MS/MS analysis (210). This results in a simplified format omitting steps which can incur sample loss normally observed with desalting, reducing the amount of protein sample required for enrichment and enabling the retention of hydrophilic phosphopeptides for LC-MS/MS. Considerations in tailoring sorbents and protocols for enrichment of target analyte can

enhance contextual biological information in proteomic investigations of interest. The comparison of porous graphitic carbon to C18 solid phase extraction columns for peptide desalting demonstrates the utility of hydrophilic sorbent in analyzing phosphopeptides derived from CK2 substrates.

The investigation of proteome preparation revealed advantages in using protein precipitation in comparison to filter-aided sample preparation for the generation of proteomes for subsequent phosphopeptide enrichment. Although both preparation methods identified nearly the same number of proteins, protein precipitation yielded more phosphorylation sites. In this thesis protein precipitation was performed using TCA and acetone overnight at -20 °C. However other protein precipitation protocols such as chloroform/methanol (211) which can be done within the span of one hour could be used in order to reduce sample processing time.

In summary, when considering the evaluation of CK2 phosphopeptides by mass spectrometry it is necessary to tailor sorbents and materials to match the unique determinants that render the substrates of CK2 hydrophilic. It was demonstrated that using porous graphitic carbon could enrich for phosphopeptides conforming to the CK2 consensus sequence. In considering the practical aspects of profiling the phosphoproteome, sample handling and instrument time are reduced when utilizing an unfractionated strategy. This resulted in similar rates of protein and phosphorylation site identification. Furthermore, comparative analysis of proteome sample preparation strategies identified that protein precipitation of samples coupled with two-step C18 and porous graphitic carbon peptide desalting in combination with phosphopeptide enrichment enables the identification of a maximum number of proteins and phosphorylation sites in a timely manner. Taken together,

these results demonstrate the utility of an unfractionated phosphoproteomics tailored with hydrophilic sorbents that should be employed when analyzing CK2 phosphopeptides.

5.3   Unbiased Proteomic Characterization of CX-4945

5.3.1   CX-4945 Results in a Dynamic Phosphoproteome

CX-4945 represents the first clinical stage ATP-competitive inhibitor of CK2 to progress into clinical trial. Despite the advances of CX-4945 in therapeutic applications and widespread utilization as the "gold standard" CK2 inhibitor in the research community, it is unclear how its effects are rendered in cells. A systematic quantitative phosphoproteomic approach was undertaken utilizing SILAC labeled cells to characterize the impact of CX-4945 treatment in HeLa cells following the optimization of a phosphoproteomics workflow tailored to identify phosphopeptides derived from CK2 substrates. This approach enabled the identification of phosphorylation sites indicating CK2 inhibition that exhibited dynamic de-phosphorylation over a period of 240 minutes. Several of these sites displayed a magnitude of change that was greater than that of EIF2S2 Ser2, a bona fide substrate of CK2 that has been previously exploited to monitor CK2 inhibition in cells. This included the identification of topo-isomerase II alpha (TOP2A) Ser1377 and presents an opportunity to use this phosphorylation site as an indicator of CK2 inhibition in cells. Furthermore, identification of differential de-phosphorylation on EIF2S2 at Ser2 and Thr111 in response to CX-4945 highlights a previously underappreciated role of phosphatase activity towards CK2 phosphorylation sites on the same protein.

Overall, analysis of CK2 phosphorylation sites that decreased in response to CX-4945 utilizing gene set enrichment analysis identified biological processes involved in DNA repair and translation. Previous studies have also highlighted the role that CK2 plays in regulating

proteins that are components of these processes (29, 212). Collectively, these findings suggest that these biological processes may be representative of the most critical pathways involved in the maintenance of cellular homeostasis that are first affected upon inhibition of CK2.

The phosphoproteomics approach presented in chapter 3 also enabled the profiling of phosphorylation sites attributed to other kinases that were revealed using kinase substrate enrichment analysis. Inhibition of CK2 may lead to the indirect regulation of other kinases in the cell. There is precedence for the regulation of kinases through the activity of CK2 towards the phosphorylation of cdc37 Ser13, a kinase co-chaperone (136). Interestingly, treatment with CX-4945 within the period of time up to 240 minutes affected several other kinases such as Akt1 and mTOR as concluded by the phosphorylation status of target substrates.

MIB profiling was performed in order to investigate whether changes observed in the phosphoproteomic profiling would correlate with the change in activity of the respective upstream kinases. Indeed when this investigation was followed up, kinases in the PI3K/Akt/mTOR pathways were affected by CX-4945. Although the quantification of activity in mTOR did not change drastically as well as CK2, other kinases that are downstream of mTOR such as Akt1, Sgk1 and Ulk1 changed in activity suggesting mTOR inhibition.

5.3.2   Limitations of Profiling Effects of CX-4945 in HeLa Cells Using MIBs

One potential limitation in using MIBs to determine the activity of kinases that are targets of CX-4945 in cells is that the residual amount of CX-4945 in the lysate that could interfere with the ability of kinases to bind to the MIBs. Considering that the protein extracts

from treated and untreated samples are mixed 1:1 prior to MIB profiling, residual CX-4945 from the treated samples may interfere with the CK2 catalytic subunits derived from cells that were treated with DMSO. Consequently, this may also impact the putative off-targets of CX-4945, thus explaining why regulation of mTOR was not apparent although downstream targets were quantified.

Another limitation may relate to the composition of the inhibitor mix used for profiling. In this respect, a recent investigation of kinase activity profiling methods such as MIBs identified cases where capture of kinases by MIBs was independent of kinase activity (213). The MIB strategy by Duncan *et al*. (84) is intended to isolate the active kinome. Ruprecht *et al.* (214) noted that the type inhibitor mix used could affect the conformation-dependent binding. On a related note, determining which variable modifications are included for peptides derived from kinases that are used for quantification may also obscure the activity of a kinase by MIB profiling. Typically peptides with variable modifications that could play a regulatory role are excluded in the quantitation at the protein level, and only modifications that result because of sample handling, as in the case of methionine oxidation are included in such searches. This was the case for ERK1/2 where the quantification at the protein level revealed no apparent change but the phosphorylation status of Thr202/Tyr204 and Thr185/Tyr187 increased. In these analyses, peptides with phosphorylation as a variable modification were excluded in the calculation of protein abundance considering it was unknown beforehand whether phosphorylation sites on kinases which change but do not confer activation status could result in quantification unrepresentative of biochemical function. Despite this limitation, utilizing the phosphorylation specific data collected in these experiments still enabled investigation of kinase activity. Efforts to overcome the limitations

of affinity-capture strategies, such as MIBs for profiling the active kinome, represent an active area of investigation. In this respect, a very recent study presented an optimized MIB mix using 12 different inhibitors that when coupled with improvements in liquid chromatography using monolithic columns and targeted mass spectrometry enabled the reliable quantification of active kinases (215). Looking to the future, it can be expected that further technological developments in this field will improve the systematic quantification of kinase activity by MIB profiling.

5.3.3 Differential Effects of CX-4945 and Inhibitor VIII in HeLa cells

The phosphoproteomic and kinome profiling suggested that mTOR was also affected in addition to inhibition of CK2. By comparison, treatment of HeLa cells with an unrelated inhibitor, "Inhibitor VIII" identified a differential effect upon the PI3K/Akt/mTOR pathway in contrast to CX-4945, with both inhibitors displaying a decrease in phosphorylation of EIF2S2 Ser2. This result suggests that CX-4945 is also a putative inhibitor of mTOR in HeLa cells and warrants further investigation. This contrasted to the observation that both Inhibitor VIII and CX-4945 treatment resulted in activation of the ERK MAPK pathway. Interestingly, when cell cycle analysis was performed by flow cytometry, CX-4945 and Inhibitor VIII treatment also resulted in distinct effects on phospho-histone H3 Ser10. Collectively, these results raise questions about the specificity of these CK2 inhibitors and emphasize the need for systematic characterization of kinase inhibitors to both validate inhibition of the intended target and identify potential downstream effects of target inhibition or potential off-targets. Furthermore, the results presented in this thesis highlight the underappreciated complexity of the phosphoproteome when challenged with CX-4945,

which has been used extensively as the "gold standard" CK2 inhibitor given its emergence in ongoing clinical trial.

5.4   Future Directions

5.4.1   Characterization of CK2-independent Effects of CX-4945 in cells

Given the utility of small molecule inhibitors in delineating signaling pathways in cells, it is critical to understand the potential off-target effects that may incorrectly attribute protein function to a pathway. The identification of the PI3K/Akt/mTOR pathway as a putative target of CX-4945 raises questions about the precise mechanisms of action of CX-4945 in cells. There is previous literature which suggests that CX-4945 can down-regulate the PI3K/Akt/mTOR pathway (51, 54, 189): however, in this thesis comparative investigation using another unrelated CK2 inhibitor revealed differential effects on this pathway. In particular, treatment with CX-4945 and Inhibitor VIII displayed differences in the phosphorylation of 4E-BP1, although both inhibitors decreased the phosphorylation of EIF2S2 Ser2. The phosphorylation status of substrates of kinases is one approach that has been utilized to understand drug-target engagement in cells but is considered an indirect read-out. A recent study proposed an innovative assay as an alternative strategy in drug discovery to examine drug-target engagement in cells, cell extracts and tissues. The cellular thermal shift assay (CETSA) relies on the biophysical concept of ligand-induced thermal stabilization of proteins and enables the assessment of drug binding to a protein (216). By incubating aliquots of cell lysate with a drug and subjecting each aliquot to a different temperature, the amount of the target protein of interest that remains soluble can be measured and a thermal melt curve can be calculated. Stabilization of the target protein by the drug will result in a shifted melt curve, and can be used to identify drug-target protein interaction. This

application can be adapted for western blotting or in micro-titer plates for increased throughput (217). Recent developments in mass spectrometry technology coupled with tandem mass tag labeling reagents have also enabled the monitoring of several thousand proteins and the respective melt curves in response to inhibitor treatment (218). This analysis identified ferrochelatase as a novel target of vemurafenib and alectinib, highlighting a previously unreported mechanism of action that explains known photosensitivity side effects. Although the application of thermal proteome profiling by mass spectrometry requires the use of specific mass spectrometry instrumentation and reagents, it would be feasible on a smaller scale to begin to study the effect of CX-4945 on constituents of the PI3K/Akt/mTOR pathway by utilizing protein specific antibodies in an adaption of CETSA for western blotting.

5.4.2   Investigating the CK2-dependent Phosphoproteome Using Cells Engineered to express CX-4945-resistant CK2

The phosphoproteomics workflow investigating the effect of CX-4945 treatment on HeLa cells presented in this thesis identified its broad impact on the phosphoproteome. Considering that CX-4945 treatment resulted in the regulation of several different kinases, it would be of interest to be able to delineate which of the signaling events observed are indirect effects of CK2 inhibition as opposed to off-targets. Another factor in the CK2 field that has been underappreciated is the ability to discriminate between the isoform specificity of CK2α and CK2α phosphorylation, as CX-4945 can inhibit both isoforms (44). In an effort to understand the structural basis of CK2 inhibition by ATP-competitive inhibitors, previous studies have identified critical residues in the ATP-binding pocket of CK2α, including Val66 and Ile174 that are essential for inhibitor binding. Furthermore, mutation of these residues to alanine

resulted in resistance to binding with a number of CK2 inhibitors while retaining catalytic activity (219). In the case of CX-4945, structural studies have also revealed an important role of His160 for interactions between CK2α and CX-4945 (or His161 in the case of CK2α'). Increased resistance to treatment with CX-4945 is achieved by substituting His160 (or His161) to glutamic acid or aspartic acid in combination with Val66Ala/Ile174/Ala substitutions. These studies have inspired efforts in our laboratory to devise chemical proteomic strategies to investigate cellular targets of CK2 inhibitors (18). In addition, this information has also been exploited to generate cell lines harboring inhibitor-resistant forms of CK2α and CK2α', that are dramatically less sensitive to a number of CK2 inhibitors including CX-4945 and Inhibitor VIII treatment.

The work that is described in this thesis utilized duplex SILAC to enable relative quantification of peptides derived from CX-4945 treated cells versus control cells. This approach utilized labeling one set of cells with arginine ($^{13}C_6$) and lysine (4,4,5,5-d4) resulting in mass shifts of 6 and 4 Da respectively in comparison to normal isotope encoded amino acids. To extend these studies, triplex SILAC-based phosphoproteomics can be employed using the cell lines harboring inhibitor resistant forms of CK2 to distinguish between direct and indirect CK2 signaling events as well as characterizing off-target effects (Figure 5.1). Utilizing a third set of labeled arginine ($^{13}C_6$ $^{15}N_4$) and lysine ($^{13}C_6$ $^{15}N_2$) which would result in mass shifts of 10 and 8 Da respectively, a population of inhibitor-resistant cells treated with CX-4945 could be compared to DMSO and CX-4945 wild-type treated cells, enabling the identification of phosphopeptides that are affected by the inhibitor in the presence of the inhibitor-resistant forms of CK2. Furthermore, comparison of datasets obtained from inhibitor-resistant CK2α and CK2α' cells could identify sets of

phosphorylation sites that are differentially regulated, indicating isoform-specific substrates. Related experiments utilizing a triplex SILAC approach could also take advantage of different classes of CK2 inhibitors, such as those that target unique features outside of the ATP-binding pocket (220) or which abrogate the stability of the tetrameric holo-enzyme complex of CK2 (221). This would enable the identification of phosphorylation sites on substrates that require tetrameric CK2. Overall, the development of inhibitor-resistant cell lines presents interesting opportunities for studying CK2-dependent signaling events under different biological contexts and will greatly aid in the characterization of cellular processes regulated by CK2.

5.4.3 Targeted Profiling of CK2-dependent Phosphoproteome Using Mass Spectrometry

The identification of phosphorylation sites that display dynamic de-phosphorylation in response to CX-4945 will serve as a useful panel of activity markers upon which a targeted strategy to monitor the actions of CX-4945 can be developed. As these phosphorylation sites are derived from phosphopeptides that were detected using data-dependent acquisition methods, the likelihood of successfully developing a targeted mass spectrometry assay to profile CK2 activity is high (222). Historically, selected reaction monitoring (SRM) (also referred to as multiple reaction monitoring (MRM)) has been used as the gold standard for profiling proteotypic peptides (223). Further advances in mass spectrometry instrumentation have enabled the utilization of a similar technique termed parallel reaction monitoring (PRM) that can be performed on hybrid quadrupole-orbitrap instruments, such as the Q Exactive (224, 225). The advantage of PRM lies within the ability to simultaneously monitor all fragment ions from a precursor ion selected in MS1 with high resolution and high mass

accuracy in comparison to SRM, and does not require *a priori* optimization of precursor and fragment ion transitions. A recent application of a targeted PRM assay demonstrated the utility of using a panel of isotopically-labeled synthetic phosphopeptides as a readout for a phosphorylation signature that could be used to monitor the effect of different chemical inhibitors (226). PRM assays could also be used to monitor the activity of individual kinases in particular contexts. In this respect, proteomic investigations have identified CK2 phosphorylation sites that increase in response to stimuli such as DNA damage (35, 36), metformin (227), and vemurafenib (85) that could be monitored using PRM strategies. Therefore, synthesis of isotopically-labeled phosphopeptides that are representative of CK2 activity could be used to systemically profile CK2 activity using a PRM assay in cells treated with DNA damaging agents or potentially in different biological contexts. Considering the therapeutic potential of CK2 as a clinically relevant target, a panel of targeted phosphopeptides could be used to profile samples derived from patient tissues receiving CX-4945 to assess treatment efficacy or efficacy of new CK2 inhibitors as they emerge in the literature.
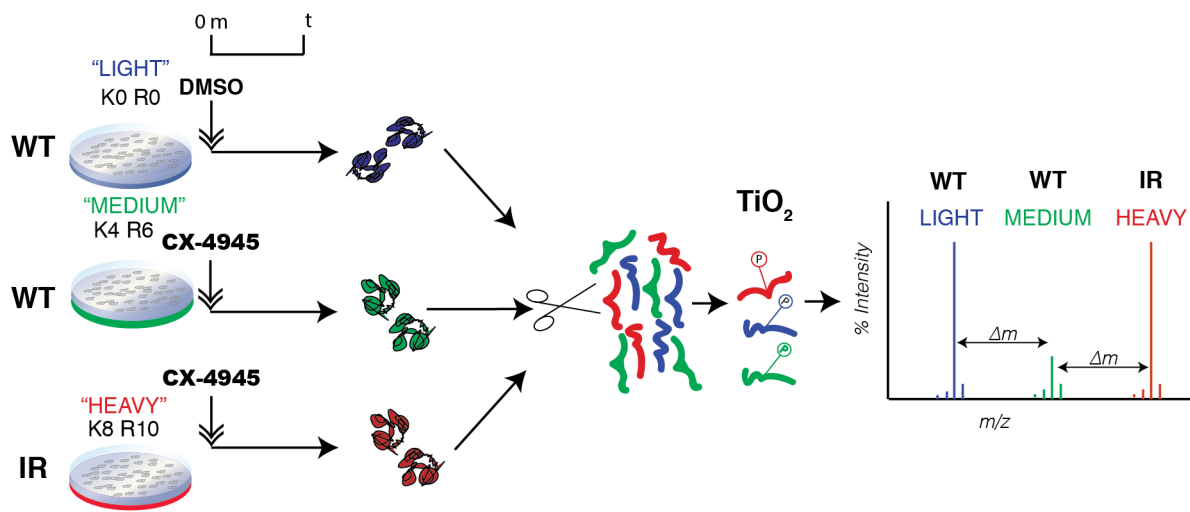
Figure 5.1 Comparative Phosphoproteomic Analysis Using Inhibitor-Resistant Cells to Identify *Bona Fide* Effects of CK2 and *Bona Fide* CK2-independent Effects of CX-4945. Cells harboring inhibitor-resistant forms of CK2 treated with CX-4945 can be compared directly to wild-type cells in a triplex SILAC approach. Quantification of phosphopeptides representing *bona fide* CK2 substrates or CK2-dependent phosphorylation sites will remain comparable in abundance between wild-type cells (WT) treated with DMSO and inhibitor-resistant cells (IR) treated with CX-4945. *Bona fide* CK2-independent effects of CX-4945 will be discernable as quantification of these phosphopeptides will differ between DMSO treated wild-type cells and CX-4945 treated inhibitor resistant cells.

5.5   Conclusion

The dynamic nature of protein phosphorylation as mediated by the activity of kinases and phosphatases renders it a critical posttranslational modification in the regulation of biological processes. The emergence of protein kinase CK2 as a therapeutic target has been met with the development of several inhibitors including CX-4945, a small molecule ATP-competitive inhibitor that has progressed into clinical trial. Furthermore, CX-4945 has been used widely in the literature in different models of cancer but these reports are anecdotal in terms of the specific signaling pathways that were studied in isolated biological contexts. Unbiased proteomic characterization of the effect of CX-4945 in human cells was undertaken in order to understand the scope of its impact on the phosphoproteome and the kinome. These studies enabled the identification of markers of CK2 activity, which can have applications for characterizing future CK2 inhibitors and also identified putative CK2-independent effects of CX-4945. The identification of CK2-independent effects raises speculation about the mechanism of action of CX-4945 in cells and highlights the need within the CK2 research community and the larger kinome research community for well-characterized chemical probes and complementary model systems in which to test hypotheses.

6   Bibliography

1.   Manning, G., Whyte, D. B., Martinez, R., Hunter, T., and Sudarsanam, S. (2002) The protein kinase complement of the human genome. *Science*. **298**, 1912–1934

2.   Hunter, T. (1995) Protein kinases and phosphatases: the yin and yang of protein phosphorylation and signaling. *Cell*. **80**, 225–236

3.   Karin, M., and Hunter, T. (1995) Transcriptional control by protein phosphorylation: signal transmission from the cell surface to the nucleus. *Curr. Biol.* **5**, 747–757

4.   Huse, M., and Kuriyan, J. (2002) The Conformational Plasticity of Protein Kinases. *Cell*. **109**, 275–282

5.   Pawson, T. (2004) Specificity in signal transduction: from phosphotyrosine-SH2 domain interactions to complex cellular systems. *Cell*. **116**, 191–203

6.   Ubersax, J. A., and Ferrell, J. E. (2007) Mechanisms of specificity in protein phosphorylation. *Nat Rev Mol Cell Biol*. **8**, 530–541

7.   Sharma, K., D'Souza, R. C. J., Tyanova, S., Schaab, C., Wisniewski, J. R., Cox, J., and Mann, M. (2014) Ultradeep human phosphoproteome reveals a distinct regulatory nature of tyr and ser/thr-based signaling. *Cell Reports*. **8**, 1583–1594

8.   Brognard, J., and Hunter, T. (2011) Protein kinase signaling networks in cancer. *Current Opinion in Genetics & Development*. **21**, 4–11

9.   Zhang, J., Yang, P. L., and Gray, N. S. (2009) Targeting cancer with small molecule kinase inhibitors. *Nat Rev Cancer*. **9**, 28–39

10.   Duncan, J. S., and Litchfield, D. W. (2008) Too much of a good thing: The role of protein kinase CK2 in tumorigenesis and prospects for therapeutic inhibition of CK2. *BBA - Proteins and Proteomics*. **1784**, 33–47

11.   Poletto, G., Vilardell, J., MARIN, O., Pagano, M. A., Cozza, G., Sarno, S., Falqués, A., Itarte, E., Pinna, L. A., and Meggio, F. (2008) The Regulatory β Subunit of Protein Kinase CK2 Contributes to the Recognition of the Substrate Consensus Sequence. A Study with an eIF2β-Derived Peptide †. *Biochemistry*. **47**, 8317–8325

12.   Buchou, T., Vernet, M., Blond, O., Jensen, H. H., Pointu, H., Olsen, B. B., Cochet, C., Issinger, O.-G., and Boldyreff, B. (2003) Disruption of the regulatory beta subunit of protein kinase CK2 in mice leads to a cell-autonomous defect and early embryonic lethality. *Molecular and Cellular Biology*. **23**, 908–915

13.   Lou, D. Y., Dominguez, I., Toselli, P., Landesman-Bollag, E., O'Brien, C., and Seldin, D. C. (2008) The alpha catalytic subunit of protein kinase CK2 is required for mouse embryonic development. *Molecular and Cellular Biology*. **28**, 131–139

14.   Ortega, C. E., Seidner, Y., and Dominguez, I. (2014) Mining CK2 in cancer. *PLoS ONE*. **9**, e115609

15.   Salvi, M., Sarno, S., Cesaro, L., Nakamura, H., and Pinna, L. A. (2009) Extraordinary pleiotropy of protein kinase CK2 revealed by weblogo phosphoproteome analysis. *Biochim. Biophys. Acta*. **1793**, 847–859

16.   Litchfield, D. W. (2003) Protein kinase CK2: structure, regulation and role in cellular decisions of life and death. *Biochem. J.* **369**, 1–15

17.   St-Denis, N. A., and Litchfield, D. W. (2009) Protein kinase CK2 in health and disease: From birth to death: the role of protein kinase CK2 in the regulation of cell proliferation and survival. *Cell. Mol. Life Sci.* **66**, 1817–1829

18.   Duncan, J. S., Gyenis, L., Lenehan, J., Bretner, M., Graves, L. M., Haystead, T. A.,

and Litchfield, D. W. (2008) An unbiased evaluation of CK2 inhibitors by chemoproteomics: characterization of inhibitor effects on CK2 and identification of novel inhibitor targets. *Mol. Cell Proteomics*. **7**, 1077–1088

19. Filhol, O., Giacosa, S., Wallez, Y., and Cochet, C. (2015) Protein kinase CK2 in breast cancer: the CK2β regulatory subunit takes center stage in epithelial plasticity. *Cell. Mol. Life Sci.* **72**, 3305–3322

20. Ruzzene, M., and Pinna, L. A. (2010) Addiction to protein kinase CK2: A common denominator of diverse cancer cells? *BBA - Proteins and Proteomics*. **1804**, 499–504

21. Krippner-Heidenreich, A., Talanian, R. V., Sekul, R., Kraft, R., Thole, H., Ottleben, H., and Luscher, B. (2001) Targeting of the transcription factor Max during apoptosis: phosphorylation-regulated cleavage by caspase-5 at an unusual glutamic acid residue in position P1. *Biochem. J.* **358**, 705–715

22. Desagher, S., Osen-Sand, A., Montessuit, S., Magnenat, E., Vilbois, F., Hochmann, A., Journot, L., Antonsson, B., and Martinou, J. C. (2001) Phosphorylation of bid by casein kinases I and II regulates its cleavage by caspase 8. *Mol. Cell*. **8**, 601–611

23. Turowec, J. P., Zukowski, S. A., Knight, J. D. R., Smalley, D. M., Graves, L. M., Johnson, G. L., Li, S. S. C., Lajoie, G. A., and Litchfield, D. W. (2014) An Unbiased Proteomic Screen Reveals Caspase Cleavage Is Positively and Negatively Regulated by Substrate Phosphorylation. *Mol. Cell Proteomics*. **13**, 1184–1197

24. Turowec, J. P., Vilk, G., Gabriel, M., and Litchfield, D. W. (2013) Characterizing the convergence of protein kinase CK2 and caspase-3 reveals isoform-specific phosphorylation of caspase-3 by CK2α′: implications for pathological roles of CK2 in promoting cancer cell survival. *Oncotarget*. **4**, 560–571

25. Torres, J., Rodriguez, J., Myers, M. P., Valiente, M., Graves, J. D., Tonks, N. K., and Pulido, R. (2003) Phosphorylation-regulated cleavage of the tumor suppressor PTEN by caspase-3: implications for the control of protein stability and PTEN-protein interactions. *J. Biol. Chem.* **278**, 30652–30660

26. Riman, S., Rizkallah, R., Kassardjian, A., Alexander, K. E., Lüscher, B., and Hurt, M. M. (2012) Phosphorylation of the transcription factor YY1 by CK2α prevents cleavage by caspase 7 during apoptosis. *Molecular and Cellular Biology*. **32**, 797–807

27. Duncan, J. S., Turowec, J. P., Duncan, K. E., Vilk, G., Wu, C., Luscher, B., Li, S. S. C., Gloor, G. B., and Litchfield, D. W. (2011) A Peptide-Based Target Screen Implicates the Protein Kinase CK2 in the Global Regulation of Caspase Signaling. *Science Signaling*. **4**, ra30–ra30

28. Chapman, J. R., and Jackson, S. P. (2008) Phospho-dependent interactions between NBS1 and MDC1 mediate chromatin retention of the MRN complex at sites of DNA damage. *EMBO Rep.* **9**, 795–801

29. Spycher, C., Miller, E. S., Townsend, K., Pavic, L., Morrice, N. A., Janscak, P., Stewart, G. S., and Stucki, M. (2008) Constitutive phosphorylation of MDC1 physically links the MRE11-RAD50-NBS1 complex to damaged chromatin. *The Journal of Cell Biology*. **181**, 227–240

30. Ciccia, A., Huang, J.-W., Izhar, L., Sowa, M. E., Harper, J. W., and Elledge, S. J. (2014) Treacher Collins syndrome TCOF1 protein cooperates with NBS1 in the DNA damage response. *Proceedings of the National Academy of Sciences*. **111**, 18631–18636

31. Larsen, D. H., Hari, F., Clapperton, J. A., Gwerder, M., Gutsche, K., Altmeyer, M., Jungmichel, S., Toledo, L. I., Fink, D., Rask, M.-B., Grøfte, M., Lukas, C., Nielsen, M. L., Smerdon, S. J., Lukas, J., and Stucki, M. (2014) The NBS1-Treacle complex controls ribosomal RNA transcription in response to DNA damage. *Nat Cell Biol*. **16**, 792–803

32. Yata, K., Lloyd, J., Maslen, S., Bleuyard, J.-Y., Skehel, M., Smerdon, S. J., and Esashi, F. (2012) Plk1 and CK2 act in concert to regulate Rad51 during DNA double strand break repair. *Mol. Cell*. **45**, 371–383

33. Litchfield, D. W., Lozeman, F. J., Piening, C., Sommercorn, J., Takio, K., Walsh, K. A., and KREBS, E. G. (1990) Subunit structure of casein kinase II from bovine testis. Demonstration that the alpha and alpha' subunits are distinct polypeptides. *J. Biol. Chem.* **265**, 7638–7644

34. So, J., Pasculescu, A., Dai, A. Y., Williton, K., James, A., Nguyen, V., Creixell, P., Schoof, E. M., Sinclair, J., Barrios-Rodiles, M., Gu, J., Krizus, A., Williams, R., Olhovsky, M., Dennis, J. W., Wrana, J. L., Linding, R., Jørgensen, C., Pawson, T., and Colwill, K. (2015) Integrative analysis of kinase networks in TRAIL-induced apoptosis provides a source of potential targets for combination therapy. *Science Signaling*. **8**, rs3

35. Bennetzen, M. V., Larsen, D. H., Bunkenborg, J., Bartek, J., Lukas, J., and Andersen, J. S. (2010) Site-specific phosphorylation dynamics of the nuclear proteome during the DNA damage response. *Mol. Cell Proteomics*. **9**, 1314–1323

36. Bensimon, A., Schmidt, A., Ziv, Y., Elkon, R., Wang, S.-Y., Chen, D. J., Aebersold, R., and Shiloh, Y. (2010) ATM-Dependent and -Independent Dynamics of the Nuclear Phosphoproteome After DNA Damage. *Sci. Signal.* **3**, rs3–rs3

37. Yamane, K., and Kinsella, T. J. (2005) CK2 Inhibits Apoptosis and Changes Its Cellular Localization Following Ionizing Radiation. *Cancer Research*. **65**, 4362–4367

38. Loizou, J. I., El-Khamisy, S. F., Zlatanou, A., Moore, D. J., Chan, D. W., Qin, J., Sarno, S., Meggio, F., Pinna, L. A., and Caldecott, K. W. (2004) The protein kinase CK2 facilitates repair of chromosomal DNA single-strand breaks. *Cell*. **117**, 17–28

39. Koch, C. A., Agyei, R., Galicia, S., Metalnikov, P., O'Donnell, P., Starostine, A., Weinfeld, M., and Durocher, D. (2004) Xrcc4 physically links DNA end processing by polynucleotide kinase to DNA ligation by DNA ligase IV. *The EMBO Journal*. **23**, 3874–3885

40. Herhaus, L., Perez-Oliva, A. B., Cozza, G., Gourlay, R., Weidlich, S., Campbell, D. G., Pinna, L. A., and Sapkota, G. P. (2015) Casein kinase 2 (CK2) phosphorylates the deubiquitylase OTUB1 at Ser16 to trigger its nuclear localization. *Science Signaling*. **8**, ra35–ra35

41. Cozza, G., Pinna, L. A., and Moro, S. (2012) Protein kinase CK2 inhibitors: a patent review. *Expert Opin Ther Pat*. **22**, 1081–1097

42. Cozza, G., and Pinna, L. A. (2016) Casein kinases as potential therapeutic targets. *Expert Opin. Ther. Targets*. **20**, 319–340

43. Pierre, F., Chua, P. C., O'Brien, S. E., Siddiqui-Jain, A., Bourbon, P., Haddach, M., Michaux, J., Nagasawa, J., Schwaebe, M. K., Stefan, E., Vialettes, A., Whitten, J. P., Chen, T. K., Darjania, L., Stansfield, R., Anderes, K., Bliesath, J., Drygin, D., Ho, C., Omori, M., Proffitt, C., Streiner, N., Trent, K., Rice, W. G., and Ryckman, D. M.

(2011) Discovery and SAR of 5-(3-chlorophenylamino)benzo[c][2,6]naphthyridine-8-carboxylic acid (CX-4945), the first clinical stage inhibitor of protein kinase CK2 for the treatment of cancer. *J. Med. Chem.* **54**, 635–654

44. Siddiqui-Jain, A., Drygin, D., Streiner, N., Chua, P., Pierre, F., O'Brien, S. E., Bliesath, J., Omori, M., Huser, N., Ho, C., Proffitt, C., Schwaebe, M. K., Ryckman, D. M., Rice, W. G., and Anderes, K. (2010) CX-4945, an Orally Bioavailable Selective Inhibitor of Protein Kinase CK2, Inhibits Prosurvival and Angiogenic Signaling and Exhibits Antitumor Efficacy. *Cancer Research*. **70**, 10288–10298

45. Siddiqui-Jain, A., Bliesath, J., Macalino, D., Omori, M., Huser, N., Streiner, N., Ho, C. B., Anderes, K., Proffitt, C., O'Brien, S. E., Lim, J. K. C., Hoff, Von, D. D., Ryckman, D. M., Rice, W. G., and Drygin, D. (2012) CK2 Inhibitor CX-4945 Suppresses DNA Repair Response Triggered by DNA-Targeted Anticancer Drugs and Augments Efficacy: Mechanistic Rationale for Drug Combination Therapy. *Molecular Cancer Therapeutics*. **11**, 994–1005

46. Becherel, O. J., Jakob, B., Cherry, A. L., Gueven, N., Fusser, M., Kijas, A. W., Peng, C., Katyal, S., McKinnon, P. J., Chen, J., Epe, B., Smerdon, S. J., Taucher-Scholz, G., and Lavin, M. F. (2010) CK2 phosphorylation-dependent interaction between aprataxin and MDC1 in the DNA damage response. *Nucleic Acids Research*. **38**, 1489–1503

47. Olsen, B. B., Wang, S.-Y., Svenstrup, T. H., Chen, B. P., and Guerra, B. (2012) Protein kinase CK2 localizes to sites of DNA double-strand break regulating the cellular response to DNA damage. *BMC Mol. Biol.* **13**, 7

48. Quotti Tubi, L., Gurrieri, C., Brancalion, A., Bonaldi, L., Bertorelle, R., Manni, S., Pavan, L., Lessi, F., Zambello, R., Trentin, L., Adami, F., Ruzzene, M., Pinna, L. A., Semenzato, G., and Piazza, F. (2013) Inhibition of protein kinase CK2 with the clinical-grade small ATP-competitive compound CX-4945 or by RNA interference unveils its role in acute myeloid leukemia cell survival, p53-dependent apoptosis and daunorubicin-induced cytotoxicity. *J Hematol Oncol*. **6**, 78

49. Prins, R. C., Burke, R. T., Tyner, J. W., Druker, B. J., Loriaux, M. M., and Spurgeon, S. E. (2013) CX-4945, a selective inhibitor of casein kinase-2 (CK2), exhibits anti-tumor activity in hematologic malignancies including enhanced activity in chronic lymphocytic leukemia when combined with fludarabine and inhibitors of the B-cell receptor pathway. *Leukemia*. **27**, 2094–2096

50. Manni, S., Brancalion, A., Mandato, E., Tubi, L. Q., Colpo, A., Pizzi, M., Cappellesso, R., Zaffino, F., Di Maggio, S. A., Cabrelle, A., Marino, F., Zambello, R., Trentin, L., Adami, F., Gurrieri, C., Semenzato, G., and Piazza, F. (2013) Protein Kinase CK2 Inhibition Down Modulates the NF-κB and STAT3 Survival Pathways, Enhances the Cellular Proteotoxic Stress and Synergistically Boosts the Cytotoxic Effect of Bortezomib on Multiple Myeloma and Mantle Cell Lymphoma Cells. *PLoS ONE*. **8**, e75280

51. Bliesath, J., Huser, N., Omori, M., Bunag, D., Proffitt, C., Streiner, N., Ho, C., Siddiqui-Jain, A., O'Brien, S. E., Lim, J. K. C., Ryckman, D. M., Anderes, K., Rice, W. G., and Drygin, D. (2012) Combined inhibition of EGFR and CK2 augments the attenuation of PI3K-Akt-mTOR signaling and the killing of cancer cells. *Cancer Lett*. **322**, 113–118

52. Zanin, S., Borgo, C., Girardi, C., O'Brien, S. E., Miyata, Y., Pinna, L. A., Donella-

Deana, A., and Ruzzene, M. (2012) Effects of the CK2 inhibitors CX-4945 and CX-5011 on drug-resistant cells. *PLoS ONE*. **7**, e49193

53.   Borgo, C., Cesaro, L., Salizzato, V., Ruzzene, M., Massimino, M. L., Pinna, L. A., and Donella-Deana, A. (2013) Aberrant signalling by protein kinase CK2 in imatinib-resistant chronic myeloid leukaemia cells: biochemical evidence and therapeutic perspectives. *Molecular Oncology*. **7**, 1103–1115

54.   Buontempo, F., Orsini, E., Martins, L. R., Antunes, I., Lonetti, A., Chiarini, F., Tabellini, G., Evangelisti, C., Melchionda, F., Pession, A., Bertaina, A., Locatelli, F., McCubrey, J. A., Cappellini, A., Barata, J. T., and Martelli, A. M. (2013) Cytotoxic activity of the casein kinase 2 inhibitor CX-4945 against T-cell acute lymphoblastic leukemia: targeting the unfolded protein response signaling. *Leukemia*. **28**, 543–553

55.   Shu, S., Lin, C. Y., He, H. H., Witwicki, R. M., Tabassum, D. P., Roberts, J. M., Janiszewska, M., Jin Huh, S., Liang, Y., Ryan, J., Doherty, E., Mohammed, H., Guo, H., Stover, D. G., Ekram, M. B., Peluffo, G., Brown, J., D'Santos, C., Krop, I. E., Dillon, D., McKeown, M., Ott, C., Qi, J., Ni, M., Rao, P. K., Duarte, M., Wu, S.-Y., Chiang, C.-M., Anders, L., Young, R. A., Winer, E. P., Letai, A., Barry, W. T., Carroll, J. S., Long, H. W., Brown, M., Shirley Liu, X., Meyer, C. A., Bradner, J. E., and Polyak, K. (2016) Response and resistance to BET bromodomain inhibitors in triple-negative breast cancer. *Nature*. **529**, 413–417

56.   Aebersold, R., and Mann, M. (2016) Mass-spectrometric exploration of proteome structure and function. *Nature*. **537**, 347–355

57.   Thakur, S. S., Geiger, T., Chatterjee, B., Bandilla, P., Frohlich, F., Cox, J., and Mann, M. (2011) Deep and Highly Sensitive Proteome Coverage by LC-MS/MS Without Prefractionation. *Mol. Cell Proteomics*. **10**, M110.003699–M110.003699

58.   Fenn, J. B., Mann, M., Meng, C. K., Wong, S. F., and Whitehouse, C. M. (1989) Electrospray ionization for mass spectrometry of large biomolecules. *Science*. **246**, 64–71

59.   Steen, H., and Mann, M. (2004) The ABC"s (and XYZ"s) of peptide sequencing. *Nat Rev Mol Cell Biol*. **5**, 699–711

60.   Elias, J. E., and Gygi, S. P. (2007) Target-decoy search strategy for increased confidence in large-scale protein identifications by mass spectrometry. *Nat Meth*. **4**, 207–214

61.   Nesvizhskii, A. I. (2007) Protein identification by tandem mass spectrometry and sequence database searching. *Methods Mol. Biol*. **367**, 87–119

62.   Michalski, A., Damoc, E., Hauschild, J. P., Lange, O., Wieghaus, A., Makarov, A., Nagaraj, N., Cox, J., Mann, M., and Horning, S. (2011) Mass Spectrometry-based Proteomics Using Q Exactive, a High-performance Benchtop Quadrupole Orbitrap Mass Spectrometer. *Mol. Cell Proteomics*. **10**, M111.011015–M111.011015

63.   Michalski, A., Damoc, E., Lange, O., Denisov, E., Nolting, D., Müller, M., Viner, R., Schwartz, J., Remes, P., Belford, M., Dunyach, J.-J., Cox, J., Horning, S., Mann, M., and Makarov, A. (2012) Ultra High Resolution Linear Ion Trap Orbitrap Mass Spectrometer (Orbitrap Elite) Facilitates Top Down LC MS/MS and Versatile Peptide Fragmentation Modes. *Mol. Cell Proteomics*. **11**, O111.013698

64.   Eliuk, S., and Makarov, A. (2015) Evolution of Orbitrap Mass Spectrometry Instrumentation. *Annual Review of Analytical Chemistry*. **8**, 61–80

65.   Ross, P. L., Huang, Y. N., Marchese, J. N., Williamson, B., Parker, K., Hattan, S.,

Khainovski, N., Pillai, S., Dey, S., Daniels, S., Purkayastha, S., Juhasz, P., Martin, S., Bartlet-Jones, M., He, F., Jacobson, A., and Pappin, D. J. (2004) Multiplexed protein quantitation in Saccharomyces cerevisiae using amine-reactive isobaric tagging reagents. *Mol. Cell Proteomics*. **3**, 1154–1169

66.   Thompson, A., Schäfer, J., Kuhn, K., Kienle, S., Schwarz, J., Schmidt, G., Neumann, T., and Hamon, C. (2003) Tandem Mass Tags: A Novel Quantification Strategy for Comparative Analysis of Complex Protein Mixtures by MS/MS. *Anal. Chem.* **75**, 1895–1904

67.   Boersema, P. J., Raijmakers, R., Lemeer, S., Mohammed, S., and Heck, A. J. R. (2009) Multiplex peptide stable isotope dimethyl labeling for quantitative proteomics. *Nat Protoc*. **4**, 484–494

68.   Ong, S.-E., Blagoev, B., Kratchmarova, I., Kristensen, D. B., Steen, H., Pandey, A., and Mann, M. (2002) Stable isotope labeling by amino acids in cell culture, SILAC, as a simple and accurate approach to expression proteomics. *Mol. Cell Proteomics*. **1**, 376–386

69.   Ong, S.-E., and Mann, M. (2006) A practical recipe for stable isotope labeling by amino acids in cell culture (SILAC). *Nat Protoc*. **1**, 2650–2660

70.   Cox, J., and Mann, M. (2008) MaxQuant enables high peptide identification rates, individualized ppb-range mass accuracies and proteome-wide protein quantification. *Nature Biotechnology*. **26**, 1367–1372

71.   Tyanova, S., Temu, T., and Cox, J. (2016) The MaxQuant computational platform for mass spectrometry-based shotgun proteomics. *Nat. Protocols*. **11**, 2301–2319

72.   Olsen, J. V., Blagoev, B., Gnad, F., Macek, B., Kumar, C., Mortensen, P., and Mann, M. (2006) Global, In Vivo, and Site-Specific Phosphorylation Dynamics in Signaling Networks. *Cell*. **127**, 635–648

73.   Pan, C., Olsen, J. V., Daub, H., and Mann, M. (2009) Global effects of kinase inhibitors on signaling networks revealed by quantitative phosphoproteomics. *Mol. Cell Proteomics*. **8**, 2796–2808

74.   Steen, H., Jebanathirajah, J. A., Rush, J., Morrice, N., and Kirschner, M. W. (2006) Phosphorylation Analysis by Mass Spectrometry: Myths, Facts, and the Consequences for Qualitative and Quantitative Measurements. *Mol. Cell Proteomics*. **5**, 172–181

75.   Larsen, M. R., Thingholm, T. E., Jensen, O. N., Roepstorff, P., and Jørgensen, T. J. D. (2005) Highly selective enrichment of phosphorylated peptides from peptide mixtures using titanium dioxide microcolumns. *Mol. Cell Proteomics*. **4**, 873–886

76.   Sugiyama, N., Masuda, T., Shinoda, K., Nakamura, A., Tomita, M., and Ishihama, Y. (2007) Phosphopeptide Enrichment by Aliphatic Hydroxy Acid-modified Metal Oxide Chromatography for Nano-LC-MS/MS in Proteomics Applications. *Mol. Cell Proteomics*. **6**, 1103–1109

77.   Horn, H., Schoof, E. M., Kim, J., Robin, X., Miller, M. L., Diella, F., Palma, A., Cesareni, G., Jensen, L. J., and Linding, R. (2014) KinomeXplorer: an integrated platform for kinome biology studies. *Nat Meth*. **11**, 603–604

78.   Riley, N. M., and Coon, J. J. (2016) Phosphoproteomics in the Age of Rapid and Deep Proteome Profiling. *Anal. Chem.* **88**, 74–94

79.   Haystead, C. M., Gregory, P., Sturgill, T. W., and Haystead, T. A. (1993) Gamma-phosphate-linked ATP-sepharose for the affinity purification of protein kinases.

Rapid purification to homogeneity of skeletal muscle mitogen-activated protein kinase kinase. *Eur J Biochem*. **214**, 459–467

80. Knockaert, M., Gray, N., Damiens, E., Chang, Y.-T., Grellier, P., Grant, K., Fergusson, D., Mottram, J., Soete, M., Dubremetz, J.-F., Le Roch, K., Doerig, C., Schultz, P. G., and Meijer, L. (2000) Intracellular targets of cyclin-dependent kinase inhibitors: identification by affinity chromatography using immobilised inhibitors. *Chemistry & Biology*. **7**, 411–422

81. Knockaert, M., Wieking, K., Schmitt, S., Leost, M., Grant, K. M., Mottram, J. C., Kunick, C., and Meijer, L. (2002) Intracellular Targets of Paullones: IDENTIFICATION FOLLOWING AFFINITY PURIFICATION ON IMMOBILIZED INHIBITOR. *Journal of Biological Chemistry*. **277**, 25493–25501

82. Bantscheff, M., Eberhard, D., Abraham, Y., Bastuck, S., Boesche, M., Hobson, S., Mathieson, T., Perrin, J., Raida, M., Rau, C., Reader, V., Sweetman, G., Bauer, A., Bouwmeester, T., Hopf, C., Kruse, U., Neubauer, G., Ramsden, N., Rick, J., Kuster, B., and Drewes, G. (2007) Quantitative chemical proteomics reveals mechanisms of action of clinical ABL kinase inhibitors. *Nature Biotechnology*. **25**, 1035–1044

83. Daub, H., Olsen, J. V., Bairlein, M., Gnad, F., Oppermann, F. S., Körner, R., Greff, Z., Kéri, G., Stemmann, O., and Mann, M. (2008) Kinase-selective enrichment enables quantitative phosphoproteomics of the kinome across the cell cycle. *Mol. Cell*. **31**, 438–448

84. Duncan, J. S., Whittle, M. C., Nakamura, K., Abell, A. N., Midland, A. A., Zawistowski, J. S., Johnson, N. L., Granger, D. A., Jordan, N. V., Darr, D. B., Usary, J., Kuan, P.-F., Smalley, D. M., Major, B., He, X., Hoadley, K. A., Zhou, B., Sharpless, N. E., Perou, C. M., Kim, W. Y., Gomez, S. M., Chen, X., Jin, J., Frye, S. V., Earp, H. S., Graves, L. M., and Johnson, G. L. (2012) Dynamic reprogramming of the kinome in response to targeted MEK inhibition in triple-negative breast cancer. *Cell*. **149**, 307–321

85. Parker, R., Clifton-Bligh, R., and Molloy, M. P. (2014) Phosphoproteomics of MAPK inhibition in BRAF-mutated cells and a role for the lethal synergism of dual BRAF and CK2 inhibition. *Molecular Cancer Therapeutics*. **13**, 1894–1906

86. Tsai, C.-F., Wang, Y.-T., Yen, H.-Y., Tsou, C.-C., Ku, W.-C., Lin, P.-Y., Chen, H.-Y., Nesvizhskii, A. I., Ishihama, Y., and Chen, Y.-J. (2015) Large-scale determination of absolute phosphorylation stoichiometries in human cells by motif-targeting quantitative proteomics. *Nature Communications*. **6**, 6622

87. Hou, Z., Nakanishi, I., Kinoshita, T., Takei, Y., Yasue, M., Misu, R., Suzuki, Y., Nakamura, S., Kure, T., Ohno, H., Murata, K., Kitaura, K., Hirasawa, A., Tsujimoto, G., Oishi, S., and Fujii, N. (2012) Structure-based design of novel potent protein kinase CK2 (CK2) inhibitors with phenyl-azole scaffolds. *J. Med. Chem*. **55**, 2899–2903

88. Pawson, T., and Scott, J. D. (2005) Protein phosphorylation in signaling – 50 years and counting. *Trends Biochem. Sci*. **30**, 286–290

89. Roux, P. P., and Thibault, P. (2013) The coming of age of phosphoproteomics--from large data sets to inference of protein functions. *Mol. Cell Proteomics*. **12**, 3453–3464

90. Li, S., and Dass, C. (1999) Iron(III)-Immobilized Metal Ion Affinity Chromatography and Mass Spectrometry for the Purification and Characterization of

Synthetic Phosphopeptides. *Anal. Biochem.* **270**, 9–14

91.   Pinkse, M. W. H., Uitto, P. M., Hilhorst, M. J., Ooms, B., and Heck, A. J. R. (2004) Selective Isolation at the Femtomole Level of Phosphopeptides from Proteolytic Digests Using 2D-NanoLC-ESI-MS/MS and Titanium Oxide Precolumns. *Anal. Chem.* **76**, 3935–3943

92.   Pinna, L. A., Meggio, F., Marchiori, F., and Borin, G. (1984) Opposite and Mutually Incompatible Structural Requirements of Type-2 Casein Kinase and Camp-Dependent Protein-Kinase as Visualized with Synthetic Peptide-Substrates. *FEBS Letters.* **171**, 211–214

93.   Kuenzel, E. A., and KREBS, E. G. (1985) A synthetic peptide substrate specific for casein kinase II. *Proc. Natl. Acad. Sci. U.S.A.* **82**, 737–741

94.   Marin, O., Meggio, F., Marchiori, F., Borin, G., and Pinna, L. A. (1986) Site specificity of casein kinase-2 (TS) from rat liver cytosol. A study with model peptide substrates. *Eur J Biochem.* **160**, 239–244

95.   Kuenzel, E. A., Mulligan, J. A., Sommercorn, J., and Krebs, E. G. (1987) Substrate specificity determinants for casein kinase II as deduced from studies with synthetic peptides. *J. Biol. Chem.* **262**, 9136–9140

96.   Villén, J., and Gygi, S. P. (2008) The SCX/IMAC enrichment approach for global phosphorylation analysis by mass spectrometry. *Nat. Protocols.* **3**, 1630–1638

97.   Thingholm, T. E., Jørgensen, T. J. D., Jensen, O. N., and Larsen, M. R. (2006) Highly selective enrichment of phosphorylated peptides using titanium dioxide. *Nat Protoc.* **1**, 1929–1935

98.   Chin, E. T., and Papac, D. I. (1999) The use of a porous graphitic carbon column for desalting hydrophilic peptides prior to matrix-assisted laser desorption/ionization time-of-flight mass spectrometry. *Anal. Biochem.* **273**, 179–185

99.   Larsen, M. R., Cordwell, S. J., and Roepstorff, P. (2002) Graphite powder as an alternative or supplement to reversed-phase material for desalting and concentration of peptide mixtures prior to matrix-assisted laser desorption/ionization-mass spectrometry. *Proteomics.* **2**, 1277–1287

100.   Chou, M. F., and Schwartz, D. (2011) Biological sequence motif discovery using motif-x. *Curr Protoc Bioinformatics.* **Chapter 13**, Unit 13.15–24

101.   Schwartz, D., and Gygi, S. P. (2005) An iterative statistical approach to the identification of protein phosphorylation motifs from large-scale data sets. *Nature Biotechnology.* **23**, 1391–1398

102.   Manza, L. L., Stamer, S. L., Ham, A.-J. L., Codreanu, S. G., and Liebler, D. C. (2005) Sample preparation and digestion for proteomic analyses using spin filters. *Proteomics.* **5**, 1742–1745

103.   Wisniewski, J. R., Zougman, A., Nagaraj, N., and Mann, M. (2009) Universal sample preparation method for proteome analysis. *Nat Meth.* **6**, 359–362

104.   Wisniewski, J. R., Zougman, A., and Mann, M. (2009) Combination of FASP and StageTip-Based Fractionation Allows In-Depth Analysis of the Hippocampal Membrane Proteome. *J Proteome Res.* **8**, 5674–5678

105.   Jiang, L., He, L., and Fountoulakis, M. (2004) Comparison of protein precipitation methods for sample preparation prior to proteomic analysis. *Journal of Chromatography A.* **1023**, 317–320

106.   Duan, X., Young, R., Straubinger, R. M., Page, B., Cao, J., Wang, H., Yu, H., Canty,

J. M., and Qu, J. (2009) A Straightforward and Highly Efficient Precipitation/On-Pellet Digestion Procedure Coupled with a Long Gradient Nano-LC Separation and Orbitrap Mass Spectrometry for Label-Free Expression Profiling of the Swine Heart Mitochondrial Proteome. *J Proteome Res*. **8**, 2838–2850

107. Batth, T. S., Francavilla, C., and Olsen, J. V. (2014) Off-line high pH reversed-phase fractionation for in-depth phosphoproteomics. *J Proteome Res*. 10.1021/pr500893m

108. Kettenbach, A. N., and Gerber, S. A. (2011) Rapid and reproducible single-stage phosphopeptide enrichment of complex peptide mixtures: application to general and phosphotyrosine-specific phosphoproteomics experiments. *Anal. Chem.* **83**, 7635–7644

109. Beausoleil, S. A., Jedrychowski, M., Schwartz, D., Elias, J. E., Villén, J., Li, J., Cohn, M. A., Cantley, L. C., and Gygi, S. P. (2004) Large-scale characterization of HeLa cell nuclear phosphoproteins. *Proc. Natl. Acad. Sci. U.S.A.* **101**, 12130–12135

110. Larsen, M. R., Graham, M. E., Robinson, P. J., and Roepstorff, P. (2004) Improved detection of hydrophilic phosphopeptides using graphite powder microcolumns and mass spectrometry - Evidence for in vivo doubly phosphorylated dynamin I and dynamin III. *Mol. Cell Proteomics*. **3**, 456–465

111. Wolf-Yadlin, A., Hautaniemi, S., Lauffenburger, D. A., and White, F. M. (2007) Multiple reaction monitoring for robust quantitative proteomic analysis of cellular signaling networks. *Proceedings of the National Academy of Sciences*. **104**, 5860–5865

112. Pellerin, D., Gagnon, H., Dubé, J., and Corbin, F. (2015) Amicon-adapted enhanced FASP: an in-solution digestion-based alternative sample preparation method to FASP. *F1000Research*. 10.12688/f1000research.6529.1

113. Erde, J., Loo, R. R. O., and Loo, J. A. (2014) Enhanced FASP (eFASP) to Increase Proteome Coverage and Sample Recovery for Quantitative Proteomic Experiments. *J Proteome Res*. **13**, 1885–1895

114. Wisniewski, J. R. (2016) Quantitative evaluation of FASP and MED FASP protocols. *Anal. Chem.* 10.1021/acs.analchem.6b00859

115. Vilk, G., Saulnier, R. B., Pierre, R. S., and Litchfield, D. W. (1999) Inducible Expression of Protein Kinase CK2 in Mammalian Cells: EVIDENCE FOR FUNCTIONAL SPECIALIZATION OF CK2 ISOFORMS. *Journal of Biological Chemistry*. **274**, 14406–14414

116. Rappsilber, J., Ishihama, Y., and Mann, M. (2003) Stop and Go Extraction Tips for Matrix-Assisted Laser Desorption/Ionization, Nanoelectrospray, and LC/MS Sample Pretreatment in Proteomics. *Anal. Chem.* **75**, 663–670

117. Olsen, J. V., de Godoy, L. M. F., Li, G., Macek, B., Mortensen, P., Pesch, R., Makarov, A., Lange, O., Horning, S., and Mann, M. (2005) Parts per million mass accuracy on an Orbitrap mass spectrometer via lock mass injection into a C-trap. *Mol. Cell Proteomics*. **4**, 2010–2021

118. Ma, B., Zhang, K., Hendrie, C., Liang, C., Li, M., Doherty Kirby, A., and Lajoie, G. (2003) PEAKS: powerful software for peptide de novo sequencing by tandem mass spectrometry. *Rapid Commun. Mass Spectrom.* **17**, 2337–2342

119. Zhang, J., Xin, L., Shan, B., Chen, W., Xie, M., Yuen, D., Zhang, W., Zhang, Z., Lajoie, G. A., and Ma, B. (2012) PEAKS DB: De Novo Sequencing Assisted Database Search for Sensitive and Accurate Peptide Identification. *Mol. Cell*

Proteomics. **11**, M111.010587–M111.010587

120.   Cox, J., Neuhauser, N., Michalski, A., Scheltema, R. A., Olsen, J. V., and Mann, M. (2011) Andromeda: A Peptide Search Engine Integrated into the MaxQuant Environment. *J Proteome Res*. **10**, 1794–1805

121.   Tyanova, S., Temu, T., Sinitcyn, P., Carlson, A., Hein, M. Y., Geiger, T., Mann, M., and Cox, J. (2016) The Perseus computational platform for comprehensive analysis of (prote)omics data. *Nat Meth*. **13**, 731–740

122.   Hunter, T. (2000) Signaling—2000 and Beyond. *Cell*. **100**, 113–127

123.   Battistutta, R., Cozza, G., Pierre, F., Papinutto, E., Lolli, G., Sarno, S., O'Brien, S. E., Siddiqui-Jain, A., Haddach, M., Anderes, K., Ryckman, D. M., Meggio, F., and Pinna, L. A. (2011) Unprecedented Selectivity and Structural Determinants of a New Class of Protein Kinase CK2 Inhibitors in Clinical Trials for the Treatment of Cancer. *Biochemistry*. **50**, 8478–8488

124.   Manni, S., Toscani, D., Mandato, E., Brancalion, A., Quotti Tubi, L., Macaccaro, P., Cabrelle, A., Adami, F., Zambello, R., Gurrieri, C., Semenzato, G., Giuliani, N., and Piazza, F. (2014) Bone marrow stromal cell-fueled multiple myeloma growth and osteoclastogenesis are sustained by protein kinase CK2. *Leukemia*. **28**, 2094–2097

125.   Martins, L. R., Lucio, P., Melão, A., Antunes, I., Cardoso, B. A., Stansfield, R., Bertilaccio, M. T. S., Ghia, P., Drygin, D., Silva, M. G., and Barata, J. T. (2013) Activity of the clinical-stage CK2-specific inhibitor CX-4945 against chronic lymphocytic leukemia. *Leukemia*. 10.1038/leu.2013.232

126.   Franchin, C., Cesaro, L., Salvi, M., Millioni, R., Iori, E., Cifani, P., James, P., Arrigoni, G., and Pinna, L. (2014) Quantitative analysis of a phosphoproteome readily altered by the protein kinase CK2 inhibitor quinalizarin in HEK-293T cells. *Biochimica et Biophysica Acta (BBA) - Proteins & Proteomics*. 10.1016/j.bbapap.2014.09.017

127.   Franchin, C., Salvi, M., Arrigoni, G., and Pinna, L. A. (2015) Proteomics perturbations promoted by the protein kinase CK2 inhibitor quinalizarin. *BBA - Proteins and Proteomics*. **1854**, 1676–1686

128.   Weidner, C., Fischer, C., and Sauer, S. (2014) PHOXTRACK-a tool for interpreting comprehensive datasets of post-translational modifications of proteins. *Bioinformatics*. **30**, 3410–3411

129.   Reimand, J., Arak, T., Adler, P., Kolberg, L., Reisberg, S., Peterson, H., and Vilo, J. (2016) g:Profiler—a web server for functional interpretation of gene lists (2016 update). *Nucleic Acids Research*. **44**, W83–W89

130.   Geiger, T., Wehner, A., Schaab, C., Cox, J., and Mann, M. (2012) Comparative Proteomic Analysis of Eleven Common Cell Lines Reveals Ubiquitous but Varying Expression of Most Proteins. *Mol. Cell Proteomics*. **11**, M111.014050–M111.014050

131.   Bendall, S. C., Hughes, C., Stewart, M. H., Doble, B., Bhatia, M., and Lajoie, G. A. (2008) Prevention of amino acid conversion in SILAC experiments with embryonic stem cells. *Mol. Cell Proteomics*. **7**, 1587–1597

132.   Melander, F., Bekker-Jensen, S., Falck, J., Bartek, J., Mailand, N., and Lukas, J. (2008) Phosphorylation of SDT repeats in the MDC1 N terminus triggers retention of NBS1 at the DNA damage-modified chromatin. *The Journal of Cell Biology*. **181**, 213–226

133. Yamane, K., and Kinsella, T. J. (2005) Casein kinase 2 regulates both apoptosis and the cell cycle following DNA damage induced by 6-thioguanine. *Clin. Cancer Res.* **11**, 2355–2363

134. Llorens, F., Duarri, A., Sarró, E., Roher, N., Plana, M., and Itarte, E. (2006) The N-terminal domain of the human eIF2β subunit and the CK2 phosphorylation sites are required for its function. *Biochem. J.* **394**, 227–236

135. Wells, N. J., Addison, C. M., Fry, A. M., Ganapathi, R., and Hickson, I. D. (1994) Serine 1524 is a major site of phosphorylation on human topoisomerase II alpha protein in vivo and is a substrate for casein kinase II in vitro. *J. Biol. Chem.* **269**, 29746–29751

136. Miyata, Y., and Nishida, E. (2004) CK2 controls multiple protein kinases by phosphorylating a kinase-targeting molecular chaperone, Cdc37. *Molecular and Cellular Biology*. **24**, 4065–4074

137. Taipale, M., Krykbaeva, I., Koeva, M., Kayatekin, C., Westover, K. D., Karras, G. I., and Lindquist, S. (2012) Quantitative Analysis of Hsp90-Client Interactions Reveals Principles of Substrate Recognition. *Cell*. **150**, 987–1001

138. Hornbeck, P. V., Kornhauser, J. M., Tkachev, S., Bin Zhang, Skrzypek, E., Murray, B., Latham, V., and Sullivan, M. (2012) PhosphoSitePlus: a comprehensive resource for investigating the structure and function of experimentally determined post-translational modifications in man and mouse. *Nucleic Acids Research*. **40**, D261–D270

139. Consortium, T. G. O. (2015) Gene Ontology Consortium: going forward. *Nucleic Acids Research*. **43**, D1049–D1056

140. Kanehisa, M., Sato, Y., Kawashima, M., Furumichi, M., and Tanabe, M. (2016) KEGG as a reference resource for gene and protein annotation. *Nucleic Acids Research*. **44**, D457–D462

141. Croft, D., Mundo, A. F., Haw, R., Milacic, M., Weiser, J., Wu, G., Caudy, M., Garapati, P., Gillespie, M., Kamdar, M. R., Jassal, B., Jupe, S., Matthews, L., May, B., Palatnik, S., Rothfels, K., Shamovsky, V., Song, H., Williams, M., Birney, E., Hermjakob, H., Stein, L., and D'Eustachio, P. (2014) The Reactome pathway knowledgebase. *Nucleic Acids Research*. **42**, D472–7

142. Isserlin, R., Merico, D., Voisin, V., and Bader, G. D. (2014) Enrichment Map - a Cytoscape app to visualize and explore OMICs pathway enrichment results. *F1000Research*. **3**, 141

143. Llorens, F., Roher, N., MIRÓ, F. A., Sarno, S., RUIZ, F. X., Meggio, F., Plana, M., Pinna, L. A., and Itarte, E. (2003) Eukaryotic translation-initiation factor eIF2β binds to protein kinase CK2: effects on CK2α activity. *Biochem. J.* **375**, 623–631

144. Wakula, P., Beullens, M., van Eynde, A., Ceulemans, H., Stalmans, W., and Bollen, M. (2006) The translation initiation factor eIF2β is an interactor of protein phosphatase-1. *Biochem. J.* **400**, 377–383

145. St-Denis, N., Gabriel, M., Turowec, J. P., Gloor, G. B., Li, S. S. C., Gingras, A.-C., and Litchfield, D. W. (2015) Systematic investigation of hierarchical phosphorylation by protein kinase CK2. *Journal of Proteomics*. **118 IS -**, 49–62

146. Wu, R., Haas, W., Dephoure, N., Huttlin, E. L., Zhai, B., Sowa, M. E., and Gygi, S. P. (2011) A large-scale method to measure absolute protein phosphorylation stoichiometries. *Nat Meth*. **8**, 677–683

147. Di Maira, G., Salvi, M., Arrigoni, G., Marin, O., Sarno, S., Brustolon, F., Pinna, L. A., and Ruzzene, M. (2005) Protein kinase CK2 phosphorylates and upregulates Akt//PKB. *Cell Death Differ.* **12**, 668–677

148. Kim, J., Park, M., Ryu, B. J., and Kim, S. H. (2014) The Protein Kinase 2 Inhibitor CX-4945 Induces Autophagy in Human Cancer Cell Lines. *Bull Korean Chem Soc*. 10.5012/bkcs.2014.35.10.2985

149. Shang, L., Chen, S., Du, F., Li, S., Zhao, L., and Wang, X. (2011) Nutrient starvation elicits an acute autophagic response mediated by Ulk1 dephosphorylation and its subsequent dissociation from AMPK. *Proceedings of the National Academy of Sciences*. **108**, 4788–4793

150. Jiang, X., Feng, S., Chen, Y., Feng, Y., and Deng, H. (2016) Proteomic analysis of mTOR inhibition-mediated phosphorylation changes in ribosomal proteins and eukaryotic translation initiation factors. *Protein Cell*. **7**, 533–537

151. Schneider, E., Kartarius, S., Schuster, N., and Montenarh, M. (2002) The cyclin H/cdk7/Mat1 kinase activity is regulated by CK2 phosphorylation of cyclin H. *Oncogene*. **21**, 5031–5037

152. Harper, J. W., and Elledge, S. J. (1998) The role of Cdk7 in CAK function, a retro-retrospective. *Genes & Development*. **12**, 285–289

153. Morgan, D. O. (1997) Cyclin-dependent kinases: engines, clocks, and microprocessors. *Annu. Rev. Cell Dev. Biol.* **13**, 261–291

154. Schwindling, S. L., Noll, A., Montenarh, M., and Götz, C. (2004) Mutation of a CK2 phosphorylation site in cdc25C impairs importin alpha/beta binding and results in cytoplasmic retention. *Oncogene*. **23**, 4155–4165

155. Schneider, C. C., Goetz, C., Hessenauer, A., Guenther, J., Kartarius, S., and Montenarh, M. (2011) Down-regulation of CK2 activity results in a decrease in the level of cdc25C phosphatase in different prostate cancer cell lines, pp. 177–184, **356**, 177–184

156. Izeradjene, K., Douglas, L., Delaney, A., and Houghton, J. A. (2005) Casein kinase II (CK2) enhances death-inducing signaling complex (DISC) activity in TRAIL-induced apoptosis in human colon carcinoma cell lines. *Oncogene*. **24**, 2050–2058

157. Izeradjene, K. (2004) Influence of Casein Kinase II in Tumor Necrosis Factor-Related Apoptosis-Inducing Ligand-Induced Apoptosis in Human Rhabdomyosarcoma Cells. *Clinical Cancer Research*. **10**, 6650–6660

158. Kim, H., Choi, K., Kang, H., Lee, S.-Y., Chi, S.-W., Lee, M.-S., Song, J., Im, D., Choi, Y., and Cho, S. (2014) Identification of a Novel Function of CX-4945 as a Splicing Regulator. *PLoS ONE*. **9**, e94978 EP –

159. Trembley, J. H., Tatsumi, S., Sakashita, E., Loyer, P., Slaughter, C. A., Suzuki, H., Endo, H., Kidd, V. J., and Mayeda, A. (2005) Activation of Pre-mRNA Splicing by Human RNPS1 Is Regulated by CK2 Phosphorylation. *Molecular and Cellular Biology*. **25**, 1446–1457

160. Bian, Y., Ye, M., Wang, C., Cheng, K., Song, C., Dong, M., Pan, Y., Qin, H., and Zou, H. (2013) Global screening of CK2 kinase substrates by an integrated phosphoproteomics workflow. *Sci. Rep.* **3**, 3460

161. Parsons, J. L., Dianova, I. I., Finch, D., Tait, P. S., Ström, C. E., Helleday, T., and Dianov, G. L. (2010) XRCC1 phosphorylation by CK2 is required for its stability and efficient DNA repair. *DNA Repair*. **9**, 835–841

162. Marcilla, M., Alpizar, A., Paradela, A., and Albar, J. P. (2011) A systematic approach to assess amino acid conversions in SILAC experiments. *Talanta*. **84**, 430–436

163. Rappsilber, J., Mann, M., and Ishihama, Y. (2007) Protocol for micro-purification, enrichment, pre-fractionation and storage of peptides for proteomics using StageTips. *Nat Protoc*. **2**, 1896–1906

164. Cox, J., Matic, I., Hilger, M., Nagaraj, N., Selbach, M., Olsen, J. V., and Mann, M. (2009) A practical guide to the MaxQuant computational platform for SILAC-based quantitative proteomics. *Nat Protoc*. **4**, 698–705

165. Schoof, E. M., and Linding, R. (2014) Experimental and computational tools for analysis of signaling networks in primary cells. *Curr Protoc Immunol*. **104**, Unit 11.11.

166. Hornbeck, P. V., Zhang, B., Murray, B., Kornhauser, J. M., Latham, V., and Skrzypek, E. (2014) PhosphoSitePlus, 2014: mutations, PTMs and recalibrations. *Nucleic Acids Research*. 10.1093/nar/gku1267

167. Shannon, P., Markiel, A., Ozier, O., Baliga, N. S., Wang, J. T., Ramage, D., Amin, N., Schwikowski, B., and Ideker, T. (2003) Cytoscape: a software environment for integrated models of biomolecular interaction networks. *Genome Research*. **13**, 2498–2504

168. Kucera, M., Isserlin, R., Arkhangorodsky, A., and Bader, G. D. (2016) AutoAnnotate: A Cytoscape app for summarizing networks with semantic annotations. *F1000Research*. **5**, 1717

169. Daub, H. (2015) Quantitative proteomics of kinase inhibitor targets and mechanisms. *ACS Chem. Biol.* **10**, 201–212

170. Oppermann, F. S., Gnad, F., Olsen, J. V., Hornberger, R., Greff, Z., Keri, G., Mann, M., and Daub, H. (2009) Large-scale Proteomics Analysis of the Human Kinome. *Mol. Cell Proteomics*. **8**, 1751–1764

171. Qin, Y., Sundaram, S., Essaid, L., Chen, X., Miller, S. M., Yan, F., Darr, D. B., Galanko, J. A., Montgomery, S. A., Major, M. B., Johnson, G. L., Troester, M. A., and Makowski, L. (2016) Weight loss reduces basal-like breast cancer through kinome reprogramming. *Cancer Cell Int*. **16**, 1–13

172. Kurimchak, A. M., Shelton, C., Duncan, K. E., Johnson, K. J., Brown, J., O'Brien, S., Gabbasov, R., Fink, L. S., Li, Y., Lounsbury, N., Abou-Gharbia, M., Childers, W. E., Connolly, D. C., Chernoff, J., Peterson, J. R., and Duncan, J. S. (2016) Resistance to BET Bromodomain Inhibitors Is Mediated by Kinome Reprogramming in Ovarian Cancer. *Cell Reports*. **16**, 1273–1286

173. Schalm, S. S., and Blenis, J. (2002) Identification of a Conserved Motif Required for mTOR Signaling. *Curr. Biol.* **12**, 632–639

174. García-Martínez, J. M., and Alessi, D. R. (2008) mTOR complex 2 (mTORC2) controls hydrophobic motif phosphorylation and activation of serum- and glucocorticoid-induced protein kinase 1 (SGK1). *Biochem. J.* **416**, 375–385

175. Sarbassov, D. D. (2005) Phosphorylation and Regulation of Akt/PKB by the Rictor-mTOR Complex. *Science*. **307**, 1098–1101

176. Sun, Q., Chen, X., Ma, J., Peng, H., Wang, F., Zha, X., Wang, Y., Jing, Y., Yang, H., Chen, R., Chang, L., Zhang, Y., Goto, J., Onda, H., Chen, T., Wang, M.-R., Lu, Y., You, H., Kwiatkowski, D., and Zhang, H. (2011) Mammalian target of rapamycin

up-regulation of pyruvate kinase isoenzyme type M2 is critical for aerobic glycolysis and tumor growth. *Proceedings of the National Academy of Sciences*. **108**, 4129–4134

177. MacGillivray, M. K., Cruz, T. F., and McCulloch, C. A. G. (2000) The Recruitment of the Interleukin-1 (IL-1) Receptor-associated Kinase (IRAK) into Focal Adhesion Complexes Is Required for IL-1 -induced ERK Activation. *Journal of Biological Chemistry*. **275**, 23509–23515

178. Norbury, C., Blow, J., and Nurse, P. (1991) Regulatory phosphorylation of the p34cdc2 protein kinase in vertebrates. *The EMBO Journal*. **10**, 3321–3329

179. Rouse, J., Cohen, P., Trigon, S., Morange, M., Alonso-Llamazares, A., Zamanillo, D., Hunt, T., and Nebreda, Á. R. (1994) A novel kinase cascade triggered by stress and heat shock that stimulates MAPKAP kinase-2 and phosphorylation of the small heat shock proteins. *Cell*. **78**, 1027–1037

180. Han, J., Lee, J., Bibbs, L., and Ulevitch, R. (1994) A MAP kinase targeted by endotoxin and hyperosmolarity in mammalian cells. *Science*. **265**, 808–811

181. Kim, J., Kundu, M., Viollet, B., and Guan, K.-L. (2011) AMPK and mTOR regulate autophagy through direct phosphorylation of Ulk1. *Nat Cell Biol*. **13**, 132–141

182. King, A. J., Sun, H., Diaz, B., Barnard, D., Miao, W., Bagrodia, S., and Marshall, M. S. (1998) The protein kinase Pak3 positively regulates Raf-1 activity through phosphorylation of serine 338. *Nature*. **396**, 180–183

183. Chaudhary, A., King, W. G., Mattaliano, M. D., Frost, J. A., Diaz, B., Morrison, D. K., Cobb, M. H., Marshall, M. S., and Brugge, J. S. Phosphatidylinositol 3-kinase regulates Raf1 through Pak phosphorylation of serine 338. *Curr. Biol.* **10**, 551–554

184. Zimmermann, S., and Moelling, K. (1999) Phosphorylation and Regulation of Raf by Akt (Protein Kinase B). *Science*. **286**, 1741–1744

185. Rommel, C., Radziwill, G., Lovric, J., Noeldeke, J., Heinicke, T., Jones, D., Aitken, A., and Moelling, K. (1996) Activated Ras displaces 14-3-3 protein from the amino terminus of c-Raf-1. *Oncogene*. **12**, 609–619

186. Kubicek, M., Pacher, M., Abraham, D., Podar, K., Eulitz, M., and Baccarini, M. (2002) Dephosphorylation of Ser-259 Regulates Raf-1 Membrane Association. *Journal of Biological Chemistry*. **277**, 7913–7919

187. Abraham, D., Podar, K., Pacher, M., Kubicek, M., Welzel, N., Hemmings, B. A., Dilworth, S. M., Mischak, H., Kolch, W., and Baccarini, M. (2000) Raf-1-associated Protein Phosphatase 2A as a Positive Regulator of Kinase Activation. *Journal of Biological Chemistry*. **275**, 22300–22304

188. Vignon, C., Debeissat, C., Georget, M.-T., Bouscary, D., Gyan, E., Rosset, P., and Herault, O. (2013) Flow Cytometric Quantification of All Phases of the Cell Cycle and Apoptosis in a Two-Color Fluorescence Plot. *PLoS ONE*. **8**, e68425 EP –

189. Gray, G. K., McFarland, B. C., Rowse, A. L., Gibson, S. A., and Benveniste, E. N. (2014) Therapeutic CK2 inhibition attenuates diverse prosurvival signaling cascades and decreases cell viability in human breast cancer cells. *Oncotarget*. **5**, 6484–6496

190. Yanagawa, T., Funasaka, T., Tsutsumi, S., Raz, T., Tanaka, N., and Raz, A. (2005) Differential Regulation of Phosphoglucose Isomerase/Autocrine Motility Factor Activities by Protein Kinase CK2 Phosphorylation. *Journal of Biological Chemistry*. **280**, 10419–10426

191. Torres, J., and Pulido, R. (2001) The tumor suppressor PTEN is phosphorylated by

the protein kinase CK2 at its C terminus. Implications for PTEN stability to proteasome-mediated degradation. *J. Biol. Chem.* **276**, 993–998

192. Shehata, M., Schnabl, S., Demirtas, D., Hilgarth, M., Hubmann, R., Ponath, E., Badrnya, S., Lehner, C., Hoelbl, A., Duechler, M., Gaiger, A., Zielinski, C., Schwarzmeier, J. D., and Jaeger, U. (2010) Reconstitution of PTEN activity by CK2 inhibitors and interference with the PI3-K/Akt cascade counteract the antiapoptotic effect of human stromal cells in chronic lymphocytic leukemia. *Blood*. **116**, 2513–2521

193. So, K. S., Kim, C. H., Rho, J. K., Kim, S. Y., Choi, Y. J., Song, J. S., Kim, W. S., Choi, C. M., Chun, Y. J., and Lee, J. C. (2014) Autophagosome-Mediated EGFR Down-Regulation Induced by the CK2 Inhibitor Enhances the Efficacy of EGFR-TKI on EGFR-Mutant Lung Cancer Cells with Resistance by T790M. *PLoS ONE*. **9**, e114000

194. Klionsky, D. J., Abeliovich, H., Agostinis, P., Agrawal, D. K., Aliev, G., Askew, D. S., Baba, M., Baehrecke, E. H., Bahr, B. A., Ballabio, A., Bamber, B. A., Bassham, D. C., Bergamini, E., Bi, X., Biard-Piechaczyk, M., Blum, J. S., Bredesen, D. E., Brodsky, J. L., Brumell, J. H., Brunk, U. T., Bursch, W., Camougrand, N., Cebollero, E., Cecconi, F., Chen, Y., Chin, L.-S., Choi, A., Chu, C. T., Chung, J., Clarke, P. G., Clark, R. S., Clarke, S. G., Clavé, C., Cleveland, J. L., Codogno, P., Colombo, M. I., Coto-Montes, A., Cregg, J. M., Cuervo, A. M., Debnath, J., Demarchi, F., Dennis, P. B., Dennis, P. A., Deretic, V., Devenish, R. J., Di Sano, F., Dice, J. F., DiFiglia, M., Dinesh-Kumar, S., Distelhorst, C. W., Djavaheri-Mergny, M., Dorsey, F. C., Dröge, W., Dron, M., Dunn, W. A., Duszenko, M., Eissa, N. T., Elazar, Z., Esclatine, A., Eskelinen, E.-L., Fésüs, L., Finley, K. D., Fuentes, J. M., Fueyo, J., Fujisaki, K., Galliot, B., Gao, F.-B., Gewirtz, D. A., Gibson, S. B., Gohla, A., Goldberg, A. L., Gonzalez, R., González-Estévez, C., Gorski, S., Gottlieb, R. A., Häussinger, D., He, Y.-W., Heidenreich, K., Hill, J. A., Høyer-Hansen, M., Hu, X., Huang, W.-P., Iwasaki, A., Jäättelä, M., Jackson, W. T., Jiang, X., Jin, S., Johansen, T., Jung, J. U., Kadowaki, M., Kang, C., Kelekar, A., Kessel, D. H., Kiel, J. A., Kim, H. P., Kimchi, A., Kinsella, T. J., Kiselyov, K., Kitamoto, K., Knecht, E., Komatsu, M., Kominami, E., Kondo, S., Kovács, A. L., Kroemer, G., Kuan, C.-Y., Kumar, R., Kundu, M., Landry, J., Laporte, M., Le, W., Lei, H.-Y., Lenardo, M. J., Levine, B., Lieberman, A., Lim, K.-L., Lin, F.-C., Liou, W., Liu, L. F., Lopez-Berestein, G., López-Otín, C., Lu, B., Macleod, K. F., Malorni, W., Martinet, W., Matsuoka, K., Mautner, J., Meijer, A. J., Meléndez, A., Michels, P., Miotto, G., Mistiaen, W. P., Mizushima, N., Mograbi, B., Monastyrska, I., Moore, M. N., Moreira, P. I., Moriyasu, Y., Motyl, T., Münz, C., Murphy, L. O., Naqvi, N. I., Neufeld, T. P., Nishino, I., Nixon, R. A., Noda, T., Nürnberg, B., Ogawa, M., Oleinick, N. L., Olsen, L. J., Ozpolat, B., Paglin, S., Palmer, G. E., Papassideri, I., Parkes, M., Perlmutter, D. H., Perry, G., Piacentini, M., Pinkas-Kramarski, R., Prescott, M., Proikas-Cezanne, T., Raben, N., Rami, A., Reggiori, F., Rohrer, B., Rubinsztein, D. C., Ryan, K. M., Sadoshima, J., Sakagami, H., Sakai, Y., Sandri, M., Sasakawa, C., Sass, M., Schneider, C., Seglen, P. O., Seleverstov, O., Settleman, J., Shacka, J. J., Shapiro, I. M., Sibirny, A., Silva-Zacarin, E. C., Simon, H.-U., Simone, C., Simonsen, A., Smith, M. A., Spanel-Borowski, K., Srinivas, V., Steeves, M., Stenmark, H., Stromhaug, P. E., Subauste, C. S., Sugimoto, S., Sulzer, D., Suzuki,

T., Swanson, M. S., Tabas, I., Takeshita, F., Talbot, N. J., Tallóczy, Z., Tanaka, K., Tanaka, K., Tanida, I., Taylor, G. S., Taylor, J. P., Terman, A., Tettamanti, G., Thompson, C. B., Thumm, M., Tolkovsky, A. M., Tooze, S. A., Truant, R., Tumanovska, L. V., Uchiyama, Y., Ueno, T., Uzcátegui, N. L., van der Klei, I., Vaquero, E. C., Vellai, T., Vogel, M. W., Wang, H.-G., Webster, P., Wiley, J. W., Xi, Z., Xiao, G., Yahalom, J., Yang, J.-M., Yap, G., Yin, X.-M., Yoshimori, T., Yu, L., Yue, Z., Yuzaki, M., Zabirnyk, O., Zheng, X., Zhu, X., and Deter, R. L. (2008) Guidelines for the use and interpretation of assays for monitoring autophagy in higher eukaryotes. *Autophagy*. **4**, 151–175

195.   Mendoza, M. C., Er, E. E., and Blenis, J. (2011) The Ras-ERK and PI3K-mTOR pathways: cross-talk and compensation. *Trends in Biochemical Sciences*. **36**, 320–328

196.   McDermott, E. P., and O'Neill, L. A. J. (2002) Ras Participates in the Activation of p38 MAPK by Interleukin-1 by Associating with IRAK, IRAK2, TRAF6, and TAK-1. *Journal of Biological Chemistry*. **277**, 7808–7815

197.   Olsen, B. B., Svenstrup, T. H., and Guerra, B. (2012) Downregulation of protein kinase CK2 induces autophagic cell death through modulation of the mTOR and MAPK signaling pathways in human glioblastoma cells. *Int. J. Oncol.* **41**, 1967–1976

198.   Zhou, B., Ritt, D. A., Morrison, D. K., Der, C. J., and Cox, A. D. (2016) Protein Kinase CK2α Maintains Extracellular Signal-regulated Kinase (ERK) Activity in a CK2α Kinase-independent Manner to Promote Resistance to Inhibitors of RAF and MEK but Not ERK in BRAF Mutant Melanoma. *Journal of Biological Chemistry*. **291**, 17804–17815

199.   Chadee, D. N., Hendzel, M. J., Tylipski, C. P., Allis, C. D., Bazett-Jones, D. P., Wright, J. A., and Davie, J. R. (1999) Increased Ser-10 Phosphorylation of Histone H3 in Mitogen-stimulated and Oncogene-transformed Mouse Fibroblasts. *Journal of Biological Chemistry*. **274**, 24914–24920

200.   Hengeveld, R. C. C., Hertz, N. T., Vromans, M. J. M., Zhang, C., Burlingame, A. L., Shokat, K. M., and Lens, S. M. A. (2012) Development of a Chemical Genetic Approach for Human Aurora B Kinase Identifies Novel Substrates of the Chromosomal Passenger Complex. *Mol. Cell Proteomics*. **11**, 47–59

201.   Hirota, T., Lipp, J. J., Toh, B.-H., and Peters, J.-M. (2005) Histone H3 serine 10 phosphorylation by Aurora B causes HP1 dissociation from heterochromatin. *Nature*. **438**, 1176–1180

202.   Murnion, M. E., Adams, R. R., Callister, D. M., Allis, C. D., Earnshaw, W. C., and Swedlow, J. R. (2001) Chromatin-associated protein phosphatase 1 regulates aurora-B and histone H3 phosphorylation. *J. Biol. Chem.* **276**, 26656–26665

203.   Huang, W., Batra, S., Atkins, B. A., Mishra, V., and Mehta, K. D. (2005) Increases in intracellular calcium dephosphorylate histone H3 at serine 10 in human hepatoma cells: potential role of protein phosphatase 2A-protein kinase CbetaII complex. *J. Cell. Physiol.* **205**, 37–46

204.   Statsuk, A. V., Maly, D. J., Seeliger, M. A., Fabian, M. A., Biggs, W. H., Lockhart, D. J., Zarrinkar, P. P., Kuriyan, J., and Shokat, K. M. (2008) Tuning a three-component reaction for trapping kinase substrate complexes. *J. Am. Chem. Soc.* **130**, 17568–17574

205. Klutchko, S. R., Hamby, J. M., Boschelli, D. H., Wu, Z., Kraker, A. J., Amar, A. M., Hartl, B. G., Shen, C., Klohs, W. D., Steinkampf, R. W., Driscoll, D. L., Nelson, J. M., Elliott, W. L., Roberts, B. J., Stoner, C. L., Vincent, P. W., Dykes, D. J., Panek, R. L., Lu, G. H., Major, T. C., Dahring, T. K., Hallak, H., Bradford, L. A., Showalter, H. D. H., and Doherty, A. M. (1998) 2-Substituted Aminopyrido[2,3-d]pyrimidin-7(8H)-ones. Structure−Activity Relationships Against Selected Tyrosine Kinases and in Vitro and in Vivo Anticancer Activity. *J. Med. Chem.* **41**, 3276–3292

206. Wissing, J., Godl, K., Brehmer, D., Blencke, S., Weber, M., Habenberger, P., Stein-Gerlach, M., Missio, A., Cotten, M., Müller, S., and Daub, H. (2004) Chemical Proteomic Analysis Reveals Alternative Modes of Action for Pyrido[2,3-d]pyrimidine Kinase Inhibitors. *Mol. Cell Proteomics*. **3**, 1181–1193

207. Zhang, L., Holmes, I. P., Hochgräfe, F., Walker, S. R., Ali, N. A., Humphrey, E. S., Wu, J., de Silva, M., Kersten, W. J. A., Connor, T., Falk, H., Allan, L., Street, I. P., Bentley, J. D., Pilling, P. A., Monahan, B. J., Peat, T. S., and Daly, R. J. (2013) Characterization of the novel broad-spectrum kinase inhibitor CTx-0294885 as an affinity reagent for mass spectrometry-based kinome profiling. *J Proteome Res*. **12**, 3104–3116

208. Gray, N. S., Wodicka, L., Thunnissen, A.-M. W. H., Norman, T. C., Kwon, S., Espinoza, F. H., Morgan, D. O., Barnes, G., LeClerc, S., Meijer, L., Kim, S.-H., Lockhart, D. J., and Schultz, P. G. (1998) Exploiting Chemical Libraries, Structure, and Genomics in the Search for Kinase Inhibitors. *Science*. **281**, 533–538

209. Vilk, G., Weber, J. E., Turowec, J. P., Duncan, J. S., Wu, C., Derksen, D. R., Zien, P., Sarno, S., Donella-Deana, A., Lajoie, G., Pinna, L. A., Li, S. S. C., and Litchfield, D. W. (2008) Protein kinase CK2 catalyzes tyrosine phosphorylation in mammalian cells. *Cellular Signalling*. **20**, 1942–1951

210. Humphrey, S. J., Azimifar, S. B., and Mann, M. (2015) High-throughput phosphoproteomics reveals in vivo insulin signaling dynamics. *Nat Biotech*. **33**, 990–995

211. Wessel, D., and Flügge, U. I. (1984) A method for the quantitative recovery of protein in dilute solution in the presence of detergents and lipids. *Anal. Biochem.* **138**, 141–143

212. Borgo, C., Franchin, C., Salizzato, V., Cesaro, L., Arrigoni, G., Matricardi, L., Pinna, L. A., and Donella-Deana, A. (2015) Protein kinase CK2 potentiates translation efficiency by phosphorylating eIF3j at Ser127. *Biochimica et Biophysica Acta (BBA) - Molecular Cell Research*. 10.1016/j.bbamcr.2015.04.004

213. Ruprecht, B., Zecha, J., Heinzlmeir, S., Médard, G., Lemeer, S., and Kuster, B. (2015) Evaluation of Kinase Activity Profiling Using Chemical Proteomics. *ACS Chem. Biol.* **10**, 2743–2752

214. Ruprecht, B., Koch, H., Medard, G., Mundt, M., Kuster, B., and Lemeer, S. (2014) Comprehensive and reproducible phosphopeptide enrichment using Fe-IMAC columns. *Mol. Cell Proteomics*. 10.1074/mcp.M114.043109

215. Urisman, A., Levin, R. S., Gordan, J. D., Webber, J. T., Hernandez, H., Ishihama, Y., Shokat, K. M., and Burlingame, A. L. (2017) An Optimized Chromatographic Strategy for Multiplexing In Parallel Reaction Monitoring Mass Spectrometry: Insights from Quantitation of Activated Kinases. *Mol. Cell Proteomics*. **16**, 265–277

216. Molina, D. M., Jafari, R., Ignatushchenko, M., Seki, T., Larsson, E. A., Dan, C.,

Sreekumar, L., Cao, Y., and Nordlund, P. (2013) Monitoring Drug Target Engagement in Cells and Tissues Using the Cellular Thermal Shift Assay. *Science*. **341**, 84–87

217. Jafari, R., Almqvist, H., Axelsson, H., Ignatushchenko, M., Lundbäck, T., Nordlund, P., and Molina, D. M. (2014) The cellular thermal shift assay for evaluating drug target interactions in cells. *Nat Protoc*. **9**, 2100–2122

218. Savitski, M. M., Reinhard, F. B. M., Franken, H., Werner, T., Savitski, M. F., Eberhard, D., Molina, D. M., Jafari, R., Dovega, R. B., Klaeger, S., Kuster, B., Nordlund, P., Bantscheff, M., and Drewes, G. (2014) Tracking cancer drugs in living cells by thermal profiling of the proteome. *Science*. **346**, 1255784–1255784

219. Sarno, S., Ruzzene, M., Frascella, P., Pagano, M. A., Meggio, F., Zambon, A., Mazzorana, M., Maira, G. D., Lucchini, V., and Pinna, L. A. (2005) Development and exploitation of CK2 inhibitors. *Arch. Pharm. Res.* **274**, 69–76

220. Brear, P., De Fusco, C., Georgiou, K. H., Francis-Newton, N. J., Stubbs, C. J., Sore, H. F., Venkitaraman, A. R., Abell, C., Spring, D. R., and Hyvönen, M. (2016) Specific inhibition of CK2α from an anchor outside the active site. *Chemical Science*. **7**, 6839–6845

221. Raaf, J., Guerra, B., Neundorf, I., Bopp, B., Issinger, O.-G., Jose, J., Pietsch, M., and Niefind, K. (2013) First Structure of Protein Kinase CK2 Catalytic Subunit with an Effective CK2β-Competitive Ligand. *ACS Chem. Biol.* **8**, 901–907

222. Hoofnagle, A. N., Whiteaker, J. R., Carr, S. A., Kuhn, E., Liu, T., Massoni, S. A., Thomas, S. N., Townsend, R. R., Zimmerman, L. J., Boja, E., Chen, J., Crimmins, D. L., Davies, S. R., Gao, Y., Hiltke, T. R., Ketchum, K. A., Kinsinger, C. R., Mesri, M., Meyer, M. R., Qian, W.-J., Schoenherr, R. M., Scott, M. G., Shi, T., Whiteley, G. R., Wrobel, J. A., Wu, C., Ackermann, B. L., Aebersold, R., Barnidge, D. R., Bunk, D. M., Clarke, N., Fishman, J. B., Grant, R. P., Kusebauch, U., Kushnir, M. M., Lowenthal, M. S., Moritz, R. L., Neubert, H., Patterson, S. D., Rockwood, A. L., Rogers, J., Singh, R. J., Van Eyk, J. E., Wong, S. H., Zhang, S., Chan, D. W., Chen, X., Ellis, M. J., Liebler, D. C., Rodland, K. D., Rodriguez, H., Smith, R. D., Zhang, Z., Zhang, H., and Paulovich, A. G. (2016) Recommendations for the Generation, Quantification, Storage, and Handling of Peptides Used for Mass Spectrometry-Based Assays. *Clinical Chemistry*. **62**, 48–69

223. Lange, V., Picotti, P., Domon, B., and Aebersold, R. (2008) Selected reaction monitoring for quantitative proteomics: a tutorial. *Mol Syst Biol*. **4**, 222

224. Gallien, S., Duriez E., Crone C., Kellmann M., Moehring T., and Domon, B. (2012) Targeted Proteomic Quantification on Quadrupole-Orbitrap Mass Spectrometer. *Mol. Cell Proteomics*. **11**, 1709–1723

225. Peterson, A. C., Russell, J. D., Bailey, D. J., Westphall, M. S., and Coon, J. J. (2012) Parallel reaction monitoring for high resolution and high mass accuracy quantitative, targeted proteomics. *Mol. Cell Proteomics*. **11**, 1475–1488

226. Abelin, J. G., Patel, J., Lu, X., Feeney, C. M., Fagbami, L., Creech, A. L., Hu, R., Lam, D., Davison, D., Pino, L., Qiao, J. W., Kuhn, E., Officer, A., Li, J., Abbatiello, S., Subramanian, A., Sidman, R., Snyder, E., Carr, S. A., and Jaffe, J. D. (2016) Reduced-representation Phosphosignatures Measured by Quantitative Targeted MS Capture Cellular States and Enable Large-scale Comparison of Drug-induced Phenotypes. *Mol. Cell Proteomics*. **15**, 1622–1641

227.   Sacco, F., Silvestri, A., Posca, D., Pirrò, S., Gherardini, P. F., Castagnoli, L., Mann, M., and Cesareni, G. (2016) Deep Proteomics of Breast Cancer Cells Reveals that Metformin Rewires Signaling Networks Away from a Pro-growth State. *Cell Systems*. 10.1016/j.cels.2016.02.005

7 Copyright Permission

PUBLICATIONS
American Association for Cancer Research

Article Reuse by Authors

Authors of articles published in AACR journals are permitted to use their article or parts of their article in the following ways without requesting permission from the AACR. All such uses must include appropriate attribution to the original AACR publication. Authors may do the following as applicable:

1. Reproduce parts of their article, including figures and tables, in books, reviews, or subsequent research articles they write;

2. Use parts of their article in presentations, including figures downloaded into PowerPoint, which can be done directly from the journal's website;

3. Post the accepted version of their article (after revisions resulting from peer review, but before editing and formatting) on their institutional website, if this is required by their institution. The version on the institutional repository must contain a link to the final, published version of the article on the AACR journal website so that any subsequent corrections to the published record will continue to be available to the broadest readership. The posted version may be released publicly (made open to anyone) 12 months after its publication in the journal;

4. Submit a copy of the article to a doctoral candidate's university in support of a doctoral thesis or dissertation.

Article Reuse by Others

Third parties or individuals who are seeking permission to copy, reproduce, or republish content from an AACR journal and who are not the author of that content may use the Copyright Clearance Center's Rightslink® service to request permission to reuse identified content. Please see **Third Party Permission and Reprints** for detailed instructions on how to submit a request.

8 Curriculum Vitae

Name: Adam J. Rabalski

Post-secondary Education and Degrees:
University of Guelph
Guelph, Ontario, Canada
2007-2011 B.Sc. Biomedical Science

The University of Western Ontario
London, Ontario, Canada
2011-2017 Ph.D. Biochemistry

Honours and Awards:
Canadian National Proteomics Network Travel Award 2016
Let's Talk Science Male Volunteer of the Year 2015
Canadian Bioinformatics Workshops Travel Award 2015
Canadian Student Health Research Forum Travel Award 2014
Canadian National Proteomics Network Travel Award 2014
NSERC USRA 2010
Dept. of Molecular & Cellular Biology Student Research Award 2009
NSERC USRA 2008
University of Guelph Entrance Scholarship 2007

Related Work Experience
Teaching Assistant
The University of Western Ontario
Biochemistry 3382
Biochemistry 3390

Extracurricular
Let's Talk Science Activity Demonstrator
2013-2016

Biochemistry Department Outreach Committee
2013-2016

St. John the Evangelist Anglican Hospitality Meal Volunteer
2012-2016

Publications:

Rabalski, A. J., Gyenis, L., and Litchfield, D. W. (2016) Molecular Pathways: Emergence of Protein Kinase CK2 (CSNK2) as a Potential Target to Inhibit Survival and DNA Damage Response and Repair Pathways in Cancer Cells. *Clin. Cancer Res.* **22**, 2840–2847

Hawley, S. P., Wills, M. K. B., **Rabalski, A. J.**, Bendall, A. J., and Jones, N. (2011) Expression patterns of ShcD and Shc family adaptor proteins during mouse embryonic development. *Dev. Dyn.* **240**, 221–231